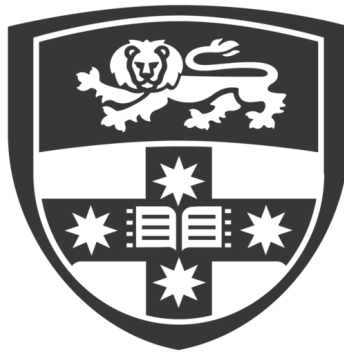


UNIVERSITY OF SYDNEY

A THESIS SUBMITTED TO FULFIL REQUIREMENTS FOR THE DOCTOR
OF PHILOSOPHY

Exactly soluble models in many-body physics



Samuel Jacob Elman

supervised by
Prof. Stephen Bartlett

April 13, 2023

Statement of originality

This is to certify that to the best of my knowledge, the content of this thesis is my own work. This thesis has not been submitted for any degree or other purposes.

I certify that the intellectual content of this thesis is the product of my own work and that all the assistance received in preparing this thesis and sources have been acknowledged.

Samuel J Elman

Abstract

Almost all phenomena in the universe are described, at the fundamental level, by quantum many-body models. In general, however, a complete understanding of large systems with many degrees of freedom is impossible. The complexity of solving such systems grows exponentially with system size, meaning that solving the governing equations is currently intractable. While in general many-body quantum systems are intractable, there are special cases for which there are techniques that allow for an exact solution. The importance of such models extends beyond the specific models in question. Exactly soluble models are interesting because they are soluble; beyond this, they can be used to gain intuition for further reaching many-body systems, including when they can be leveraged to help with numerical approximations for general models. The work presented in this thesis considers exactly soluble models of quantum many-body systems. In particular, this thesis investigates two distinct classes of exactly soluble quantum many-body systems. The first part of this thesis extends the family of many-body spin models for which we can find a free-fermion solution. A solution method that was developed for a specific free-fermion model is generalized in such a way that allows application to a broader class of many-body spin system than was previously known to be free. Further more a simple recognition test is presented to determine a system's free-fermion solubility. Models which admit a solution via this method are characterized by a graph theory invariants: in brief it is shown that a quantum spin system has an exact description via non-interacting fermions if its frustration graph is claw-free and contains a simplicial clique. The graph theoretic characterization is also connected to the developing body of work on operator Krylov subspaces; such a connection could have implications which reach beyond this class of models, and aide in our understanding of tractability in more general models. The results in this part of the thesis deepen the already existing connection between many-body physics and the mathematical theory of claw-free graphs. The second part of this thesis gives an explicit example of how the usefulness of exactly soluble models can extend beyond the solution itself. This chapter pertains to the calculation of the topological entanglement entropy in topologically ordered loop-gas states. Topological entanglement entropy gives an understanding of how correlations may extend throughout a system. In this chapter the topological entanglement entropy of two- and three-dimensional loop-gas states is calculated in the bulk and at the boundary. We obtain a closed form expression for the topological entanglement in terms of the anyonic theory that the models support. Central to the formulation of these results is the development of a generalized braiding operator.

Declaration

This thesis consists of an introduction, three main body chapters and an outlook. The body chapters, were written while completing the investigation described therein. Chapters 2 to 4 are based on three separate research articles with small edits and additions throughout. The research articles are either published or currently in progress. The introduction and outlook chapters are written by me. A statement of research contribution for each of Chapters 2 to 4 is included below.

Chapter 2: Free fermions behind the disguise

Published in: [Comm. Math Phys](#), **388**, 969–1003 (2021)

Author list: Samuel Elman, Adrian Chapman and Steve Flammia

Student contribution: I am the lead author in this publication. Adrian Chapman was a postdoc who was taking a supervisory role on this work; Steve Flammia oversaw the project. The initial idea for this project arose from a conversation between myself and Adrian, following the publication of his previous paper and the discovery of the result in Paul Fendley’s paper *Free fermions in disguise*. Following this initial discussion, Adrian and I worked closely together to complete proofs.

Chapter 3: A unified graph-theoretic approach to free fermions

Paper in preparation

Author list: Adrian Chapman, Samuel Elman and Ryan Mann

Student contribution: The authors of this paper are listed in alphabetical order. Both Adrian and Ryan Mann are postdocs working in an active and supervisory role on this project; I was the student working actively on the proofs and the manuscript. The initial idea for the project in this chapter came from an outlook point in the previous chapter. Adrian and I spoke briefly about how we might extend the proofs in Chapter 2, at the same time Ryan reached out and suggested an avenue. Following these discussions, we have all worked closely together to complete the proofs. I completed the proof of Theorem 2, and took on large integral parts of the proofs of Theorems 1 and 3.

Chapter 4: Boundary topological entanglement entropy in two and three dimensions

Published in: [Comm. Math Phys](#), **389**, 1241–1276 (2022)

Author list: Jacob Bridgeman, Benjamin Brown and Samuel Elman

Student contribution: Authors are listed in alphabetical order. I was involved in this project from the very early stages. Initially, the project was to investigate the topological entanglement entropy at the boundaries of three dimensional topologically ordered models by considering specific examples of Walker-Wang models associated with Abelian anyons. During this time I completed the calculations for these examples and was then able to prove a closed form expression for the topological entanglement entropy of Abelian (or pointed) Walker-Wang models in general based on the anyons supported by the model and a boundary algebra defined by the anyons that condense at a given boundary. The project then grew into its current form. Jacob Bridgeman was a postdoc expanding on the initial work into what it is presently; Benjamin Brown was the more senior postdoc overseeing the project.

In addition to the statements above, in cases where I am not the corresponding author of a published item, permission to include the published material has been granted by the corresponding author.

Samuel Elman
03/01/23

As supervisor for the candidature upon which this thesis is based, I can confirm that the authorship attribution statements above are correct.

Stephen Bartlett
03/01/23

Acknowledgments

I would like to thank my supervisor Stephen Bartlett, for allowing me to undertake my Doctorate at the University of Sydney in this wonderful group. I would like to acknowledge all of the people who have come through this group , and have made my time in this group such a pleasant experience. In particular, I would like to thank Adrian Chapman for his guidance and willingness to explain things slowly. I would like to thank my parents for their support throughout my various studies.

Finally I would like to thank Angela Karanjai and Maya, the lights of my life. You have been unwavering in your support and so understanding. Thank you.

Contents

1	Introduction	1
1.1	Free fermions	4
1.2	Loop-gas models	8
2	Free fermions behind the disguise	12
2.1	Introduction	12
2.2	Main Results	16
2.3	Relation to prior work	19
2.4	Proofs of Main Results	24
2.5	Examples	39
2.5.1	Small systems	40
2.5.2	Indifference Graphs	42
2.5.3	Integrable and Soluble models	48
2.6	Discussion	48
3	A unified graph theoretic approach	51
3.1	Introduction	52
3.1.1	Main Results	54
3.1.2	A worked example	56
3.2	Frustration Graphs	59
3.3	Free-Fermion Models	64
3.3.1	Exact Solution	64
3.3.2	Generalized Jordan-Wigner Solutions	67
3.3.3	“Hidden” Free-Fermion Modes	69
3.4	Claw-Free Graphs	73
3.5	Conserved Quantities	81
3.5.1	Proof of Eq. 3.80a	82
3.5.2	Proof of Eq. 3.80b	83
3.5.3	Proof of Eq. 3.80c	84
3.6	Exact Solution	94
3.7	Polynomial Division	96
3.7.1	Implications of Theorem 3.3	97
3.7.2	Induced path trees	100
3.7.3	The single-vertex-deformation closure of an induced path	102
3.7.4	Proof of Theorem 3.3	104
3.8	Numerical Example	107
3.9	Discussion	110
	Appendices	114
3.A	Proof of Lemmas 3.6, 3.7, 3.8	114
3.A.1	Proof of Lemma 3.6	114
3.A.2	Proof of Lemma 3.7	115
3.A.3	Proof of Lemma 3.8	118

CONTENTS

3.A.4	Proof of Lemma 3.9	118
3.B	Proof of Lemma 3.10	120
3.C	Proofs of Lemmas 3.1 and 3.11	122
3.D	Proof of Lemma 3.13	124
3.E	Proof of Lemma 3.14	125
3.F	Numerical model definition	126
4	Topological entanglement entropy	128
4.1	Introduction	128
4.2	Preliminaries	131
4.2.1	Examples	134
4.3	Loop-gas models in (3+1) dimensions	135
4.3.1	Bulk	135
4.3.2	Boundaries	137
4.3.3	Examples	137
4.4	Entropy diagnostics	138
4.4.1	The universal correction to the area law	138
4.4.2	(2+1)-dimensional models	139
4.4.3	(3+1)-dimensional models	140
4.5	Bulk entropy of topological loop-gasses	142
4.5.1	Levin-Wen models	144
4.5.2	Walker-Wang models	146
4.6	Boundary entropy of topological loop-gasses	149
4.6.1	Levin-Wen models	150
4.6.2	Walker-Wang models	152
4.7	Remarks	156
	Appendices	157
4.A	Properties of the connected \mathcal{S} -matrix	157
4.B	Loop-gas results	159
4.B.1	Case 1	163
4.B.2	Case 2	163
4.B.3	Case 3	164
4.B.4	Case 4	164
4.B.5	Small category data	165
5	Outlook	169

Chapter 1

Introduction

Quantum many-body systems are ubiquitous: from semiconductors [1] and superconductors [2–4] in condensed matter [5] to black holes [6, 7] and plasmas in high energy physics [8], quantum many-body systems are everywhere. Indeed, it could even be argued that the universe, and therefore all of nature, is a single, vast quantum many-body system. Of course, the universe is an impractical test subject, so research is generally restricted in purview to more manageable (and focused) settings. Certainly, a quantum mechanical treatment of the processes in systems with many more than one particle is important. Such a treatment informs our understanding of all that is around us.

Analyzing many-body systems through the lens of quantum mechanics is fundamentally different from a classical approach [9]. In classical mechanics it is conceptually possible to label all particles in a system and to follow their respective motion. In quantum mechanics, this is not possible. Particles do not have a definitive position between measurements, instead the states of a quantum system in time are described by wave-functions. The wave-function can be thought of as a probability distribution over different measurement outcomes. Furthermore, there is no experimental result that can distinguish between two states related by the exchange of identical particles. This leads to the surprising, and yet somehow satisfyingly simple, binary classification of all particles that can naturally exist in terms of their wave-function. Wave-functions are either symmetric or anti-symmetric, with symmetric wave-functions reserved for bosons, while anti-symmetric wave-functions describe fermions. This dichotomy means, among other things, that wave-functions acquire a negative (fermionic) phase or remain invariant (bosons) under exchange of indistinguishable particles [10]. The anti-symmetry of the fermionic wave-function further gives rise to the Pauli exclusion principle, which states that two (or more identical) fermions cannot occupy the same quantum state within a quantum system

simultaneously. Bosons, however, have no such restriction. Thus, studying quantum many-body systems, that is systems with many more than one degree of freedom, or particles, that obey the laws of quantum mechanics, necessitates the development of a new paradigm with which to describe the system in terms of the wave-functions, rather than the dynamics of the constituent particles. Such a paradigm relates the state of a system at any given time to a previous state by the exchange statistics of particles within, rather than the trajectories of particles, or other classical properties with similar analogues.

One of the key goals of the field of quantum many-body physics is to understand the dynamics of a system that is cannot be experimentally controlled. To do this we develop a model which attempts to describe the system, and tune parameters until the dynamics of the model most closely resemble the system itself. The task is then to understand how and why the model describes the system of interest, not simply to emulate the system entirely; a complete and exact emulation would only be as useful as looking at the original system itself. Certainly, in terms of naturally occurring systems, it is clear that there is already a perfect simulation of any phenomena already in existence, the system itself. Rather, the objective is to develop models which embody the characteristics of a physical system, so that the processes behind the characteristics may then be understood through the models. While this distinction may seem arbitrary, it is in fact a poignant contrast, one which allows us to probe the underlying nature of systems of interest, rather than to simply observe. This task of understanding a model designed to describe a process is motivated from both the perspectives of the fundamental (as in gaining a understanding of naturally occurring phenomena), as well as for potential applications (as in designing new materials).

In general, models that are developed to describe quantum many-body systems are so-called ‘toy’ models: deliberately over-simplistic models which neglect, or remove completely, many details so that they can be used to explain a specific mechanism concisely. In many cases these toy models are defined by ensembles of spins particles which are coupled by finite-range, (semi-)local, Pauli interaction terms [11–14]; or finite-range, (semi-)local, spin-less (boson or fermion) creation and annihilation operators; which negate coupling terms that are known to weakly persist at extreme distances in reality.

Even with the restriction to the simplistic, time-independent toy models, there remains a major challenge within the field, due to the inherent difficulty in solving the equation that governs the dynamics of a the degrees of freedom in a system: the time-independent Schrödinger equation [9]. The Schrödinger equation relates the state of a system after a given time to the energetic spectrum of the

model, which is determined by a system specific operator called the Hamiltonian. The Schrödinger equation is mathematically complete, in that in principle, all properties of any system can be obtained by solving it exactly. In practice however, for a system with many degrees of freedom, this is not feasible. The Hilbert space dimension, the dimension of the Hamiltonian, and therefore the computational power required to solve the equation, scales exponentially in the number of degrees of freedom in a system. Thus, for systems with a large number of degrees of freedom (literally) astronomically large computers would be necessary to solve exactly an arbitrary system of interest. For example, the computational power achieved by a computer the size of the Andromeda galaxy would barely be sufficient to solve the equation for a singular caffeine molecule [15]; a computer made by all of the atoms in the observable universe would only be powerful enough to solve the Schrödinger equation for a system of one hundred particles [10, 15, 16].

Quantum computers promise to deliver a performance advantage for some problems which are currently intractable on a classical computer. [17–19]. One of the main areas in which quantum computers are expected to provide computational speedups is in the area of quantum many-body systems [10]. However, quantum devices that are capable of reliable and large-scale computations are not yet available. Furthermore, the link between building a reliable large scale quantum computers and understanding the dynamics of many-body systems is a two-way street. Many of the tasks for which a quantum computer is purported to produce an advantage in run time require the preparation and control of large and highly entangled quantum systems [15]. Thus, it is important to develop an understanding of how to manipulate systems with a large number of degrees of freedom in some regimes in order to even build a quantum computer. For this reason, a number of approximate techniques have been developed to probe the physics of many-body systems. For example, one numerical technique that has great success at determining the low energy properties of one-dimensional systems is tensor networks [20], the decomposition of a global quantum state into the product of smaller, local tensors. Another technique that has seen promising results is that of mean-field theory, where the interactions are averaged in a self consistent way, rather than considered individually [21]. A third method is perturbation theory, where a difficult to solve problem is treated as a small deviation from a system with a known solution, is a prevalent methodology at use throughout physics and applied mathematics [9].

When there exists a special structure within a model that results in the Hamiltonian admitting a tractable, exact solution without any approximations, the model is called *exactly soluble*. Exactly soluble models are extremely useful in many-body physics for a number of reasons [22, 23]. Models

that have a tractable, exact solution provide fundamental insight into physics without the need for difficult numerical methods or perturbation theory. But the common use of perturbation theory in the field makes plain the necessity for some exactly soluble models for another reason, they can also be used as starting points for perturbation theory. For perturbation theory to remain valid, the deviation from a system with a known solution must be small; therefore it is of the utmost importance to find solvable systems which are most similar to the one of interest. A larger class of systems which are known to be solvable makes this easier. This thesis considers two distinct classes of exactly soluble many-body quantum systems: many-body spin systems with free-fermion solutions [24] and string-net condensates [13], also known as loop-gas models [25].

1.1 Free fermions

Fermions are one of the two types of particles that exist in nature. Fermions are those with an anti-symmetric wave-function, and thus obey the Pauli exclusion principle, which precludes the event that two fermions occupy the exact same state at the same time. For this reason, when we think about a fermionic system, the picture that generally comes to mind is that of a set of billiard-ball-like particles which move around a lattice of ‘sites’. That is, we tend to think of Dalton-esque atoms (solid spheres) which move between sites and occasionally bump into one another, such as the image shown in Fig. 1.1. Obviously this is a false image: fermions are not solid spheres of matter. However, the image is an intuitive, and even informative one. In a toy model of a spin-less fermionic system the degrees of freedom are positions and momenta; similarly, in the analogy of solid spheres, the degrees of freedom of interest are their positions and momenta. Furthermore, the solidity of the balls means that they cannot occupy the same space at the same time, this exclusion due to solidity is a reasonable representation for the fact that the fermions obey the Pauli exclusion principle [9]. It is then tempting to equate to the interactions between fermions an attractive or repulsive force between the balls which draws them together or apart, impeding the natural flow and increasing the likelihood of collisions. Although this is not a perfect analogy, and fermion interactions are more nuanced and complicated, it does serve the purpose of differentiating between the images of a system of interacting and non-interacting fermions.

The dynamical equations of a fermionic system can thus be written in terms of Majorana creation and annihilation operators which, as the name suggests, either create and remove a fermion at a given location. The terms of the Hamiltonian that are quadratic describe hopping amplitudes; these terms denote fermions moving from one site to another. We could also think about these terms as paths or

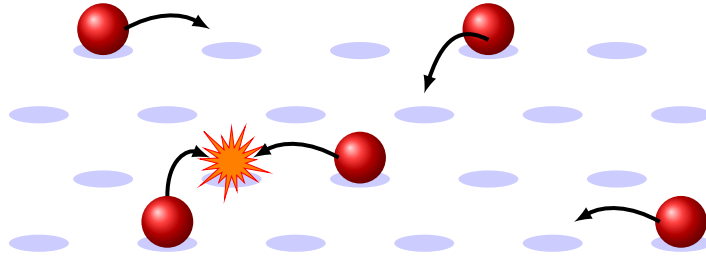


Figure 1.1: A fermionic system is often thought of as a set of solid spheres which move between sites of a lattice and occasionally collide.

roads between sites and the quadratic terms can be thought of as describing the presence of a road with coefficients describing the width and speed of the road between two specific sites [10, 16]. The higher order terms (those which are comprised of a product of three or more creation or annihilation operators) describe interactions [26]. A dynamical equation which only contains bilinear terms (that is, terms which are a product of no more than two fermionic operators) is therefore non-interacting or free. In the billiard ball picture, this means that the balls are able to travel along the paths unimpeded by any attractive and repulsive forces from other balls, as a result, the billiard balls do not collide. The balls do not interact, and so the energies of each fermion can be calculated individually. Crucially, this leads to an exponential decrease in Hilbert space dimension and therefore size of the Hamiltonian. This means that finding the energy spectrum of the model no longer requires diagonalizing the full Hamiltonian. Instead, we need only consider a new Hamiltonian of with an exponentially reduced dimension, that describes the location of any given single particle, called the *single-particle Hamiltonian*. The spectrum of the single-particle Hamiltonian gives us the single-particle energies, and from here we are able to construct the full spectrum by summing together the occupied particle sites. Because of this, the spectrum of a non-interacting (or free-fermion) model has a distinct and easily recognizable form. Indeed, how different a given model's spectrum is from this specific structure has been used to quantify interactions [26, 27]. Since it is possible to exactly compute the spectrum using classical means, free-fermion models are considered exactly soluble.

On the other hand, when we think of a quantum many-body spin model, the image that comes to mind is much more like a set of compass-like vector states that themselves are fixed in space but that are able to point in arbitrary directions [15]. Phenomena such as entanglement and superposition mean that the direction in which the compass needles point may be correlated, or that they can move in unison, or even that we need to consider super-positions of sets of directions. This image could hardly be further removed from the picture of the solid balls hopping around a lattice. Nevertheless, in the particular setting of a many-body spin- $\frac{1}{2}$ system, a duality occurs between the spin and fermionic

systems due to the fact that for given n spins and n fermions the two systems will occupy Hilbert spaces of the same dimension. In each case adding a spin or fermion doubles the Hilbert space dimension. Thus, there exists a mathematical map, which can take a model consisting of n fermions and rewrite it in terms of n spins, or vice versa [16, 28].

The construction of such a map, however, requires a little bit more than the same dimension of Hilbert space of the two systems. The dimension of the Hilbert space of a fermionic system is determined by the Pauli exclusion principle, which prevents two fermions from residing at the same site at the same time. However, as we have seen, this is not the only property of a fermionic system determined by the Pauli exclusion principle: the anti-symmetric wave-function of a system of fermions also requires that the fermionic operators satisfy the canonical anti-commutation relations. Thus, any map from spins to fermions must require that the mapped fermions also obey these relations. Such a map is necessarily non-local [28]. Indeed, this non-locality has lead some physicists to imply that if nature did not provide us with fermions, then no physicist in their right mind would want to study them [29].

We may now question why we would even want to map from a spin model to a fermion model. The map is surjective, and so every spin model can be mapped to a fermion model. In many cases the fermion model to which the spin system can be mapped is interacting, and so such a map has not made understanding the model any simpler. However, there is a special case in which solving the model becomes more tractable: there are examples in which the fermion model to which the model is mapped is *non-interacting* [24, 30–40], and thus, the full spectrum of the spin model is easily obtained. The spectrum of the fermion model is exactly the spectrum of the spin model. For this reason a spin model that can be mapped to non-interacting fermions is also referred to as a free-fermion model.

The quintessential example of a qubit-to-fermion mapping is the Jordan-Wigner transformation [28]. The Jordan-Wigner transformation requires the ordering of spins in a model, and then maps creation and annihilation operators to one-dimensional strings of Pauli operators [24]. Other maps have also been discovered, most of which are generator-to-generator mappings, meaning that each Pauli term in the spin Hamiltonian is mapped to an individual term in the fermion formalism [22, 41]. However, this is not the case for all spin models with a free-fermion solution that the map takes a generator-to-generator form. Indeed, there are examples of models with a free-fermion solution for which the Jordan-Wigner mapping, or any generator-to-generator generalization of the map, produces a highly interacting fermion model, but notwithstanding, the model is free [23]. Thus, an important task in quantum many-body physics is to develop new maps between spin models and their

fermionic counterparts, which may lead to the discovery of free-fermion models which were previously considered be interacting, and to develop a mechanism through which to recognize models that are to be considered free via the new maps.

In Chapters 2 and 3 of this thesis, we develop a new mathematical framework for the recognition of a new class of many-body spin- $\frac{1}{2}$ models which are described by free fermions, and provide a solution to those models. The new framework is expansive, in that it encompasses previous results [22, 41], and provides a sufficient condition for the recognition of a free-fermion model with regards to the new map. However, the framework is not complete, in that the condition provided for the recognition of free-fermion models is not necessary; there are examples of models which are free but do not meet the criteria.

One key feature that might inform the definition of an effective fermion description of a many-body spin Hamiltonian is the frustration between the Hamiltonian terms [16]. Frustration describes the commutation (or anti-commutation) relationship between the Hamiltonian terms. If two terms in the Hamiltonian commute, the spins on which they act can align to obey the action of both terms at the same time; on the contrary, if two terms do not commute, the spins on which they act cannot simultaneously align to obey both terms; thus the terms are frustrated. Pauli operators obey a strict binary commutation relationship with one another; that is, if a pair of Pauli operators do not commute, they necessarily anti-commute [15]. Similarly fermionic operators also either commute or anti-commute. Because of this binary relationship graph theory presents itself as a natural mathematical framework in which to investigate a correspondence between these systems based on the frustration.

Graph theory is a branch of pure mathematics that is often considered abstract. Graph theory is the study of graphs: structures comprising of a (finite) set of objects, represented by vertices, in which some pairs of the objects are in some sense “related,” with the relationship represented by edges between the corresponding vertices. In a simple graph, the edges have no direction and are unweighted, this means that the relationship between pairs of connected vertices is uniform. A simple graph also contains no self-loops, that is, no node is connected to itself.

The abstract nature of graph theory, and perhaps pure mathematics in general means that results in the field have no *inherent* correspondence to the ‘real world’. However, it is exactly this lack of intrinsic relationship to the real world, that means we are free to interpret and find correspondences in whichever way we so choose [42]. As it happens, graph theory can be interpreted in such a way that the axioms and theorems in graph theory have direct applications to the real world in a myriad of ways; graph theory has found applications in computer science [43, 44], genetics [45, 46], chemistry [47–49],

engineering [44, 50] and also in many-body physics.

In Chapters 2 and 3 a many-body Hamiltonian is represented by a graph by assigning a vertex to every Hamiltonian term, and joining them by an edge if and only if they anti-commute. We then look for restrictions on these graphs such that all corresponding models within the class admit a free-fermion solution. For a generator-to-generator map from spins to fermions (such as Jordan-Wigner) it is evident that the frustration between terms in the fermionic Hamiltonian must naturally be isomorphic to the frustration relationships in the spin description. For any Hamiltonian written in terms of spin there is an associated graph. Similarly, all Hamiltonians in terms of fermionic operators also have an associated graph. Given a spin model and a fermionic model, if their two graphs are isomorphic to one another this represents a valid generator-to-generator map [22]. For the more complicated maps developed in Chapters 2 and 3 the restrictions on the graphs are less intuitive, nevertheless we are able to find a broad class of graphs for which the corresponding spin models admit a free-fermion solution.

An interesting consequence of the graph theoretic approach to free-fermion solubility is that the maps identified are necessarily generic in that the existence of a free-fermion solution is not dependent on coupling strengths of any Hamiltonian terms. Indeed, even the mathematical form of the solution is independent of the coupling strength of any of the individual terms. One could imagine a particular Hamiltonian which admits a free-fermion solution for a particular regime for a subset of Hamiltonian terms, these models exist outside of the classes that we consider. The free-fermion solutions in this thesis occur merely a result of the underlying frustration structure.

1.2 Loop-gas models

The second class of exactly soluble quantum many-body system considered in this thesis is topologically ordered systems known as loop-gas models. These families of models were designed not to describe any known physical system; but rather precisely because they are topologically ordered and can be solved exactly [13, 25, 29, 51–54]. A topologically ordered quantum system is one whose ground space degeneracy depends on the topology, and in particular the genus, of the manifold on which it is supported [10]. Another key identifying feature of topologically ordered systems is the ability to support anyonic excitations. Full analysis of loop-gas models requires category theory (and string diagrams), which we leave for Chapter 4, but here give a basic understanding.

An anyon is a particle which can have *any* exchange statistics. As we have seen, in nature, all particles are either fermions or bosons. Under exchange, a wave-function describing a pair of fermions

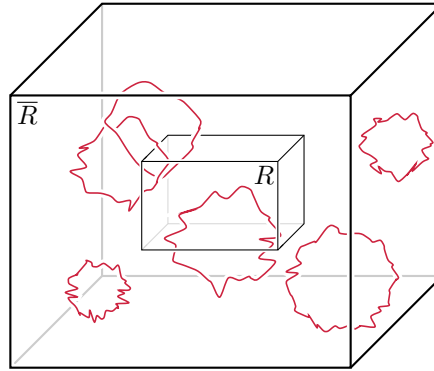


Figure 1.2: The ground state of a loop-gas model is defined as superposition of closed string configurations. Here we depict a single loop configuration, which is partitioned for entropy calculations in Chapter 4. Each loop is closed, and the Hamiltonian of the model is written explicitly as the sum of commuting projectors.

will acquire a phase of negative one, while the wave-function that describes a pair of bosons will acquire no phase under exchange. However, it is possible to engineer localized excitations, which behave like particles, for which this dichotomy of particles is no longer true. If we restrict ourselves to two spatial dimensions, particles can be constructed from low-energy, local excitations, such that these point-like excitations acquire arbitrary phases under exchange, as opposed to the binary pair of particle types that exist in the three spatial dimensions of nature.

Particles in two dimensions can have rich statistical behaviors; in fact, it is possible to construct a model for particles in two dimensions, so that they have any exchange statistics, which leads to the name ‘anyon.’ While any phase is possible, the statistics of a given species of anyon within a model are always well defined, and consistent such that for a pair of anyons the statistical phase acquired will always be the same. Abelian anyons are the class of anyons for which this acquired scalar phase is the only change to the wave-function of the system. However, beyond a scalar phase factor, it is also possible for the statistical evolution to be more complex, and actually lead to a higher-dimensional unitary matrix applied to the wave-function. These anyons are called non-Abelian, because unitary matrices do not necessarily commute.

A consistent anyon theory is defined by a finite set of anyons, including the vacuum or no anyon, a set of fusion rules and a consistent set of braiding statistics (exchange statistics). Given an anyon theory, a loop-gas model can be defined on a physical lattice in two dimensions, as a Levin-Wen string-net condensate [13, 29, 51] or in three dimensions, as a Walker-Wang model [25, 52–54] as follows: Hilbert spaces with dimension equal to the number of anyons in the theory reside on the links of a trivalent lattice in either two or three spatial dimensions. A set of Hamiltonian coupling terms are then defined by the following rules. At each vertex of the lattice an operator enforces the fusion rules

of the anyon theory. These terms ensure that the ground space of the model only includes closed anyonic loops. For each face or plaquette of the lattice, a family of operators describe the process of fusing each of the anyon types to the face. The terms in the Hamiltonian project the system into its ground space and also commute on the ground space, ensuring the solubility of the model. The ground state of these loop-gas models are a superposition of all possible closed string configurations, such as the one shown in Fig. 1.2, with coefficients determined by the braiding and fusion rules of the anyon theory. Higher energy eigenstates of the models are also well understood, because excitations in the model are localized, appearing as point-like excitations with exotic braiding statistics, they are the very anyons used to construct the model.

One may now be wondering how a three-dimensional loop-gas model can support anyonic excitations if in three dimensions all particles are fermions or bosons. There are two distinct families of topologically ordered loop-gas models in three spatial dimensions. The first family has a ground-space degeneracy that depends on the topology of three-dimensional space. Models in this family support localized point-like excitations in their bulk and as well as ‘loop-like’ excitations, both of which are ‘deconfined’ in their bulk; meaning that these excitations can move or expand with low energy cost. The point-like particles behave as fermions or bosons when exchanged, while interesting statistics may occur between when these point-like excitations are threaded through the loop-like excitations. The second family, however, has a unique ground state on any closed 3-manifolds. Such a unique ground-state also results in a complete lack of deconfined excitations in the bulk. Nonetheless, the introduction of a boundary to the manifold on which these models are supported results in a degenerate ground space, the dimension of which is dependent on the topology of the boundary. Furthermore, while the bulk of these models confine any excitations, there are deconfined excitations which are restricted to the boundary. This restriction to the boundary is effectively a restriction onto two-dimensional space; thus, these excitations can exhibit complex anyonic statistics [55].

The ground-states of loop-gas models demonstrate long-range entanglement that is not present in non-topologically ordered systems, sometimes referred to as the ‘trivial’ phase. Typically, we expect the entanglement between a subsystem of a ground state and the rest of the system to respect an area law; that is, the entanglement will scale with the size of the surface area of the subsystem. For most models, we expect that entanglement may be present between two subsystems which in close proximity to one another; however, we also expect the correlations to diminish rapidly as the distance between the two subsystems increases. For topologically ordered models, however, there is a long-range entanglement present that means subsystems at vast differences share the same correlations as

those in direct contact. This long-range entanglement manifests as a correction to the area law of the entanglement entropy, with the correction being dependent on the anyon theory supported by the model. In Chapter 4 we calculate this correction both in the bulk and at the boundary of topological loop-gas models in two and three dimensions.

Summary

In this thesis we have looked closely at two classes of quantum many-body systems which admit an exact solution. The first part of this thesis focuses on expanding the class of models which are known to admit a free-fermion solution. In Chapters 2 and 3, a new recognition criteria and solution method is developed for many-body spin models that admit a free-fermion solution; first in one spatial dimension and then in arbitrary dimensions. The second part of this thesis, Chapter 4, concerns the calculation of the entanglement properties of exactly soluble, topologically ordered many-body systems. The consequences of this calculation extend beyond limited reach of these specific exactly soluble models; the results derived in this chapter also offer insight into other classes of topological systems that have a closer alignment with physical systems that can be fabricated in a lab.

Chapter 2

Free fermions behind the disguise

An invaluable method for probing the physics of a quantum many-body spin system is a mapping to non-interacting effective fermions. We find such mappings using only the frustration graph G of a Hamiltonian H , i.e., the network of anti-commutation relations between the Pauli terms in H in a given basis. Specifically, when G is (even-hole, claw)-free, we construct an explicit free-fermion solution for H using only this structure of G , even when no Jordan-Wigner transformation exists. The solution method is generic in that it applies for any values of the couplings. This mapping generalizes both the classic Lieb-Schultz-Mattis solution of the XY model and an exact solution of a spin chain recently given by Fendley, dubbed “free fermions in disguise.” Like Fendley’s original example, the free-fermion operators that solve the model are generally highly nonlinear and non-local, but can nonetheless be found explicitly using a transfer operator defined in terms of the independent sets of G . The associated single-particle energies are calculated using the roots of the independence polynomial of G , which are guaranteed to be real by a result of Chudnovsky and Seymour. Furthermore, recognizing (even-hole, claw)-free graphs can be done in polynomial time, so recognizing when a spin model is solvable in this way is efficient. We give several example families of solvable models for which no Jordan-Wigner solution exists, and we give a detailed analysis of such a spin chain having 4-body couplings using this method.

2.1 Introduction

A notorious challenge for the simulation of quantum many-body systems is the exponential growth of the Hilbert space dimension in the number of constituent degrees of freedom. Systems for which

this difficulty can be circumvented via an analytic solution are invaluable for at least two reasons. First, the discovery of a new class of analytic solutions opens up the prospect of tractable simulation to a new family of models, and potentially of new phenomenology. Second, analytic solutions can be taken as starting points for approximations to more realistic models, thus extending the reach of these methods.

For a quantum spin- $\frac{1}{2}$ (qubit) system, one remarkable type of analytic solution comes in the form of a duality to effective fermions. When the effective fermions are non-interacting, it can be said that we have found a means of restricting the model's essential behavior to the low-dimensional subspace of a single fermion, and the physics of the model is well-understood. The textbook example of a free-fermion mapping is the Jordan-Wigner transformation [28], which was famously employed to solve the one-dimensional XY model by Lieb, Schultz, and Mattis [24]. The key insight is the identification of non-local Pauli operators with fermionic ladder operators. In the fermionic picture, the n -qubit XY-model Hamiltonian is mapped to a free-fermion Hamiltonian on $2n$ fermionic modes. The model is then completely solved by exactly diagonalizing the model's $2n \times 2n$ free-fermion Hamiltonian, an exponential simplification from the naive brute-force diagonalization that one might expect to need in the qubit picture. This solution method is *generic*, meaning it applies regardless of the values taken by the nonzero coupling constants in the Hamiltonian. This is because the Jordan-Wigner transformation maps each term in the Hamiltonian linearly to a fermionic bilinear operator.

One physical signature of models that are solvable in this way is an energy spectrum $\{E_{\mathbf{x}}\}$ that is given in terms of a number α of single-particle energies ε_k by

$$E_{\mathbf{x}} = \sum_{k=1}^{\alpha} (-1)^{x_k} \varepsilon_k, \quad (2.1)$$

where $\alpha \leq n$ and $\mathbf{x} \in \{0, 1\}^{\alpha}$ is a binary vector describing the occupation of each canonical fermionic mode. We will refer to a spectrum of the form in Eq. (2.1) as *free*. We say that a Hamiltonian is *solvable* if it has a free spectrum and it can be written in terms of its eigenmodes ψ_j as

$$H = \sum_{k=1}^{\alpha} \varepsilon_k [\psi_k, \psi_k^{\dagger}], \quad (2.2)$$

where the ψ_k obey the *canonical anti-commutation relations*, $\{\psi_j, \psi_k\} = 0$ and $\{\psi_j, \psi_k^{\dagger}\} = \delta_{jk}I$. When $\alpha < n$, a free spectrum will necessarily have degeneracies, since this is equivalent to the case where a subset of the energies $\{\varepsilon_k\}_{k=1}^n$ are equal to zero.

Recently, two of the authors [22] have given a simple necessary and sufficient condition for a

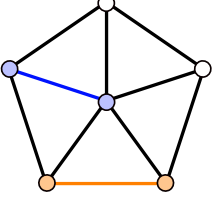
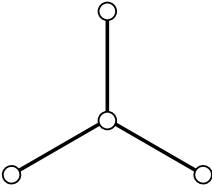
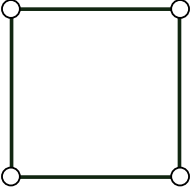
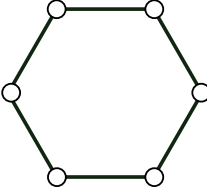
<i>Includes</i>		<i>Forbidden</i>	
2-4 Simplicial Clique	Claw, $K_{1,3}$	Even hole, C_{2k}	
(a) 	(b) 	(c) 	 ...
		$k = 2$	$k = 3$

Table 2.1: (a) A graph has a simplicial clique (orange in the example) if it has a clique where the neighborhood of each constituent vertex, minus the original clique, induces another clique (see Def. 2.1). The blue nodes are the induced neighbors of the left orange vertex and they induce a clique. The induced neighbors of the right orange vertex similarly induce a clique, so this graph is simplicial. A graph is claw-free or even-hole-free if none of its vertex-induced subgraphs contain (b) the “claw” $K_{1,3}$ or (c) an even hole C_{2k} . If a graph is (even-hole, claw)-free, it necessarily contains a simplicial clique [56].

qubit Hamiltonian H to be solvable via a Jordan-Wigner mapping by looking at properties of the *frustration graph* of H (see Def. 2.2). This gives a complete solution for this best-known class of solvable models. However, there exist models that are free and solvable, but that cannot be solved via any Jordan-Wigner mapping. Such a model has been introduced by Fendley [23] as free fermions “in disguise”. Fendley solves this model by directly defining the single-particle eigenstates for the Hamiltonian through its interaction terms. The free fermions manifest nonlinearly and non-locally in a basis which is dependent on the specific interaction strengths, but they remain free for all values of the couplings. The solution is therefore generic. This solution method has since been reproduced in a family of generalized spin-chain models [57, 58], including *qudit* models, where the system is dual to so-called free parafermions [59]. The generic nature of the free spectrum in these models would suggest that the frustration-graph formalism of Ref. [22] could be applied to understand this solution. However, since these models provably do not admit a Jordan-Wigner mapping, it would seem the solution relies on much subtler commutation structures than previously understood.

In this work, we go behind the disguise and clarify the role that the frustration graph plays in solving these models. We develop an infinite family of free-fermion solutions which generalizes Ref. [23] by finding specific graph-theoretic conditions for when such a solution is possible. Specifically, when the frustration graph of H avoids certain obstructions known as claws and even holes (see Table 2.1 and Def. 2.3), then H is solvable.

Result 2.1. (Informal version of Thm. 2.1 and Thm. 2.2.) If a Hamiltonian has an (even-hole, claw)-free frustration graph, then it has an explicit free-fermion solution.

The proof proceeds by considering the independence polynomial of the frustration graph. The independence polynomial of a graph is the polynomial generating function that counts the independent sets in the graph. We prove that these independent sets give us families of conserved charges for the model whenever the frustration graph is claw-free; meaning that when the frustration graph of H avoids claws the model is integrable.

Result 2.2. (Corollary of Lemma 2.1.) If a Hamiltonian has a claw-free frustration graph, then the model is integrable.

We can incorporate detailed information about the Hamiltonian into the independence polynomial by attaching certain vertex weights given in terms of squares of Hamiltonian coupling strengths. We then prove that when the frustration graph is additionally even-hole-free, the independence polynomial factorizes into a quadratic of a certain transfer operator. The single-particle spectrum can then be derived by looking at the zeros of the vertex-weighted independence polynomial. Given knowledge of the spectrum, the transfer operator then acts like a raising operator when acting on a fiducial mode whose existence is guaranteed by the structure of (even-hole, claw)-free graphs. The modes generated in this way allow us to define the eigenmodes of the free-fermionic Hamiltonian.

As in Fendley’s original model [23], there are no “physical modes” to speak of from this derivation as there would be from a Jordan-Wigner transformation. The eigenmodes are “disguised”, and then emerge directly as nonlinear, non-local combinations of the underlying spin operators. We call the eigenmodes revealed by this procedure *incognito modes*.

We then describe explicit families of models with frustration graphs that satisfy the (even-hole, claw)-free condition. The first of these examples is a small system, which is chosen explicitly as it has no generalized Jordan-Wigner solution and yet has a free-fermion solution of the form we consider. We show that this particular model is in fact related to one with a Jordan-Wigner solution by a local rotation. We next demonstrate how the family of generalized spin chain models included in Refs. [23,57,58] fit into our formalism. These models have a particular one-dimensional structure which makes their asymptotic dispersion relations amenable to the techniques of Toeplitz-matrix analysis. Though this is not expected to be true of general (even-hole, claw)-free graphs, a structure theorem for these graphs demonstrates that we should expect their coarse topology to be one-dimensional, or possibly treelike.

The structure of the chapter is as follows: in Section 2.2, we formally state all definitions and our main results. In Section 2.3, we discuss our result in the context of prior work. In Section 2.4 we prove the main results as Thm. 2.1 and Thm. 2.2. In Section 2.5, we demonstrate how specific examples fit

into our formalism, and in Section 2.6 we close with a discussion of possible future work.

2.2 Main Results

We begin with self-contained statements of our main theorems and necessary supporting definitions. First, let us fix graph-theoretic conventions. A graph $G := (V, E)$ consists of a set of vertices V together with a set of 2-element subsets $E \subset V^{\times 2}$ called edges. All graphs we consider are finite and simple: every pair of vertices neighbors by at most one edge, and the graphs contain no self loops. An *induced subgraph* is a graph $G[S] := (S, E \cap S^{\times 2})$ whose vertex set is $S \subseteq V$ and whose edge set consists of all of the edges in E with both endpoints in S . We denote the vertex and edge sets of $G[S]$ by V_S and E_S , respectively. We will also use the notation $G - W := G[V \setminus W]$ to denote the induced subgraph of the graph G by removing the set of vertices W . We will often refer to a subset of vertices interchangeably with the subgraph it induces. The open neighborhood of a vertex, $\Gamma(v)$ is the set of vertices neighboring the vertex, v . The closed neighborhood of a vertex, $\Gamma[v]$, is the set of vertices neighboring the vertex, v , together with v itself. An *independent set*, or *stable set*, of a graph $G = (V, E)$ is a subset of vertices $S \subseteq V$ which induces a subgraph with no edges, $G[S] = (S, \{\})$. Notice that our definition includes the empty set and sets of one vertex as independent sets.

A clique is a graph where every pair of vertices is neighboring. For us, a particularly important type of clique in a graph is a simplicial clique (See Table 2.1 (a)):

Definition 2.1 (Simplicial clique). A *simplicial clique* K_s in G is a non-empty clique such that for every vertex, $v \in K_s$, the (closed or open) neighborhood of v induces a clique in $G - K_s$. That is, for each $v \in K_s$ we have that $K_v := \Gamma[v] \setminus (K_s \setminus v)$ induces a clique in G .

The claw, $K_{1,3}$, is the complete bipartite graph between one vertex and a set of three non-neighboring vertices (See Table 2.1 (b)). A path of length ℓ is a connected graph of $\ell + 1$ vertices and ℓ edges such that every vertex has at most two neighbors. A cycle, C_ℓ , is a connected graph of ℓ edges and ℓ vertices such that each vertex has exactly two neighbors. Informally, a path of length ℓ is a cycle $C_{\ell+1}$ with one edge removed. A hole in a graph G is a subset of ℓ vertices $W \subseteq V$ such that $G[W] \cong C_\ell$ (i.e. an induced cycle of G), where $\ell \geq 4$. A hole is called *even* if it has an even number of vertices and edges. Importantly, our definition of an even hole includes holes of four vertices (See Table 2.1 (c)).

Next we turn to definitions involving a physical many-body qubit model. Consider an n -qubit

Hamiltonian, H , written in a given basis of Pauli operators $\{\sigma^j\}$ as

$$H := \sum_{j \in V} h_j := \sum_{j \in V} b_j \sigma^j, \quad (2.3)$$

where $V \subseteq \{0, x, y, z\}^{\otimes n}$ is a set of strings labeling the n -qubit Pauli operators in the natural way. A frustration graph describes the commutation relations between the Hamiltonian terms as follows:

Definition 2.2 (Frustration graph). The *frustration graph* of a Hamiltonian of the form in Eq. (2.3) is a graph, $G(H) = (V, E)$, with vertices in V in one-to-one correspondence with the Pauli terms $\{\sigma^j\}_{j \in V}$ in H , and edge set E defined by the commutation relations between the Hamiltonian terms:

$$E = \{(j, k) \mid \{\sigma^j, \sigma^k\} = 0\}. \quad (2.4)$$

That is, two vertices in V are adjacent in $G(H)$ if and only if their corresponding Paulis anti-commute.

The frustration graph is the complement of the Pauli graph introduced by Planat [60]. Notice that it is always simple by construction. Where clear from context, we will drop the dependence on the Hamiltonian from $G(H)$.

Definition 2.3 (ECF). A graph G is said to be *(even-hole, claw)-free*, or *ECF*, if it contains no even holes and no claws among its induced subgraphs (see Table 2.1). A Hamiltonian H is ECF if its frustration graph $G(H)$ is ECF.

It can be shown that all (even-hole, claw)-free graphs are *simplicial*, meaning they contain a simplicial clique [56]. If a Hamiltonian H is ECF then its frustration graph is necessarily simplicial, so we say that H is simplicial as well.

Our first main result says that the spectrum of an ECF Hamiltonian is free, with single-particle energies given by the roots of a certain polynomial.

Theorem 2.1. Every ECF Hamiltonian H has a free spectrum of the form in Eq. (2.1). In particular, the single-particle energies $\{\varepsilon_j\}_{j=1}^{\alpha(G)}$ satisfy

$$P_G(-1/\varepsilon_j^2) = 0, \quad (2.5)$$

where $P_G(x)$ is the vertex-weighted independence polynomial of the frustration graph $G(H)$,

$$P_G(x) := \sum_{k=0}^{\alpha(G)} \sum_{S \in \mathcal{S}^{(k)}} \left(\prod_{j \in S} b_j^2 \right) x^k. \quad (2.6)$$

$\mathcal{S}^{(k)}$ is the set of k -vertex independent sets of $G(H)$, and $\alpha(G)$ is the independence number of $G(H)$.

Here we note that when $\alpha < n$ each energy level of the model's spectrum will necessarily have a $2^{n-\alpha}$ degeneracy. An important result that we will show is that even if the frustration graph is only claw-free, then the Hamiltonian is still integrable, as there exists a set of mutually commuting conserved charges.

Definition 2.4 (Independent-set charges). Given a Hamiltonian of the form in Eq. (2.3) with frustration graph $G(H)$, we define the $\alpha(G) + 1$ *independent-set charges* as

$$Q^{(k)} := \sum_{S \in \mathcal{S}^{(k)}} \prod_{\mathbf{m} \in S} h_{\mathbf{m}}, \quad k \in \{0, 1, \dots, \alpha(G)\}, \quad (2.7)$$

with the convention that $Q^{(0)} := I$. Additionally, notice that $Q^{(1)} = H$.

As we will prove in Lemma 2.1 below, the independent-set charges satisfy

$$[Q^{(r)}, Q^{(s)}] = 0, \quad \forall r, s \in \{1, \dots, \alpha(G)\}. \quad (2.8)$$

Since $Q^{(1)} = H$, this demonstrates that the charges are conserved. To take advantage of the independent-set charges, we exploit the simplicial property of H and define a fiducial mode, χ , in terms of which we can express the “incognito modes”.

Definition 2.5 (Incognito mode, simplicial mode). Given a simplicial Hamiltonian of the form in Eq. (2.3) with frustration graph $G(H)$, we define a *simplicial mode* χ to be any Pauli operator which is not present in the original Hamiltonian and which anti-commutes with all of the operators in a simplicial clique of $G(H)$. The $\alpha(G)$ *incognito modes* of H are defined with respect to a given simplicial mode χ as

$$\psi_j = N_j^{-1} T_G(-u_j) \chi T_G(u_j), \quad j \in \{1, \dots, \alpha(G)\}, \quad (2.9)$$

where $u_j := 1/\varepsilon_j$ for the single-particle energy ε_j satisfying Eq. (2.5), $T_G(u)$ is a transfer operator

$$T_G(u) := \sum_{j=0}^{\alpha(G)} (-u)^j Q^{(j)}, \quad (2.10)$$

and N_j^{-1} is a normalization factor which is computable (see Eq. (2.70)).

Note that we can always construct a simplicial mode for any simplicial Hamiltonian. To do so we introduce an additional (fictitious) spin to the system and augment each Hamiltonian term in the simplicial clique with a Pauli-X applied to the extra spin — notice that this will not affect the frustration graph. The simplicial mode is then defined by a Pauli-Z operator applied to the additional spin; clearly, the simplicial mode will anti-commute with all terms in the simplicial clique, but no other Hamiltonian terms.

Theorem 2.2. An ECF Hamiltonian H is free-fermion-solvable via Eq. (2.2) with eigenmodes given by its incognito modes.

Our proofs of Theorem 2.1 and Theorem 2.2 closely resemble the solution method introduced by Fendley in Ref. [23]. The operative technical insight is that many of the key properties of that model, and its generalizations in Refs. [57, 58], are actually special cases of more general recursion relations in the class of models we identify.

2.3 Relation to prior work

Since its discovery, the Jordan-Wigner transformation [28] and subsequent generalizations [12, 30–33, 39, 61–64] have enjoyed great success in probing the fundamental physics of quantum many-body spin models, as well as classical statistical mechanics models through so-called transfer-matrix methods [65–67]. An understanding of these mappings has furthermore proven useful for designing fermion-to-qubit mappings with desired properties for simulating fermionic systems on a quantum computer [34–36, 68–74]. Here, operator locality in the dual spin model is generally enabled through coupling to an auxiliary gauge field [37, 38, 40], which endows fermionic-pair excitations with the structure of freely deformable strings on the spin lattice [75]. The preponderance of these mappings suggests that a fundamental theory of physics containing fermionic degrees of freedom need not hold fermions as fundamental objects [29, 76].

Free-fermion models have an interesting connection to graph theory. The dynamics of free-fermion models are equivalent to matchgate circuits [77–82], which were originally developed in the context

of counting perfect matchings in graphs [83–86]. Independently, graph-theoretic methods have been utilized in quantum information in the context of variational quantum eigensolvers [87–93], where the frustration graph is commonly known as the *anticompatibility* graph. Inspired by these methods, two of the authors have shown that a generalized Jordan-Wigner transformation exists for exactly those models for which the frustration graph is a line graph [22].

Definition 2.6 (Line Graph). A *line graph* $L(R) := (E, F)$ is a graph whose vertex set is in one-to-one correspondence with the edges E of a *root graph* $R := (V, E)$. Vertices in $L(R)$, $e_1, e_2 \in E$, are neighboring if and only if $|e_1 \cap e_2| = 1$, i.e. the edges in R are incident at a vertex in V .

We note that line graphs also play an important role in understanding the spectrum of certain tight-binding models [94, 95], but we will not discuss these models further here.

A generalized Jordan-Wigner transformation maps a spin Hamiltonian of the form in Eq. (2.3) to one which is quadratic in *Majorana fermion* modes $\{\gamma_j\}$. These are Hermitian operators, which satisfy canonical anti-commutation relations

$$\{\gamma_j, \gamma_k\} = 2\delta_{jk}I \quad \text{and} \quad \gamma_j^\dagger = \gamma_j \quad \forall j, k. \quad (2.11)$$

That is, when solving a Hamiltonian of the form in Eq. (2.3) by Jordan-Wigner, we are asking whether there exists a mapping $\phi : V \mapsto \tilde{V}^{\times 2}$ acting on the Pauli terms of H , and effecting

$$\sigma^{\mathbf{j}} \mapsto i\gamma_{\phi_1(\mathbf{j})}\gamma_{\phi_2(\mathbf{j})} \quad \forall \mathbf{j} \in V \quad (2.12)$$

such that

$$H \mapsto \tilde{H} := \frac{i}{2} \sum_{j,k \in \tilde{V}} h_{jk} \gamma_j \gamma_k := \frac{i}{2} \boldsymbol{\gamma} \cdot \mathbf{h} \cdot \boldsymbol{\gamma}^T, \quad (2.13)$$

in a way that preserves the commutation relations between terms, i.e. $G(H) \simeq G(\tilde{H})$. The coefficient matrix \mathbf{h} — called the single-particle Hamiltonian — is necessarily anti-symmetric, since any symmetric part will vanish under the sum in Eq. (2.13), and we may take H to be traceless without loss of generality. The central theorem of Ref. [22] gives a necessary and sufficient criterion for a generalized Jordan-Wigner solution to exist for a particular qubit Hamiltonian.

Theorem 2.3 (Thm. 1 of Ref. [22]). An injective map ϕ as defined in Eq. (2.12) and Eq. (2.13) such that $G(H) \simeq G(\tilde{H})$ exists for the Hamiltonian H as defined in Eq. (2.3) if and only if there exists a

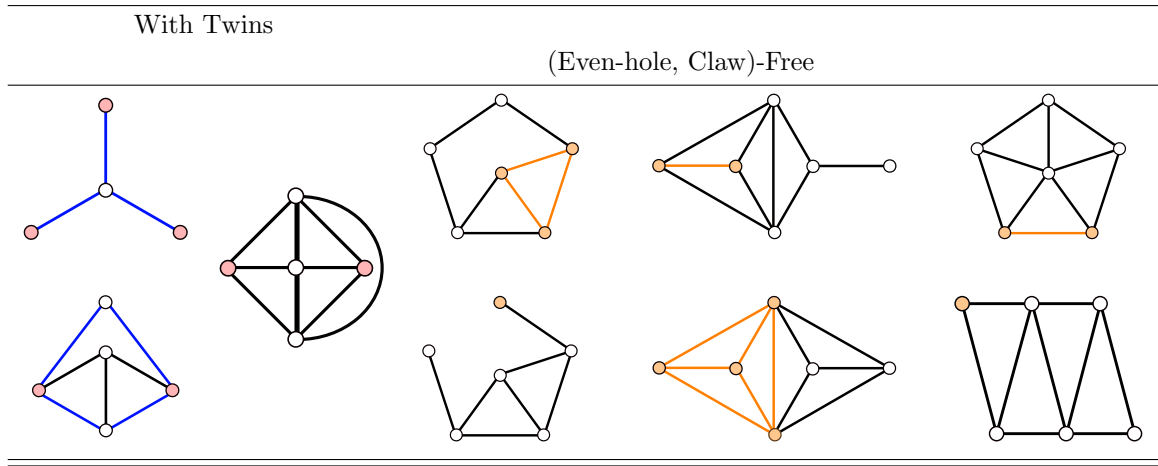


Table 2.2: Nine forbidden induced subgraphs for line graphs. No model containing a subset of terms inducing any of the above frustration graphs admits a generalized Jordan-Wigner solution, unless the global frustration graph contains twin vertices which may then be removed via a symmetry to give a line graph [22]. Note that we define twin vertices to be non-neighboring, and that all but the claw and the graphs in the rightmost column above contain at least one pair of *neighboring* vertices with the same closed neighborhoods. Vertices from these pairs may be removed through a unitary rotation as described in Section 2.5.1. The six-qubit instance of the four-fermion model introduced by Fendley has the frustration graph shown at the very bottom right, and larger instances clearly contain a subset of terms inducing this graph. Surprisingly, each of these graphs describes a standalone model with a free-fermion solution, as the graphs themselves either contain twins or are (even-hole, claw)-free. What is important, therefore, is the precise way that these graphs are connected to a global frustration graph that determines whether or not a generic free-fermion solution is possible. **Left column:** Forbidden subgraphs which contain twin vertices, highlighted in red, but also contain either a claw or an even-hole, highlighted by blue edges. **Middle column:** This forbidden subgraph contains twin vertices, but no claws or even holes. Each red highlighted vertex is also simplicial. **Right column:** These graphs do not contain twins, but are (even-hole, claw)-free. Though they contain many simplicial cliques, an example is highlighted for each graph in orange. Importantly, note that the simplicial vertex highlighted in the four-fermion model is necessary for Fendley’s exact solution of this model.

root graph R such that

$$G(H) \simeq L(R). \quad (2.14)$$

Upon constructing a free-fermion solution for a given Hamiltonian, we find that \mathbf{h} gives an edge-weighted skew-adjacency matrix of the root graph R . The graph R may therefore be seen as the Majorana-fermion hopping graph. A full solution for H is found by a linear transformation on the Majorana modes in Eq. (2.13) to diagonalize the Hermitian matrix $i\mathbf{h}$. Letting the nonzero eigenvalues of $i\mathbf{h}$ be given by $\{\pm\varepsilon_j\}_{j=1}^\alpha$ with $\varepsilon_j > 0$ for all $j \in \{1, \dots, \alpha\}$, this brings the Hamiltonian to the form in Eq. (2.2) with single-particle energies given by the $\{\varepsilon_j\}$.

Claw-free graphs were originally investigated as natural generalizations to line graphs [96] and have since developed into the subject of a rich area of study in graph theory [97]. Line graphs are claw-free,

as no three edges in R can be incident to another edge without at least two of them being incident to each other. Remarkably, the free-fermion solution method presented in this work extends the generalized Jordan-Wigner solution in a way that parallels the relationship between claw-free graphs and line graphs. Specifically, the single-particle energies obtained from Eq. (2.13) satisfy Eq. (2.5) when $L(R)$ is an ECF graph. Every vertex of R corresponds to a simplicial clique of $L(R)$. Clearly, the edges incident to a given vertex in R are mapped to the vertices of a clique in $L(R)$, and since every edge is incident to two vertices in R , the open neighborhood of a vertex in $L(R)$ induces two vertex-disjoint cliques [98]. When a line graph is even-hole-free, the corresponding root graph is even-cycle-free, as any even cycle in R will be mapped to an even hole in $L(R)$. Suppose that a given Hamiltonian satisfies Eq. (2.14) with $L(R)$ an ECF graph. The single particle energies are zeros of

$$f_R(u) = \det(i\mathbf{h} - u\mathbf{I}) . \quad (2.15)$$

Equivalently, we may consider the reciprocal polynomial f_R^* to f_R ,

$$f_R^*(u) := u^n f_R(1/u) = (-1)^n \det(\mathbf{I} - iu\mathbf{h}) , \quad (2.16)$$

where n is the number of vertices in R . For an arbitrary simple graph R , the characteristic polynomial f_R (and thus f_R^*) would only depend on products of elements from \mathbf{h} from matchings and even cycles of R [99]. Since R is an even-cycle-free graph however, only the matchings are relevant. Let \mathcal{M}_k be the set of all k -edge matchings M of R . We have

$$f_R^*(u) = (-1)^n \sum_{k=0}^{\lfloor n/2 \rfloor} (-u^2)^k \left[\sum_{M \in \mathcal{M}_k} \prod_{(i,j) \in M} h_{ij}^2 \right] \quad (2.17)$$

$$f_R^*(u) = (-1)^n P_{L(R)}(-u^2) . \quad (2.18)$$

The last equality follows because the matchings of a graph correspond to the independent sets of its line graph. Therefore, $\pm\varepsilon_j$ are an eigenvalue pair of $i\mathbf{h}$ if and only if Eq. (2.5) is satisfied for $G(H) \simeq L(R)$. Though even-hole-free line graphs are a rather limited set of frustration graphs, what is incredibly surprising is that Theorem 2.1 holds when $G(H)$ is relaxed to be a general ECF graph, though there is no fermion-hopping graph R for this set of graphs in general. We remark that for any claw-free graph, the vertex-weighted independence polynomial, $P_G(x)$, is real-rooted for all values of the Hamiltonian couplings by the results given in Refs. [100, 101]. This generalizes the result for

the un-weighted independence polynomial originally proved by Chudnovsky and Seymour [102]. Since $P_G(x)$ has non-negative coefficients and real roots, all of its roots must be negative by Descartes' rule of signs [103], and therefore all of the single-particle energies $\{\varepsilon_j\}$ are themselves real. The free-fermion solution method presented here therefore includes systems for which we can prove that no generalized Jordan-Wigner solution is possible, as we shall now see.

Line graphs can be characterized by the set of nine forbidden subgraphs [104], shown in Table 2.2. No model containing a subset of terms inducing any of the frustration graphs in Table 2.2 admits a generalized Jordan-Wigner solution. One possible exception is when the Jordan-Wigner mapping is allowed to be non-injective; i.e. there is a mapping satisfying Eq. (2.12) and preserving the frustration graph which takes multiple Pauli terms to the same fermionic pair. These Pauli terms must then correspond to *twin vertices* in $G(H)$: vertices with identical open neighborhoods, $\Gamma(v)$. Notice that twin vertices are never neighboring by this definition, as a vertex is not included in its own open neighborhood.¹ Since operators corresponding to twin vertices anti-commute with the same set of operators in the Hamiltonian, the product of any pair of such operators commutes with every term in the Hamiltonian and so constitutes a symmetry. We can thus project onto the eigenspace of this symmetry operator to replace one operator in the set of twins with another, thus removing its vertex from the frustration graph. If twins can be removed in such a way as to change the frustration graph into a line graph, then the Hamiltonian is still solvable via Jordan-Wigner. This will sometimes be possible, as some of the forbidden subgraphs in Table 2.2 themselves contain twins. From Table 2.2, we see that all forbidden subgraphs for line graphs either contain twins, are simplicial ECF, or both. They therefore surprisingly all have a free spectrum, and it is truly how these graphs are connected to one another that allows us to infer the existence of a free-fermion solution.

The class of ECF graphs is generalized by the set of so-called (even-hole, pan)-free graphs [105]. A *pan* is a graph consisting of a hole together with an additional vertex with exactly one neighbor on the hole. A pan contains a claw as an induced subgraph, and so an (even-hole, pan)-free graph is necessarily ECF. The structure of (even-hole, pan)-free graphs has been completely characterized, and this allows the authors of Ref. [105] to give an $O(mn)$ -time algorithm for recognizing them, where m is the number of edges in the graph and n is the number of vertices. Specifically, the authors of Ref. [105] show that (even-hole, pan)-free graphs either: (i) have a clique cutset, (ii) are unit circular-arc graphs, (iii) are a clique, (iv) are the join of a clique and a unit circular-arc graphs. A unit circular-arc graph is one whose vertices correspond to distinct arcs of unit length on a circle, such that vertices are

¹Here we caution the reader that this definition differs slightly from that used in the graph-theory literature, where vertices with identical closed neighborhoods (which are therefore neighboring) are also referred to as twins. We will return to pairs of vertices with identical closed neighborhoods in Section 2.5.1.

neighboring if and only if their corresponding arcs intersect. A clique cutset is a subset of vertices inducing a clique whose removal disconnects the graph. The join of two graphs $G_1 := (V_1, E_1)$ and $G_2 := (V_2, E_2)$ is the graph with vertex-set $V_1 \cup V_2$ and edge-set $E_1 \cup E_2 \cup \{(u, v) | u \in V_1, v \in V_2\}$. Though the theorem of Ref. [105] completely describes the structure of these graphs, we can intuitively expect that the coarse topology of these models is fundamentally one-dimensional or treelike.

As general claw-free graphs can also be recognized efficiently [106], we have an efficient algorithm for recognizing ECF graphs. In Ref. [107], a polynomial time algorithm is given for detecting whether a general claw-free graph contains a simplicial clique. It is therefore computationally efficient to recognize a simplicial clique in an ECF graph. Moreover, every (nonempty) ECF graph has at least one simplicial clique [56].

2.4 Proofs of Main Results

In this section we prove the two main results presented in Section 2.2. We restate these theorems here for convenience. The first main result tells us that an ECF model will have a free spectrum, of the form Eq. (2.1), and provides an explicit form of the single-particle energies.

Theorem 2.1. (Restatement.) Every ECF Hamiltonian H has a free spectrum of the form in Eq. (2.1). In particular, the single-particle energies $\{\varepsilon_j\}_{j=1}^{\alpha(G)}$ satisfy

$$P_G(-1/\varepsilon_j^2) = 0, \quad (2.19)$$

where $P_G(x)$ is the vertex-weighted independence polynomial of the frustration graph $G(H)$,

$$P_G(x) := \sum_{k=0}^{\alpha(G)} \sum_{S \in \mathcal{S}^{(k)}} \left(\prod_{j \in S} b_j^2 \right) x^k. \quad (2.20)$$

$\mathcal{S}^{(k)}$ is the set of k -vertex independent sets of $G(H)$, and $\alpha(G)$ is the independence number of $G(H)$.

The second main result gives an explicit realization of the canonical modes of an ECF model in terms of independent sets of Hamiltonian terms, and the simplicial mode, χ .

Theorem 2.2. (Restatement.) An ECF Hamiltonian H is free-fermion-solvable via Eq. (2.2) with eigenmodes given by its incognito modes.

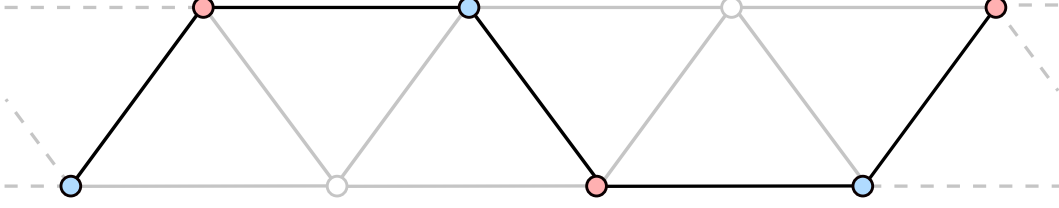


Figure 2.1: The frustration graph of the model introduced in Ref. [23], which is (even-hole, claw)-free. Each of the sets of colored (red and blue) vertices are independent sets, and together they induce a path in the frustration graph. In a general claw-free graph, the symmetric difference of any pair of independent sets induces a bipartite subgraph of maximum degree two: all of the components of the subgraph are induced paths and even-holes. If the graph is furthermore even-hole free, then the symmetric difference induces a set of disjoint paths.

Recall that the incognito modes are defined in terms of the simplicial mode, χ , as

$$\psi_j = N_j^{-1} T_G(-u_j) \chi T_G(u_j), \quad j \in \{1, \dots, \alpha(G)\}, \quad (2.21)$$

where $u_j := 1/\varepsilon_j$ for the single-particle energy ε_j satisfying Eq. (2.19), $T_G(u)$ is a transfer operator

$$T_G(u) := \sum_{j=0}^{\alpha(G)} (-u)^j Q^{(j)}, \quad (2.22)$$

and N_j^{-1} is a normalization factor which is computable.

We proceed by making successively more restrictive assumptions on $G(H)$: first that it is claw-free, then (even-hole, claw)-free. We begin by proving the following lemma, regarding claw-free Hamiltonians and the independent-set charges.

Lemma 2.1. Given a Hamiltonian with claw-free frustration graph $G(H)$, the independent-set charges are mutually commuting:

$$[Q^{(r)}, Q^{(s)}] = 0, \quad \forall r, s \in \{1, \dots, \alpha(G)\}. \quad (2.23)$$

Proof. We may assume $r \neq s$, since Eq. (2.23) clearly holds if r and s are equal. For a given independent set S , define

$$h_S := \prod_{j \in S} h_j. \quad (2.24)$$

and notice that, since operators belonging to an independent set in $G(H)$ are commuting, the order in which we take the product is unimportant in this definition. For two independent sets S, S' of a

claw-free graph

$$[h_S, h_{S'}] = \begin{cases} \pm 2 \left(\prod_{j \in S \cap S'} b_j^2 \right) \prod_{j \in S \oplus S'} h_j & |E_{S \oplus S'}| \text{ odd} \\ 0 & |E_{S \oplus S'}| \text{ even} \end{cases} \quad (2.25)$$

where $S \oplus S' := (S \cup S') \setminus (S \cap S')$, the symmetric difference of S with S' . When it is not empty, the graph $G[S \oplus S']$ is bipartite, since S and S' are both independent sets. Commuting h_S through $h_{S'}$ thus gives a factor of -1 for every edge in this graph, and so Eq. (2.25) holds. From here, we naturally restrict to the case where $|E_{S \oplus S'}|$ is odd.

As G is claw-free, we must furthermore have that every vertex of $G[S \oplus S']$ has degree at most two in this graph, since once again, $G[S \oplus S']$ is bipartite. Every component of $G[S \oplus S']$ is therefore either an isolated vertex, path, or even cycle (odd cycles are not bipartite). We have assumed that $G[S \oplus S']$ has odd-many edges, and so this graph must have an odd number (and thus at least one) of odd-length-path components. Such paths have the same number of vertices from both S and S' and so cannot be the only component of $G[S \oplus S']$, since we have assumed $r \neq s$. Pick one such odd path, $L \subseteq V$, and note that

$$\{h_{S \cap L}, h_{S' \cap L}\} = 0. \quad (2.26)$$

Since $G[L]$ has the same number of vertices from both S and S' , we can exchange the subsets $S \cap L$ and $S' \cap L$ between S and S' , respectively, to obtain a new unique pair of independent sets without changing the number of vertices in either, while also preserving the sets $S \cap S'$ and $S \oplus S'$. This gives

$$[h_{S/L} h_{S \cap L}, h_{S'/L} h_{S' \cap L}] = -[h_{S/L} h_{S' \cap L}, h_{S'/L} h_{S \cap L}], \quad (2.27)$$

and so these terms cancel in the commutator $[Q^{(r)}, Q^{(s)}]$. Letting N be the number of odd-length-path components in $G[S \oplus S']$, there are 2^N pairs of independent sets (S, S') , related by these exchanges, for which the graph $G[S \oplus S']$ is fixed. The contributions to the commutator $[Q^{(r)}, Q^{(s)}]$ from each (S, S') therefore cancel pairwise, and we have $[Q^{(r)}, Q^{(s)}] = 0$ for all r and s . \square

Lemma 2.1 implies that all claw-free models have a set of conserved quantities whose size generally grows with system size, since $Q^{(1)} := H$. Thus, we can conclude that, in the traditional sense, claw-free models are *integrable*. Consider as an example the frustration graph of the model introduced in Ref. [23], as shown in Fig. 2.1. The graph is always claw-free, although contains even holes when the

model has periodic boundary conditions. Two independent sets of vertices (highlighted in red and blue) induce a path in the frustration graph. In a general claw-free graph, the symmetric difference of any pair of independent sets induces a bipartite subgraph of maximum degree two: all of the components of the subgraph are induced paths and even-holes. Lemma 2.1 also implies that the transfer operator, $T_G(u)$, defined in Eq. (2.22), will commute with the Hamiltonian.

Next consider the following lemma regarding the transfer operators, $T_G(u)$, of even-hole-free models.

Lemma 2.2. If G is an (even-hole, claw)-free graph, the transfer matrix, $T_G(u)$, satisfies

$$T_G(u)T_G(-u) = P_G(-u^2) \quad (2.28)$$

where P_G is the vertex-weighted independence polynomial, defined in Eq. (2.6).

Proof. Let G be an ECF graph. Using Eq. (2.22) we have

$$T_G T_G^- = \sum_{s,t=0}^{\alpha(G)} (-1)^s u^{s+t} Q^{(s)} Q^{(t)}, \quad (2.29)$$

where we have used the abbreviated notation $T_G(-u) := T_G^-$. If s and t have opposite parity, then $Q^{(s)} Q^{(t)}$ and $Q^{(t)} Q^{(s)}$ have a relative minus sign in the sum, and so these terms vanish in the sum since $Q^{(s)}$ and $Q^{(t)}$ commute.

Thus we need only consider terms for which s and t have the same parity

$$T_G T_G^- = \sum_{\substack{s,t=0 \\ s+t \text{ even}}}^{\alpha(G)} (-1)^s u^{s+t} Q^{(s)} Q^{(t)}, \quad (2.30)$$

By expanding the $Q^{(k)}$ in terms of independent sets, h_S , we can write

$$T_G T_G^- = \sum_{\substack{s,t=0 \\ s+t \text{ even}}}^{\alpha(G)} (-1)^s u^{s+t} \sum_{\substack{S \in \mathcal{S}^{(s)} \\ S' \in \mathcal{S}^{(t)} \\ |E_{S \oplus S'}| \text{ even}}} \left(\prod_{j \in S \cap S'} b_j^2 \right) h_{S \cap (S \oplus S')} h_{S' \cap (S \oplus S')}. \quad (2.31)$$

The constraint that $s + t$ is even implies that the number of vertices $|V_{S \oplus S'}|$ is even, and we require that $|E_{S \oplus S'}|$ be even because the operators h_S and $h_{S'}$ will anti-commute otherwise and cancel in the sum over S, S' . It thus suffices to consider induced subgraphs, $G[S \oplus S']$, with even-many edges and even-many vertices. Once again, such graphs must be bipartite and, furthermore, must be a union of

disjoint isolated vertices, paths, and even cycles.

By a similar argument as above, we will show that the contributions from any such graphs containing an odd-length path will cancel in the sum. Assume that $G[S \oplus S']$ does contain an odd-length path L . Since $|E_{S \oplus S'}|$ must be even, L cannot be the only component of $G[S \oplus S']$, and in fact one of the additional components of $G[S \oplus S']$ must be another odd-length path (otherwise the total number of edges in $G[S \oplus S']$ cannot be made even). Exchanging $S \cap L$ and $S' \cap L$ between S and S' gives another pair of distinct independent sets for the same s , t , $S \cap S'$, and $S \oplus S'$, but for which the operator $h_{S \cap (S \oplus S')} h_{S' \cap (S \oplus S')}$ appears with a minus sign in the sum and cancels the term corresponding to S and S' . The contributions from $G[S \oplus S']$ therefore cancel pairwise in this case.

Next, we will show that contributions from any such graphs containing an even-length path will cancel in the sum, and therefore non-vanishing contributions must come from graphs containing no paths at all. Once again, assume $G[S \oplus S']$ does contain such a path L of even length (which may be an isolated vertex, i.e. a path of length zero). Since L has an odd number of vertices, L cannot be the only component of $G[S \oplus S']$ and in fact one of the additional components of $G[S \oplus S']$ must be another even-length path (otherwise the total number of vertices in $G[S \oplus S']$ cannot be made even). Both of the endpoints of L must belong to the same independent set, either S or S' . If L is an isolated vertex, then it trivially belongs to the same independent set as itself. Exchanging $S \cap L$ and $S' \cap L$ between S and S' in this case gives another pair of distinct independent sets for the same value of $s + t$, $S \cap S'$, and $S \oplus S'$, for which the operator $h_{S \cap (S \oplus S')} h_{S' \cap (S \oplus S')}$ appears with the same sign in the sum since L has even-many edges. Both of the parities of s and t are changed in this exchange, and so s and t have the same parity still, but this term appears with an overall relative minus sign in the sum due to the factor of $(-1)^s$. This therefore cancels the term corresponding to S and S' , and so the contributions from $G[S \oplus S']$ cancel pairwise.

The only allowed graphs $G[S \oplus S']$ whose term in the sum is not canceled by something else are those for which $G[S \oplus S']$ consists of a set of disconnected even cycles. However, we have assumed that G is even-hole free. Therefore, these contributions do not appear, and we will have

$$T_G T_G^- = P_G(-u^2), \quad (2.32)$$

if there are no even holes in G . □

Note that P_G has strictly positive coefficients, which do not depend on the signs of the Hamiltonian coefficients $\{b_j\}_{j \in V}$. Thus, as discussed in Sect. 2.3, $P_G(-x)$ will have all positive roots, denoted by

$$x := u_\ell^2.$$

We next consider the commutation of the incognito modes, ψ_ℓ , with the Hamiltonian. Here we further use the fact that an ECF graph, $G(H)$, contains a simplicial clique, K_s . Recall that the simplicial mode, χ , commutes with all terms in the Hamiltonian outside of K_s , but anti-commutes with all terms in K_s , $\{\chi, h_v\} = 0$ for all $v \in K_s$. Thus, we can write the commutation of $T_G \chi T_G^-$ with the Hamiltonian for arbitrary u as

$$[H, T_G(u) \chi T_G(-u)] = 2 \sum_{v \in K_s} T_G(u) h_v \chi T_G(-u). \quad (2.33)$$

For an ECH model, we require that when $u = -u_\ell$, the right-hand-side of Eq. (2.33) is equal to $2\varepsilon_\ell \psi_\ell$, where $1/\varepsilon_\ell := u_\ell$ (similarly when $u = u_\ell$, it is equal to $-2\varepsilon_\ell \psi_\ell^\dagger$). A crucial step for proving this is the following lemma:

Lemma 2.3. Let K_s be a simplicial clique in $G(H)$, and let χ be a simplicial mode, as defined in Def. 2.5, then

$$T_G \left(1 + u \sum_{v \in K_s} h_v \right) \chi T_G^- = P_G(-u^2) \left(1 - u \sum_{v \in K_s} h_v \right) \chi. \quad (2.34)$$

Proof. We first express important recurrence relations for both T_G and P_G . For any clique $K \subseteq G$ we have

$$T_G = T_{G-K} - u \sum_{v \in K} h_v T_{G-\Gamma[v]}. \quad (2.35)$$

This follows from the fact that independent sets of G can be partitioned into two groups: (i) sets which do not contain $v \in K$, corresponding to the first term T_{G-K} ; and (ii) sets which contain a single $v \in K$, and thus contain none of its neighbors, corresponding to the second term, $-u \sum_{v \in K} h_v T_{G-\Gamma[v]}$. When K is simplicial, $K := K_s$, we can show the additional recursion relation

$$T_G = T_{G-K_s} - u \sum_{v \in K_s} h_v T_{G-K_v} \quad (2.36)$$

where $K_v := \Gamma[v] \setminus (K_s \setminus v)$ is a clique in G for all $v \in K_s$, since K_s is simplicial. We show Eq. (2.36)

by applying the recursion relation in Eq. (2.35) twice in succession

$$T_G = T_{G-K_s} - u \sum_{v \in K_s} h_v T_{G-K_s-K_v} \quad (2.37)$$

$$T_G = T_{G-K_s} - u \sum_{v \in K_s} h_v \left(T_{G-K_v} + u \sum_{w \in K_s \setminus \{v\}} h_w T_{G-K_s-K_v-K_w} \right) \quad (2.38)$$

where we have rearranged the expansion Eq. (2.35) by the clique K_s in the graph $G - K_v$ and substituted into Eq. (2.37) to obtain Eq. (2.38) (recall that, by definition, $K_v \cap K_s = \{v\}$). Expanding Eq. (2.38), we see that the operators h_v and h_w anti-commute since v and w are distinct vertices both belonging to the clique K_s . However, the subscript of the transfer matrix is symmetric under the exchange of v and w in the double sum. This double sum over $v \neq w \in K_s$ therefore vanishes and we obtain the desired relation in Eq. (2.36).

Notice that both Eqs. (2.35) and (2.36) have analogues in terms of T_G^- , given by substituting u for $-u$ in these identities. Additionally, both Eqs. (2.35) and (2.36) have analogues with h_v to the right of the transfer operator instead of to the left. It is especially surprising that this is true for Eq. (2.36), since h_v does not commute with T_{G-K_v} in general. Examining the proof however, we see that we can equivalently pull h_v to the right instead of to the left everywhere, and the proof goes through. In the forthcoming proofs, we will often refer to our use of these analogous identities as Eqs. (2.35) and (2.36), as the specific form of the identity we are using will be clear from context.

By similar reasoning as for T_G , we have the corresponding recurrence relation for $P_G(-u^2)$

$$P_G = P_{G-K} - u^2 \sum_{v \in K} b_v^2 P_{G-\Gamma[v]} \quad (2.39)$$

Note that, since any induced subgraph of G is also ECF, we can expand Eq. (2.28) in Lemma 2.2 by

Eq. (2.35) for some clique K to obtain

$$P_G(-u^2) = T_G T_G^- \quad (2.40)$$

$$= \left(T_{G-K} - u \sum_{v \in K} h_v T_{G-\Gamma[v]} \right) \left(T_{G-K}^- + u \sum_{v \in K} h_v T_{G-\Gamma[v]}^- \right) \quad (2.41)$$

$$= P_{G-K} - u^2 \sum_{v \in K} b_v^2 P_{G-\Gamma[v]} + u \sum_{v \in K} \left(T_{G-K} h_v T_{G-\Gamma[v]}^- - h_v T_{G-\Gamma[v]} T_{G-K}^- \right) \\ - u^2 \sum_{v \neq w \in K} h_v T_{G-\Gamma[v]} h_w T_{G-\Gamma[w]}^- \quad (2.42)$$

$$P_G(-u^2) = P_G(-u^2) + u \sum_{v \in K} \left(T_{G-K} h_v T_{G-\Gamma[v]}^- - h_v T_{G-\Gamma[v]} T_{G-K}^- \right) \\ - u^2 \sum_{v \neq w \in K} h_v T_{G-\Gamma[v]} h_w T_{G-\Gamma[w]}^- \quad (2.43)$$

In the last line, we used the recurrence relation in Eq. (2.39). This gives

$$u^2 \sum_{v \neq w \in K} h_v T_{G-\Gamma[v]} h_w T_{G-\Gamma[w]}^- = u \sum_{v \in K} \left(T_{G-K} h_v T_{G-\Gamma[v]}^- - h_v T_{G-\Gamma[v]} T_{G-K}^- \right). \quad (2.44)$$

Now we expand the left-hand side of Equation (2.34), and compute each of the two terms:

$$T_G \left(1 + u \sum_{v \in K_s} h_v \right) \chi T_G^- = T_G \chi T_G^- + u \sum_{v \in K_s} T_G h_v \chi T_G^- \quad (2.45)$$

For the first term, we make use of the recurrence relation Eq. (2.35) for the simplicial clique, K_s , noting that χ anti-commutes with h_v for all $v \in K_s$ and commutes with h_v for $v \notin K_s$

$$T_G \chi T_G^- = \left(T_{G-K_s} - u \sum_{v \in K_s} h_v T_{G-\Gamma[v]} \right) \left(T_{G-K_s}^- - u \sum_{v \in K_s} h_v T_{G-\Gamma[v]}^- \right) \chi \quad (2.46)$$

$$= \left[P_{G-K_s} + u^2 \sum_{v \in K_s} b_v^2 P_{G-\Gamma[v]} - u \sum_{v \in K_s} \left(T_{G-K_s} h_v T_{G-\Gamma[v]}^- + h_v T_{G-\Gamma[v]} T_{G-K_s}^- \right) \right. \\ \left. + u^2 \sum_{v \neq w \in K_s} h_v T_{G-\Gamma[v]} h_w T_{G-\Gamma[w]}^- \right] \chi \quad (2.47)$$

$$T_G \chi T_G^- = \left(P_G + 2u^2 \sum_{v \in K_s} b_v^2 P_{G-\Gamma[v]} - 2u \sum_{v \in K_s} h_v T_{G-\Gamma[v]} T_{G-K_s}^- \right) \chi \quad (2.48)$$

In the last line, we used the recurrence relation Eq. (2.39) and the identity Eq. (2.44).

Turning to the second term in Eq. (2.45), we consider the individual terms in the sum separately.

For each $v \in K_s$, we expand by K_v using Eq. (2.35). We then use the fact that $h_v \chi$ anti-commutes

with h_w for all $w \in K_v$ and commutes with h_w for all $w \notin K_v$. A similar set of steps as above gives

$$T_G h_v \chi T_G^- = \left(2P_{G-K_v} - P_G - 2u \sum_{w \in K_v} h_w T_{G-\Gamma[w]} T_{G-K_v}^- \right) h_v \chi, \quad (2.49)$$

where we have used a different rearrangement of Eq. (2.39) from that in Eq. (2.48) to simplify the expression. We next combine Eqs. (2.48) and (2.49) according to the linear combination on the left-hand side of Eq. (2.34) to obtain

$$\begin{aligned} T_G \left(1 + u \sum_{v \in K_s} h_v \right) \chi T_G^- &= P_G \left(1 - u \sum_{v \in K_s} h_v \right) \chi \\ &\quad + 2u \sum_{v \in K_s} (u b_v^2 P_{G-\Gamma[v]} - h_v T_{G-\Gamma[v]} T_{G-K_s}^-) \chi \\ &\quad + 2u \sum_{v \in K_s} \left(P_{G-K_v} - u \sum_{w \in K_v} h_w T_{G-\Gamma[w]} T_{G-K_v}^- \right) h_v \chi. \end{aligned} \quad (2.50)$$

We next proceed to prove that the last two terms in Eq. (2.50) evaluate to zero. Denote these terms by Δ . What follows is a tedious yet straightforward rearrangement of the expression for Δ :

$$\begin{aligned} \Delta &= 2u \sum_{v \in K_s} (u b_v^2 P_{G-\Gamma[v]} - h_v T_{G-\Gamma[v]} T_{G-K_s}^-) \chi \\ &\quad + 2u \sum_{v \in K_s} \left(P_{G-K_v} - u \sum_{w \in K_v} h_w T_{G-\Gamma[w]} T_{G-K_v}^- \right) h_v \chi \end{aligned} \quad (2.51)$$

We begin by separating the sum over $w \in K_v$ into the cases where $w = v$ term and $w \neq v$ terms, and make other minor rearrangements for simplification. We also commute the operators χ and h_v to the left of each expression, taking care to keep track of the sign changes and employ $h_v^2 = b_v^2$ in the $w = v$ term. Finally, we have made use of the identification $G - \Gamma[v] \simeq G - K_s - K_v$ for $v \in K_s$ in the subscripts of the first two terms. Thus we can write Δ as

$$\begin{aligned} \Delta &= 2\chi \left\{ \left[u^2 \sum_{v \in K_s} b_v^2 P_{G-K_s-K_v} + u \left(\sum_{v \in K_s} h_v T_{G-K_s-K_v} \right) T_{G-K_s}^- \right] \right. \\ &\quad \left. - u \sum_{v \in K_s} \left[P_{G-K_v} h_v + u \left(\sum_{\substack{w \in K_v \\ w \neq v}} h_v h_w T_{G-\Gamma[w]} + b_v^2 T_{G-K_s-K_v} \right) T_{G-K_v}^- \right] \right\} \end{aligned} \quad (2.52)$$

Next, we expand the factor of $T_{G-K_v}^-$, for the $w = v$ term, by the recursion relation Eq. (2.35) for the

clique $K_s \setminus \{v\}$, so that Δ becomes

$$\begin{aligned} \Delta = 2\chi \Big\{ & \left[u^2 \sum_{v \in K_s} b_v^2 P_{G-K_s-K_v} + u \left(\sum_{v \in K_s} h_v T_{G-K_s-K_v} \right) T_{G-K_s}^- \right] \\ & - u \sum_{v \in K_s} \left[P_{G-K_v} h_v + u \sum_{\substack{w \in K_v \\ w \neq v}} h_v h_w T_{G-\Gamma[w]} T_{G-K_v}^- \right. \\ & \left. + u b_v^2 T_{G-K_s-K_v} \left(T_{G-K_s-K_v}^- + u \sum_{\substack{w \in K_s \\ w \neq v}} h_w T_{G-K_v-\Gamma[w]}^- \right) \right] \Big\} \end{aligned} \quad (2.53)$$

We next simplify the first of the terms in the final parenthesis of Eq. (2.53) expansion using Lemma 2.2 to give

$$\begin{aligned} \Delta = 2\chi \Big\{ & \left[u^2 \sum_{v \in K_s} b_v^2 P_{G-K_s-K_v} + u \left(\sum_{v \in K_s} h_v T_{G-K_s-K_v} \right) T_{G-K_s}^- \right] \\ & - u \sum_{v \in K_s} \left[P_{G-K_v} h_v + u \sum_{\substack{w \in K_v \\ w \neq v}} h_v h_w T_{G-\Gamma[w]} T_{G-K_v}^- \right. \\ & \left. + u b_v^2 P_{G-K_s-K_v} + u^2 b_v^2 T_{G-K_s-K_v} \sum_{\substack{w \in K_s \\ w \neq v}} h_w T_{G-K_v-\Gamma[w]}^- \right] \Big\}. \end{aligned} \quad (2.54)$$

Here, we notice that the first term and second-to-last term in Eq. (2.54) cancel to give

$$\begin{aligned} \Delta = 2\chi \Big[& u \left(\sum_{v \in K_s} h_v T_{G-K_s-K_v} \right) T_{G-K_s}^- - u \sum_{v \in K_s} \left(P_{G-K_v} h_v + u \sum_{\substack{w \in K_v \\ w \neq v}} h_v h_w T_{G-\Gamma[w]} T_{G-K_v}^- \right. \\ & \left. + u^2 b_v^2 T_{G-K_s-K_v} \sum_{\substack{w \in K_s \\ w \neq v}} h_w T_{G-K_v-\Gamma[w]}^- \right) \Big] \end{aligned} \quad (2.55)$$

We again make minor rearrangements using the factorizations $P_{G-K_v} = T_{G-K_v} T_{G-K_v}^-$ and $b_v^2 = h_v^2$, together with the fact that the term χh_v commutes with all operators outside of the clique $K_v \subseteq \Gamma[w]$ for $w \in K_v$, so that

$$\begin{aligned} \Delta = 2u\chi \sum_{v \in K_s} h_v \Big(& T_{G-K_s-K_v} T_{G-K_s}^- - u^2 h_v T_{G-K_s-K_v} \sum_{\substack{w \in K_s \\ w \neq v}} h_w T_{G-K_v-\Gamma[w]}^- \Big) \\ & - 2u \sum_{v \in K_s} \left(T_{G-K_v} - u \sum_{\substack{w \in K_v \\ w \neq v}} h_w T_{G-\Gamma[w]} \right) T_{G-K_v}^- \chi h_v \end{aligned} \quad (2.56)$$

Making use of Eq. (2.35), we can rewrite the parentheses in the second term as T_G plus the missing

term from the sum over K_v , again making use of the identification $G - \Gamma[v] \simeq G - K_s - K_v$ for $v \in K_s$:

$$\begin{aligned} \Delta &= 2u\chi \sum_{v \in K_s} h_v \left(T_{G-K_s-K_v} T_{G-K_s}^- - u^2 h_v T_{G-K_s-K_v} \sum_{\substack{w \in K_s \\ w \neq v}} h_w T_{G-K_v-\Gamma[w]}^- \right) \\ &\quad - 2u \sum_{v \in K_s} (T_G + u h_v T_{G-K_s-K_v}) T_{G-K_v}^- \chi h_v \end{aligned} \quad (2.57)$$

Next, we collect the residual term from the sum over K_s in the second parentheses with the final term in the first parentheses, to obtain

$$\begin{aligned} \Delta &= 2u\chi \sum_{v \in K_s} \left[h_v T_{G-K_s-K_v} T_{G-K_s}^- + u b_v^2 T_{G-K_s-K_v} \left(-u \sum_{\substack{w \in K_s \\ w \neq v}} h_w T_{G-K_v-\Gamma[w]}^- + T_{G-K_v}^- \right) \right] \\ &\quad - 2u \sum_{v \in K_s} T_G T_{G-K_v}^- \chi h_v \end{aligned} \quad (2.58)$$

Expanding the second term in parentheses using the recurrence relation Eq. (2.35) for the clique $K_s \setminus \{v\}$, we find

$$\begin{aligned} \Delta &= 2u\chi \sum_{v \in K_s} \left[h_v T_{G-K_s-K_v} T_{G-K_s}^- \right. \\ &\quad \left. + u b_v^2 T_{G-K_s-K_v} \left(-u \sum_{\substack{w \in K_s \\ w \neq v}} h_w T_{G-K_v-\Gamma[w]}^- + T_{G-K_s-K_v}^- + u \sum_{\substack{w \in K_s \\ w \neq v}} h_w T_{G-K_v-\Gamma[w]}^- \right) \right] \\ &\quad - 2u \sum_{v \in K_s} T_G T_{G-K_v}^- \chi h_v \end{aligned} \quad (2.59)$$

The first and third terms in parentheses in Eq. (2.59) cancel, and by Lemma 2.4, the remaining term is $P_{G-K_s-K_v}$. Thus

$$\Delta = 2u\chi \sum_{v \in K_s} \left(h_v T_{G-K_s-K_v} T_{G-K_s}^- + u b_v^2 P_{G-K_s-K_v} \right) - 2u \sum_{v \in K_s} T_G T_{G-K_v}^- \chi h_v \quad (2.60)$$

Finally, we employ the recursion relation Eq. (2.36) to obtain

$$\Delta = 2u\chi \sum_{v \in K_s} (h_v T_{G-K_s-K_v} T_{G-K_s}^- + u b_v^2 P_{G-K_s-K_v}) + 2T_G (T_G^- - T_{G-K_s}^-) \chi \quad (2.61)$$

$$= -2 \left(T_G + u \sum_{v \in K_s} h_v T_{G-K_s-K_v} \right) T_{G-K_s}^- \chi + 2u^2 \chi \sum_{v \in K_s} b_v^2 P_{G-K_s-K_v} + 2T_G T_G^- \chi \quad (2.62)$$

$$= -2T_{G-K_s} T_{G-K_s}^- \chi + 2u^2 \chi \sum_{v \in K_s} b_v^2 P_{G-K_s-K_v} + 2T_G T_G^- \chi \quad (2.63)$$

$$= -2 \left(P_{G-K_s} - u^2 \sum_{v \in K_s} b_v^2 P_{G-K_s-K_v} \right) \chi + 2T_G T_G^- \chi \quad (2.64)$$

$$\Delta = -2P_G \chi + 2P_G \chi = 0 \quad (2.65)$$

Therefore, Eq. (2.50) evaluates to

$$T_G \left(1 + u \sum_{v \in K_s} h_v \right) \chi T_G^- = P_G \left(1 - u \sum_{v \in K_s} h_v \right) \chi \quad (2.66)$$

and this proves the lemma. \square

Since u_ℓ is a root of $P_G(-u^2)$, the right-hand-side of Equation (2.34) becomes zero for $u = u_\ell$. The left-hand side can then be rearranged, such that we can rewrite Eq. (2.33) as

$$[H, T_G(\pm u_\ell) \chi T_G(\mp u_\ell)] = \mp \frac{2}{u_\ell} T_G(\pm u_\ell) \chi T_G(\mp u_\ell). \quad (2.67)$$

Thus, Equation (2.67) implies that the incognito modes of the model act as canonical ladder operators and the Hamiltonian of the ECH model can be written as Eq. (2.2) in terms of the incognito modes, ψ_ℓ .

Finally, to show that the canonical modes of the Hamiltonian are fermionic, we must confirm that the incognito modes obey the canonical anti-commutation relations. It is straightforward to see from the definition of ψ_ℓ that $(\psi_\ell)^2 \propto P(-u_\ell^2)^2 = 0$ (remember the simplicial mode χ is defined as a Pauli operator, so $\chi^2 = I$). Further, since the transfer matrix and the simplicial mode are both Hermitian, we have

$$\psi_\ell^\dagger = \frac{1}{N_\ell} (T(u_\ell) \chi T(-u_\ell)) := \psi_{-\ell}. \quad (2.68)$$

Lemma 2.4. The incognito modes, $\{\psi_\ell\}$ (Def. 2.5), satisfy the canonical anti-commutation relations,

$$\{\psi_\ell, \psi_{-m}\} = \delta_{m,\ell} \quad (2.69)$$

with normalization

$$(N_\ell)^2 = 16u_\ell^2 P_{G-K_s}(-u_\ell^2) \partial_x (P_G(x))_{x=-u_\ell^2}, \quad (2.70)$$

where $\partial_x (P_G(x))_{x=-u_\ell^2}$ denotes the derivative of $P_G(x)$ with respect to x , evaluated at $-u_\ell^2$.

Proof. This proof closely follows the derivation by Fendley [23], again with generalizations to the graph recursion relations. To find the anticommutator between any two fermionic operators, we take the limit of

$$\{\psi_\ell, \psi_{-m}\} = \frac{1}{N_m} \lim_{u \rightarrow u_m} \{\psi_\ell, T_G(u) \chi T_G(-u)\} \quad (2.71)$$

We start by finding the explicit relationship acquired by commuting ψ_ℓ and $T_G(u)$. To do this we expand $T_G(u) \chi T_G(-u)$, using Eq. (2.34) and Lemma 2.3, noting that the transfer matrices commute, even at different u , due to Lemma 2.1, so that

$$T_G(u) \psi_\ell T_G(-u) = \frac{1}{N_\ell} T_G(-u_\ell) \left[-u T_G(u) \left(\sum_{v \in K_s} h_v \chi \right) T_G(-u) + P_G(-u^2) \left(1 - u \sum_{v \in K_s} h_v \right) \chi \right] T_G(u_\ell) \quad (2.72)$$

$$= -\frac{u}{2} T_G(u) [H, \psi_\ell] T_G(-u) + P_G(-u^2) \left(\psi_\ell - \frac{u}{2} [H, \psi_\ell] \right) \quad (2.73)$$

$$T_G(u) \psi_\ell T_G(-u) = \frac{1}{u_\ell} \left(-u T_G(u) \psi_\ell T_G(-u) + P_G(-u^2) (u_\ell - u) \psi_\ell \right) \quad (2.74)$$

By rearranging the expression in Eq. (2.74), we find algebra obeyed by the transfer matrices and ψ_ℓ as

$$(u_\ell + u) T_G(u) \psi_\ell = (u_\ell - u) \psi_\ell T_G(u). \quad (2.75)$$

Thus, the argument of Equation (2.71) becomes

$$\{\psi_\ell, T_G(u) \chi T_G(-u)\} = \frac{u_\ell + u}{u_\ell - u} T_G(u) \{\psi_\ell, \chi\} T_G(-u). \quad (2.76)$$

The anticommutator between ψ_ℓ and χ can be calculated explicitly using the recursion relation Equation (2.35),

$$\{\psi_\ell, \chi\} = \frac{4}{N_\ell} P_{G-K_s}(-u_\ell^2). \quad (2.77)$$

Since the right hand side of Eq. (2.77) is scalar, we can commute the transfer matrix, $T(u)$, in Eq. (2.71) through the anticommutator and use Equation (2.6) to write explicitly

$$\{\psi_\ell, T_G(u_m) \chi T_G(-u_m)\} = \lim_{u \rightarrow u_m} \frac{4}{N_\ell} P_{G-K_s}(-u_\ell^2) P_G(-u^2) \frac{u_\ell + u}{u_\ell - u}. \quad (2.78)$$

In this limit we find that the polynomial $P_G(-u^2) \rightarrow 0$, except in the case when $\ell = m$. Here, this limit requires the use of L'Hôpital's rule, since both the numerator and denominator of the expression go to zero. Doing so gives

$$\{\psi_\ell, \psi_{-m}\} = \delta_{\ell,m} \frac{16u_\ell^2}{N_\ell^2} P_{G-K_s}(-u_\ell^2) \partial_x (P_G(x))_{x=-u_\ell^2}. \quad (2.79)$$

Thus, we define the normalization factor of the incognito modes to be

$$(N_\ell)^2 = 16u_\ell^2 P_{G-K_s}(-u_\ell^2) \partial_x (P_G(x))_{x=-u_\ell^2}, \quad (2.80)$$

revealing that the $\{\psi_\ell\}$ do indeed satisfy the algebra of fermions. \square

Finally, we prove Theorems 2.1 and 2.2. In general, the existence of fermionic ladder operators satisfying Eqs. (2.67) and (2.69) is only enough to show that the Hamiltonian block-diagonalizes into sectors (i.e. multiplets). In each sector, the Hamiltonian has the same free spectrum up to a sector-dependent constant shift. In our case, however, the transfer matrix formalism allows us to prove the stronger statements of Theorems 2.1 and 2.2. Having proven the necessary lemmas, this proof is straightforward, as it matches exactly to the proof given by Fendley in Ref. [23]. We restate the essential steps of this proof here for completeness.

Proof of Thms. 2.1 and 2.2. In Ref. [23], the *higher Hamiltonians* $\{H^{(k)}\}_{k=1}^\infty$ are defined as operators generated by the logarithmic derivative of T_G

$$\mathcal{H}(u) := \sum_{k=1}^\infty H^{(k)} u^{k-1} := -\partial_u \ln [T_G(u)] = -\frac{1}{P_G(-u^2)} T_G(-u) T'_G(u). \quad (2.81)$$

The last equality follows from Lemma 2.2, where T'_G is the derivative of T_G with respect to u . Substituting $u = 0$ into the second and fourth expressions in this definition demonstrates that $H^{(1)} := H$. The operator $\mathcal{H}(u)$ is a meromorphic function of u whose only singularities are at the roots of $P_G(-u^2)$, since $T_G(-u)T'_G(u)$ is a finite series in u with bounded-operator coefficients. Since $P_G(x)$ has a constant term, none of the roots of $P_G(-u^2)$ are at $u = 0$, and so $\mathcal{H}(u)$ is analytic on a small disk centered at this point. Therefore, we can write each of the higher Hamiltonians as an integral over a small oriented contour C around $u = 0$

$$H^{(k)} = \frac{1}{2\pi i} \oint_C du u^{-k} \mathcal{H}(u). \quad (2.82)$$

Changing variables to $u = 1/\varepsilon$ gives

$$H^{(k)} = \frac{1}{2\pi i} \oint_{\tilde{C}} d\varepsilon \varepsilon^{k-2} \mathcal{H}(\varepsilon) \quad (2.83)$$

where the new contour \tilde{C} encircles all of the poles at the zeros of $P_G(-u^2)$ with the same orientation as C (reversing this orientation incurs a sign change). This gives

$$H^{(k)} = -\frac{1}{2\pi i} \oint_{\tilde{C}} d\varepsilon \frac{\varepsilon^{2\alpha+k-2}}{\prod_{j=1}^{\alpha} (\varepsilon^2 - \varepsilon_j^2)} T_G(-1/\varepsilon) T'_G(1/\varepsilon) \quad (2.84)$$

where we have utilized the factorization $P_G(-u^2) = \prod_{j=1}^{\alpha} (1 - \varepsilon_j^2 u^2)$ and multiplied numerator and denominator by $u^{-2\alpha} := \varepsilon^{2\alpha}$ in the integral ($u \neq 0$ over C). Note here that T'_G is still the derivative of T_G with respect to its argument and not the derivative with respect to ε in the equation above. Since the maximum power of u in $T_G(u)$ is α , the minimum power of ε in $T_G(-1/\varepsilon) T'_G(1/\varepsilon)$ is $-2\alpha + 1$, and so the integrand has no poles at $\varepsilon = 0$ for $k \geq 1$. The only poles of the integrand are therefore at $\pm \varepsilon_j$, and so the Cauchy residue theorem gives

$$H^{(k)} = -\sum_{j=1}^{\alpha} \frac{\varepsilon_j^{2\alpha+k-2}}{\prod_{\ell=1, \ell \neq j}^{\alpha} (\varepsilon_j^2 - \varepsilon_{\ell}^2)} \left[\frac{1}{2\varepsilon_j} T_G(-1/\varepsilon_j) T'_G(1/\varepsilon_j) - \frac{(-1)^k}{2\varepsilon_j} T_G(1/\varepsilon_j) T'_G(-1/\varepsilon_j) \right] \quad (2.85)$$

Using

$$\partial_u [P_G(-u^2)]_{u=u_j} = -2\varepsilon_j \prod_{\ell=1, \ell \neq j}^{\alpha} (1 - \varepsilon_{\ell}^2 u_j^2) \quad (2.86)$$

gives

$$H^{(k)} = \sum_{j=1}^{\alpha} \frac{u_j^{-k}}{\partial_u [P_G(-u^2)]_{u=u_j}} [T_G(-u_j) T'_G(u_j) - (-1)^k T_G(u_j) T'_G(-u_j)] \quad (2.87)$$

Next we evaluate the commutator

$$[\psi_j, \psi_j^{\dagger}] = [\psi_j, \psi_{-j}] \quad (2.88)$$

$$= \frac{1}{N_j} \lim_{u \rightarrow u_j} [\psi_j, T_G(u) \chi T_G(-u)] \quad (2.89)$$

$$[\psi_j, \psi_j^{\dagger}] = \frac{1}{N_j} \lim_{u \rightarrow u_j} \left\{ \left(\frac{u_j + u}{u_j - u} \right) T_G(u) [\psi_j, \chi] T_G(-u) \right\} \quad (2.90)$$

This follows by similar steps to Eqs. (2.71) and (2.76). Our definition of the incognito modes, together

with Lemma 2.2, implies

$$T_G(u_j)\psi_j = \psi_{-j}T_G(u_j) = 0 \quad (2.91)$$

both numerator and denominator of Eq. (2.90) vanish in the limit, so we have

$$[\psi_j, \psi_j^\dagger] = -\frac{2u_j}{N_j} (T'_G(u_j)\psi_j\chi T_G(-u_j) + T_G(u_j)\chi\psi_j T'_G(-u_j)) . \quad (2.92)$$

Exchanging χ and ψ_j using the anticommutator, Eq. (2.77), gives

$$[\psi_j, \psi_j^\dagger] = -\frac{8u_j}{N_j^2} P_{G-K_s}(-u_j^2) (T'_G(u_j)T_G(-u_j) + T_G(u_j)T'_G(-u_j)) \quad (2.93)$$

as the additional terms vanish by Eq. (2.91). Rewriting the normalization condition of Eq. (2.70) as,

$$(N_j)^2 = -8u_j P_{G-K_s}(-u_j^2) \partial_u [P_G(-u^2)]_{u=u_j}, \quad (2.94)$$

and then substituting into the above expression gives

$$[\psi_j, \psi_j^\dagger] = \frac{1}{\partial_u [P_G(-u^2)]_{u=u_j}} (T'_G(u_j)T_G(-u_j) + T_G(u_j)T'_G(-u_j)) \quad (2.95)$$

Comparing Eq. (2.87) for $k = 1$ to Eq. (2.95) proves both Theorems 2.1 and 2.2. \square

In this way we can see that a ECH model is described by non-interacting fermions, with single particle energies given by the reciprocals of the roots of the vertex-weighted independence polynomial, Eq. (2.6), and canonical modes given by the incognito modes (Def. 2.5). This constitutes a complete solution to any model of this kind.

2.5 Examples

In this section we analyze explicitly two sets of models whose Hamiltonians are (even hole, claw)-free, thus admitting a free-fermion solution via Theorems 2.1 and 2.2. The first set includes a pair of examples of models realized on small systems, including a model whose frustration graph is a line graph and a simple extension whose frustration graph is one of the nine forbidden subgraphs of a line graph (see Table 2.2). The second example is a class of graphs we call *equipartition indifference* graphs. This family of models generalizes the well-known XY-model and was exactly solved at their

critical points in Refs. [57, 58]. In the third subsection we define a new set of integrable and soluble models constructed by fusing the equipartition indifference graphs into more complex structures.

2.5.1 Small systems

Here we look at two related models on three qubits. The Hamiltonians of the models, denoted H_5 and H_6 , and are related by the addition of a single term

$$H_5 = aX_1X_2 + bZ_2 + cY_1Y_2X_3 + dY_1Z_2 + eX_1Z_2 \quad (2.96)$$

$$H_6 = aX_1X_2 + bZ_2 + cY_1Y_2X_3 + dY_1Z_2 + eX_1Z_2 + fY_1Y_2Z_3, \quad (2.97)$$

where $\{X_i, Y_i, Z_i\}$ refer to Pauli operators applied to the i -th spin in the natural way and the coupling strengths $\{a, b, c, d, e, f\}$ are arbitrary real numbers. The frustration graphs for H_5 and H_6 are depicted in Figure 2.2, with vertices labeled by their corresponding field strengths.

The frustration graph of the first model, $G(H_5)$, is a five-cycle, as depicted in Fig. 2.2 (a): the five Hamiltonian terms anti-commute only with those directly before and after it in a closed chain. $G(H_5)$ is a line graph, as such this model admits a Jordan-Wigner solution [22]. Let $R(H_5)$ be the root graph of $G(H_5)$; this graph is also a five-cycle. Each Hamiltonian term is mapped to a Majorana bilinear with Majorana modes $\{\gamma_j\}_{j=1}^5$ assigned to each vertex of the root graph. Using this method, the Hamiltonian is mapped to

$$H = \frac{i}{2} \sum_{j,k=0}^4 \gamma_j h_{j,k} \gamma_k \quad (2.98)$$

where the single particle Hamiltonian is given by

$$\frac{i}{2} \mathbf{h} = \frac{i}{2} \begin{pmatrix} 0 & a & 0 & 0 & -e \\ -a & 0 & b & 0 & 0 \\ 0 & -b & 0 & c & 0 \\ 0 & 0 & -c & 0 & d \\ e & 0 & 0 & -d & 0 \end{pmatrix}. \quad (2.99)$$

Note here that the orientation of $R(H_5)$ given by the signs of the elements in \mathbf{h} is arbitrary, i.e. we can change the sign of any coupling coefficient without affecting the spectrum.

The frustration graph of $G(H_5)$ is also an (even hole, claw)-free graph: every edge induces a simplicial clique. Thus, the model can be solved using the method developed here. The vertex-

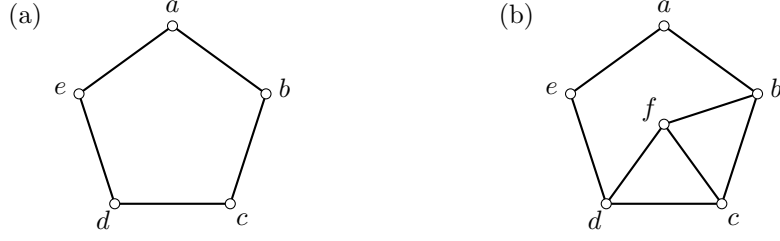


Figure 2.2: Frustration graphs for small system sizes solved in this section: (a) a five-cycle, which admits a generator-to-generator mapping, but is both even hole and claw free also, thus admitting a solution by the method developed in the present work, (b) one of the six forbidden subgraphs of a line graph with no twins, created by adding a single additional Hamiltonian term to the five-cycle, thus when $f \rightarrow 0$, this model is identical to (a). This model does not admit a generator-to-generator mapping, but is solvable using the method developed here.

weighted independence polynomial of $G(H_5)$ is

$$P_{G(H_5)}(-u^2) = 1 - u^2 (a^2 + b^2 + c^2 + d^2 + e^2) + u^4 [a^2 (c^2 + d^2) + b^2 (d^2 + e^2) + c^2 e^2]. \quad (2.100)$$

$P_{G(H_5)}$ can be factored simply as a quadratic polynomial in u^2 . The roots of $P_{G(H_5)}$ provide the the single particle energies, as well as the spectral parameters for the incognito modes, $\{\psi_k\}_k$ in Eq. (2.9). Note that, as discussed in Sect. 2.3, $P_{G(H_5)}$ is exactly the characteristic polynomial of the single-particle Hamiltonian $i\mathbf{h}$

$$P_{G(H_5)}(-u^2) = \det(\mathbf{I} - iu\mathbf{h}). \quad (2.101)$$

Thus, we can see the direct link between the two approaches for a solution when the model is an even hole-free line graph. Furthermore, the eigenvectors of the single particle Hamiltonian, \mathbf{h} , elucidate the non-locality of the canonical modes, $\{\psi_k\}_k$.

The frustration graph $G(H_6)$ is depicted in Fig. 2.2 (b). In direct contrast to H_5 , this graph is one of the six forbidden subgraphs of a line graph that does not contain twins and admits no Jordan-Wigner mapping to non-interacting fermions. Nevertheless, Fig. 2.2 (b) contains no even holes or claws, and each maximal clique of the graph is simplicial. Thus, by Theorem 2.1 the model must be free.

The vertex-weighted independence polynomial of $G(H_6)$ is

$$P_{G(H_6)}(-u^2) = 1 - u^2 (a^2 + b^2 + c^2 + d^2 + e^2 + f^2) + u^4 [a^2 (c^2 + d^2 + f^2) + b^2 (d^2 + e^2) + c^2 e^2 + e^2 f^2] \quad (2.102)$$

and so the single particle energies can be found by again solving a simple quadratic equation.

Despite the similarities between the two models, H_5 admits a solution in terms of individual fermions localized to physical modes, while H_6 does not. It therefore remains an open question to clarify the intrinsic link (if any) between the graphical and spatial structures for models with ECF frustration graphs, a stark contrast from the line-graph setting.

While the spectrum, and fermionization, of the models is independent of the explicit Pauli realization, the qubitization of the graphs given does elucidate an interesting link between the ECF models and those that have a Jordan-Wigner mapping (line-graph models). Here H_5 and H_6 are related via a single-qubit rotation on the third qubit. To see this, rewrite the Hamiltonian as

$$H_6 = aX_1X_2 + bZ_2 + Y_1Y_2(cX_3 + fZ_3) + dY_1Z_2 + eX_1Z_2. \quad (2.103)$$

By applying the coupling strength dependent rotation $(cX_3 + fZ_3) \rightarrow \pm\sqrt{c^2 + f^2}X_3$, we can see the direct relation between models H_5 and H_6 . In general, the transformation from an arbitrary (even-hole, claw)-free model to a similar line-graph model is nontrivial, requiring complicated, multi-qubit rotations. However, this particular example shows when two vertices share the same *closed neighborhood* we can always perform a rotation to remove one of them, without altering the spectrum. This is analogous to the situation involving twin vertices – i.e. vertices sharing an open neighborhood – discussed in Sect. 2.3. The difference is that vertices sharing a closed neighborhood are themselves neighboring. Similarly to removing twin vertices by projecting onto a subspace, we remove these pairs by performing a rotation.

2.5.2 Indifference Graphs

An infinite family of ECF graphs is given by the set of *indifference graphs*. Indifference graphs are defined by placing vertices on the real line and connecting two vertices if and only if they are separated by a distance $\leq k$, for some fixed and finite k . Such graphs are ECF since they have a known forbidden induced subgraph characterization that forbids (among others) the claw and even holes [108]. They are therefore also simplicial. In fact, the closed neighborhood of the vertex corresponding to the least real number is always a simplicial clique (its neighbors are all within distance 1 of each other, hence induce a clique). Finally, it is simple to identify the independent sets for these graphs: they are the subsets of vertices whose pairwise separation on the real line is greater than 1. Some examples of indifference graphs are shown in Fig. 2.3. Given an indifference graph G , there is no unique way to

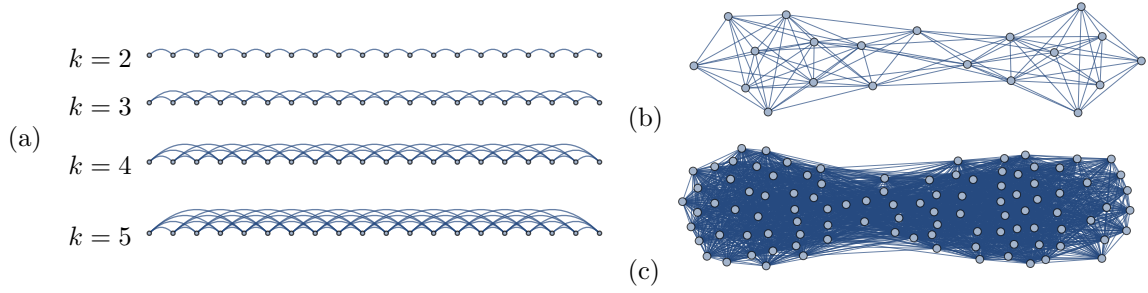


Figure 2.3: Indifference frustration graphs for some ECF models (see text). **(a)** Equipartition indifference graphs arise, for example, as frustration graphs for the translation-invariant spin chain (having open boundary conditions) with Hamiltonian $H_k = \sum_i X_i X_{i+1} \cdots X_{i+k-2} Z_{i+k-1}$. The frustration graph is shown for $k = 2, \dots, 5$. When $k = 2$, a Hadamard rotation on every second spin shows that this model is equivalent to the XY model with half of its terms removed, and it can be solved by a Jordan-Wigner transformation. The $k = 3$ model is the model studied by Fendley [23]. When $k > 2$, the graph is not a line graph, so it cannot be solved by any Jordan-Wigner transformation [22], but since it is ECF by construction, it can be solved by the methods introduced in this chapter. **(b,c)** Two examples of ECF graphs that arise as indifference graphs with randomly chosen points at different densities. It is evident that, depending on the point density, the connectivity of interval graphs can look rather complex.

find a spin model Hamiltonian having G as its frustration graph, though such models will always exist. To get a natural mapping to spin models, we will specialize to the set of graphs (shown in Fig. 2.3(a)) where the vertices are equally spaced on the real line.

We therefore consider a particularly nice family of spin models, which generalizes the XY-model and the four-fermion model in Ref. [23]. This family was originally introduced in Refs. [57, 58] and the critical behavior analyzed there as well. Here we demonstrate how this family fits into our formalism. Each model in the family is indexed by an integer k . When $k = 2$, we get an XY-chain, albeit with half the terms removed. This model is still solvable by a Jordan-Wigner transformation. When $k = 3$, we get the four-fermion model solved in Ref. [23]. When $k \geq 4$, we get an infinite family of free-fermion-solvable models with translation-invariant frustration graphs. The construction of the associated frustration graph with N unit cells, $G(N, k)$, is simple: fix k , and consider the set of integers $M(N, k) \subset \mathbb{Z}$

$$M(N, k) := \bigcup_{n=0}^{N-1} \bigcup_{j=0}^{k-1} (nk + j) . \quad (2.104)$$

Let $m(n, j) := nk + j$. Associate a vertex of $G(N, k)$ to each point in $M(N, k)$, and join vertices corresponding to $m(n, j)$ and $m(n', j')$ by an edge if $|m(n, j) - m(n', j')| < k$. Then $G(N, k)$ is equivalent to the indifference graph of $M(N, k)$ after rescaling our distance function appropriately. We will often refer to the vertices of $G(N, k)$ by their corresponding points in $M(N, k)$ directly. We will shortly see that $N = \alpha$, the independence number of $G(N, k)$. See Fig. 2.4 for an example when

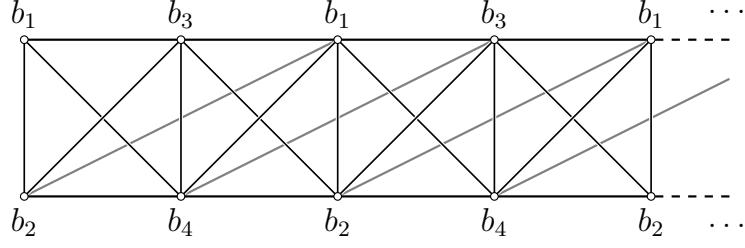


Figure 2.4: Equipartition indifference graph for $k = 4$, formed from the frustration graph of the Hamiltonian in Eq. (2.105). The Hamiltonian couplings are 4-periodic and are labeled b_1, b_2, b_3 , and b_4 .

$k = 4$.

An explicit qubit Pauli Hamiltonian realizing $G(N, k)$ is given in Refs. [57, 58]

$$H = \sum_{n=0}^{N-1} \sum_{j=0}^{k-1} b_{nk+j} X_{nk+j} \prod_{\ell=1}^{k-1} Y_{nk+j+\ell}. \quad (2.105)$$

Similarly to these references, we consider staggered, uniform couplings: k different couplings which are repeated periodically as

$$b_{nk+j} := b_j, \quad (2.106)$$

For simplicity of expression we collect the squares of the coupling strengths in a vector

$$\mathbf{b} = (b_0^2, b_1^2, b_2^2, \dots, b_{k-1}^2). \quad (2.107)$$

Define the *elementary symmetric polynomials* in \mathbf{b} as

$$e_j(\mathbf{b}) := \sum_{0 \leq i_1 < i_2 < \dots < i_j \leq k-1} \prod_{\ell=1}^j b_{i_\ell}^2 \quad (2.108)$$

for $j \in \{0, \dots, k\}$, with $e_0 := 1$. Finally, denote the clique induced by the vertices corresponding to the points $\{m(n, 0), m(n, 1), \dots, m(n, k-1)\} \subset M(N, k)$ in $G(N, k)$ by K_n . Notice that

$$G(N, k) - \left(\sum_{p=0}^{\ell} K_p \right) = G(N - \ell - 1, k). \quad (2.109)$$

Since any independent set can contain at most one vertex from each clique K_n , we have that $\alpha \leq N$.

An explicit independent set with N vertices is given by $\cup_{n=0}^{N-1} m(n, 0)$. Therefore, $\alpha = N$.

Let us first show that $P_{G(N, k)}$ satisfies a recursion relation which is symmetric in the entries of \mathbf{b} ,

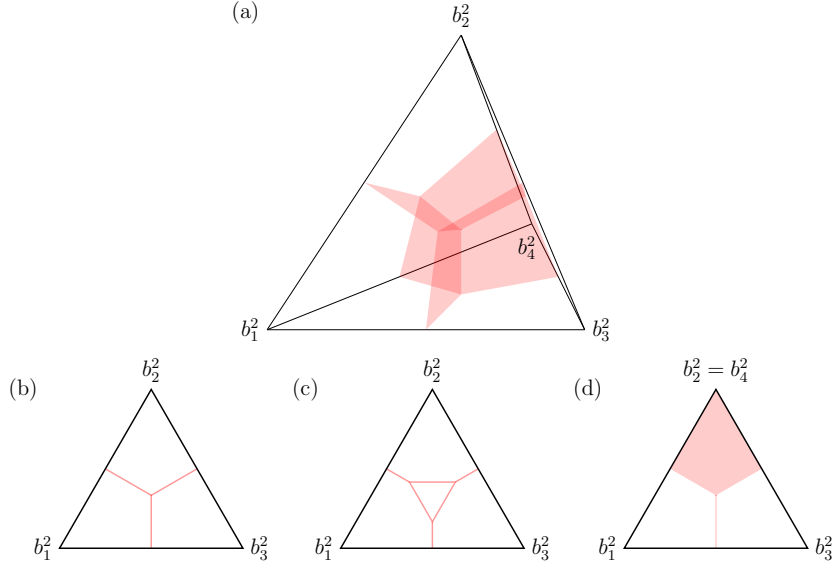


Figure 2.5: Phase diagram for the *equipartition indifference graph* Hamiltonian for $k = 4$, with staggered uniform couplings, b_1, b_2, b_3, b_4 . (a) shows a three dimensional simplex, with parameters. (b) shows a cross section of the plane at $b_4 = 0$. (c) shows a cross section parallel to that in (a), but with $b_4 > b_1, b_2, b_3$, (d) shows a cross section at a diagonal through the tetrahedron where $b_2^2 = b_4^2$ at all times

which follows from the graph-theoretic recurrence relations.

$$P_{G(N,k)} = P_{G(N-1,k)} - \sum_{\ell=1}^k u^{2\ell} e_{\ell}(\mathbf{b}) P_{G(N-\ell,k)} \quad (2.110)$$

For $k = 4$, for example

$$P_{G(N,4)} = [1 - u^2 e_1(\mathbf{b})] P_{G(N-1,4)} - u^4 e_2(\mathbf{b}) P_{G(N-2,4)} - u^6 e_3(\mathbf{b}) P_{G(N-3,4)} - u^8 e_4(\mathbf{b}) P_{G(N-4,4)}. \quad (2.111)$$

We show Eq. (2.110) by first expanding $P_{G(N,k)}$ via the recursion relation Eq. (2.39) in the clique K_0 , with the convention in Eq. (2.109). Note that the neighbors to each vertex $m(0,j) \in K_0$, besides K_0 itself, are given by translations $\{m(1,\ell)\}_{\ell=1}^{j-1}$. This gives,

$$P_{G(N,k)} = P_{G(N-1,k)} - u^2 \sum_{j=0}^{k-1} b_j^2 P_{G(N-1,k) - \sum_{\ell=0}^{j-1} m(1,\ell)}. \quad (2.112)$$

We can rearrange similar expansions in the induced subgraphs of K_1 , which are also cliques, to obtain

$$P_{G(N-1,k) - \sum_{\ell=0}^{j-1} m(1,\ell)} = P_{G(N-1,k)} + u^2 \sum_{\ell=0}^{j-1} b_{\ell}^2 P_{G(N-2,k) - \sum_{p=0}^{\ell-1} m(1,p)} \quad (2.113)$$

for $j \in \{1, \dots, k-1\}$. Substituting Eq. (2.113) into Eq. (2.112) gives

$$P_{G(N,k)} = [1 - u^2 e_1(\mathbf{b})] P_{G(N-1,k)} - u^4 \sum_{j=0}^{k-1} \sum_{\ell=0}^{j-1} b_j^2 b_\ell^2 P_{G(N-2,k) - \sum_{p=0}^{\ell-1} m(1,p)} \quad (2.114)$$

We can iterate this procedure by substituting Eq. (2.113), with $G(N-1, k)$ replaced by $G(N-2, k)$, back into the sum over j and ℓ in Eq. (2.114). Notice that each time we do this, the sum over single vertices p in the subscript of the summand contains one fewer term, the equipartition indifference graph in this subscript contains one fewer clique K_n , and the coefficient in the summand acquires another factor from \mathbf{b} . Iterating $k-1$ times gives the desired recurrence relation, Eq. (2.110).

We next assemble a vector with entries

$$v_s(\varepsilon^2) = \varepsilon^{2s} P_{G(s-1,k)}(\varepsilon^{-2}), \quad (2.115)$$

such that the recursion relation, Eq. (2.110), can be rewritten as

$$v_{N+1} = \varepsilon^2 v_N - \sum_{\ell=1}^k e_\ell(\mathbf{b}) v_{N-\ell+1}. \quad (2.116)$$

As this recursion relation holds for any value of N , we can define the matrix \mathcal{R} with elements

$$\mathcal{R}_{ss'} = \sum_{\ell=0}^k \delta_{s-\ell+1, s'} e_\ell(\mathbf{b}), \quad (2.117)$$

such that Eq. (2.116) has the form of an eigenvalue equation

$$\mathcal{R} \cdot \mathbf{v} = \varepsilon^2 \mathbf{v}. \quad (2.118)$$

When the eigenvalue corresponds to a root ε_j^{-2} of $P_{G(N,k)}$, the corresponding eigenvector \mathbf{v} satisfies the boundary condition $v_{N+1}(\varepsilon_j^2) = 0$. We further require \mathbf{v} satisfy the boundary conditions $v_0 = \dots = v_{-k+2} = 0$ (by our convention, $v_1 \propto P_{G(0,k)} = 1$).

These models exhibit critical behavior when any subset of the coupling coefficients become equal. For all k -sized equipartition indifference models, the phase diagram is a $(k-1)$ -dimensional simplex with k -critical point at the center. The phase diagram for $k=4$ is shown in Fig. 2.5 as both a three dimensional tetrahedron, as well as three cross sections of the depicting the gapped regions in white, with gapless regions in red. Here we see the two-dimensional semi-hyperplanes meeting at the center

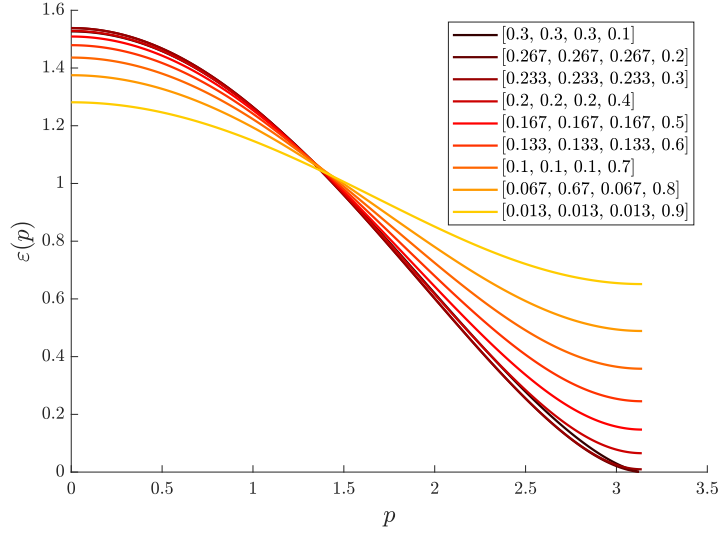


Figure 2.6: Dispersion relations for the $k = 4$ instance of equipartition indifference models, with $b_4^2 \in \{0.1, 0.2, \dots, 0.9\}$, and other couplings equal such that the sum of their squares is normalized to 1. For $b_4^2 \leq 0.25$, the model is critical at momentum $p = \pi$, as our numerics indicate.

point of the tetrahedron, where $b_1^2 = b_2^2 = b_3^2 = b_4^2$, as well as along one dimensional lines.

It is clear from the cross section in Fig. 2.5 (b) that the class of models is hereditary as boundary of the phase diagram corresponds directly to the phase diagram of the $k = 3$ model (see Ref. [23]). Interestingly, Fig. 2.5 (c) shows that as we increase the fourth parameter, b_4^2 , the central, tri-critical point in the model opens and a gapless phase emerges. Fig. 2.5 (d) shows the cross-section through the center of the tetrahedron when $b_2^2 = b_4^2$. We see that there is a regime in which there is a large gapped phase, as well as two symmetric gapless phases separated by a gapped region.

The critical behavior of these models has been exactly analyzed in Refs. [57, 58] (and indeed, extended to parafermionic systems as well), and the authors find a dynamical critical exponent of k/d for general qudits of dimension d ($d = 2$ in our setting). We add that the model can be numerically analyzed over the entire phase diagram using the fact that \mathcal{R} is a banded Toeplitz matrix with bandwidth $k + 1$ and applying the algorithm in Ref. [109] to find the dispersion relation in the asymptotic limit. Figure 2.6 shows the dispersion relations along the central axis from one vertex ($b_4^2 = 1$) to the center of the opposite face ($b_4^2 = 0$), with other coefficients equal and normalized. We find that the model is indeed critical when $b_4^2 \leq 0.25$, and the dispersion relation is nonlinear about this point.

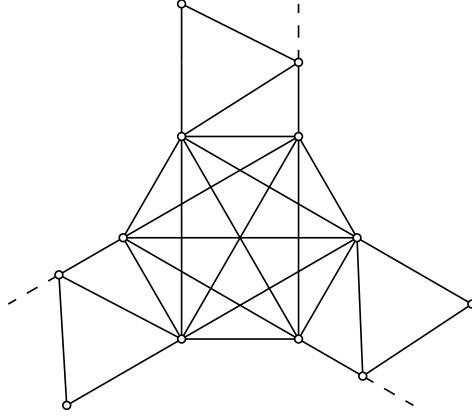


Figure 2.7: An example frustration graph of a junction for more complex models which are either integrable or soluble.

2.5.3 Integrable and Soluble models

Here we define a new class of two-dimensional models not previously discussed in the literature. The models are formed by attaching the one-dimensional chains from Sect. 2.5.2 to one another via interaction terms with clique-like frustration graphs. In order to ensure that the graphs remain claw-free, at each point of attachment, or junction, the clique must contain at least twice as many vertices as attached chains. Consider the example frustration graph depicted in Fig. 2.7, the junction is trivalent; however, in order to ensure that the model remains claw-free, the junction contains a sixth order clique (K_6). Notice, that if the new structure formed from the joining of the chains is a quasi-two-dimensional structure (such as a tree), the model will be even-hole-free, and thus free-fermion soluble using the methods developed here. On the contrary, if the new structure is two dimensional, then the frustration graph will necessarily contain even-holes. Nevertheless, the model will still be integrable, due to Lemma 2.1.

2.6 Discussion

We have proven that Hamiltonians with (even-hole, claw)-free frustration graphs in a given basis admit a solution by non-interacting fermions, even when such models provably do not admit a Jordan-Wigner solution. Though our result considerably expands the set of known free-fermion solutions, we should note that it clearly does not capture all of them. First, there exist models whose free-fermion solution is *non-generic*, in that they only hold for specific values of the coupling strengths. As an example, we

can consider the following model on three qubits:

$$H = aZ_2 + bY_1X_2 + cX_1Y_2 + dZ_1Y_3 + eY_1X_3 + fZ_3 \quad (2.119)$$

The frustration graph of the model is depicted in Fig. 2.8. The graph clearly contains both claws and even holes, and is thus outside the class of models discussed in this chapter. In general, the model is not free for arbitrary couplings. Nevertheless, the model does have a free spectrum for all equal couplings ($a = b = c = d = e = f$). Further, we can numerically verify that the single particle energies of the model are the reciprocals of the roots of the vertex weighted independence polynomial of the graph.

A perhaps much deeper open question concerns the relationship between the spatial structure of a given model and the associated free-fermion modes which emerge from this solution. We have structured our argument to draw a parallel between the way in which these mappings generalize the Jordan-Wigner transformation—whose spatial structure is evident—with the way claw-free graphs generalize line graphs. Carrying this argument through, one might ask whether the even-hole-free assumption can be relaxed, as Hamiltonians whose frustration graphs are arbitrary line graphs still admit a Jordan-Wigner free-fermion solution. From a technical perspective, simplicial claw-free graphs enjoy many of the properties that we relied on to prove our general solution. Models with simplicial claw-free frustration graphs admit an extensive number of commuting conserved charges defined through their independent sets (i.e., they satisfy Lemma 2.1), and their independence polynomials are also real-rooted [100–102]. One might attempt to incorporate even holes into this formalism by defining spatial hopping terms $\psi_j\psi_k^\dagger$. The simplicial mode cancels in the definition of these quadratic operators, leaving them defined only in terms of Hamiltonian terms. However, the resulting expressions are very complicated. Furthermore, allowing for even holes requires us to generalize Lemma 2.2, which was crucial for the following proof. Though we cannot say anything definitive about the more general class of simplicial claw-free graphs currently (indeed, they may not admit a free-fermion solution at all), we remark that they would be a natural class of models for further study.

Another clear open question concerns whether this construction could be generalized to solutions of qudit models in terms of *parafermions* [110]. The concept of free parafermions has been developed by Fendley [59], and Refs. [57, 58] consider non-Hermitian qudit generalizations of the equipartition indifference graphs which have free parafermionic spectra. It is known that, unlike fermions, bilinear parafermions are not always free, yet our formalism may provide a clue to recognizing such systems. Recall that the structure theorem of Ref. [105] states that (even-hole, pan)-free graphs (which

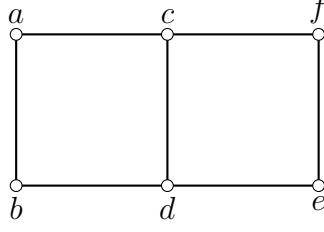


Figure 2.8: The frustration graph of the model, defined in Equation (2.119). This model has claws and even holes, nevertheless for all-equal-coefficients the model has a free fermion spectrum.

generalize our class of graphs) are essentially unit circular-arc graphs connected by clique cutsets. Incidentally, a subset of bilinear parafermion models have frustration graphs given by oriented unit circular-arc graphs, where the orientation captures the fact that the group-commutator between bilinear parafermionic terms is a complex phase, and this orientation is inherited from an underlying orientation on the circular-arc representation. This characterization could therefore clarify the relationship between free-parafermion models, the models considered in Refs. [57, 58], and more general bilinear parafermion models.

One strength of the solution method developed in the present work is that it could in principle be applied to *interacting* fermion models in addition to qubit models. Indeed, Fendley’s four-fermion model is an obvious example. This is because the existence of the solution is independent of the Pauli realization and relies only on the graph structure of the model. In Ref. [23], Fendley suggests applying this solution method to the cooper pair model of Refs. [111, 112], which represents one other such fermion model. However, the frustration graph of this model has even holes, and so is ineligible for solution by our method. Nevertheless, it would be interesting to investigate our method as a starting point for approximate solutions to non-integrable models such as quantum impurity models [113]. One potential application would be to extend the exact analysis of Fendley’s four-fermion model to an approximate one on periodic boundary conditions. We leave such questions for future work.

Chapter 3

A unified graph theoretic approach to free fermions

We show that a quantum spin system has an exact description by noninteracting fermions when its frustration graph is claw-free and contains a simplicial clique. Our result captures a vast family of known free-fermion solutions. In particular, it generalizes graph-theoretic characterizations given in previous work, where it was shown that a free-fermion solution exists if the frustration graph is either a line graph, or (even-hole, claw)-free. The former case includes the celebrated Jordan-Wigner transformation and the exact solution to the Kitaev honeycomb model. The latter case generalizes a nonlocal solution to the four-fermion model given by Fendley. Our characterization unifies these two approaches, extending generalized Jordan-Wigner solutions to the nonlocal setting and extending the generalized four-fermion solution to models of arbitrary spatial dimension. Our key technical insight is the identification of a class of cycle symmetries for all models with claw-free frustration graphs. We prove that these symmetries commute, and this allows us to apply Fendley's solution method to each symmetric subspace independently. Finally, we give a physical description of the fermion modes in terms of operators generated by repeated commutation with the Hamiltonian, connecting our framework to the developing body of work on operator Krylov subspaces. Our results establish a deep connection between many-body physics and the mathematical theory of claw-free graphs.

3.1 Introduction

The Jordan-Wigner transformation represents a fascinating insight into the physics of quantum many-body spin systems. It identifies collective spin degrees of freedom with those of fermions, resulting in a fermionic model with the same energy spectrum as the spin system of interest [28]. It is perhaps best-known for its application to models where the effective fermions are non-interacting, allowing for an exact solution to these otherwise non-trivial systems [24]. Since its discovery, the Jordan-Wigner transformation has been generalized to a family of exact free-fermion solutions [30–40], yielding new understanding for a wide class of spin models.

In addition to the setting of exactly solvable systems, an understanding of effective fermions is important for applications in quantum information. Interacting fermionic systems are foundational to quantum chemistry [114–117], which motivates the design of good fermion-to-qubit mappings [34, 69–74, 76, 118–120]. These mappings can, in some sense, be considered the reverse problem of finding a free-fermion solution to a spin model. Further, Majorana fermions represent a promising avenue for the topological protection of quantum information [11, 121–124] which is promising for experimental realization [125].

Concretely, the Jordan-Wigner transformation and its generalizations map many-qubit Pauli observables directly to fermionic operators: the *Majorana modes*. These mappings are generator-to-generator, as they identify a direct correspondence between Hamiltonian terms in the spin system and its dual fermion model. Additionally, they are *generic*, meaning that the solution method applies for all values of the Hamiltonian couplings. In Ref. [22], a connection was shown between a system’s solvability by this method and its *frustration graph*. This is the graph whose vertices correspond to terms in the spin Hamiltonian written in the given Pauli basis and are neighboring if the associated Pauli operators anticommute. It is shown in Ref. [22] that a generator-to-generator free-fermion solution is only possible if the frustration graph is a line graph. This property corresponds to the absence of certain *forbidden induced subgraphs* of the Hamiltonian frustration graph: anticommutation structures among subsets of Hamiltonian terms that obstruct a free-fermion solution. The line-graph characterization captures generator-to-generator mappings, and these generally accompany a set of symmetries associated to induced cycles — or holes — of the frustration graph.

More recently, a free-fermion-solvable model outside of the generalized Jordan-Wigner framework, called the four-fermion model, was given in a remarkable result by Fendley [23]. Here, the fermions correspond to nonlinear polynomials in the Pauli terms of the spin Hamiltonian, rather than individual terms. This solution maps the entire spin Hamiltonian onto the entire free-fermion Hamiltonian and is

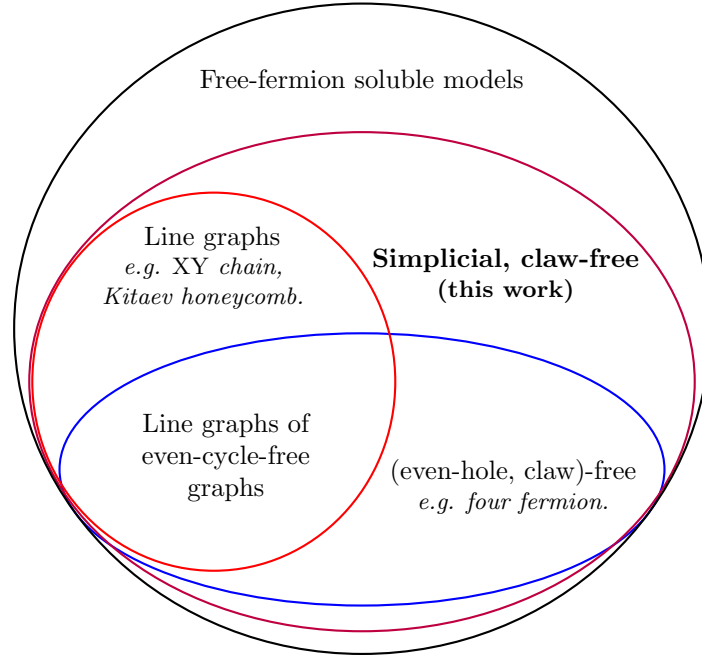


Figure 3.1: Summary of this work in relation to earlier results. In Ref. [22], it was shown that a generalized Jordan-Wigner (generator-to-generator) mapping exists if and only if the frustration graph of a given spin model is a line graph. In Ref. [126], it was shown that a more complicated solution of the type given in Ref. [23] holds when the graph is (even-hole, claw)-free. Though these two graph classes intersect at the class of line graphs of even-cycle-free graphs, neither class contains the other. In the present work, these methods to show that a somewhat more complicated free-fermion structure exists for simplicial, claw-free frustration graphs. We expect that there are still free-fermion solution methods beyond this characterization, including non-generic solutions.

generic despite apparently transcending the generator-to-generator structure. Surprisingly, a solution of this form is also revealed by the absence of certain forbidden induced subgraphs of the Hamiltonian frustration graph [126]. These forbidden subgraphs include $K_{1,3}$, or *the claw* — which is also a forbidden induced subgraph for line graphs — as well as all even holes. The two graph classes share some overlap, but also each include cases not present in the other. In a generalized Jordan-Wigner solution, even holes correspond to the aforementioned Pauli symmetries, and this strongly suggests the existence of a free-fermion solution framework unifying these two methods.

In this work, we formalize a graph-theoretic characterization unifying these two approaches. Our main result is summarized in Fig. 3.1. We show that if the frustration graph is claw-free and contains a structure called a simplicial clique, then it admits an exact free-fermion solution. We refer to this set of graphs as *simplicial, claw-free*. Both graph classes of Refs. [22, 126] have this property. It is an interesting consequence of our characterization that free-fermion solutions are generalized much in the same way as the graphs that describe them. Importantly, our result removes the even-hole assumption of Ref. [126], and so extends the non-local solution method given by Fendley to graphs with arbitrary spatial dimension in their coarse topology. We are able to relax this assumption by identifying a class of cycle-like symmetries, which generalize the cycle symmetries of generalized Jordan-Wigner solutions. This identification can be seen as our main technical insight.

This chapter is organized as follows. In the remainder of the introduction, we summarize our main results and analyze a small illustrative example. In Section 3.2 we review the concept of frustration graphs and standardize our notation. Section 3.3 gives a thorough background on free-fermion models. In Section 3.4, we review some properties of claw-free graphs. In the following sections, we prove our main results. Finally, we give a numerical example of a two-dimensional model which is not obviously free-fermion-solvable in Section 3.8. We conclude with a discussion of future work in Section 3.9.

3.1.1 Main Results

We consider many-body spin systems on n qubits with Hamiltonians written in the Pauli basis as

$$\begin{aligned} H &= \sum_{j \in V} b_j \sigma^j \\ &:= \sum_{j \in V} h_j \end{aligned} \tag{3.1}$$

where $V \subseteq \{I, x, y, z\}^{\times n}$ is a set of strings labeling the n -qubit Pauli operators in the natural way, and $h_j := b_j \sigma^j$ with $b_j \in \mathbb{R} \setminus \{0\}$.

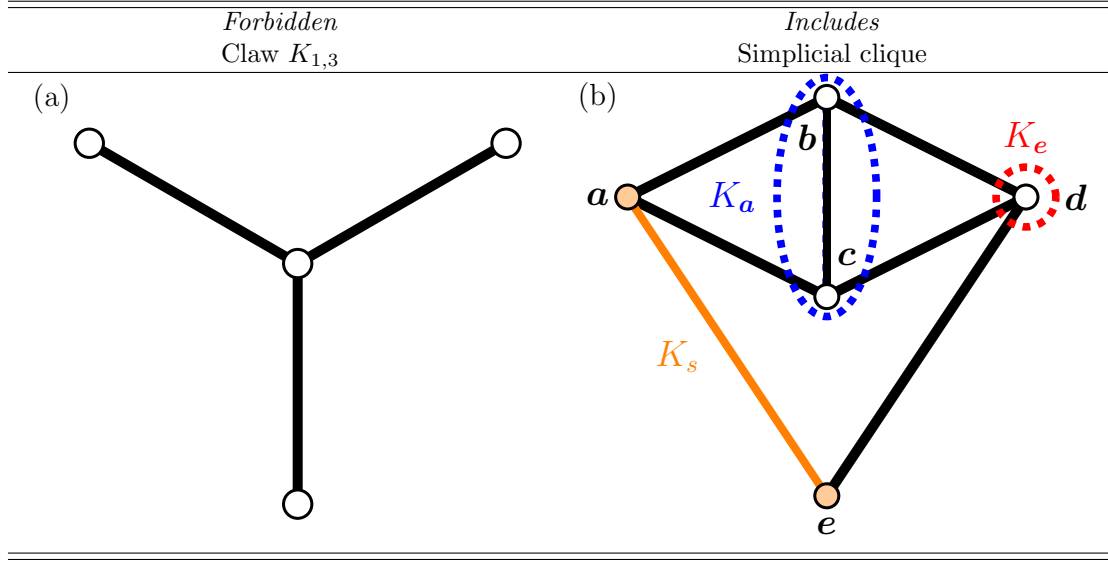


Table 3.1: (a) A graph is claw-free if no subset of its vertices induces a claw, $K_{1,3}$. (b) A simplicial clique, K_s (orange), is a clique such that the neighborhood of each vertex in K_s induces a clique in the graph $G \setminus K_s$. The simplicial clique is depicted in orange consisting of the vertices $\{a, e\}$. The neighborhood of the vertex a in $G \setminus K_s$ is the clique $K_a = \{b, c\}$. Similarly, the neighbourhood of e in $G \setminus K_s$ is the single vertex clique $K_e = d$. Crucially, our result captures frustration graphs containing even holes.

The *frustration graph* of H , $G := (V, E)$, is the graph with vertices given by nonzero Pauli terms in H , neighboring if the corresponding Paulis anticommute. Our main result extends the class of free-fermion-solvable spin Hamiltonians H based on their frustration graphs G .

Result 3.1 (Theorems 3.1 and 3.2). Let H be a Hamiltonian whose frustration graph, G , is claw-free and contains a simplicial clique. There exist commuting symmetries $\{J_G[\langle C_0 \rangle]\}_{\langle C_0 \rangle}$, defined in terms of induced cycles of G , such that each symmetric subspace with projector $\Pi_{\mathcal{J}}$ admits a free-fermion solution

$$H = \sum_{\mathcal{J}} \left(\sum_{j=1}^{\alpha(G)} \varepsilon_{\mathcal{J},j} [\psi_{\mathcal{J},j}, \psi_{\mathcal{J},j}^\dagger] \right) \Pi_{\mathcal{J}}. \quad (3.2)$$

where $\alpha(G)$ is the independence number of G . The fermionic ladder operators, $\{\psi_{\mathcal{J},j}\}_{\mathcal{J},j}$, are constructed from another set of commuting symmetries $\{Q_G^{(k)}\}_{k=0}^{\alpha(G)}$ defined in terms of independent sets of G . The single particle energies, $\{\varepsilon_{\mathcal{J},j}\}_{\mathcal{J},j}$, can be calculated from the roots of a generalized characteristic polynomial, $Z_G(-u^2)$, over each symmetric subspace specified by the $\Pi_{\mathcal{J}}$. Finally, the $\{J_G[\langle C_0 \rangle]\}_{\langle C_0 \rangle}$ and $\{Q_G^{(k)}\}_{k=0}^{\alpha(G)}$ commute with each other.

We prove the result by applying the solution method of Refs. [23, 126] independently to each symmetric subspace of H specified by the projector $\Pi_{\mathcal{J}}$. Notice that when there are no even holes,

there is only a single such subspace, and we recover the result proven in Ref. [126].

While our result gives an exact, explicit means to solve the Hamiltonian in Eq. (3.1), it is difficult to extract a physical picture for the fermion modes from the solution. We address this with our second main result.

Result 3.2 (Theorem 3.3 and Corollary 3.6). Given a Hamiltonian, H , with a simplicial, claw-free frustration graph, G . Let $\chi := \sigma^{\mathbf{j}^*}$ be a Pauli operator such that $\mathbf{j}^* \notin V$, and χ only anticommutes with every operator corresponding to the vertices in a simplicial clique of G . There exists a real matrix \mathbf{A} , whose elements are indexed by induced paths in $G \cup \{\mathbf{j}^*\}$, such that, over each mutual eigenspace of the $\{J_G[\langle C_0 \rangle]\}_{\langle C_0 \rangle}$, we have

$$\text{ad}_{iH}^k \chi = (-2i)^k \sum_{\mathcal{J}} \left[\sum_P (\mathbf{A}_{G,\mathcal{J}}^k)_{\{\mathbf{j}^*\},P} h_P \right] \Pi_{\mathcal{J}}. \quad (3.3)$$

where $\text{ad}_{iH} \chi := [iH, \chi]$. The matrix \mathbf{A} is the weighted adjacency matrix of a directed bipartite graph. The operators generated by repeated commutation with H satisfy

$$\{\text{ad}_{iH}^j \chi, \text{ad}_{iH}^k \chi\} = 2 \sum_{\mathcal{J}} (\mathbf{M}_{G,\mathcal{J}})_{jk} \Pi_{\mathcal{J}} \quad (3.4)$$

where the real matrix \mathbf{M} is positive definite.

Before we prove these results, we first consider a small, illustrative example, to see how they can be applied in practice.

3.1.2 A worked example

We consider the model defined on four qubits by the following Hamiltonian

$$\begin{aligned} H = & \sigma_1^x + \sigma_1^z + \sigma_1^x \sigma_2^x + \sigma_1^z \sigma_2^x \sigma_3^x + \sigma_1^y \sigma_2^z + \sigma_1^z \sigma_3^z \\ & + \sigma_1^z \sigma_2^x \sigma_3^y \sigma_4^x + \sigma_1^y \sigma_2^y \sigma_3^y \sigma_4^z. \end{aligned} \quad (3.5)$$

where we have set $b_j = 1$ for all $\mathbf{j} \in V$ for succinctness. Additionally, we denote each of the Hamiltonian terms as h_j , for $j \in \{1, 2, \dots, 8\}$, based on the order in which the term appears in Eq. (3.5).

The frustration graph of this model, shown in Fig. 3.2 claw-free, and contains the simplicial cliques

$$h_{C_1} = h_1 h_3 h_2 h_4 = \sigma_3^x$$

$$h_{C_2} = h_1 h_3 h_2 h_6 = \sigma_2^x \sigma_3^z$$

$$h_{C_3} = h_1 h_3 h_2 h_7 = \sigma_3^y \sigma_4^x$$

$$h_{C_4} = h_8 h_3 h_2 h_4 = -\sigma_1^z \sigma_2^y \sigma_3^z \sigma_4^z$$

$$h_{C_5} = h_5 h_3 h_2 h_6 = \sigma_1^z \sigma_2^y \sigma_3^z$$

$$h_{C_6} = h_8 h_3 h_2 h_7 = \sigma_1^z \sigma_2^y \sigma_4^y$$

$$h_{C_7} = h_8 h_7 h_6 h_4 = \sigma_4^z$$

$$h_{C_8} = h_8 h_6 h_5 h_7 = -\sigma_3^z \sigma_4^y.$$

This gives the following generalized cycle symmetries

$$J_1 \equiv J_G[\langle C_1 \rangle] = \sum_{k=1}^6 h_{C_k} \quad (3.6)$$

$$J_2 \equiv J_G[\langle C_7 \rangle] = \sum_{k=7}^8 h_{C_k} \quad (3.7)$$

Unlike in the case where G is a line graph, these cycle symmetries do not generally square to an operator proportional to the identity, and so they are not proportional to Pauli operators in any basis. Rather, we have

$$J_1^2 = 6I - 2J_2 \quad (3.8)$$

$$J_2^2 = 2I \quad (3.9)$$

Thus, J_1 and J_2 commute, as we expect. The generalized characteristic polynomial of a model is constructed by taking the independence polynomial of the frustration graph, G , and then subtracting the generalized even hole operators. Since these operators commute, we can then simultaneously diagonalize them and find a distinct polynomial over each symmetric subspace. For this model, we arrive at the polynomial

$$Z_G(x) = 1 + 8x + 9x^2 - 2(J_1 + J_2)x^2. \quad (3.10)$$

By solving $Z_G(-u^2)$ for u for the various eigenvalues of the even hole operators, we are able to calculate the single particle energies of the model in each of the mutual eigenspaces.

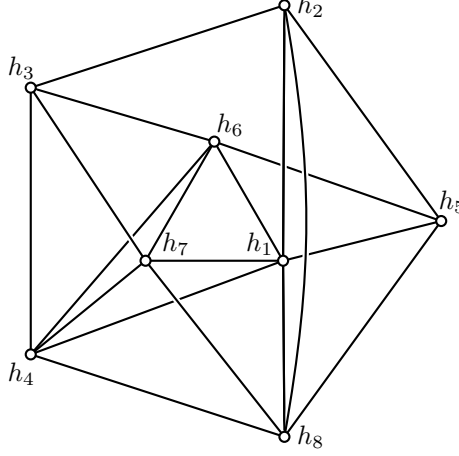


Figure 3.2: The frustration graph of a small, illustrative example on four qubits. Clearly the graph is not a line graph, but it is claw-free and contains a simplicial clique.

Let $\Pi_{\mathcal{J}}$ be the projector onto the eigenspace of J_1 with eigenvalue \mathcal{J}_1 , corresponding to the eigenspace of J_2 with eigenvalue \mathcal{J}_2 as $\mathcal{J}_1 = \pm\sqrt{6-2\mathcal{J}_2}$. Additionally, let us identify the simplicial clique formed by the vertices associated with the terms $\{h_1, h_2, h_5, h_8\}$ and define

$$\chi = \sigma_1^y \sigma_2^y \sigma_3^x \sigma_4^z. \quad (3.11)$$

Finally, let $K^{(\ell)}$ be the sum of all path operators with endpoint \mathbf{j}^* and length ℓ , where we take $K^{(0)} = \chi$ as our convention. We complete the free fermion solution by taking repeated commutators

$$\text{ad}_{iH}^0 \chi = K^{(0)} \quad (3.12)$$

$$\text{ad}_{iH}^1 \chi = -2iK^{(1)} \quad (3.13)$$

$$\text{ad}_{iH}^2 \chi = (-2i)^2(4K^{(0)} + K^{(2)}) \quad (3.14)$$

$$\text{ad}_{iH}^3 \chi = (-2i)^3 \left[(4K^{(1)} + K^{(3)}) \right. \quad (3.15)$$

$$\left. + (3\chi h_1 + \chi h_2 + \chi h_5 + 2\chi h_8) \right]$$

$$\text{ad}_{iH}^4 \chi = (-2i)^4 \left\{ [23 - 2(J_1 + J_2)] K^{(0)} + 8K^{(2)} \right\} \quad (3.16)$$

$$\text{ad}_{iH}^4 \chi = -(-2i)^4 (9 + 2J_1 + 2J_2) (\text{ad}_{iH}^0 \chi) \quad (3.17)$$

$$+ 8(2)^2 (\text{ad}_{iH}^2 \chi)$$

In the last line, we see that the fourth nested commutator is a linear combination of the previous

ones, so we have the characteristic polynomial

$$f_{\mathcal{J}_1, \mathcal{J}_2}(u) = u^4 - 32u^2 + 16(9 + 2\mathcal{J}_1 + 2\mathcal{J}_2) \quad (3.18)$$

and single particle energies given by

$$\varepsilon_{\mathcal{J}, \mathcal{J}_2, \pm} = \sqrt{4 \pm \sqrt{7 - 2\mathcal{J}_1 - 2\mathcal{J}_2}}. \quad (3.19)$$

3.2 Frustration Graphs

Here we explain frustration graphs in-detail and standardize our graph-theoretic notation. A graph $G = (V, E)$ is a set V of vertices, together with a set $E \subset V^{\times 2}$ of two-element subsets of V called edges. Vertices $\mathbf{j}, \mathbf{k} \in V$ are said to be *neighboring* if there is an edge $(\mathbf{j}, \mathbf{k}) \in E$. Edges $(\mathbf{j}, \mathbf{k}), (\mathbf{u}, \mathbf{v}) \in E$ are said to be *incident* if they share a vertex: $|\{\mathbf{j}, \mathbf{k}\} \cap \{\mathbf{u}, \mathbf{v}\}| = 1$. A vertex $\mathbf{j} \in V$ and edge $(\mathbf{u}, \mathbf{v}) \in E$ are similarly incident if $\mathbf{j} \in \{\mathbf{u}, \mathbf{v}\}$. The *order* of a graph is the cardinality $|V|$ of its vertex set; the *size* of a graph is the cardinality $|E|$ of its edge set.

Because Pauli operators only either commute or anticommute, it is convenient to describe these relations between terms in a spin Hamiltonian by a graph.

Definition 3.1 (Frustration Graph). The frustration graph of the Hamiltonian H in Eq. (3.1) is the graph $G = (V, E)$ with

$$E := \{(\mathbf{j}, \mathbf{k}) \mid h_{\mathbf{j}}h_{\mathbf{k}} = -h_{\mathbf{k}}h_{\mathbf{j}}\}. \quad (3.20)$$

The frustration graph is always simple; there are no self loops because every Hamiltonian term commutes with itself, and there is at most one edge per pair of terms. For this work, we additionally assume all models have finitely many terms, so the frustration graphs we consider are finite. Without loss of generality, we assume that distinct vertices in the frustration graph correspond to linearly independent Pauli terms in H . We can always collect repeated Paulis by adding their coefficients $b_{\mathbf{j}}$. The commutation relation between Pauli terms is clearly unchanged by including the coefficients in their definitions, so we prefer to give statements in terms of the $h_{\mathbf{j}}$ rather than the $\sigma^{\mathbf{j}}$, with the understanding that $h_{\mathbf{j}}^2 = b_{\mathbf{j}}^2$. The frustration graph thus naturally captures properties of the spin model that do not depend on the coefficients. We refer to such properties as *generic*.

We next consider subsets of Hamiltonian terms and the associated induced subgraphs of the frustration graph. To this end, we define our labeling scheme in Eq. (3.1) more precisely. We can equivalently describe a Pauli string $\mathbf{j} \in \{I, x, y, z\}^{\times n}$ by a binary string on $2n$ bits by associating each single-qubit pauli label to a 2-bit string as $I \rightarrow \begin{pmatrix} 0 & 0 \end{pmatrix}$, $x \rightarrow \begin{pmatrix} 1 & 0 \end{pmatrix}$, $z \rightarrow \begin{pmatrix} 0 & 1 \end{pmatrix}$, and $y \rightarrow \begin{pmatrix} 1 & 1 \end{pmatrix}$. Let $\mathbf{j} := \begin{pmatrix} \mathbf{j}_x & \mathbf{j}_z \end{pmatrix} \in \{0, 1\}^{\times 2n}$ be the binary vector such that the k th component of \mathbf{j}_x , $j_{x,k}$, is the first bit of the k th qubit label according to this association, and, similarly, $j_{z,k}$ is the second bit of the k th qubit label. This gives

$$\sigma^{\mathbf{j}} = i^{\mathbf{j}_x \cdot \mathbf{j}_z} \left[\bigotimes_{k=1}^n (\sigma_k^x)^{j_{x,k}} \right] \left[\bigotimes_{k=1}^n (\sigma_k^z)^{j_{z,k}} \right] \quad (3.21)$$

where $\mathbf{j}_x \cdot \mathbf{j}_z := \sum_{k=1}^n j_{x,k} j_{z,k}$ denotes the Euclidean inner product.

The scalar commutator between Paulis is defined implicitly via

$$\sigma^{\mathbf{j}} \sigma^{\mathbf{k}} = \llbracket \sigma^{\mathbf{j}}, \sigma^{\mathbf{k}} \rrbracket \sigma^{\mathbf{k}} \sigma^{\mathbf{j}}. \quad (3.22)$$

Since Pauli operators only commute or anticommute, we have $\llbracket \sigma^{\mathbf{j}}, \sigma^{\mathbf{k}} \rrbracket = \pm 1$. This sign factor is given by

$$\llbracket \sigma^{\mathbf{j}}, \sigma^{\mathbf{k}} \rrbracket = (-1)^{\langle \mathbf{j}, \mathbf{k} \rangle}, \quad (3.23)$$

where $\langle \mathbf{j}, \mathbf{k} \rangle := \sum_{m=1}^n (j_{x,m} k_{z,m} + j_{z,m} k_{x,m}) \pmod{2}$ is the binary symplectic inner product. The scalar commutator distributes over multiplication as

$$\llbracket A, BC \rrbracket = \llbracket A, B \rrbracket \llbracket A, C \rrbracket, \quad (3.24)$$

and, accordingly, the binary symplectic inner product is linear in \mathbf{j} and \mathbf{k} . Because commutation relations between operators are unchanged upon multiplying the operators by nonzero constants, the scalar commutator and binary symplectic inner product are well-defined for the operators $\{h_{\mathbf{j}}\}_{\mathbf{j} \in V}$ as well.

For a subset $U \subset V$, the *induced subgraph* $G[U]$ is the subgraph of G whose vertex set is U and whose edge set $E[U] = E \cap U^{\times 2}$ consists of all edges in G which have both endpoints in U . We will often refer to the vertex subset interchangeably with the subgraph it induces. Similarly, we will use set-theoretic notation to denote the exclusion of vertices, e.g., $G \setminus U = G[V \setminus U]$.

An important family of vertex-subsets is given by the neighborhoods of vertices in the graph.

Definition 3.2 (Open and closed neighborhoods, degree). The *open neighborhood* of $\mathbf{j} \in V$ is the set given by

$$\Gamma(\mathbf{j}) := \{\mathbf{k} \mid (\mathbf{j}, \mathbf{k}) \in E\}, \quad (3.25)$$

and the *closed neighborhood* of \mathbf{j} is $\Gamma[\mathbf{j}] := \Gamma(\mathbf{j}) \cup \{\mathbf{j}\}$. The *degree* of \mathbf{j} , $\Delta(\mathbf{j}) := |\Gamma(\mathbf{j})|$, is the order of its open neighborhood.

We often refer to the open or closed neighborhood of a vertex \mathbf{j} in a subset of vertices $U \subset V$ by $\Gamma_U(\mathbf{j}) := \Gamma(\mathbf{j}) \cap U$. Similarly, $\Gamma_U[\mathbf{j}] := \Gamma_U(\mathbf{j}) \cup \{\mathbf{j}\}$. Note that we do not necessarily assume $\mathbf{j} \in U$ for this definition. Accordingly, we refer to the degree in a subset by $\Delta_U(\mathbf{j}) := |\Gamma_U(\mathbf{j})|$. We will also refer to the closed neighborhood of a subset $U \subseteq V$ by $\Gamma[U] = \bigcup_{\mathbf{j} \in U} \Gamma[\mathbf{j}]$, and similarly for the open neighborhood where there is no ambiguity.

One useful consequence of the binary linear structure of the commutation relations between Hamiltonian terms is that it allows us to talk about commutation relations between products over subsets of terms. We can thus extract such commutation relations from the graph itself. In general, we will let

$$h_U := \prod_{\mathbf{j} \in U} h_{\mathbf{j}} \quad (3.26)$$

be the product of all operators whose vertices in G are members of a particular subset $U \subseteq V$. Because re-ordering the operators in this product contributes an overall sign factor to h_U , the operator ordering is irrelevant to the commutation relations between h_U and other products of Hamiltonian terms. We will define the operator ordering for specific families of vertex subsets on a case-by-case basis. With these definitions, we have

$$[h_{\mathbf{j}}, h_U] = (-1)^{\Delta_U(\mathbf{j})} \quad (3.27)$$

for any $\mathbf{j} \in V$. That is, $\langle \mathbf{j}, \sum_{\mathbf{k} \in U} \mathbf{k} \rangle = \Delta_U(\mathbf{j}) \pmod{2}$ as we expect. We denote the symmetric difference between vertex subsets $U, W \subseteq V$ by $U \oplus W := (U \setminus W) \cup (W \setminus U)$. Applying the constraint that $h_{\mathbf{j}}^2 \propto I$ gives

$$[h_{\mathbf{j}}, h_{U \oplus W}] = [h_{\mathbf{j}}, h_U][h_{\mathbf{j}}, h_W], \quad (3.28)$$

so the commutation relation between h_j and h_U is only changed by taking the symmetric difference with W if h_j and h_W anticommute. When the graph is claw-free, often the parity of the degree alone is enough to fix the neighboring relation between j and a particular graph structure U . We go on to define several important such structures.

An *independent set* S in G is a subset of vertices with no edges between them (i.e. $E[S] = \emptyset$). For the corresponding operator, h_S , the ordering of the factors in the product is irrelevant, as these factors commute with one another. The independence number $\alpha(G)$ is the order of the largest independent set in G . We denote \mathcal{S}_G as the collection of all independent sets from G and let $\mathcal{S}_G^{(k)}$ denote the collection of all independent sets of order k from G . A *matching* M in G is a subset of edges such that no two edges in M are incident. A *perfect matching* is a matching such that every vertex in V is incident to exactly one edge in the matching. Clearly, a graph can only have a perfect matching if its order is even. We denote \mathcal{M}_G as the collection of all matchings in G and let $\mathcal{M}_G^{(k)}$ denote the collection of all matchings of k edges from G .

The *claw* is the graph consisting of a central vertex neighboring to every vertex in an independent set of order three (see Table 3.1). That is, it is the complete bipartite graph $K_{1,3}$. The vertices in the three-vertex independent set are called the *leaves* of the claw. A graph is *claw-free* if it does not include the claw as an induced subgraph. When we list a subset of vertices that induces a claw, we will generally order the list by the central vertex followed by the leaves.

A *path* is a set of distinct vertices $P = \{j_i\}_{i=0}^\ell$ with j_i neighboring to j_{i+1} for $i \in \{0, \dots, \ell-1\}$. The vertices $\{j_0, j_\ell\}$ are the *endpoints* of the path, and the quantity ℓ is the *length* of the path. When $P \subseteq V$ is a subset of vertices such that $E[P] = \{(j_i, j_{i+1})\}_{i=0}^{\ell-1}$, we say P is an *induced path*. That is, there are no edges in $G[P]$ other than those between vertices with consecutive indices in the path, of which there are ℓ . We refer to the index i as the *distance* from j_i to j_0 along P in this case, and we give the vertex labeling for P as

$$P := j_0 - j_1 - \dots - j_\ell. \quad (3.29)$$

For the corresponding operator, h_P , we similarly order the factors from left to right according to their distance from an endpoint in accordance with the labeling above. We denote the set of all induced paths in G by \mathcal{P}_G and the set of all induced paths in G of length ℓ by $\mathcal{P}_G^{(\ell)}$. We also define P_k as the subpath of P induced by the vertices up to j_k : $P_k = \{j_i\}_{i=0}^k$.

A *cycle* is a set of distinct vertices $C = \{j_i\}_{i=0}^{\ell-1}$ with j_i neighboring to j_{i+1} for $i \in \{0, \dots, \ell-1\}$ with index addition taken modulo ℓ . The quantity ℓ is the length of the cycle. When $C \subseteq V$ is a

subset of vertices such that $E[C] = \{(\mathbf{j}_i, \mathbf{j}_{(i+1) \pmod{\ell}})\}_{i=0}^{\ell-1}$ for $\ell \geq 4$, we say C is an *induced cycle* or *hole*. In this case, $\ell = |C|$ is the number of vertices and edges of the hole. An *even hole* is a hole with an even number of vertices and edges. If C is an even hole with length $\ell = 2k$, then there are two unique independent sets of size $k > 1$ in C , which we refer to as the coloring classes of C . Let these coloring classes be C_a and C_b . We label the vertices of C with distinct labels for the vertices in each coloring class as

$$C := \mathbf{b}_0\text{-}\mathbf{a}_0\text{-}\mathbf{b}_1\text{-}\mathbf{a}_1\text{-}\dots\text{-}\mathbf{b}_{k-1}\text{-}\mathbf{a}_{k-1}\text{-}\mathbf{b}_0 \quad (3.30)$$

where $\{\mathbf{a}_j\}_{j=0}^{k-1} := C_a$ and $\{\mathbf{b}_j\}_{j=0}^{k-1} := C_b$. Here, we take addition in the indices of these vertices modulo k . We choose the factor-ordering for the operator corresponding to C as $h_C = h_{C_a}h_{C_b}$, where the ordering within each of the coloring-class factors is again irrelevant as these are independent sets. Furthermore, we are free to exchange the ordering of h_{C_a} and h_{C_b} , as these operators commute. We denote the set of all even holes in G by $\mathcal{C}_G^{(\text{even})}$ and the set of all even holes in G of length ℓ by $\mathcal{C}_G^{(\ell)}$. We say two even holes $C, C' \in \mathcal{C}_G^{(\text{even})}$ are compatible if and only if $G[C \cup C']$ is a disconnected graph whose components are $G[C]$ and $G[C']$. We let $\mathcal{C}_G^{(\text{even})}$ denote the collection of all subsets of $\mathcal{C}_G^{(\text{even})}$ that are pairwise compatible. For a given such subset $\mathcal{X} \subseteq \mathcal{C}_G^{(\text{even})}$ (i.e. $\mathcal{X} \in \mathcal{C}_G^{(\text{even})}$), we take

$$\partial\mathcal{X} := \bigcup_{C \in \mathcal{X}} C \quad (3.31)$$

to be the set of vertices in \mathcal{X} . Let $|\mathcal{X}|$ denote the number of even-hole components in \mathcal{X} , and $|\partial\mathcal{X}|$ be the total length of all the elements of \mathcal{X} .

A *clique* K in G is a subset of vertices such that every pair of vertices in K is neighboring. A *simplicial clique* K_s is a clique such that, for every vertex $\mathbf{j} \in K_s$, $\Gamma(\mathbf{j})$ induces a clique in $G \setminus K_s$ (see Table 3.1). A graph is *simplicial* if it contains a simplicial clique. We say that a Hamiltonian is *simplicial*, *claw-free* (SCF) if its frustration graph is claw-free and contains a simplicial clique.

The aforementioned graph structures all play important roles in the free-fermion solvability of a Hamiltonian with frustration graph G , as we will see.

3.3 Free-Fermion Models

3.3.1 Exact Solution

A free-fermion Hamiltonian has the form

$$H_f = i \sum_{(j,k) \in E_f} h_{jk} \gamma_j \gamma_k \quad (3.32)$$

$$:= \frac{i}{2} \boldsymbol{\gamma}^T \cdot \mathbf{h} \cdot \boldsymbol{\gamma} \quad (3.33)$$

where we collect the set of *Majorana fermion modes* in the vector $\boldsymbol{\gamma} := (\gamma_j)$ and the Hamiltonian coefficients in the *single-particle Hamiltonian* $\mathbf{h} := (h_{ij})$. We denote the set of Majorana indices by V_f and the set of pairs (j, k) of distinct elements of V_f for which h_{jk} is nonzero as E_f . The graph $R := (V_f, E_f)$ is the *Majorana hopping graph*.

The Majorana modes satisfy the canonical anticommutation relations

$$\{\gamma_j, \gamma_k\} := \gamma_j \gamma_k + \gamma_k \gamma_j = 2\delta_{jk} I \quad (3.34)$$

Products of Majorana operators only commute or anticommute and square to $\pm I$. Without loss of generality, we take \mathbf{h} to be antisymmetric, since any symmetric part of \mathbf{h} will only contribute a physically irrelevant identity term to H_f by Eq. (3.34).

The relations in Eq. (3.34) imply that linear combinations of the Majorana modes are preserved under commutation with the Hamiltonian

$$\text{ad}_{H_f} \gamma_j := [H_f, \gamma_j] = -2i (\mathbf{h} \cdot \boldsymbol{\gamma})_j \quad (3.35)$$

where we remind the reader of our definition of ad_{H_f} below Result 3.2. This gives

$$e^{iH_f t} \gamma_j e^{-iH_f t} = (e^{2\mathbf{h}t} \cdot \boldsymbol{\gamma})_j, \quad (3.36)$$

and $e^{2\mathbf{h}t}$ is called the *single-particle transition matrix*. Because \mathbf{h} is antisymmetric, $e^{2\mathbf{h}t}$ is an orthogonal matrix in the group $SO(|V_f|)$. Thus, conjugation by free-fermion unitary evolution preserves the canonical anticommutation relations (3.34).

Similarly, we can find an orthogonal matrix $e^{\mathbf{w}}$ that block-diagonalizes \mathbf{h} as

$$e^{-\mathbf{w}} \cdot \mathbf{h} \cdot e^{\mathbf{w}} = \bigoplus_{j=1}^{|V_f|/2} \begin{pmatrix} 0 & -\varepsilon_j \\ \varepsilon_j & 0 \end{pmatrix} \quad (3.37)$$

if $|V_f|$ is even. If $|V_f|$ is odd, then the tensor sum runs to $\lfloor |V_f|/2 \rfloor$, and \mathbf{h} has an additional zero eigenvalue. Choosing $W := e^{-\frac{i}{4}(\gamma^T \cdot \mathbf{w} \cdot \gamma)}$ gives

$$W^\dagger H_f W = -i \sum_{j=1}^{\lfloor |V_f|/2 \rfloor} \varepsilon_j \gamma_{2j-1} \gamma_{2j}. \quad (3.38)$$

It is convenient to pair the Majorana modes in this basis to define the fermionic *eigenmodes* $\{\psi_j\}_{j=1}^{\lfloor |V_f|/2 \rfloor}$ as

$$W^\dagger \psi_j W = \frac{1}{2} (\gamma_{2j-1} + i\gamma_{2j}) \quad j \in \{1, \dots, \lfloor |V_f|/2 \rfloor\} \quad (3.39)$$

These operators satisfy the canonical anticommutation relations for fermionic ladder operators

$$\{\psi_j, \psi_k\} = 0 \quad \{\psi_j, \psi_k^\dagger\} = \delta_{jk} I, \quad (3.40)$$

and this gives

$$H_f = \sum_{j=1}^{\lfloor |V_f|/2 \rfloor} \varepsilon_j [\psi_j, \psi_j^\dagger]. \quad (3.41)$$

The linear map ad_{H_f} satisfies the conventional eigenvector relation with respect to the eigenmodes

$$[H_f, \psi_j] = \varepsilon_j \psi_j \quad (3.42)$$

and we see that the free-fermion Hamiltonian H_f has spectrum given by

$$\mathcal{E}_{\mathbf{x}} = \sum_{j=1}^{\lfloor |V_f|/2 \rfloor} (-1)^{x_j} \varepsilon_j \quad \mathbf{x} \in \{0, 1\}^{\times \lfloor |V_f|/2 \rfloor}. \quad (3.43)$$

The quantities $\{\varepsilon_j\}$ are called the *single-particle energies*, and we can generate eigenstates of H_f by applying W^\dagger to the mutual eigenstates of the operators $\{-i\gamma_{2j-1}\gamma_{2j}\}$.

The single-particle energies are the reciprocals of the roots of the polynomial

$$f_{\mathbf{h}}(u) = \det(\mathbf{I} - iu\mathbf{h}) \quad (3.44)$$

$$= \sum_{U \subseteq V_{\mathbf{f}}} (-iu)^{|U|} \det(\mathbf{h}_{UU}) \quad (3.45)$$

where \mathbf{h}_{UU} is the principal submatrix of \mathbf{h} with rows and columns indexed by the elements of U . This polynomial is in-fact the reciprocal polynomial to the characteristic polynomial of \mathbf{h} . We will need the expression of this polynomial in terms of the graph structures of R . Because \mathbf{h}_{UU} is antisymmetric, its determinant is the square of the Pfaffian:

$$\det(\mathbf{h}_{UU}) = \text{Pf}(\mathbf{h}_{UU})^2. \quad (3.46)$$

The Pfaffian is defined to be zero if $|U|$ is odd, and

$$\text{Pf}(\mathbf{h}_{UU}) = \sum_{M \in \mathcal{M}_{R[U]}^{(|U|/2)}} (-1)^{\pi(M)} \prod_{\substack{(j,k) \in M \\ j < k}} h_{jk} \quad (3.47)$$

if $|U|$ is even. The sign factor $(-1)^{\pi(M)}$ is defined implicitly as the factor incurred upon sorting the individual Majorana-mode factors in $\prod_{\{(j,k) \in M | j < k\}} (\gamma_j \gamma_k)$ such that indices are ascending from left to right. This gives

$$\begin{aligned} f_{\mathbf{h}}(u) &= \sum_{\substack{M, M' \in \mathcal{M}_R \\ |M| = |M'|}} (-u^2)^{|M|} (-1)^{\pi(M) + \pi(M')} \\ &\quad \times \left(\prod_{\substack{(j,k) \in M \\ j < k}} h_{jk} \right) \left(\prod_{\substack{(j,k) \in M' \\ j < k}} h_{jk} \right) \end{aligned} \quad (3.48)$$

We will return to this explicit expression in the following sections.

In Eq. (3.35) we show that a single commutation of a given Majorana mode with the free-fermion Hamiltonian gives a linear combination of the Majorana modes transformed by the single-particle Hamiltonian. Let us now consider nesting these commutators - note that we now include a factor of i , as in Theorem 3.3, with the Hamiltonian to ensure that the resulting linear map is positive

$$\text{ad}_{iH_{\mathbf{f}}}^k \gamma_j = (-2)^k (\mathbf{h}^k \cdot \boldsymbol{\gamma})_j. \quad (3.49)$$

Therefore, we can see that H_f will satisfy the characteristic polynomial (the reciprocal polynomial of Eq. (3.45)).

Furthermore, we have

$$\{\text{ad}_{iH_f}^k \gamma_j, \text{ad}_{iH_f}^\ell \gamma_j\} = (-2)^{k+\ell} (\mathbf{h}^{k+\ell})_{jj} I \quad (3.50)$$

Analogous to the relations above are indicative of the existence of a free-fermion solution, as we will see in Sect. 3.7.

3.3.2 Generalized Jordan-Wigner Solutions

Remarkably, the exact solvability of free-fermion models can be leveraged to find exact solutions to spin models, which are not explicitly given in terms of free fermions. If one can find the proper identification of spin and fermionic degrees of freedom, one can treat the spin model as an effective free-fermion model and apply the exact solution method. One way to do this is to identify each term in a given spin model H with a corresponding term in H_f such that commutation relations between terms are preserved. Such a solution is called a *generator-to-generator mapping*. This family of solutions includes the celebrated Jordan-Wigner transformation as well as the exact solution to the Kitaev honeycomb model. For this reason, it is also called a *generalized Jordan-Wigner solution*.

Graph theory allows us to make this procedure systematic using the frustration graph of H . Note that, for a given free-fermion Hamiltonian H_f , the frustration graph has a particular structure due to the canonical anticommutation relations (3.34). It is the graph whose vertices are the edges of the fermion hopping graph, R , with vertices adjacent in the frustration graph if and only if the corresponding edges of R are incident. That is, the frustration graph of H_f is the *line graph* of R .

Definition 3.3 (Line graph). Given a graph $R := (V, E)$, the *line graph* of R , $L(R) := (E, F)$, is the graph whose vertices correspond to the edges of R , and

$$F := \{(e, f) \mid e, f \in E, |e \cap f| = 1\}. \quad (3.51)$$

R is called the *root graph* of $L(R)$.

Not every graph can be realized as the line graph of another graph. In particular, note that a line graph is always claw-free, as three edges cannot all be incident to a fourth edge without at least two of those edges being incident to each other. In fact, line graphs are characterized by a complete set of

nine forbidden subgraphs that includes the claw [104]. Using the notation of Def. 3.3, a vertex $j \in V$ in R is mapped to the clique $K_j := \{(j, k)\}_{k \in \Gamma(j)} \subseteq E$ in $L(R)$ under the line graph mapping. Because every edge has two vertices, it is an equivalent characterization of line graphs that the edges of a line graph $L(R)$ can be partitioned into cliques such that every vertex in $L(R)$ is a member of at most two cliques [98]. Furthermore, every such clique K_j in $L(R)$ is *simplicial* because $\Gamma_{L(R) \setminus K_j}[e] = K_k$ for $e = (j, k) \in E$. Thus, line graphs are automatically simplicial and claw-free. Similarly, a path of length ℓ in R is mapped to an induced path of length $\ell - 1$ in $L(R)$, and a cycle of length ℓ in R is mapped to a hole of length ℓ in $L(R)$. Conversely, for every induced path in $L(R)$, there is a unique corresponding path in R ; for every hole in $L(R)$, there is a unique corresponding cycle in R . A matching of size k in R is mapped to an independent set of order k in $L(R)$, and for every independent set in $L(R)$, there is a unique matching in R .

In Ref. [22], it was shown that an injective generator-to-generator mapping from H to a free-fermion Hamiltonian H_f exists if and only if its frustration graph is a line graph. This allows us to associate each vertex $\mathbf{j} \in V$ of the frustration graph G with an edge $\varphi(\mathbf{j}) := (\varphi_1(\mathbf{j}), \varphi_2(\mathbf{j})) \in E_f$ of the fermion hopping graph R . We choose an ordering on the vertices V_f , and our convention on φ is such that $\varphi_1(\mathbf{j}) < \varphi_2(\mathbf{j})$. While this mapping guarantees that commutation relations between terms are preserved, it does not necessarily give the correct products of free-fermion terms, since, for example, we can multiply a free-fermion term by any real number without changing the commutation relations. The products between free-fermion terms are enforced through constraints. The constraint that $h_j^2 = b_j^2$ guarantees that we must identify h_j with one of $\pm i|b_j|\gamma_{\varphi_1(\mathbf{j})}\gamma_{\varphi_2(\mathbf{j})}$. Because $\gamma_j\gamma_k = -\gamma_k\gamma_j$ for $j \neq k$, we can equivalently consider that R is a directed graph with arc $(j \rightarrow k) \in E_f$ if $ih_{jk}\gamma_j\gamma_k$ appears in H_f and $h_{jk} > 0$. The association of a direction to every edge in R is called an orientation of R , which we denote by τ . Concretely, we say that τ fixes the free-fermion mapping by identifying h_j with $i(-1)^{\tau(\mathbf{j})}|b_j|\gamma_{\varphi_1(\mathbf{j})}\gamma_{\varphi_2(\mathbf{j})}$ with $\tau(\mathbf{j}) \in \{0, 1\}$ for all $\mathbf{j} \in V$. We choose the orientation τ by imposing additional constraints, which correspond to restricting H to a mutual eigenspace of its commuting *cycle symmetries*.

Let $C_f := \{j_i\}_{i=0}^{\ell-1} \subseteq V_f$ be a cycle in R , and denote $C := \{\mathbf{j}_i\}_{i=0}^{\ell-1} \subseteq V$ as the *hole* in G such that $\varphi(\mathbf{j}_i) = (j_i, j_{i+1}) \in E_f$, with index addition taken modulo ℓ . We have

$$\prod_{i=0}^{\ell-1} (\gamma_{j_i} \gamma_{j_{i+1}}) = \prod_{j \in C_f} \gamma_j^2 = I. \quad (3.52)$$

Thus, we have that the *cycle symmetry*

$$h_C := \prod_{j \in C} h_j \quad (3.53)$$

commutes with every term in H by the requirement that the generator-to-generator mapping preserve commutation relations. Furthermore, cycle symmetry operators $h_C, h_{C'}$ mutually commute for distinct holes $C, C' \subset V$ because they themselves are products of terms from H . While h_C is not proportional to the identity in general, h_C^2 is. Under the free-fermion solution, h_C maps to

$$\prod_{j \in C} \left(i(-1)^{\tau(j)} |b_j| \gamma_{\varphi_1(j)} \gamma_{\varphi_2(j)} \right) = \pm i^{|C|} \left(\prod_{j \in C} |b_j| \right) \quad (3.54)$$

Thus, choosing an orientation τ is equivalent to fixing a mutual set of symmetry eigenvalues, and we have a unique free-fermion solution for every such restriction. It is shown in Ref. [22] that every mutual set of symmetry eigenvalues corresponds to an orientation of R .

Finally, the parity operator

$$P := i^{\frac{1}{2}|V_f|(|V_f|-1)} \prod_{j \in V_f} \gamma_j \quad (3.55)$$

is always a symmetry of H_f . When $|V_f|$ is even, this operator can be constructed from terms in H_f using edges from a structure called a *T-join* of R . A perfect matching is a special case of a *T-join*, and a graph with even order will have a *T-join* even if it does not have a perfect matching. If M is a perfect matching in R , then P can be constructed as the product $\left(\prod_{(j,k) \in M} i \gamma_j \gamma_k \right)$. However, the corresponding product, h_M , of terms from H may give the identity, so we must only consider a fixed-parity restriction of H_f as a solution to the spin model.

3.3.3 “Hidden” Free-Fermion Modes

We now consider the much more detailed problem of finding a free-fermion solution to a spin model whose frustration graph is not a line graph. In this case, there is no direct mapping from terms in H to terms in *any* free-fermion Hamiltonian H_f of the form in Eq. (3.32). However, it may still be possible to find a free-fermion solution to H . The essential idea is to treat independent sets, cliques, induced paths, and holes algebraically as though they result from a line graph mapping, even though there is no associated root graph. Our foray into this problem is the machinery of transfer matrices. We first need to define the following set of operators, related to independent sets of the frustration

graph G .

Definition 3.4 (Independent-set charges). The independent-set charges $\{Q_G^{(k)}\}_{k=0}^{\alpha(G)}$ are defined as the sum over independent sets of order k in G by

$$Q_G^{(k)} = \sum_{S \in \mathcal{S}_G^{(k)}} h_S. \quad (3.56)$$

Note that $Q_G^{(1)} := H$. By convention, $Q_G^{(0)} := I$, and $Q_G^{(k)} = 0$ for $k < 0$.

It is shown in Ref. [126] that the independent-set charges $Q_G^{(k)}$ commute with each other when G is claw-free. Because $Q_G^{(1)} = H$, the independent-set charges are conserved as well.

The independent set charges satisfy a recursion relation due to the fact that no independent set can have more than one vertex in a clique of G . For a given clique $K \subseteq V$, we partition terms in $Q_G^{(k)}$ according to independent sets with no vertices in K and those with exactly one vertex in K . This gives

$$Q_G^{(k)} = Q_{G \setminus K}^{(k)} + \sum_{j \in K} h_j Q_{G \setminus \Gamma[j]}^{(k-1)}. \quad (3.57)$$

When $K = K_s$ is a simplicial clique, we define

$$K_j \equiv \Gamma[j] \setminus (K_s \setminus \{j\}) \quad (3.58)$$

as the clique such that $\Gamma[j] = K_s \cup K_j$. Note that we define K_j such that $j \in K_j$. In this case, we can show the following lemma

Lemma 3.1. With the definitions above, we have

$$Q_G^{(k)} = Q_{G \setminus K_s}^{(k)} + \sum_{j \in K_s} Q_{G \setminus K_j}^{(k-1)} h_j \quad (3.59)$$

where K_s is a simplicial clique in the claw-free graph G .

We prove Lemma 3.1 in Sect. 3.C. We next define the transfer operator.

Definition 3.5 (Transfer operator [23]). Let H be a Hamiltonian with frustration graph G . The

transfer operator $T_G(u)$ is defined as the generating function of independent set charges

$$T_G(u) := \sum_{S \in \mathcal{S}_G} (-u)^{|S|} h_S \quad (3.60)$$

$$= \sum_{k=0}^{\alpha(G)} (-u)^k Q_G^{(k)}, \quad (3.61)$$

where $u \in \mathbb{R}$ is the *spectral parameter*.

The transfer operator can be viewed as the operator analogue for the independence polynomial of a graph.

Definition 3.6 (Vertex-weighted independence polynomial).

$$I_G(x) = \sum_{S \in \mathcal{S}_G} x^{|S|} \prod_{j \in S} b_j^2 \quad (3.62)$$

Both the transfer operator and the independence polynomial satisfy similar recursion relations to Eq. (3.57)

$$T_G(u) = T_{G \setminus K}(u) - u \sum_{j \in K} h_j T_{G \setminus \Gamma[j]}(u) \quad (3.63)$$

$$I_G(x) = I_{G \setminus K}(x) + x \sum_{j \in K} b_j^2 I_{G \setminus \Gamma[j]}(x). \quad (3.64)$$

A special case of these recursion relations is that for which K consists of a single vertex.

The transfer operator bears an interesting relation to the characteristic polynomial for the free-fermion model.

Definition 3.7 (Generalized characteristic polynomial). Let H be an SCF Hamiltonian with frustration graph G . The *generalized characteristic polynomial* Z_G of G is defined as

$$Z_G(-u^2) := T_G(u) T_G(-u). \quad (3.65)$$

with the transfer operator defined as in Def. 3.5.

Strictly speaking, Z_G is an operator-valued polynomial, but reduces to an ordinary polynomial when restricted to a mutual eigenspace of the $J_G[\langle C_0 \rangle]$. The reason for calling Z_G the generalized

characteristic polynomial becomes clear when we consider the case where G is a line graph $L(R)$. Suppose this is the case. In Sect. 3.B, Eq. (3.225), we show

$$Z_G(-u^2) = \sum_{\substack{S, T \in \mathcal{S}_G \\ S \oplus T = \partial \mathcal{X} \\ \mathcal{X} \in \mathcal{C}_G^{(\text{even})}}} (-u^2)^{|S|} h_S h_T \quad (3.66)$$

$$= \sum_{\substack{S, T \in \mathcal{S}_G \\ S \oplus T = \partial \mathcal{X} \\ \mathcal{X} \in \mathcal{C}_G^{(\text{even})}}} (-u^2)^{|S|} \left(\prod_{j \in S \cap T} b_j^2 \right) \prod_{C \in \mathcal{X}} h_C. \quad (3.67)$$

Because the h_C are symmetries of the Hamiltonian, we can restrict to a mutual eigenspace of these symmetries through the orientation of R implicit in \mathbf{h} . Denote $M_S \in \mathcal{M}_R^{(|S|)}$ as the matching of R corresponding to the independent set S in $L(R)$, and similarly for M_T . Under the free-fermion solution, the operator $h_S h_T$ maps to

$$\begin{aligned} & \left[\prod_{\substack{(j,k) \in M_S \\ j < k}} (i h_{jk} \gamma_j \gamma_k) \right] \left[\prod_{\substack{(j,k) \in M_T \\ j < k}} (i h_{jk} \gamma_j \gamma_k) \right] \\ &= (-1)^{\pi(M_S) + \pi(M_T)} \left(\prod_{\substack{(j,k) \in M_S \\ j < k}} h_{jk} \right) \left(\prod_{\substack{(j,k) \in M_T \\ j < k}} h_{jk} \right) \end{aligned} \quad (3.68)$$

since every Majorana mode is either included zero times or twice in this product by the constraint on $S \oplus T$. The phase factor is calculated by sorting the Majorana modes in each matching individually, giving a factor of $(-1)^{\pi(M_S) + \pi(M_T)}$. Squaring the sorted operator gives a factor of $i^{2|M|} (-1)^{\frac{1}{2}(2|M|)(2|M|-1)} =$

1. Comparing Eqs. (3.66) and (3.68) to Eq. (3.48) gives

$$Z_{L(R)}(-u^2) = f_{\mathbf{h}}(u). \quad (3.69)$$

In the case where G is a general SCF graph, Eqs. (3.66) and (3.67) still hold, but the h_C are not symmetries of the Hamiltonian in general. To recover a set of cycle-like symmetries, we need to sum these operators over subsets of even-holes with the same neighborhood, and the solution follows analogously.

To finally give the full solution, we need to describe the fermionic eigenmodes. These are given in terms of the roots $\{\pm u_j\}$ of $Z_G(-u^2)$ over a fixed symmetric subspace via the transfer operator and a so-called *simplicial mode*.

Definition 3.8 (Simplicial mode). Let H be an SCF Hamiltonian with frustration graph G . A

simplicial mode with respect to a simplicial clique K_s is a Pauli operator $\chi := \sigma^{\mathbf{j}^*}$ such that $\mathbf{j}^* \notin V$, and χ satisfies

$$\langle \mathbf{j}^*, \mathbf{k} \rangle = \delta_{\mathbf{k} \in K_s} \quad (3.70)$$

That is, χ only anticommutes with terms in H whose vertices in G are in the simplicial clique K_s .

In Ref. [126], the corresponding result is proven in the special case that G is even-hole-free and claw-free. It is shown in Ref. [127] that these graphs are always simplicial. In this case, there is only one symmetry sector \mathcal{J} , for which $\Pi_{\mathcal{J}} = I$, so the mapping to the free-fermion model is “direct” in this sense. Additionally, considering Eq. (3.67) when there are no even holes in G , we see that the only nonvanishing terms in Eq. (3.66) are those for which $S = T$, and the generalized characteristic polynomial coincides with the vertex-weighted independence polynomial

$$Z_G(-u^2) = I_G(-u^2). \quad (3.71)$$

It is a well-known result that the independence polynomial of a claw-free graph has real negative roots [102], and the generalization to the vertex-weighted case can be seen from [100].

3.4 Claw-Free Graphs

We review some properties of claw-free graphs that are important for our purposes. The following is a well-known fact about claw-free graphs, which we set apart by stating as a lemma and briefly prove for completeness.

Lemma 3.2. Let S and S' be independent sets. The graph $G[S \oplus S']$ induced by the symmetric difference of S and S' is a bipartite graph of maximum degree at most two.

Proof. Clearly $G[S \oplus S']$ is bipartite with coloring classes $S \setminus S'$ and $S' \setminus S$, which are both independent sets by definition. If any vertex $\mathbf{j} \in S \oplus S'$ has degree greater than two in $G[S \oplus S']$, then \mathbf{j} , together with any three of its neighbors in $G[S \oplus S']$, induce a claw in G . \square

Lemma 3.2 implies that $G[S \oplus S']$ is a union of disjoint isolated vertices, induced paths, and even holes (odd holes are not bipartite).

Induced paths and even holes are *triangle-free* (they do not contain a clique of three vertices). As we might expect, the tension between this triangle-free constraint and the claw-free constraint on the

Commuting		Anticommuting	
(a.i)		(b.i)	
(a.ii)			
(a.iii)			
Hole	Path	Hole	Path
(a.iv)	(a.v)	(b.ii)	(b.iii)
		(b.iv)	

Table 3.2: Summary of the possible neighboring relations between a hole or induced path L and a vertex $j \notin L$ in a claw-free graph. (a) The Hamiltonian term h_j commutes with h_L only if j has at most four neighbors in L . If j has two neighbors in L , they must be (a.ii) neighboring, or (a.v) the endpoints of an induced path of at least one edge. If j has four neighbors in L , they may (a.iii) induce two disjoint edges, a path of length three, or (a.iv) a hole of length four in L . (b) The Hamiltonian term h_j anticommutes with h_L only if j has at most five neighbors in L . If j has three neighbors in L , they must (b.i) induce a path of length two in L , unless (b.iv) L is an induced path, in which case j can neighbor an endpoint and any pair of neighboring vertices in L . (b.i) The only possibility for j to have one neighbor in L is if L is an induced path, and j is neighboring its endpoint. (b.ii) The only possibility for j to have five neighbors in L is if L is a hole of length five. In case (b.i), we can define a unique additional hole or induced path by the single-vertex deformation $(L \setminus \{k\}) \cup \{j\}$.

entire graph tightly restricts the neighboring relations between these structures and other vertices in the graph.

Lemma 3.3. Given an induced path or hole L in a claw-free graph G and a vertex $j \notin L$, then the only possible neighboring relations between j and L are given in Table 3.2.

Proof. Rather than list the cases here, we give their definitions in the caption under Table 3.2. These cases are not necessarily mutually exclusive, such as for L an induced path of length one. Note that, while we consider general holes in this lemma, we define a hole to have length greater than three, so $G[L]$ contains no triangles. Additionally, any induced subgraph of $G[L]$ must either be bipartite (an even hole, or a disjoint union of induced paths) or an odd hole. Since any bipartite graph of at least five vertices or odd hole of more than five vertices contains an independent set of at least three vertices, j cannot have five or more neighbors in L unless L is a hole of five vertices. This gives case (b.ii). Clearly, there are no claws in $G[\{j\} \cup L]$ if j has no neighbors in L , so this gives case (a.i). We consider each additional case according to the number of neighbors to j in L .

Suppose j has exactly one neighbor, $k \in L$. If k has two neighbors, $u, v \in L$, then $\{k, j, u, v\}$ induces a claw in G . Thus, the only possibility is for k to have exactly one neighbor in L . This gives case (b.iii), where L is an induced path, and k is an endpoint of L .

More generally, if $k \in L$ is a neighbor to $j \notin L$, and k has two neighbors $u, v \in L$, then at least one of u, v must be a neighbor to j as well. If j has exactly two neighbors, $\Gamma_L(j) := \{k_0, k_1\} \subseteq L$, this gives case (a.ii) when at least one of k_0, k_1 has two neighbors in L . If both of k_0 and k_1 have exactly one neighbor in L , this gives case (a.v).

If j has exactly three neighbors $\Gamma_L(j) := \{k_0, k_1, k_2\} \subseteq L$, then at least two of these vertices must be neighboring in L . This gives case (b.i) when all of k_0, k_1 , and k_2 have two neighbors in L . If at least one of k_0, k_1 , or k_2 has one neighbor in L , then we have case (b.iv).

If j has four neighbors $\Gamma_L(j) := \{k_0, k_1, k_2, k_3\} \subseteq L$, then we have case (a.iv) if L is a hole of length four. In general, any subset of three vertices in L has an independent set of at least two vertices, since $G[L]$ does not contain triangles. Thus, $G[\Gamma_L(j)]$ cannot contain an isolated vertex. Assuming $\Gamma_L(j)$ not to be a hole, there is a pair of vertices in $\Gamma_L(j)$ with only one neighbor in $\Gamma_L(j)$. Without loss of generality, suppose these vertices are $\{k_0, k_3\}$. If these vertices are neighboring, then k_1 and k_2 must be neighboring, so as not to be isolated. This gives case (a.iii). If k_0 and k_3 have the same unique neighbor, say k_1 , then k_2 must also neighbor k_1 since it again cannot be isolated in $G[\Gamma_L(j)]$, and we have assumed k_0 and k_3 each only have one neighbor in $\Gamma_L(j)$. However, this gives that k_1 has degree three in $G[L]$ (and accordingly $\{k_1, k_0, k_2, k_3\}$ induces a claw in G), so we must have that

\mathbf{k}_0 and \mathbf{k}_3 have distinct unique neighbors in $G[\Gamma_L(\mathbf{j})]$ if they are not neighboring. Suppose \mathbf{k}_1 is the unique neighbor to \mathbf{k}_0 , and \mathbf{k}_2 is the unique neighbor to \mathbf{k}_3 . This again gives case (a.iii). \square

In the forthcoming graph-theoretic proofs, Lemma 3.3 is very important insofar as it allows us to infer neighboring relations based on partial information. We state this explicitly as a pair of useful corollaries

Corollary 3.1. If \mathbf{j} is neighboring to \mathbf{k} in an even hole, C , then \mathbf{j} is also neighboring to a neighbor of \mathbf{k} in C .

Corollary 3.2. Let \mathbf{j} be such that $\mathbf{k}_0\text{-}\mathbf{k}_1\text{-}\mathbf{k}_2 \subseteq \Gamma_L(\mathbf{j})$ for an induced path or even hole L . If \mathbf{j} has an additional neighbor $\mathbf{u} \in L$, then \mathbf{u} must neighbor at least one of \mathbf{k}_0 or \mathbf{k}_2 .

We make the distinction between the case where $h_{\mathbf{j}}$ commutes with h_L and the case where $h_{\mathbf{j}}$ anticommutes with h_L in Table 3.2, as the latter is especially important from a physical perspective. Interestingly, there is only one possibility for $h_{\mathbf{j}}$ to anticommute with h_C when C is an even hole, which is Table 3.2 (b.i). When this case holds, and L is either an induced path or even hole, there is a unique additional induced path or even hole defined informally as a *rerouting* of L through \mathbf{j} .

Definition 3.9 (Single-vertex deformation). Let L be a hole or an induced path, and let $\mathbf{j} \notin L$ be a vertex with neighborhood $\Gamma_L(\mathbf{j}) := \mathbf{u}\text{-}\mathbf{k}\text{-}\mathbf{v}$ as in case (b.i) of Table 3.2. The *single-vertex deformation* L' of L by \mathbf{j} is given by

$$L' := (L \setminus \{\mathbf{k}\}) \cup \{\mathbf{j}\}. \quad (3.72)$$

The vertex \mathbf{k} is called the *clone* to \mathbf{j} in L and is denoted by $\mathbf{j} \prec_L \mathbf{k}$.

Note that single-vertex deformations are “reversible”; if $\mathbf{j} \prec_L \mathbf{k}$, then $\mathbf{k} \prec_{L'} \mathbf{j}$.

There is a kind of generalization of a deformation that we need for our proof of Result 3.2.

Definition 3.10 (Bubble wand, handle, hoop). Suppose \mathbf{j} neighbors a path P as in case (b.iv) with $\Gamma_P(\mathbf{j}) = \{\mathbf{j}_i\text{-}\mathbf{j}_{i+1}, \mathbf{j}_\ell\}$ as labeled in Eq. (3.29). We define the *bubble wand* graph to be $B := P \cup \{\mathbf{j}\}$ and define the *handle* of the wand as the path $P_i := \{\mathbf{j}_k\}_{k=0}^i$, with the *hoop* defined as $C := B \setminus P_i$. We denote this relationship by $B = P_i \triangleleft C$.

We will return to this structure in Sect. 3.7.

We collect all of the holes or induced paths related by sequences of single-vertex deformations into sets called deformation closures.

Definition 3.11 (Deformation closure). Let L_0 be a hole or an induced path. The *deformation closure* $\langle L_0 \rangle$ of L_0 is the set such that $L_0 \in \langle L_0 \rangle$ and, for any hole or induced path $L \in \langle L_0 \rangle$ and single-vertex deformation L' of L , $L' \in \langle L_0 \rangle$ as well.

Note that a given hole or induced path cannot belong to more than one deformation closure. If $L \in \langle L_0 \rangle$ and $L' \in \langle L'_0 \rangle$, then L and L_0 are related by a deformation, and so are L and L'_0 . Thus, L_0 is related to L'_0 by the deformation that first takes L_0 to L and then from L to L'_0 . This therefore gives $\langle L_0 \rangle = \langle L'_0 \rangle$. Additionally, all of the holes in a deformation closure have the same length, so the deformation closures partition the holes in the graph such that all of the holes in a given deformation closure have a fixed length. The induced paths in a given deformation closure have the same length and endpoints, so their deformation closures partition them similarly.

The structures of the deformation closures can be complicated, with certain single-vertex deformations either enabled or prevented by other ones. In particular, this happens when a given vertex t is neighboring to exactly one of $\{s, a\}$ with $s \prec_L a$. In this case, we say that t is *dependent* on the deformation by $s \prec_L a$. We will especially be interested in the instance where L is an even hole, for which we have the following lemma.

Lemma 3.4. Let C be an even hole with labeling defined as in Eq. (3.30). If $s \prec_C a_0$ and t neighbors exactly one of $\{s, a_0\}$, then we must have either

$$\Gamma_{\{s\} \cup C}(t) = \begin{cases} a_{k-1}-b_0-u & \text{(i)} \\ b_{k-1}-a_{k-1}-b_0-u & \text{(ii)} \\ u-b_1-a_1 & \text{(iii)} \\ u-b_1-a_1-b_2 & \text{(iv)} \end{cases} \quad (3.73)$$

where $u = s$ or $u = a_0$. If $k = 2$, then cases (ii) and (iv) coincide.

Proof. Without loss of generality, suppose $u = s$, and let $C' := (C \setminus a_0) \cup \{s\}$ be the single-vertex deformation of C by s . By Corollary 3.1, t must neighbor at least one vertex in $\Gamma_{C'}(s) = \{b_0, b_1\}$. Once again without loss of generality, suppose t neighbors b_0 . Again by Corollary 3.1, t must neighbor at least one vertex in $\Gamma_C(b_0) = \{a_{k-1}, a_0\}$, so it must neighbor a_{k-1} . This gives case (i). If t has an additional neighbor in C' , then by Corollary 3.2, it must be either b_{k-1} or b_1 . If $k = 2$, then $b_{k-1} = b_1$, cases (ii) and (iv) coincide, and this gives that case. If $k > 2$, then t cannot neighbor b_1 , as $\{b_1, t, a_0, a_1\}$ would induce a claw, and t cannot have any additional neighbors in C' in this case.

Thus, \mathbf{t} must neighbor \mathbf{b}_{k-1} , and this gives case (ii). A similar argument applies for the case where $\mathbf{b}_1 \in \Gamma_C(\mathbf{t})$ and the case where $\mathbf{u} = \mathbf{a}_0$. \square

Lemma 3.4 gives the following useful corollaries.

Corollary 3.3. If \mathbf{t} neighbors exactly one of $\{\mathbf{s}, \mathbf{a}_0\}$ in the setting of Lemma 3.4 with $k > 2$, it must neighbor exactly one of $\{\mathbf{b}_0, \mathbf{b}_1\}$.

Corollary 3.4. If \mathbf{t} neighbors at least one of $\{\mathbf{s}, \mathbf{a}_0\}$ and both of $\{\mathbf{b}_0, \mathbf{b}_1\}$ in the setting of Lemma 3.4 with $k > 2$, it must neighbor both of $\{\mathbf{s}, \mathbf{a}_0\}$.

As stated previously, Lemma 3.4 allows us to consider *sequences* of deformations. The following lemma is a simple example

Lemma 3.5. If $\mathbf{t} \in \Gamma[C_0]$ for an even hole C_0 , then $\mathbf{t} \in \Gamma[C]$ for any even hole $C \in \langle C_0 \rangle$.

Proof. It is sufficient to prove that $\mathbf{t} \in \Gamma[C]$ for C a single-vertex deformation of C_0 . Thus, let

$$C := (C_0 \setminus \{\mathbf{a}_0\}) \cup \{\mathbf{s}\} \quad (3.74)$$

with $\mathbf{s} \prec_{C_0} \mathbf{a}_0$. Suppose that $\mathbf{t} \notin \Gamma[C]$, then $\mathbf{t} \notin C \cup C_0$ since $C \cup C_0 \subset \Gamma[C]$, and $\Gamma_{C \cup C_0}(\mathbf{t}) = \mathbf{a}_0$ since $\mathbf{t} \in \Gamma[C_0]$. However, this is a contradiction to Lemma 3.4. Therefore, if $\mathbf{t} \in \Gamma[C_0]$, then $\mathbf{t} \in \Gamma[C]$ for any single-vertex deformation C of C_0 . For an even hole $C \in \langle C_0 \rangle$ that is not necessarily a single-vertex deformation of C_0 , applying this result iteratively to the sequence of deformations from C_0 to C gives the lemma. \square

Lemma 3.5 shows that $\Gamma[C] = \Gamma[C_0]$ for any $C \in \langle C_0 \rangle$. Conversely, if $\mathbf{t} \notin \Gamma[C_0]$, then $\mathbf{t} \notin \Gamma[C]$ for any $C \in \langle C_0 \rangle$. Recall from Sect. 3.2 that two even holes C and C' are said to be compatible if $\mathbf{j} \notin \Gamma[C']$ for every $\mathbf{j} \in \Gamma[C]$. We thus have the following corollary

Corollary 3.5. If an even hole C is compatible with an even hole C_0 , then C is compatible with any even hole $C' \in \langle C_0 \rangle$.

These results will allow us to collect statements about individual even holes into statements about their deformation closures.

We now turn to the structures of deformation sequences. We give two important examples of deformation sequences in Fig. 3.3. In each, we deform the hole C by each vertex in $S := \{\mathbf{s}_j\}_{j=0}^{\ell-1}$ successively in j . Let $C^{(j)}$ be the hole following the deformation by \mathbf{s}_j , with the last hole in the deformation denoted by $\tilde{C} := C^{(\ell-1)}$.

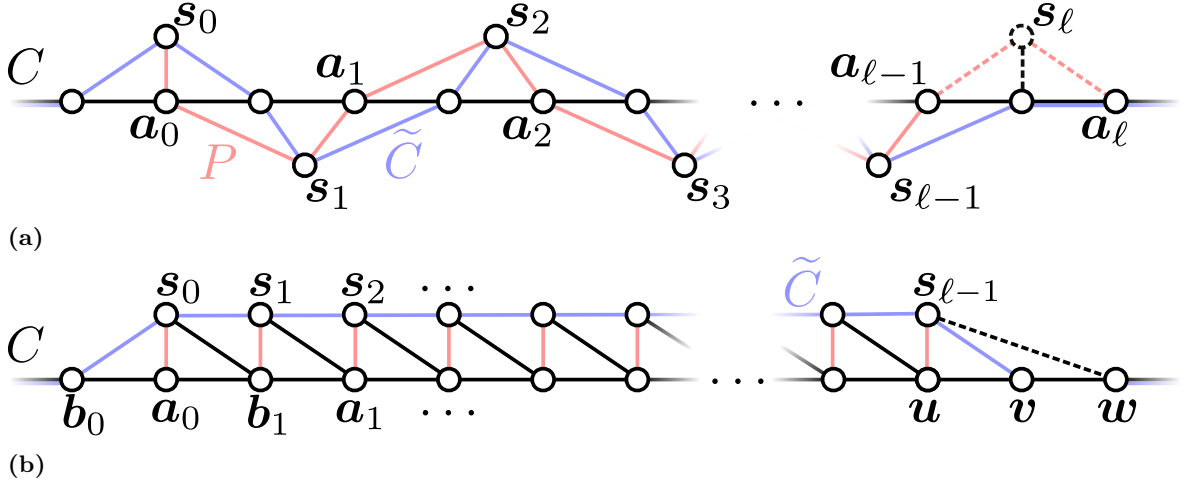


Figure 3.3: Two special cases for deformations of an even hole C by a sequence of vertices $S := \{s_j\}_{j=0}^{\ell-1}$. (a) The deformation along a path P when S is an independent set, defined as the path component of $G[S \oplus C_a]$ with endpoint s_0 , where C_a is the coloring class to which the clone of s_0 in C belongs. If s_ℓ is present, then we cannot deform by s_ℓ , and we say that s_0 is tethered to s_ℓ . Otherwise, the path P has odd length. (b) Deformation by a sequence of length-one paths. If $s_{\ell-1}$ has three neighbors in C , then we can not deform by $s_{\ell-1}$, and s_0 and $s_{\ell-1}$ are similarly uniquely paired.

In Fig. 3.3a, we consider the case where S is an independent set in G . That is, s_{j+1} is not neighboring to s_j , but is neighboring to its clone, a_j , in $C^{(j-1)}$. If we can deform $C^{(j)}$ by s_{j+1} , then $s_{j+1} \prec_{C^{(j)}} a_{j+1}$ by Lemma 3.4. Because none of the $\{s_j\}$ are neighboring, s_{j+1} is not neighboring to b_j for $j > 0$. Otherwise, s_{j+1} would be neighboring to s_{j-1} by Lemma 3.4 applied to the hole $C^{(j-1)}$. Thus, the deformation must continue in the “direction” specified by s_0 and s_1 .

There is a unique path associated to the sequence of deformations shown in Fig. 3.3a. This is the path component of $G[S \oplus C_a]$ with endpoint s_0 , where the independent set C_a is operationally defined as the coloring class of C to which the clone to s_0 belongs. (Because s_0 has only one neighbor in C_a , it is the endpoint of a path component of $G[S \oplus C_a]$.) We call this sequential deformation by vertices in $P \cap S$ a deformation *along* the path P , and we call P the deformation path. We call s_0 the *initializing vertex* of the deformation. We can continue the deformation until we reach a vertex s_ℓ with only three neighbors in C , as shown in Fig. 3.3a, and we cannot deform by s_ℓ if it is present. Letting P' be the path component of $G[S \oplus C_b]$ with s_ℓ as an endpoint, we could similarly deform C along P' until we reach the vertex s_0 , so s_0 and s_ℓ can be uniquely associated this way. We say that s_0 and s_ℓ are *tethered* with respect to C . If s_0 is untethered with respect to C (i.e. s_ℓ is not present), the path P has odd length $2\ell - 1$, so is given by

$$P := s_0 - a_0 - \dots - s_{\ell-1} - a_{\ell-1}. \quad (3.75)$$

Note that for $|C| = 2k$, we must have $\ell \leq k$. Otherwise, this contradicts the requirement that P is a path. Given a vertex $\mathbf{j} \notin C \cup S$, we show in Sect. 3.5.3 that requiring that \mathbf{j} satisfy Lemma 3.3 simultaneously with respect to both P and C tightly constrains its neighboring relations.

In Fig. 3.3b, we demonstrate an opposite extreme, whereby we deform along a sequence of length-one untethered paths. Here S is not an independent set, and \mathbf{s}_{j+1} neighbors \mathbf{s}_j , but not its clone in C (which may be in either coloring class). Because each untethered path in the deformation has length one, \mathbf{s}_{j+1} is the unique vertex dependent on the deformation by \mathbf{s}_j . We can continue this sequential deformation by vertices in S until we again reach a vertex $\mathbf{s}_{\ell-1}$ with three neighbors in C . Starting the deformation instead from $\mathbf{s}_{\ell-1}$ and deforming by each vertex $\mathbf{s}_{\ell-j}$ successively in j , we see we can continue until we reach \mathbf{s}_0 . Thus, \mathbf{s}_0 and \mathbf{s}_ℓ can be uniquely associated in this way.

We close this section with an overall summary in relation to previous results. Deformations for holes and induced paths are closely related to well-studied *reconfiguration problems* for claw-free graphs. A reconfiguration problem considers whether a graph structure, such as an independent set or shortest path, can be reached from another one by a sequence of allowed moves. We consider the following important reconfiguration move for independent sets

Definition 3.12 (Token sliding [128]). Given independent sets S, S' in a claw-free graph G , S and S' are related by a *token slide* if there is a pair of neighboring vertices \mathbf{u}, \mathbf{v} with $\mathbf{u} \in S \setminus S'$ and $\mathbf{v} \in S' \setminus S$ such that

$$S' = (S \setminus \mathbf{u}) \cup \{\mathbf{v}\} \quad (3.76)$$

That is, we consider a set of *tokens* placed on the independent set S and ask whether we can obtain S' from S by sliding a token along an edge of G . Note that if S' is reachable from S by a token sliding move, then S is similarly reachable from S' . We say that $S \leftrightarrow_{\text{TS}} S'$ if S and S' are related by a sequence of token-sliding moves.

Reachability is described by the solution graph $\text{TS}_k(G)$, whose vertices correspond to k -vertex independent sets in G and are neighboring if they are related by a token slide. Two k -vertex independent sets S, S' satisfy $S \leftrightarrow_{\text{TS}} S'$ if S, S' are in the same connected component of $\text{TS}_k(G)$. Let Ξ_k be the set of connected components of $\text{TS}_k(G)$.

We see that the token sliding operation closely resembles a single-vertex deformation. We can consider a connected component of $\text{TS}_k(G)$ as a corresponding “closure” of independent sets, and define the following conserved charges of Theorem 3.1 as sums over the appropriate closures

Definition 3.13 (Token-sliding charges, generalized cycle symmetries). The token-sliding charge $Q_G^{(k,\mu)}$ is defined as

$$Q_G^{(k,\mu)} = \sum_{S \in \mu} h_S \quad (3.77)$$

where $\mu \in \Xi_k$ is a connected component of $\text{TS}_k(G)$.

These are related to the independent-set charges from Def. 3.4 via

$$\sum_{\mu} Q_G^{(k,\mu)} = Q_G^{(k)}. \quad (3.78)$$

The $Q_G^{(k,\mu)}$ can thus be thought of a fine-graining of the independent set charges to account for the case where G is not connected or contains a certain kind of even hole. That is, the independent set charge is a sum over the connected components of $\text{TS}_k(G)$.

The generalized cycle symmetries are defined by

$$J_G[\langle C_0 \rangle] = \sum_{C \in \langle C_0 \rangle} h_C \quad (3.79)$$

Note that if G is itself not connected, then neither is $\text{TS}_k(G)$, and we have token-sliding charge for each component of $\text{TS}_k(G)$. However, even when G is connected, $\text{TS}_k(G)$ may not be. The case where G is an even hole and $k = \alpha(G)$ is a clear example, since any token slide will take a coloring class of G to a set which is not independent. Ref. [128] gives necessary and sufficient conditions for $\text{TS}_k(G)$ to be connected. In fact, it is only possible for $\text{TS}_k(G)$ to be disconnected with G connected when $k = \alpha(G)$ and when G contains an even hole. This implies that Lemma 1 of Ref. [126] (corresponding to Theorem 3.1 in this work) is already the strongest possible when H has connected frustration graph. However, when G contains even holes, we may have additional token-sliding charges. Note that the single-vertex deformation of a hole is the special case of a token sliding on one of its coloring classes that preserves the structure of the even hole.

3.5 Conserved Quantities

A crucial component to the proof of Result 3.1 is the identification of the conserved charges via their graphical structures. In this section we prove the following theorem

Theorem 3.1 (Conserved Charges). Consider a Hamiltonian, H , with frustration graph, G , that is claw-free. There exist a set of operators $\{Q_G^{(s,\mu)}, J_G[\langle C_0 \rangle]\}$ defined in Def. 3.13 that obey

$$[Q_G^{(s,\mu)}, Q_G^{(t,\nu)}] = 0, \quad (3.80a)$$

$$[J_G[\langle C_0 \rangle], Q_G^{(s,\mu)}] = 0, \quad (3.80b)$$

$$[J_G[\langle C_0 \rangle], J_G[\langle C'_0 \rangle]] = 0. \quad (3.80c)$$

In particular, $\sum_{\mu} Q_G^{(1,\mu)} = H$, which implies that $\{Q_G^{(s,\mu)}, J_G[\langle C_0 \rangle]\}$ are conserved charges of the model.

This theorem alone gives further evidence for the idea proposed in Ref. [126] that Hamiltonians with claw-free frustration graphs are integrable. Our proof strategy is to expand each operator as a sum in the commutator. For each non-vanishing contribution to the sum, we will show there is a unique additional term to cancel it. This is simply illustrated with our proof of Eq. (3.80a).

3.5.1 Proof of Eq. 3.80a

We have

$$[Q_G^{(s,\mu)}, Q_G^{(t,\nu)}] = \sum_{S \in \mu, S' \in \nu} [h_S, h_{S'}] \quad (3.81)$$

In general

$$h_S h_{S'} = (-1)^{\sum_{j \in S} \Delta_{S'}(j)} h_{S'} h_S \quad (3.82)$$

$$= (-1)^{|E[S \oplus S']|} h_{S'} h_S. \quad (3.83)$$

Eq. (3.82) follows from Eq. (3.27). Using the fact that both S and S' are independent sets, we have $\Delta_{S'}(j) = \Delta_{S' \setminus S}(j)$ for $j \in S$, and $\Delta_{S'}(j) = 0$ for $j \in S \cap S'$. This gives

$$\sum_{j \in S} \Delta_{S'}(j) = \sum_{j \in S \setminus S'} \Delta_{S' \setminus S}(j) = |E[S \oplus S']| \quad (3.84)$$

since $S \oplus S' = (S \setminus S') \cup (S' \setminus S)$, and $G[S \oplus S']$ is bipartite.

Consider the terms in Eq. (3.81) that are nonvanishing, for which h_S and $h_{S'}$ anticommute. By Lemma 3.2, there must be at least one (and odd many in general) path component of $G[S \oplus S']$ with

odd length. Choose a fiducial such path P , and let

$$P := \mathbf{s}'_0 - \mathbf{s}_0 - \dots - \mathbf{s}'_{\ell-1} - \mathbf{s}_{\ell-1} \quad (3.85)$$

with $\{\mathbf{s}_j\}_{j=0}^{\ell-1} = S \cap P$ and $\{\mathbf{s}'_j\}_{j=0}^{\ell-1} = S' \cap P$, so P has length $2\ell - 1$. Define

$$\tilde{S} := S \oplus P$$

$$\tilde{S}' := S' \oplus P$$

We can reach \tilde{S} from S by successively sliding \mathbf{s}_j to \mathbf{s}'_j for $j \in \{0, \dots, \ell - 1\}$. Thus, $S \leftrightarrow_{\text{TS}} \tilde{S}$, and $\tilde{S} \in \mu$. Similarly, $S' \leftrightarrow_{\text{TS}} \tilde{S}'$, and $\tilde{S}' \in \nu$. Because $S \oplus S' = \tilde{S} \oplus \tilde{S}'$, $G[\tilde{S} \oplus \tilde{S}']$ has odd-many edges, so there is an additional nonvanishing term in Eq. (3.81) indexed by (\tilde{S}, \tilde{S}') . We have

$$\begin{aligned} [h_S, h_{S'}] + [h_{\tilde{S}}, h_{\tilde{S}'}] &= 2(h_S h_{S'} + h_{\tilde{S}} h_{\tilde{S}'}) \\ &= 2h_{S \setminus P} (h_{S \cap P} h_{S' \cap P} + h_{S' \cap P} h_{S \cap P}) h_{S' \setminus P} \\ &= 0 \end{aligned}$$

For a collection of nonvanishing terms indexed by (S, S') in Eq. (3.81) with fixed graph $G[S \oplus S']$, fix a fiducial path component of $G[S \oplus S']$ by which to similarly pair corresponding terms. Therefore, terms in Eq. (3.81) can be made to cancel pairwise, and this proves Eq. (3.80a).

3.5.2 Proof of Eq. 3.80b

We next consider Eq. (3.80b)

$$[J_G[\langle C_0 \rangle], Q_G^{(s, \mu)}] = \sum_{C \in \langle C_0 \rangle, S \in \mu} [h_C, h_S]. \quad (3.86)$$

If h_C and h_S anticommute, then there is at least one (and odd many in general) vertex, $\mathbf{s}_0 \in S$ such that $h_{\mathbf{s}_0}$ anticommutes with h_C . As shown in the previous section, each such vertex is the endpoint of a (possibly tethered) deformation path, and is called the initializing vertex to the deformation. If every deformation path is tethered, then we can uniquely pair initializing vertices, and this contradicts the assumption that h_S and h_C anticommute. Thus, there must be at least one untethered path P , and we assume we have chosen our labeling such that \mathbf{s}_0 is the endpoint of this path, with $\mathbf{s}_0 \prec_C \mathbf{a}_0$,

and

$$P := s_0\text{-}a_0\text{-}\dots\text{-}s_{\ell-1}\text{-}a_{\ell-1} \quad (3.87)$$

as shown in Fig. 3.3a. Once again, we define

$$\tilde{C} := C \oplus P$$

$$\tilde{S} := S \oplus P$$

We have shown in the previous section that $\tilde{C} \in \langle C_0 \rangle$, and it is clear from the proof of Eq. (3.80a) that $\tilde{S} \in \mu$.

We have that h_P anticommutes with both h_S and h_C because only h_{s_0} anticommutes with h_C , and only $h_{a_{\ell-1}}$ anticommutes with h_S . Thus, $h_{\tilde{S}}$ and $h_{\tilde{C}}$ anticommute by Eq. (3.28) because h_S and h_C do. We have

$$\begin{aligned} [h_C, h_S] + [h_{\tilde{C}}, h_{\tilde{S}}] &= 2(h_C h_S + h_{\tilde{C}} h_{\tilde{S}}) \\ &= 2h_{C \setminus P}(h_{C \cap P} h_{S \cap P} + h_{S \cap P} h_{C \cap P}) h_{S \setminus P} \\ &= 0 \end{aligned}$$

where last line follows because $S \cap P$ and $C \cap P$ are the coloring classes of a path of odd length. For a given collection of nonvanishing terms in Eq. (3.86) related by a fixed set of untethered paths, we choose a fiducial path by which to cancel terms pairwise. This therefore proves Eq. (3.80b).

3.5.3 Proof of Eq. 3.80c

Finally, we consider Eq. (3.80c)

$$[J_G[\langle C_0 \rangle], J_G[\langle C'_0 \rangle]] = \sum_{C \in \langle C_0 \rangle, C' \in \langle C'_0 \rangle} [h_C, h_{C'}] \quad (3.88)$$

Fix a pair C, C' such that h_C and $h_{C'}$ anticommute. Let us choose the vertex labeling according to Eq. (3.30) as

$$C := b_0\text{-}a_0\text{-}b_1\text{-}a_1\text{-}\dots\text{-}b_{k-1}\text{-}a_{k-1}\text{-}b_0 = C_a \cup C_b \quad (3.89)$$

$$C' := d_0\text{-}c_0\text{-}d_1\text{-}c_1\text{-}\dots\text{-}d_{k'-1}\text{-}c_{k'-1}\text{-}d_0 = C'_c \cup C'_d \quad (3.90)$$

where $C_a := \{\mathbf{a}_j\}_{j=0}^{k-1}$ and $C_b := \{\mathbf{b}_j\}_{j=0}^{k-1}$ are the coloring classes of C , and $C'_c := \{\mathbf{c}_j\}_{j=0}^{k'-1}$ and $C'_d := \{\mathbf{d}_j\}_{j=0}^{k'-1}$ are the coloring classes of C' . We sequentially deform C by vertices in C' along an ordered collection of deformation paths $\mathcal{O} := (P^{(j)})_{j=0}^m$ such that

$$\begin{cases} \tilde{C} := C \oplus (\cup_{j=0}^m P^{(j)}) \in \langle C_0 \rangle \\ \tilde{C}' := C' \oplus (\cup_{j=0}^m P^{(j)}) \in \langle C'_0 \rangle \end{cases} \quad (3.91)$$

The term corresponding to (\tilde{C}, \tilde{C}') is also nonvanishing in Eq. (3.88) and can be uniquely paired to cancel the (C, C') term. The deformation \mathcal{O} is such that

$$\begin{cases} P^{(j)} \subseteq G[C_a \oplus C'_c] \quad \text{or} \quad P^{(j)} \subseteq G[C_b \oplus C'_d] \quad (\text{i}) \\ P^{(j)} \subseteq G[C_a \oplus C'_d] \quad \text{or} \quad P^{(j)} \subseteq G[C_b \oplus C'_c] \quad (\text{ii}) \end{cases} \quad (3.92)$$

for all $j \in \{0, \dots, m\}$. In case (i), we say that \mathcal{O} is (a, c) -pairing, and in case (ii), we say that \mathcal{O} is (a, d) -pairing. We refer to this property as the *pairing type* of \mathcal{O} . Similarly, we say that each $P^{(j)}$ is either (a, c) - or (a, d) -pairing. Note that when vertices are tethered, their respective deformation paths have opposite pairing type, Fig. 3.3a.

Let $U \subseteq C' \setminus C$ be the set of vertices $\mathbf{j} \in C'$ such that $h_{\mathbf{j}}$ anticommutes with $h_{C'}$. Because h_C and $h_{C'}$ anticommute, $|U|$ must be odd. For each $\mathbf{j} \in U$, we define a unique deformation $\mathcal{O}_{\mathbf{j}} := (P_{\mathbf{j}}^{(j)})_{j=0}^m$ initialized by \mathbf{j} , in that \mathbf{j} is the endpoint of $P_{\mathbf{j}}^{(0)}$ in $C' \setminus C$. Here, we will potentially allow for $\mathcal{O}_{\mathbf{j}}$ to be empty, i.e., $\mathcal{O}_{\mathbf{j}} = ()$, but we will still associate a unique pairing type to $\mathcal{O}_{\mathbf{j}}$ even in this case, and our desired deformation \mathcal{O} will never be empty. If a particular deformation $\mathcal{O}_{\mathbf{j}}$ fails to give us this desired deformation, then it is *obstructed* by another vertex $\mathbf{j}' \in U$. When this happens, $\mathcal{O}_{\mathbf{j}'}$ has the opposite pairing type to $\mathcal{O}_{\mathbf{j}}$. We thus define a bipartite directed graph $\mathcal{D} \equiv (U, D)$ such that $(\mathbf{j} \rightarrow \mathbf{j}') \in D$ if \mathbf{j}' obstructs $\mathcal{O}_{\mathbf{j}}$. The coloring classes of \mathcal{D} are naturally given by the two pairing types.

Because a given deformation $\mathcal{O}_{\mathbf{j}}$ can be obstructed by at most one additional vertex in U , there is at most one outgoing arc from each vertex in \mathcal{D} . We will also see that the obstructions come in two varieties, which we will call *type-I* and *type-II* obstructions. A given vertex cannot obstruct two distinct deformations in the same way, so there are at most two incoming arcs to each vertex in \mathcal{D} . Because \mathcal{D} is bipartite with odd-many vertices, there is thus either at least one vertex in \mathcal{D} with no outgoing arc or at least one vertex in \mathcal{D} with two incoming arcs. In the former case, we have

a deformation \mathcal{O}_j with no obstruction, and this will be seen to be the desired deformation \mathcal{O} . In the latter case, there is a vertex j'' which obstructs \mathcal{O}_j and $\mathcal{O}_{j'}$ for vertices $j, j' \in U$. Note that $\mathcal{O}_{j''}$ must have the opposite pairing type to both \mathcal{O}_j and $\mathcal{O}_{j'}$, so \mathcal{O}_j and $\mathcal{O}_{j'}$ must have the same pairing type as each other. Suppose j'' is a type-I obstruction for \mathcal{O}_j and a type-II obstruction for $\mathcal{O}_{j'}$, then we will see that the deformation given by $\mathcal{O}'_j := (\mathcal{O}_{j'}, \mathcal{O}_j, \mathcal{O}_{[j, j'']})$ is not obstructed by j'' . Here, parentheses denotes concatenation of the deformations as ordered sets of deformation paths, and $\mathcal{O}_{[j, j'']}$ is the set of ordered paths resulting from *continuing* the deformation \mathcal{O}_j through j'' after $\mathcal{O}_{j'}$ has been applied. We will see that \mathcal{O}'_j has the same pairing type as \mathcal{O}_j and $\mathcal{O}_{j'}$. We thus construct a new bipartite directed graph $\mathcal{D}^{(0)}$ resulting from replacing \mathcal{O}_j with \mathcal{O}'_j in \mathcal{D} , and continue this reconfiguration procedure on \mathcal{D} until we reach a graph $\mathcal{D}^{(p)}$ with some unobstructed deformation. Because this procedure is guaranteed to never reach the same directed graph twice, we will eventually find the unobstructed deformation.

We next describe our process to associate a unique deformation \mathcal{O}_j to the initializing vertex $j \in C' \setminus C$. For concreteness, let us, without loss of generality, fix our labeling such that $j := c_0 \prec_C a_0$. In this case, we say that \mathcal{O}_j is (a, c) -pairing. If c_0 is tethered to another vertex $c_g \in C' \setminus C$, then let $j' := c_g$. We say that j' is a type-I obstruction to \mathcal{O}_j , and we take $\mathcal{O}_j = ()$. As shown previously, this definition similarly gives that j is a type-I obstruction to $\mathcal{O}_{j'} = ()$, and $\mathcal{O}_{j'}$ is (a, d) -pairing as desired. This will be the only case where \mathcal{O}_j is empty as a subset of induced paths, so we will see that no such empty subset can have a type-II obstruction.

Next, suppose that c_0 is untethered with respect to C , and assume we have chosen our labeling for $P^{(0)} \subseteq G[C_a \oplus C'_c]$ such that

$$P_j^{(0)} = c_0 - a_0 - \dots - c^{(j)} - a_j - \dots - c^{(\ell-1)} - a_{\ell-1} \quad (3.93)$$

Again without loss of generality, we assume to have chosen our labeling such that

$$\Gamma_C(c^{(j)}) = a_{j-1} - b_j - a_j - b_{j+1} \quad (3.94)$$

for $j > 0$ if $\ell > 1$, but we do not assume $c^{(j)} = c_j$ for $j > 0$ (hence the use of superscript labeling). Notably, we do not assume that $c^{(j)}$ and $c^{(j+1)}$ share a neighbor in C'_d for any $j \in \{0, \dots, \ell-2\}$ with the convention that $c^{(0)} = c_0$.

If a_j is neighboring to both vertices in $\Gamma_{C'}(c^{(j)})$ for all $j \in \{0, \dots, \ell-1\}$, then $\mathcal{O}_j = (P_j^{(0)})$ is unobstructed, and we take $\mathcal{O} := \mathcal{O}_j$ as our desired deformation. We thus consider the cases where

there is a vertex $\mathbf{d}^{(s)} \in \Gamma_{C'}(\mathbf{c}^{(s)}) \setminus \Gamma_{C'}(\mathbf{a}_s)$. In this case, $\mathbf{d}^{(s)}$ is dependent on the deformation $\mathbf{c}^{(s)} \prec_{C^{(0), s-1}} \mathbf{a}_s$. Let $C^{(0)} := C \oplus P_{\mathbf{j}}^{(0)}$, $C^{(0, s)} := C \oplus (\{\mathbf{c}^{(j)}\}_{j=0}^s \cup \{\mathbf{a}_j\}_{j=0}^s)$. We will utilize the following Lemmas concerning this situation, given the definitions above

Lemma 3.6. If there is a vertex $\mathbf{d}^{(s)} \in C'_d$ such that

$$\mathbf{d}^{(s)} \in \Gamma_{C'}(\mathbf{a}_s) \setminus \Gamma_{C'}(\mathbf{c}^{(s)}) \quad (3.95)$$

then

- (a) $s < \ell - 1$ (and thus $\ell > 1$).
- (b) there exists an $s' > s$ such that

$$\mathbf{d}^{(s)} \in \Gamma_{C'}(\mathbf{c}^{(s')}) \setminus \Gamma_{C'}(\mathbf{a}_{s'}). \quad (3.96)$$

Lemma 3.6 shows that we do not need to consider vertices $\mathbf{d}^{(s)} \in \Gamma_{C'}(\mathbf{a}_s) \setminus \Gamma_{C'}(\mathbf{c}^{(s)})$ when considering deformations with respect to entire paths, as this will reduce to the case where $\mathbf{d}^{(s)} \in \Gamma_{C'}(\mathbf{c}^{(s')}) \setminus \Gamma_{C'}(\mathbf{a}_{s'})$ for some $s' > s$.

Lemma 3.7. If there is a vertex $\mathbf{d}^{(s)} \in C'_d$ such that

$$\mathbf{d}^{(s)} \in \Gamma_{C'}(\mathbf{c}^{(s)}) \setminus \Gamma_{C'}(\mathbf{a}_s) \quad (3.97)$$

then we have the following

- (a) If $\Delta_C(\mathbf{d}^{(s)}) = 4$, then $\Delta_{C^{(0)}}(\mathbf{d}^{(s)}) = 4$, and there is another vertex

$$\mathbf{d}^{(s')} \in \Gamma_{C'}(\mathbf{c}^{(s')}) \setminus \Gamma_{C'}(\mathbf{a}_{s'}) \quad (3.98)$$

with $s' < s$ and $\Delta_C(\mathbf{d}^{(s')}) < 4$. This vertex lies in the same path component of $G[C_b \oplus C'_d]$ as $\mathbf{d}^{(s)}$, and $h_{\mathbf{d}^{(s)}}$ commutes with h_P in this case.

- (b) Otherwise, $h_{\mathbf{d}^{(s)}}$ anticommutes with h_P , and we have

$$\Delta_{C^{(0)}}(\mathbf{d}^{(s)}) = \Delta_C(\mathbf{d}^{(s)}) + 1 \quad (3.99)$$

with

$$\begin{cases} \mathbf{d}^{(s)} \prec_C \mathbf{u} \in C_a & \Delta_C(\mathbf{d}^{(s)}) = 3 \\ \mathbf{d}^{(s)} \prec_{C^{(0)}} \mathbf{u} \in C_b & \Delta_{C^{(0)}}(\mathbf{d}^{(s)}) = 3 \end{cases}. \quad (3.100)$$

Lemma 3.7(a) essentially allows us to only consider dependent vertices $\mathbf{d}^{(s)}$ whose degree in C is either 2 or 3, and Lemma 3.7(b) conveniently relates the degree of $\mathbf{d}^{(s)}$ in C to its degree in the path with (a, c) pairing type.

Lemma 3.8. There is no other path $P \subseteq G[C_a \oplus C'_c] \setminus P^{(0)}$

$$P := \mathbf{j}^{(0)} - \mathbf{k}^{(0)} - \dots - \mathbf{j}^{(\ell'-1)} - \mathbf{k}^{(\ell'-1)} \quad (3.101)$$

such that $\mathbf{d}^{(s)} \in \Gamma_{C'}(\mathbf{j}^{(s')}) \setminus \Gamma_{C'}(\mathbf{k}^{(s')})$.

That is, a given vertex in C' can depend on at most one deformation path of a fixed pairing type. By utilizing Lemma 3.8 and Lemma 3.7 successively, we can see how vertices' neighboring relationships change under continued deformation of C .

We continue to construct \mathcal{O}_j through our iterative method. Recall that we have assumed our deformation is (a, c) -pairing, and assume that we have constructed it out to step $s-1$ with $\mathcal{O}_j^{(s-1)} = (P_j^{(r)})_{j=0}^{s-1}$ for $s \geq 0$. Let $C^{(s-1)} := C \oplus (\cup_{j=0}^{s-1} P_j^{(r)})$. In this construction, we have

$$P_j^{(r)} := \mathbf{j}^{(r,0)} - \mathbf{k}^{(r,0)} - \dots - \mathbf{j}^{(r,\ell_r-1)} - \mathbf{k}^{(r,\ell_r-1)} \quad (3.102)$$

for $r \in \{0, \dots, s-1\}$ such that $\mathbf{j}^{(r,0)} \in C' \setminus C^{(r-1)}$ is untethered with respect to $C^{(r-1)}$. If $s = 0$, let $\mathbf{u} := \mathbf{j}$, in which case $\mathcal{O}^{(-1)} := ()$, $C^{(-1)} = C$, so $\Delta_{C^{(s-1)}}(\mathbf{u}) = 3$. If $s > 0$, let $\mathbf{u}^{(r,t)}$ be the sole element (by Corollary 3.1) of $[\Gamma_{C'}(\mathbf{j}^{(r,t)}) \setminus \Gamma_{C'}(\mathbf{k}^{(r,t)})] \setminus C^{(s-1)}$ if it exists and satisfies $\Delta_C(\mathbf{u}^{(r,t)}) < 4$. If there is no such vertex, then take $\mathcal{O}_j = \mathcal{O}_j^{(s-1)}$. In this case, \mathcal{O}_j is unobstructed, so we take $\mathcal{O}_j = \mathcal{O}$. Otherwise, let

$$\mathbf{u} := \max_{(\sum_{q=0}^{r-1} \ell_q) + t} \{\mathbf{u}^{(r,t)}\}_{0 \leq t \leq \ell_r-1, 0 \leq r \leq s-1} \quad (3.103)$$

By assumption, \mathbf{u} is dependent on at least one deformation path in $\mathcal{O}^{(s-1)}$, and so it is dependent on exactly one deformation path by Lemma 3.8. If $\Delta_C(\mathbf{u}) = 2$, then $\Delta_{C^{(s-1)}}(\mathbf{u}) = 3$ by Lemma 3.7(b). If \mathbf{u} is untethered with respect to $C^{(s-1)}$, then let $P_j^{(s)}$ be the path with (a, c) -pairing and endpoint

\mathbf{u} . Let $\mathcal{O}_j^{(s)} = (\mathcal{O}_j^{(s-1)}, P_j^{(s)})$ and continue the construction. If $\Delta_C(\mathbf{u}) = 2$ and \mathbf{u} is tethered to \mathbf{j}' with respect to $C^{(s-1)}$, then take $\mathcal{O}_j = \mathcal{O}_j^{(s-1)}$, and \mathbf{j}' is a type-I obstruction for \mathcal{O}_j . Because the deformation path of $C^{(s-1)}$ initialized by \mathbf{j}' has (a, d) -pairing, it cannot be dependent on any path in \mathcal{O}_j , so $\mathbf{j}' \in U$. If $\Delta_C(\mathbf{u}) = 3$ and \mathbf{u} is untethered with respect to C , then take $\mathcal{O}_j = \mathcal{O}_j^{(s-1)}$, and \mathbf{u} is a type-II obstruction for \mathcal{O}_j . If $\Delta_C(\mathbf{u}) = 3$ and \mathbf{u} is tethered to \mathbf{v} with respect to C , then consider \mathbf{v} . If \mathbf{v} is untethered with respect to $C^{(s-1)}$, let $P_j^{(s)}$ be the path with (a, c) -pairing and endpoint \mathbf{v} . Let $\mathcal{O}_j^{(s)} = (\mathcal{O}_j^{(s-1)}, P_j^{(s)})$ and continue the construction. If \mathbf{v} is tethered to \mathbf{j}' with respect to $C^{(s-1)}$, then take $\mathcal{O}_j = \mathcal{O}_j^{(s-1)}$, and \mathbf{j}' is a type-I obstruction for \mathcal{O}_j . This completes our description of our unique deformation process \mathcal{O}_j .

Suppose there are two such deformations $\mathcal{O}_j, \mathcal{O}_{j'}$ that share \mathbf{j}'' as an obstruction. We show that \mathbf{j}'' cannot be a type-I obstruction for both, nor a type-II obstruction for both. First, note that $\mathcal{O}_j := \{P_j^{(r)}\}_{r=0}^m$ and $\mathcal{O}_{j'} := \{P_{j'}^{(r)}\}_{r=0}^{m'}$ are disjoint as induced path subsets because every path $P_j^{(s)} \in \mathcal{O}_j$ is determined uniquely by its initializing vertex $\mathbf{j}^{(s,0)} \in C' \setminus C^{(s-1)}$ and pairing type, and all such initializing vertices in \mathcal{O}_j and $\mathcal{O}_{j'}$ except \mathbf{j} and \mathbf{j}' are dependent on a previous deformation path. Since $\mathbf{j} \neq \mathbf{j}'$, by Lemma 3.8, no initializing vertex is common to $\cup_{r=0}^m P_j^{(r)}$ and $\cup_{r=0}^{m'} P_{j'}^{(r)}$, so \mathcal{O}_j and $\mathcal{O}_{j'}$ are disjoint as induced path subsets. If \mathbf{j}'' is a type-II obstruction for both \mathcal{O}_j and $\mathcal{O}_{j'}$, then it must be dependent on both $P_j^{(m)}$ and $P_{j'}^{(m')}$, again contradicting Lemma 3.8.

If \mathbf{j}'' is a type-I obstruction for both \mathcal{O}_j and $\mathcal{O}_{j'}$, then there is some path P with (a, c) -pairing in which \mathbf{j}'' is a degree-2 vertex. Furthermore, one endpoint of P is dependent on some path deformation in \mathcal{O}_j and the other is dependent on some path deformation in $\mathcal{O}_{j'}$. Let $\Gamma_C(\mathbf{j}'') = \mathbf{u}-\mathbf{k}-\mathbf{v}$, with $\mathbf{u}, \mathbf{v} \in P$. Because $\mathbf{u}, \mathbf{v} \in C$, they cannot be the endpoints of P , so let $\mathbf{w}-\mathbf{u}-\mathbf{j}''-\mathbf{v}-\mathbf{r} \subseteq P$. Both \mathbf{w} and \mathbf{r} neighbor \mathbf{k} , the clone to \mathbf{j}'' in C , so $\{\mathbf{k}, \mathbf{j}'', \mathbf{w}, \mathbf{r}\}$ gives a claw. Therefore, \mathbf{j}'' cannot be a type-I obstruction for both \mathcal{O}_j and $\mathcal{O}_{j'}$.

Suppose \mathbf{j}'' is a type-I obstruction to \mathcal{O}_j and a type-II obstruction to $\mathcal{O}_{j'}$. Let $C^{(m')} := C \oplus (\cup_{r=0}^{m'} P_{j'}^{(r)})$. By Lemma 3.7, $\Delta_{C^{(m')}}(\mathbf{j}'') = 4$. Additionally, no vertex that initializes a path deformation in \mathcal{O}_j can be dependent on a path deformation in $\mathcal{O}_{j'}$. The vertex \mathbf{j} cannot be dependent on $\mathcal{O}_{j'}$, as it would have the wrong pairing type, and any additional initializing vertices also cannot be dependent on $\mathcal{O}_{j'}$ by Lemma 3.8. By Lemma 3.7(a) and Lemma 3.8, any vertex $\mathbf{u} \in \cup_{r=0}^{m'} P_{j'}^{(r)}$ with $\Delta_C(\mathbf{u}) = 4$ must also have $\Delta_{C^{(m')}}(\mathbf{u}) = 4$, so we can perform the deformation by the same paths in \mathcal{O}_j after deforming by $\mathcal{O}_{j'}$. However, because $\Delta_{C^{(m')}}(\mathbf{j}'') = 4$ and \mathbf{j}'' cannot be dependent on any path deformation in \mathcal{O}_j by Lemma 3.8, \mathbf{j}'' is not an obstruction to the deformation given by $(\mathcal{O}_{j'}, \mathcal{O}_j)$. This allows us to continue the deformation through \mathbf{j}'' and reroute the graph \mathcal{D} to \mathcal{D}' as

described. Note that, now $\mathcal{O}'_j := (\mathcal{O}_{j'}, \mathcal{O}_j, \mathcal{O}_{[j, j']})$ is not disjoint from $\mathcal{O}_{j'}$ as a path subset. However, this method gives that if \mathbf{j}'' is a type-II obstruction to $\mathcal{O}_{j'}$, then it cannot be a type-II obstruction to \mathcal{O}'_j . Since this is the only situation under which deformations intersect, we see that no vertex can be a type-II obstruction to two deformations in any rerouted graph $\mathcal{D}^{(p)}$. Furthermore, every such rerouting $\mathcal{D}^{(p)}$ differs from $\mathcal{D}^{(p-1)}$ by exactly one arc, and no graph can repeat under this rerouting process. Therefore, we must eventually find a deformation \mathcal{O} with no obstruction. Finally, Lemma 3.7 guarantees that any vertex $\mathbf{u} \in \Gamma_{C'}(\mathbf{j}^{(r,t)}) \setminus \Gamma_{C'}(\mathbf{k}^{(r,t)})$ with $\Delta_C(\mathbf{u}) = 4$ also lies in a deformation path of \mathcal{O} .

We next show that this guarantees the reverse deformation sequence to \mathcal{O} is also a deformation of C' : $\tilde{C}' := C' \oplus (\cup_{r=0}^m P^{(r)}) \in \langle C'_0 \rangle$. Let

$$\begin{cases} \mathbf{j} := \cup_{r=0}^m \{\mathbf{j}^{(r,t)}\}_{t=0}^{\ell_r-1} \\ \mathbf{k} := \cup_{r=0}^m \{\mathbf{k}^{(r,t)}\}_{t=0}^{\ell_r-1} \end{cases}. \quad (3.104)$$

Considering the last deformation in the sequence

$$\tilde{C} = (C^{(m, \ell_m-2)} \setminus \mathbf{k}^{(m, \ell_m-1)}) \cup \mathbf{j}^{(m, \ell_m-1)} \quad (3.105)$$

where we have $\mathbf{k}^{(m, \ell_m-1)} \prec_{\tilde{C}} \mathbf{j}^{(m, \ell_m-1)}$, there can be no vertex in C' that neighbors exactly one of $\{\mathbf{k}^{(m, \ell_m-1)}, \mathbf{j}^{(m, \ell_m-1)}\}$, since this vertex is in \tilde{C} by assumption on \mathcal{O} , and so this would contradict the fact that $\mathbf{k}^{(m, \ell_m-1)} \prec_{\tilde{C}} \mathbf{j}^{(m, \ell_m-1)}$. This gives that $\mathbf{k}^{(m, \ell_m-1)} \prec_{C'} \mathbf{j}^{(m, \ell_m-1)}$.

Now suppose we can perform the reverse deformation out to step g on path s , and let

$$\begin{cases} \mathbf{j}^{(s,g)} := \cup_{r=0}^{s-1} \{\mathbf{j}^{(r,t)}\}_{t=0}^{\ell_r-1} \cup \{\mathbf{j}^{(s,t)}\}_{t=0}^g \\ \bar{\mathbf{k}}^{(s,g)} := \cup_{r=s+1}^m \{\mathbf{k}^{(r,t)}\}_{t=0}^{\ell_r-1} \cup \{\mathbf{k}^{(s,t)}\}_{t=g+1}^{\ell_s-1} \end{cases} \quad (3.106)$$

with

$$\begin{cases} C^{(s,g)} = (C \setminus \mathbf{k}) \cup \mathbf{j}^{(s,g)} \cup \bar{\mathbf{k}}^{(s,g)} \\ C'^{(s,g)} = (C' \setminus \mathbf{j}) \cup \mathbf{j}^{(s,g)} \cup \bar{\mathbf{k}}^{(s,g)} \end{cases} \quad (3.107)$$

That is,

$$C'^{(s,g)} = [C^{(s,g)} \setminus (C \setminus \mathfrak{k})] \cup (C' \setminus \mathfrak{j}) \quad (3.108)$$

we have $\mathbf{k}^{(s,g)} \prec_{C^{(s,g)}} \mathbf{j}^{(s,g)}$. Finally, note

$$\mathbf{j}^{(s,g)} \in C^{(s,g)} \cap C'^{(s,g)} \quad (3.109)$$

with

$$C^{(s,g)} \cap C'^{(s,g)} = [(C \setminus \mathfrak{k}) \cap (C' \setminus \mathfrak{j})] \cup \mathfrak{j}^{(s,g)} \cup \bar{\mathfrak{k}}^{(s,g)} \quad (3.110)$$

To prove that $\mathbf{k}^{(s,g)} \prec_{C'^{(s,g)}} \mathbf{j}^{(s,g)}$, we require that $\Gamma_{C'^{(s,g)}}(\mathbf{k}^{(s,g)}) = \Gamma_{C'^{(s,g)}}[\mathbf{j}^{(s,g)}]$. Since $\mathbf{k}^{(s,g)} \prec_{C^{(s,g)}} \mathbf{j}^{(s,g)}$, if there is a vertex \mathbf{u} in exactly one of $\{\Gamma_{C'^{(s,g)}}(\mathbf{k}^{(s,g)}), \Gamma_{C'^{(s,g)}}[\mathbf{j}^{(s,g)}]\}$, it must be in $C'^{(s,g)} \setminus C^{(s,g)}$. Thus, it is in $(C' \setminus \mathfrak{j})$ but not $(C \setminus \mathfrak{k})$. However, such a vertex would be a vertex in C' neighboring precisely one of $\{\mathbf{j}^{(s,g)}, \mathbf{k}^{(s,g)}\}$, so it would be in \tilde{C} by our construction. This is a contradiction, since there is no vertex in

$$[(C' \setminus \mathfrak{j}) \setminus (C \setminus \mathfrak{k})] \cap [(C \setminus \mathfrak{k}) \cup \mathfrak{j}] = (C' \setminus \mathfrak{j}) \cap \mathfrak{j} = \emptyset. \quad (3.111)$$

Next, we show that the term indexed by (\tilde{C}, \tilde{C}') is nonvanishing in Eq. (3.88). Let $h_{\mathcal{O}} = \prod_{r=0}^m h_{P(r)}$. We have

$$[h_{\tilde{C}}, h_{\tilde{C}'}] = [h_{\tilde{C}}, h_{C'} h_{\mathcal{O}}] \quad (3.112)$$

$$= [h_{\tilde{C}}, h_{C'} h_C h_{\tilde{C}}] \quad (3.113)$$

$$= [h_{\tilde{C}}, h_{C'}][h_{\tilde{C}}, h_C] \quad (3.114)$$

Note that there are odd-many vertices in $\cup_{r=0}^m P^{(r)}$ whose corresponding operator anticommutes with h_C . Clearly $h_{\mathbf{j}}$ anticommutes with h_C if \mathbf{j} is the initializing vertex of \mathcal{O} . If there is a dependent vertex in the deformation whose corresponding operator anticommutes with h_C , then it must be tethered to another such vertex with respect to C , or there is another initializing vertex that will allow us to continue the deformation. Thus, such vertices come in pairs, and we have that the total number of vertices whose corresponding operator anticommutes with h_C is odd. This gives $[h_{\tilde{C}}, h_C] = -1$, since odd many vertices whose operator commutes with h_C have been replaced by vertices for which

the corresponding operator anticommutes. Additionally, this gives $\llbracket h_{\tilde{C}}, h_{C'} \rrbracket = 1$, since odd many vertices in C' whose operator anticommutes with h_C have been replaced by vertices for which the corresponding operator commutes with $h_{\tilde{C}}$, and the total number of such vertices in C' was odd. Therefore, we have

$$\llbracket h_{\tilde{C}}, h_{\tilde{C}'} \rrbracket = -1. \quad (3.115)$$

Finally, we show that corresponding terms indexed by (C, C') and (\tilde{C}, \tilde{C}') cancel in Eq. (3.88). We have

$$[h_C, h_{C'}] + [h_{\tilde{C}}, h_{\tilde{C}'}] = 2(h_C h_{C'} + h_{\tilde{C}} h_{\tilde{C}'}). \quad (3.116)$$

Because h_C and $h_{C'}$ anticommute, exactly one of $h_{C'_e}$ or $h_{C'_d}$ anticommutes with h_C . Suppose $h_{C'_d}$ commutes, so we have

$$h_C h_{C'} = (h_{C_a} h_{C_b})(h_{C'_e} h_{C'_d}) \quad (3.117)$$

$$= h_{C'_d}(h_{C_b} h_{C_a}) h_{C'_e} \quad (3.118)$$

$$= (h_{C'_d \setminus \mathcal{O}} h_{(C'_d \cap \mathcal{O})}) [(h_{(C_b \cap \mathcal{O})} h_{C_b \setminus \mathcal{O}})] \quad (3.119)$$

$$\times (h_{C_a \setminus \mathcal{O}} h_{(C_a \cap \mathcal{O})}) [(h_{(C'_e \cap \mathcal{O})} h_{C'_e \setminus \mathcal{O}})]$$

$$= (-1)^{m+1} (h_{C'_d \setminus \mathcal{O}} h_{(C_b \cap \mathcal{O})}) [(h_{(C'_d \cap \mathcal{O})} h_{C_b \setminus \mathcal{O}})] \quad (3.120)$$

$$\times (h_{C_a \setminus \mathcal{O}} h_{(C'_e \cap \mathcal{O})}) [(h_{(C_a \cap \mathcal{O})} h_{C'_e \setminus \mathcal{O}})]$$

$$h_C h_{C'} = (-1)^{m+1} h_{\tilde{C}'_d} (h_{\tilde{C}'_b} h_{\tilde{C}'_a}) h_{\tilde{C}'_e} \quad (3.121)$$

where, e.g. $\tilde{C}_a := C_a \oplus (\cup_{r=0}^m P^{(r)})$, and similarly for the other coloring classes of \tilde{C} , \tilde{C}' . Next we check

$$\llbracket h_{\tilde{C}'_d}, h_{\tilde{C}} \rrbracket = \llbracket h_{C'_d} h_{[\mathcal{O} \cap (C_b \cup C'_d)]}, h_C h_{\mathcal{O}} \rrbracket \quad (3.122)$$

$$= \llbracket h_{C'_d}, h_C \rrbracket \llbracket h_{C'_d}, h_{\mathcal{O}} \rrbracket$$

$$\times \llbracket h_{[\mathcal{O} \cap (C_b \cup C'_d)]}, h_C \rrbracket \llbracket h_{[\mathcal{O} \cap (C_b \cup C'_d)]}, h_{\mathcal{O}} \rrbracket \quad (3.123)$$

If h_j anticommutes with $h_{\mathcal{O}}$ for $j \in C'_d$, then either h_j anticommutes with $h_{P^{(r)}}$ for exactly one (by Lemma 3.8) path component $P^{(r)} \subseteq G[C_a \oplus C'_c]$ of \mathcal{O} , or h_j anticommutes with $h_{P^{(r)}}$ for exactly

one path component $P^{(r)} \subseteq G[C_b \oplus C'_d]$. If $\Delta_C(\mathbf{j}) = 2$ and $h_{\mathbf{j}}$ anticommutes with $h_{P^{(r)}}$ for $P^{(r)} \subseteq G[C_a \oplus C'_c]$, then $h_{\mathbf{j}}$ satisfies both cases, so it commutes with $h_{\mathcal{O}}$. If $\Delta_C(\mathbf{j}) = 4$, then $h_{\mathbf{j}}$ satisfies neither case. Thus, the only vertices $\mathbf{j} \in \mathcal{O}$ for which $h_{\mathbf{j}}$ anticommutes with $h_{\mathcal{O}}$ are those for which $h_{\mathbf{j}}$ also anticommutes with h_C and for which $\mathbf{j} \in \mathcal{O} \cap C'_d$. Thus, we have

$$[[h_{C'_d}, h_{\mathcal{O}}]] = [[h_{\mathcal{O} \cap C'_d}, h_C]] = [[h_{[\mathcal{O} \cap (C_b \cup C'_d)]}, h_C]] \quad (3.124)$$

and

$$[[h_{\tilde{C}'_d}, h_{\tilde{C}}]] = [[h_{C'_d}, h_C]] [[h_{[\mathcal{O} \cap (C_b \cup C'_d)]}, h_{\mathcal{O}}]] \quad (3.125)$$

$$= [[h_{C'_d}, h_C]] [[h_{[\mathcal{O} \cap (C_b \cup C'_d)]}, h_{[\mathcal{O} \cap (C_a \cup C'_c)]]]] \quad (3.126)$$

We have

$$\begin{cases} h_{[\mathcal{O} \cap (C_b \cup C'_d)]} = \prod_{\{r | P^{(r)} \subseteq G[C_b \oplus C'_d]\}} h_{P^{(r)}} \\ h_{[\mathcal{O} \cap (C_a \cup C'_c)]} = \prod_{\{r | P^{(r)} \subseteq G[C_a \oplus C'_c]\}} h_{P^{(r)}} \end{cases} \quad (3.127)$$

To complete the proof, we consider the frustration graph G_P whose vertices correspond to the path operators $h_{P^{(r)}}$ for $P^{(r)} \in \mathcal{O}$. We will show that this graph captures the dependencies between the paths in the deformation \mathcal{O} in the following way

Lemma 3.9. Given the definitions above, suppose $P^{(r)}$ precedes $P^{(s)}$ in the deformation \mathcal{O} , then $h_{P^{(r)}}$ and $h_{P^{(s)}}$ will anticommute if and only if $P^{(s)}$ is dependent on $P^{(r)}$ in \mathcal{O} .

By the construction of \mathcal{O} together with Lemma 3.9, G_P is a connected tree with coloring classes given by $\mathcal{O} \cap (C_b \cup C'_d)$ and $\mathcal{O} \cap (C_a \cup C'_c)$, so

$$[[h_{[\mathcal{O} \cap (C_b \cup C'_d)]}, h_{[\mathcal{O} \cap (C_a \cup C'_c)]]] = (-1)^m. \quad (3.128)$$

Therefore,

$$[[h_{\tilde{C}'_d}, h_{\tilde{C}}]] = (-1)^m [[h_{C'_d}, h_C]] \quad (3.129)$$

$$[[h_{\tilde{C}'_d}, h_{\tilde{C}}]] = (-1)^m \quad (3.130)$$

by our assumption that $\llbracket h_{C'_d}, h_C \rrbracket = 1$, and we have

$$h_C h_{C'} = -h_{\tilde{C}'_d} h_{\tilde{C}'_c} (h_{\tilde{C}'_b} h_{\tilde{C}'_a}) h_{\tilde{C}'_c} = -h_{\tilde{C}} h_{\tilde{C}'} \quad (3.131)$$

and

$$[h_C, h_{C'}] + [h_{\tilde{C}}, h_{\tilde{C}'}] = 0 \quad (3.132)$$

For each collection of terms indexed by (C, C') sharing a fixed deformation \mathcal{O} , we can uniquely pair them using this deformation. This therefore proves Eq. (3.80c) and completes our proof of Theorem 3.1.

3.6 Exact Solution

With the identification of the conserved charges, we can then proceed to show the rest of Result 3.1. In particular, we show that within each symmetric subspace of the generalized-even-hole operators, a Hamiltonian with a simplicial, claw-free frustration graph exhibits a free fermion solution. Formally:

Theorem 3.2 (Exact Solution). Given a Hamiltonian, H , with frustration graph, G , which is claw-free and contains a simplicial clique. There exists a set of mutually commuting cycle symmetries $\{J_G[\langle C_0 \rangle]\}$ for H , such that we can write

$$H = \sum_{\mathcal{J}} \left(\sum_{j=1}^{\alpha(G)} \varepsilon_{\mathcal{J},j} [\psi_{\mathcal{J},j}, \psi_{\mathcal{J},j}^\dagger] \right) \Pi_{\mathcal{J}} \quad (3.133)$$

with

$$\psi_{\mathcal{J},j} := N_{\mathcal{J},j}^{-1} \Pi_{\mathcal{J}} T(-u_{\mathcal{J},j}) \chi T(u_{\mathcal{J},j}) \quad (3.134)$$

where the $\{\Pi_{\mathcal{J}}\}_{\mathcal{J}}$ are a complete set of projectors onto the mutual eigenspaces of the $\{J_G[\langle C_0 \rangle]\}$, and $u_{\mathcal{J},j}$ satisfies $Z_G(-u_{\mathcal{J},j}^2) \Pi_{\mathcal{J}} = 0$. Furthermore, the projectors $\Pi_{\mathcal{J}}$ satisfy

$$[\Pi_{\mathcal{J}}, \psi_{\mathcal{J}',j}] = 0 \quad (3.135)$$

for all \mathcal{J} , \mathcal{J}' , and j . The single-particle energies in the subspace labeled by \mathcal{J} are given by $\varepsilon_{\mathcal{J},j} = 1/u_{\mathcal{J},j}$.

The proof closely follows the analysis given in Refs. [23, 126] with slight modifications and generalizations where necessary. We first prove the following lemma relating the transfer operators to the generalized characteristic polynomial Z_G of the frustration graph G .

Lemma 3.10. Let H be a Hamiltonian with claw-free frustration graph G . The generalized characteristic polynomial, Z_G is given by

$$Z_G(-u^2) = \sum_{\mathcal{X} \in \mathcal{C}_G^{(\text{even})}} (-u^2)^{|\partial \mathcal{X}|/2} 2^{|\mathcal{X}|} I_{G \setminus \Gamma[\mathcal{X}]}(-u^2) \prod_{C \in \mathcal{X}} h_C \quad (3.136)$$

We prove Lemma 3.10 in Appendix 3.B. We also require the following lemma.

Lemma 3.11. Let H be an SCF Hamiltonian with frustration graph G . Further let K_s be a simplicial clique and let χ be a simplicial mode with respect to K_s . Then

$$\begin{aligned} T_G(u) \left(1 + u \sum_{j \in K_s} h_j \right) \chi T_G(-u) \\ = Z_G(-u^2) \left(1 - u \sum_{j \in K_s} h_j \right) \chi. \end{aligned} \quad (3.137)$$

We prove Lemma 3.11 in Appendix 3.C. Lemma 3.11 immediately shows that the incognito modes satisfy the eigenmode condition for the Hamiltonian over the subspace specified by \mathcal{J} .

Lemma 3.12. Let H be an SCF Hamiltonian with frustration graph G . The single particle energies $\{\varepsilon_{\mathcal{J},j}\}$ and incognito modes $\{\psi_{\mathcal{J},j}\}$ satisfy

$$[H, \psi_{\mathcal{J},\pm j}] = \pm 2\varepsilon_{\mathcal{J},j} \psi_{\mathcal{J},\pm j}. \quad (3.138)$$

Proof. We have

$$[H, \psi_{\mathcal{J},\pm j}] = N_{\mathcal{J},j}^{-1} \Pi_{\mathcal{J}} T(\mp u_{\mathcal{J},j}) [H, \chi] T(\pm u_{\mathcal{J},j}) \quad (3.139)$$

$$= 2N_{\mathcal{J},j}^{-1} \Pi_{\mathcal{J}} T(\mp u_{\mathcal{J},j}) \left(\sum_{j \in K_s} h_j \chi \right) T(\pm u_{\mathcal{J},j}) \quad (3.140)$$

Applying Lemma 3.11, together with the definition of $u_{\mathcal{J},j}$ that $\Pi_{\mathcal{J}} Z_G(-u_{\mathcal{J},j}^2) = 0$ gives

$$[H, \psi_{\mathcal{J}\pm j}] = \pm \frac{2}{u_{\mathcal{J},j} N_{\mathcal{J},j}} \Pi_{\mathcal{J}} T(\mp u_{\mathcal{J},j}) \chi T(\pm u_{\mathcal{J},j}) \quad (3.141)$$

$$= \pm 2\varepsilon_{\mathcal{J},j} \psi_{\mathcal{J},\pm j}, \quad (3.142)$$

completing the proof. \square

We now show that the incognito modes $\{\psi_{\mathcal{J},\pm j}\}$ obey the canonical anticommutation relations.

Lemma 3.13. Let H be an SCF Hamiltonian with frustration graph G . The incognito modes $\{\psi_{\mathcal{J},\pm j}\}$ satisfy the following anticommutation relations.

$$\{\psi_{\mathcal{J},+j}, \psi_{\mathcal{J}',-k}\} = \delta_{\mathcal{J},\mathcal{J}'} \delta_{jk} \Pi_{\mathcal{J}}. \quad (3.143)$$

We prove Lemma 3.13 in Appendix 3.D. Finally, we show that we can write the Hamiltonian H as a free-fermion Hamiltonian in the eigenmode basis.

Lemma 3.14. Let H be an SCF Hamiltonian with frustration graph G . The single particle energies $\{\varepsilon_k\}_{k=1}^{\alpha(G)}$ and incognito modes $\{\psi_{\pm j}\}_{j=1}^{\alpha(G)}$ satisfy

$$H = \sum_{\mathcal{J}} \left(\sum_{j=1}^{\alpha(G)} \varepsilon_{\mathcal{J},j} [\psi_{\mathcal{J},+j}, \psi_{\mathcal{J},-j}] \right) \Pi_{\mathcal{J}}. \quad (3.144)$$

We prove Lemma 3.14 in Appendix 3.E. Combining Lemma 3.12, Lemma 3.13, and Lemma 3.14 proves Theorem 3.1.

3.7 Polynomial Division

We next present an alternative solution method inspired by a well-known polynomial divisibility result of Godsil [129] and a recently emerging body of work on operator Krylov subspaces [130–132]. As such, we expect the method to provide a strategy for applying graph theory to more general models, and, for our purposes, it will provide a better physical intuition for the free-fermion modes in the Pauli basis where H is defined. The technical content of the method is captured by the following theorem

Theorem 3.3 (Polynomial Divisibility). There exists a real matrix \mathbf{A} with elements indexed by

induced paths in G such that

$$\mathrm{ad}_{iH}^k \chi = (-2)^k \sum_{P \in \mathcal{P}} (\mathbf{A}^k)_{\{j^*\}, P} h_P. \quad (3.145)$$

over each mutual eigenspace of the $\{J_G[\langle C_0 \rangle]\}$, where χ is a simplicial mode corresponding to the vertex $j^* \notin V$, and we define $\mathrm{ad}_{iH} \chi := [iH, \chi]$. The matrix \mathbf{A} is the weighted adjacency matrix of a directed bipartite graph.

3.7.1 Implications of Theorem 3.3

Before continuing to the proof, let us elaborate on some implications of Theorem 3.3. The theorem already appears very “holographic” in the sense that commutation with the Hamiltonian only changes path operators at the endpoints. This is entirely due to the fact that the frustration graph is claw-free. We make this precise by showing that the theorem implies a set of fermion modes given by repeated commutators with the Hamiltonian.

Corollary 3.6. The operators generated by repeated commutation with H satisfy

$$\{\mathrm{ad}_{iH}^j \chi, \mathrm{ad}_{iH}^k \chi\} = 2M_{jk}I \quad (3.146)$$

where the matrix \mathbf{M} is real symmetric.

Proof. We show Eq. (3.146) by induction on j . Note that, for all k

$$\begin{aligned} \{\mathrm{ad}_{iH}^0 \chi, \mathrm{ad}_{iH}^k \chi\} &= \{\chi, \mathrm{ad}_{iH}^k \chi\} \\ &= (-i)^k 2^{k+1} (\mathbf{A}^k)_{\{j^*\}, \{j^*\}} I \end{aligned} \quad (3.147)$$

by applying Theorem 3.3 to $\mathrm{ad}_{iH}^k \chi$ together with the fact that the only operator in the sum that does not anticommute with χ is itself. Thus, the corollary holds for $j = 0$ with

$$M_{0,k} = (-2i)^k (\mathbf{A}^k)_{\{j^*\}, \{j^*\}}. \quad (3.148)$$

Now assume that

$$\{\mathrm{ad}_{iH}^\ell \chi, \mathrm{ad}_{iH}^k \chi\} = 2M_{\ell,k}I, \quad (3.149)$$

for all k , for some matrix \mathbf{M} , and all $\ell < \{0, \dots, j-1\}$. Then

$$\begin{aligned} [\mathrm{ad}_{iH}^j \chi, \mathrm{ad}_{iH}^k \chi] &= [\mathrm{ad}_{iH} \left(\mathrm{ad}_{iH}^{j-1} \chi \right), \mathrm{ad}_{iH}^k \chi] \\ &= [H, [\mathrm{ad}_{iH}^{j-1} \chi, \mathrm{ad}_{iH}^k \chi]] - [\mathrm{ad}_{iH}^{j-1} \chi, \mathrm{ad}_{iH}^{k+1} \chi] \\ &= -2M_{j-1, k+1} I - 2 \mathrm{ad}_{iH}^k \chi \mathrm{ad}_{iH}^j \chi, \end{aligned} \quad (3.150)$$

The second line follows by the Jacobi identity. The third line follows from applying the inductive hypothesis with the identity

$$[A, B] = \{A, B\} - 2BA \quad (3.151)$$

and canceling terms. Applying Eq. (3.151) again to Eq. (3.150) gives.

$$\{\mathrm{ad}_{iH}^j \chi, \mathrm{ad}_{iH}^k \chi\} = -2M_{j-1, k+1} I.$$

This shows the first part of the corollary. By solving the recursion relation for \mathbf{M} , we have

$$\begin{aligned} \{\mathrm{ad}_{iH}^j \chi, \mathrm{ad}_{iH}^k \chi\} &= 2(-i)^j M_{0, j+k} I \\ \{\mathrm{ad}_{iH}^j \chi, \mathrm{ad}_{iH}^k \chi\} &= (-i)^{j+k} 2^{j+k+1} (\mathbf{A}^{j+k})_{\{j^*\}, \{j^*\}} I \end{aligned} \quad (3.152)$$

This gives

$$M_{jk} = (-2i)^{j+k} (\mathbf{A}^{j+k})_{\{j^*\}, \{j^*\}} \quad (3.153)$$

so \mathbf{M} is real symmetric. \square

While we may take as many commutators with H as we like, the fact that the set of induced paths of G is finite implies that there is a minimal rank, r , such that $\mathrm{ad}_{iH}^r \chi$ is a linear combination of the elements of $\{\mathrm{ad}_{iH}^j \chi\}_{j=0}^{r-1}$. Suppose we have

$$\mathrm{ad}_{iH}^r \chi = \sum_{k=0}^{r-1} v_k \mathrm{ad}_{iH}^k \chi \quad (3.154)$$

this gives

$$\{\text{ad}_{iH}^j \chi, \text{ad}_{iH}^r \chi\} = \sum_{k=0}^{r-1} v_k \{\text{ad}_{iH}^j \chi, \text{ad}_{iH}^k \chi\} \quad (3.155)$$

$$= 2(\mathbf{M} \cdot \mathbf{v})_j I. \quad (3.156)$$

Thus, it suffices to consider only the spanning set given by the elements of $\{\text{ad}_{iH}^j \chi\}_{j=0}^{r-1}$, and we take \mathbf{M} to be an $r \times r$ matrix. We will see that, in fact, the value of this rank is generally much lower than the number of induced paths in G .

By the definition of \mathbf{M} , we have

$$(\mathbf{v}^T \cdot \mathbf{M} \cdot \mathbf{v}) = \frac{1}{2d} \sum_{j,k=0}^{r-1} v_j v_k \text{tr}(\{\text{ad}_{iH}^j \chi, \text{ad}_{iH}^k \chi\}) \quad (3.157)$$

$$= \frac{1}{d} \text{tr} \left[\left(\sum_{j=0}^{r-1} v_j \text{ad}_{iH}^j \chi \right)^2 \right] \quad (3.158)$$

Because this is the trace of the square of a non-zero Hermitian matrix, it is positive. Thus, \mathbf{M} is positive definite. This allows us to define a set of “physical” Majorana modes $\{\gamma_j\}_{j=0}^{r-1}$ by diagonalizing \mathbf{M} as

$$\mathbf{M} = \mathbf{U}^T \mathbf{D} \mathbf{U} \quad (3.159)$$

where \mathbf{U} is an orthogonal matrix and \mathbf{D} is a diagonal matrix with positive elements $D_{jj} \equiv \lambda_j$ along the main diagonal. We next define

$$\gamma_j = i^{(j \bmod 2)} \lambda_j^{-1/2} \sum_{k=0}^{r-1} U_{jk} \text{ad}_{iH}^k \chi. \quad (3.160)$$

These operators are Hermitian and satisfy the canonical anticommutation relations for fermions

$$\{\gamma_j, \gamma_k\} = 2\delta_{jk} I. \quad (3.161)$$

As a result, they are trace-orthogonal

$$d^{-1} \text{tr}(\gamma_j \gamma_k) = \frac{1}{2d} \text{tr}(\{\gamma_j, \gamma_k\}) = \delta_{jk} \quad (3.162)$$

where d is the Hilbert-space dimension. We can write the elements of an effective single-particle

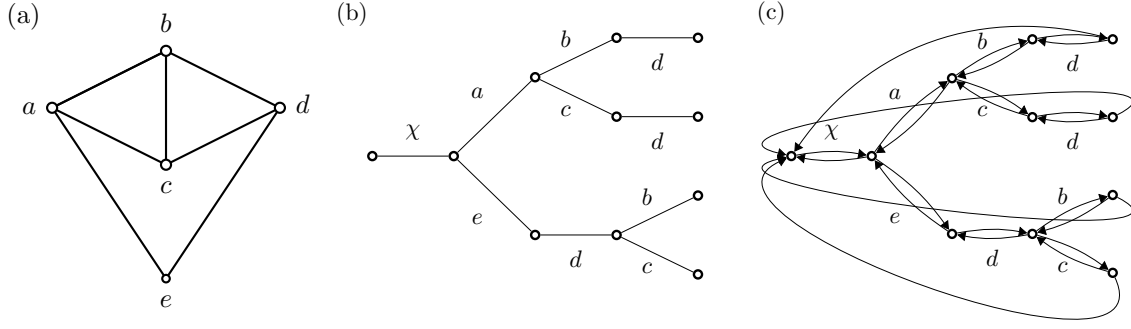


Figure 3.4: The induced path tree: (a) a simplicial, claw-free graph with an even hole; (b) a path tree from a simplicial vertex attached to the simplicial clique $\{a, e\}$ in the graph; (c) the hopping graph of a walk induced by the nested commutators of χ with the Hamiltonian H for which the graph is the frustration graph.

Hamiltonian by

$$h_{jk} = -\frac{i}{2d} \text{tr}[\gamma_j \text{ad}_H(\gamma_k)] \quad (3.163)$$

Formally, \mathbf{h} is given by the inverse transformation relating the $\{\gamma_j\}_{j=0}^{r-1}$ to the $\{\text{ad}_{i_H}^j \chi\}_{j=0}^{r-1}$ applied to the companion matrix for ad_{i_H} on the cyclic subspace generated by χ .

3.7.2 Induced path trees

We next turn to the proof of Theorem 3.3. While the only specific property of \mathbf{A} that we rely on is the fact that it is the weighted adjacency matrix of a directed bipartite graph, it will be helpful to propose the specific form of \mathbf{A} here. For this purpose, we define the *induced path tree* $\Upsilon(G)$ of G . The definition of $\Upsilon(G)$ is given in Ref. [100] and we repeat it here with our conventions.

Definition 3.14 (Induced path tree with respect to \mathbf{j} [100]). For $\mathbf{j} \in V$, the *induced path tree*, $\Upsilon_{\mathbf{j}}(G)$, of G with respect to \mathbf{j} is defined recursively. If G is a tree, then $\Upsilon_{\mathbf{j}}(G) = G$, and we say that \mathbf{j} is the root of $\Upsilon_{\mathbf{j}}(G)$. Otherwise, we consider the forest of disjoint trees $\Upsilon_{\mathbf{k}}((G \setminus \Gamma[\mathbf{j}]) \cup \{\mathbf{k}\})$ with root \mathbf{k} for each $\mathbf{k} \in \Gamma(\mathbf{j})$. We then define $\Upsilon_{\mathbf{j}}(G)$ by appending a root vertex corresponding to \mathbf{j} and connecting it to the roots of each of these trees.

As in Ref. [100], we also define an induced path tree with respect to a clique, $K \subseteq G$.

Definition 3.15 (Induced path tree with respect to K [100]). Let K be a clique. The induced path tree $\Upsilon_K(G)$ of G with respect to K is defined as follows. Let G^* be the graph formed by attaching a new vertex \mathbf{j}^* to G with the property that $(\mathbf{j}^*, \mathbf{k}) \in E(G^*)$ for all $\mathbf{k} \in K$. Then $\Upsilon_K(G) := \Upsilon_{\mathbf{j}^*}(G^*)$.

Note that G^* from Def. 3.15 is also simplicial, claw-free. Clearly it is simplicial since \mathbf{j}^* is a simplicial vertex. Suppose that it contains a claw, then that claw must contain \mathbf{j}^* since G is claw-free. However, $\Gamma(\mathbf{j}^*) = K_s$, so there must be some vertex $\mathbf{k} \in \Gamma(\mathbf{j}^*)$ that neighbors an independent set of order at least three. Suppose that this is the case, then the set $\Gamma[\mathbf{k}] \setminus \Gamma[\mathbf{j}^*]$ must contain a pair of non-neighboring vertices, but this contradicts our assumption that K_s is simplicial. Therefore, we must have that G^* is a simplicial, claw-free graph as well. In particular, we shall use the fact that all of the neighboring relations in Table 3.2 hold for induced paths containing \mathbf{j}^* as an endpoint in G^* . Also note that $G \setminus K$ is also simplicial, with simplicial cliques defined by $\Gamma_{G \setminus K}(v)$ for all $v \in K$ [100].

Fig. (3.4a) shows a small example of a claw-free simplicial graph, we have identified the simplicial clique $K = \{a, e\}$ and constructed the induced path tree $\Upsilon_K(G)$ (equivalently $\Upsilon_{\mathbf{j}^*}(G^*)$) in Fig. (3.4b). In what follows, we shall always consider the induced path tree with respect to a fixed simplicial clique of G , so we drop the explicit \mathbf{j}^* -dependence in our notation as $\Upsilon(G^*) \equiv \Upsilon_{\mathbf{j}^*}(G^*)$.

The graph, Λ , is related to the graph Υ by replacing each edge in Υ with a pair of directed arcs, and we additionally add a set of arcs corresponding to the generalized cycles in G as follows. There is an arc from P to P' in Λ if there is a vertex $\mathbf{k} \notin P$ such that $P \cup \{\mathbf{k}\}$ is a bubble wand (see Def. 3.10) with P' the handle, and the hoop is an even hole. An example of the graph Λ is shown in Fig. (3.4c).

We now define the matrix elements, $A_{PP'}$, for $(P, P') \in E_\Lambda$, as

$$A_{PP'} \equiv \begin{cases} 1 & |P'| > |P| \\ b_j^2 & P' = P \setminus \{\mathbf{j}\} \\ \frac{\mathcal{J}_{\langle C_0 \rangle}}{N_{P, P', \langle C_0 \rangle}} & \text{hoop in } \langle C_0 \rangle \end{cases} \quad (3.164)$$

and zero otherwise. The normalization factor is chosen such that $\frac{1}{2} \sum_{P'} N_{P, P', \langle C_0 \rangle}^{-1} = 1$. Each of these cases corresponds to a particular non-vanishing contribution from an additional application of ad_{iH} in a fixed mutual subspace of the generalized cycle symmetries. In the first two cases, the induced path can transition to an adjacent induced path in the induced path tree. In the last case, the induced path “wraps around” an even hole, and this even-hole part contributes a factor of the generalized cycle eigenvalue in the given subspace. There is an additional factor of two due to the fact that the path can wrap around the hole in either direction.

To prove Theorem 3.3, we will also consider a particular Pauli representation of G^* , and we will prove particular properties of G^* using this representation. Since the result will be a property of G^* alone, it will not depend on the representation, and we can conclude that it holds for all representations

of G^* . We choose the representation to have the property that

$$d^{-1} \operatorname{tr} \left(h_P^\dagger h_{P'} \right) = \delta_{PP'} \quad (3.165)$$

for any pair of induced paths $P, P' \in \mathcal{P}_{G^*}$. For an explicit instance of such a representation, we can take the so-called *fiducial bosonization* from Ref. [124]. In this representation, we assign a qubit to each edge $e = (\mathbf{j}, \mathbf{k}) \in E_G$ of the frustration graph. Without loss of generality, we choose one of the terms from $h_{\mathbf{j}}$ and $h_{\mathbf{k}}$ to act on this qubit as σ_e^z , and we let the other term act as σ_e^x (e.g. $h_{\mathbf{j}}$ acts as σ_e^z and $h_{\mathbf{k}}$ acts as σ_e^x). Additionally the only terms acting on the qubit corresponding to edge e are $h_{\mathbf{j}}$ and $h_{\mathbf{k}}$. Thus, h_P is the only induced-path operator acting as σ^y only on the qubits corresponding to the edges in $E[P]$, so it satisfies the property above.

3.7.3 The single-vertex-deformation closure of an induced path

We now prove the following lemma regarding paths within the same single-vertex-deformation closure.

Lemma 3.15. Given an induced path

$$P := \mathbf{j}^* - \mathbf{j}_1 - \dots - \mathbf{j}_\ell \quad (3.166)$$

with $\ell \geq 2$, then we have

$$(\mathbf{A}^k)_{\{\mathbf{j}^*\}, P} = (\mathbf{A}^k)_{\{\mathbf{j}^*\}, \tilde{P}} \quad (3.167)$$

for all $\tilde{P} \in \langle P \rangle$ and all $k \geq 0$.

Proof. It is sufficient to prove the lemma for \tilde{P} given by a single-vertex deformation of P . By convention, we take $\mathbf{j}_0 \equiv \mathbf{j}^*$, and we let

$$\tilde{P} \equiv (P \setminus \{\mathbf{j}_i\}) \cup \{\mathbf{k}\} \quad (3.168)$$

for $\mathbf{k} \prec_P \mathbf{j}_i$, with $i \in \{1, \dots, \ell - 1\}$. It is useful to consider $(\mathbf{A}^k)_{P, P'}$ as the weighted sum of walks

from P to P' on $\Lambda(G^*)$ in k steps. Let $P_m := \mathbf{j}^* - \mathbf{j}_1 - \dots - \mathbf{j}_m$ for $m \leq \ell$, with $P_\ell := P$, and define

$$\tilde{P}_m := \begin{cases} P_m & m < i \\ (P_m \setminus \{\mathbf{j}_i\}) \cup \{\mathbf{k}\} & m \geq i \end{cases}. \quad (3.169)$$

We first show that, if a weighted arc $P_r \rightarrow P_s$ is present in Λ for $r, s \in \{i, i+1, \dots, \ell\}$, then there is a corresponding arc $\tilde{P}_r \rightarrow \tilde{P}_s$ with the same weight present as well. Suppose P_r and P_s are neighboring in $\Upsilon(G^*)$. If $s > r$, then $P_r \subset P_s$ with $P_s \setminus P_r = \{\mathbf{j}_s\}$. Because $r \geq i$, we must have $s \geq i+1$, so $\tilde{P}_r \subset \tilde{P}_s$ with $\tilde{P}_s \setminus \tilde{P}_r = \{\mathbf{j}_s\}$. Thus, there is an arc $P_r \rightarrow P_s$ with weight 1 present in Λ in this case. If $s < r$, $P_s \subset P_r$ with $P_r \setminus P_s = \{\mathbf{j}_r\}$. Because $s \geq i$, we must have $r \geq i+1$, so $\tilde{P}_r \subset \tilde{P}_s$ with $\tilde{P}_s \setminus \tilde{P}_r = \{\mathbf{j}_r\}$. Thus, there is an arc $P_r \rightarrow P_s$ with weight $b_{\mathbf{j}_r}^2$ present in Λ in this case.

If $(P_r, P_s) \notin E_{\Upsilon(G^*)}$, then there is a vertex $\mathbf{s} \in \Gamma(\mathbf{j}_r) \setminus \Gamma[\mathbf{j}_{r-1}]$ such that $P_r \cup \{\mathbf{s}\} = P_s \cup C$ with $C \in \langle C_0 \rangle$. Restricting to this case, if $s = i$, then we must have that \mathbf{s} and \mathbf{k} are neighboring. If this is not the case, then $\{\mathbf{j}_{i+1}, \mathbf{s}, \mathbf{k}, \mathbf{j}_{i+2}\}$ induces a claw in G . Thus, we have $\Gamma_{\tilde{P}_r}(\mathbf{s}) = \{\mathbf{j}_r, \mathbf{k}, \mathbf{j}_{i+1}\}$ and so $\tilde{P}_r \cup \{\mathbf{s}\} = \tilde{P}_s \cup C$ with $C \in \langle C_0 \rangle$. If $s > i$, then $\tilde{P}_r \cup \{\mathbf{s}\} = \tilde{P}_s \cup C$ with $C \in \langle C_0 \rangle$. Thus, there is an arc $\tilde{P}_r \rightarrow \tilde{P}_s$ with the same weight as that from $P_r \rightarrow P_s$.

Consider the weighted sum of walks from $\{\mathbf{j}^*\}$ to P on Λ in k steps. Since every walk in this sum must end at P , there must be a step $m \leq k$, which is the last step in which the arc $P_{i-1} \rightarrow P_i$ is traversed. After this, no arcs $P_r \rightarrow P_s$ can be traversed where $s < i$. Otherwise, the walk would need to traverse the arc $P_{i-1} \rightarrow P_i$ again. Thus, all arcs $P_r \rightarrow P_s$ traversed after step m will have $r, s \in \{i, i+1, \dots, \ell\}$. Since $A_{P_{i-1}, P_i} = A_{P_{i-1}, \tilde{P}_i} = 1$, we can substitute $A_{P_{i-1}, P_i} \rightarrow A_{P_{i-1}, \tilde{P}_i}$ at step m and $A_{P_r, P_s} \rightarrow A_{\tilde{P}_r, \tilde{P}_s}$ thereafter. This gives a walk with an equal weight that ends at \tilde{P} , and since this substitution can be performed for each term in the sum, we therefore we have

$$(\mathbf{A}^k)_{\{\mathbf{j}^*\}, P} = (\mathbf{A}^k)_{\{\mathbf{j}^*\}, \tilde{P}}, \quad (3.170)$$

proving the lemma. \square

We note that a single-vertex deformation of a path P is a special case of a bubble wand with the hoop being a cycle of length three. Thus, we expect there to be a similar result, regarding bubble wands when the hoops are even holes and describe symmetries of the model, which we shall see in the following proof.

3.7.4 Proof of Theorem 3.3

We proceed to prove Theorem 3.3 by induction on the power, k , of ad_{iH} . Clearly, we have

$$\text{ad}_{iH}^0 \chi = \chi = (-2i)^0 \sum_{P \in \mathcal{P}} (\mathbf{A}^0)_{\{j^*\}, P} h_P \quad (3.171)$$

$$\text{ad}_{iH} \chi = -2i \sum_{j \in K_s} \chi h_j = -2i \sum_{P \in \mathcal{P}} (\mathbf{A})_{\{j^*\}, P} h_P \quad (3.172)$$

so the theorem holds for $k \in \{0, 1\}$. Now assume it is true for all powers $m < k$,

$$\text{ad}_{iH}^m \chi = \sum_P (\mathbf{A}^m)_{\{j^*\}, P} h_P \quad (3.173)$$

for $m < k$, and take

$$(-2i)^{-k} \text{ad}_{iH}^k \chi = (-2i)^{-k} [iH, \text{ad}_{iH}^{k-1} \chi] \quad (3.174)$$

$$= -\frac{1}{2} \sum_P (\mathbf{A}^{k-1})_{\{j^*\}, P} [iH, h_P] \quad (3.175)$$

$$\begin{aligned} &= \sum_{P \equiv j^* \dots j_\ell} (\mathbf{A}^{k-1})_{\{j^*\}, P} b_{j_\ell}^2 h_{P \setminus j_\ell} \\ &\quad + \sum_P (\mathbf{A}^{k-1})_{\{j^*\}, P} \sum_{\substack{j \notin P \\ \llbracket h_j, h_P \rrbracket = -1}} h_P h_j \end{aligned} \quad (3.176)$$

From the second to the third line, we have expanded the commutator by linearity in $H = \sum_{j \in V} h_j$ and grouped terms according to whether $j \in P$ or $j \notin P$. In the former case, the only operator h_j with $j \in P$ that anticommutes with h_P is h_{j_ℓ} , and this gives the first term in Eq. (3.176). By Lemma 3.3, there are three cases whereby h_j can anticommute with h_P for $j \notin P$. In case (b.i), where $j \prec_P k$, we have a unique additional term corresponding to $\tilde{P} \equiv (P \setminus k) \cup \{j\}$ and $k \notin \tilde{P}$, which cancels that corresponding to P and j as

$$(\mathbf{A}^{k-1})_{\{j^*\}, P} h_P h_j + (\mathbf{A}^{k-1})_{\{j^*\}, \tilde{P}} h_{\tilde{P}} h_k \quad (3.177)$$

$$\begin{aligned} &= \left[(\mathbf{A}^{k-1})_{\{j^*\}, P} - (\mathbf{A}^{k-1})_{\{j^*\}, \tilde{P}} \right] h_P h_j \\ &= 0. \end{aligned} \quad (3.178)$$

In case (b.iv), we have that $\Gamma_P(j) = \{j_s, j_{s+1}, j_\ell\}$ for $0 \leq s < \ell - 2$ (if $s = \ell - 2$, then we again have case (b.i)). Let $P' := j^* \dots j_1 \dots j_s$, then we have that $C := (P \setminus P') \cup \{j\}$ gives a hole in G . Next, let

$P^* \equiv (P \cup \{j\}) \setminus \{j_{s+1}\}$ be the path traversing C in the “opposite direction” to P . We will show that

$$(\mathbf{A}^m)_{\{j^*\}, P} = (\mathbf{A}^m)_{\{j^*\}, P^*} \quad (3.179)$$

for all powers $m < k$. We have

$$(\mathbf{A}^m)_{\{j^*\}, P} = \sum_{\mathbf{P} \in \mathcal{P}_G^{\times m-1}} A_{\{j^*\}, P^{(1)}} A_{P^{(1)}, P^{(2)}} \dots A_{P^{(m-1)}, P} \quad (3.180)$$

where $\mathbf{P} = \{P^{(1)}, \dots, P^{(m-1)}\}$ is a walk on the directed graph with weighted adjacency matrix \mathbf{A} .

Let us group terms in this sum by walks which pass P' for the last time at step g . This gives

$$\begin{aligned} (\mathbf{A}^m)_{\{j^*\}, P} &= \sum_{g=0}^m \sum_{\mathbf{P} \in \mathcal{P}_G^{\times g-1}} A_{\{j^*\}, P^{(1)}} \dots A_{P^{(g-1)}, P'} \\ &\quad \times \left(\mathbf{A}_{G \setminus (P' \cup \{j, j_{s+1}\})}^{m-g} \right)_{\{j_{s+1}\}, (P \setminus P')} \end{aligned} \quad (3.181)$$

where $\mathbf{A}_{G \setminus (P' \cup \{j, j_{s+1}\})}$ is the graph corresponding to the weighted adjacency matrix $G \setminus (P' \cup \{j, j_{s+1}\})$ in the natural way. It is a result of Ref. [102] that $h_{j_{s+1}}$ is a simplicial mode for $P' \cup \{j, j_{s+1}\}$, so this matrix is well defined.

First, note that, strictly speaking, we cannot have $g = m$ by the requirement that $s < \ell - 2$ and the fact that the length of a path can increase by at most one at any step in the walk. This implies that the largest g can be is $m - 3$, but we will include all values of g that are not obviously forbidden in Eq. (3.181) with the understanding that there are no terms in the sum when g is too large. Next, we see that once the walk passes through P' for the last time, it must immediately next pass through $P' \cup \{j_{s+1}\}$, or it will eventually have to return to P' again to proceed to P . Since j neighbors j_s and j_{s+1} , if the walk passes through any path containing j from this point, it will again return to P' by the definition of \mathbf{A} . Finally, if the walk ever passes through a path $P_r := j^* - j_1 - \dots - j_r$ for $r \leq s$, then it must pass through P' again. Thus, our requirement that the walk passes through P' for the last time at step g gives Eq. (3.181). To prove Eq. (3.179), it is sufficient to prove

$$\left(\mathbf{A}_{G \setminus \{j, k\}}^m \right)_{\{j\}, (P \setminus \{j^*\})} = \left(\mathbf{A}_{G \setminus \{j, k\}}^m \right)_{\{k\}, (P^* \setminus \{j^*\})} \quad (3.182)$$

for $j, k \in K_s$ with simplicial mode corresponding to vertex j^* , and $P^* := (P \cup \{k\}) \setminus \{j\}$ with $(P \setminus \{j^*\}) \cup \{k\} = (P^* \setminus \{j^*\}) \cup \{j\} \in \mathcal{C}_G$. We thus proceed to prove Eq. (3.182).

Letting

$$H' \equiv H - h_j - h_{\mathbf{k}} \quad (3.183)$$

we next apply the inductive hypothesis and assume the fiducial bosonization of Ref. [124] to obtain

$$\left(\mathbf{A}_{G \setminus \{j, \mathbf{k}\}}^m \right)_{\{j\}, (P \setminus \{j^*\})} = \left(d \prod_{\mathbf{u} \in P} b_{\mathbf{u}}^2 \right)^{-1} \text{tr} \left[h_P^\dagger \text{ad}_{H'}^m (\chi h_j) \right] \quad (3.184)$$

where

$$h_P^\dagger = \left(\prod_{\mathbf{u} \in C} b_{\mathbf{u}}^2 \right) (h_C^\dagger h_C) h_P^\dagger \quad (3.185)$$

$$h_P^\dagger = b_{\mathbf{k}}^{-2} h_C^\dagger (h_{\mathbf{k}} \chi) \quad (3.186)$$

This gives

$$\begin{aligned} & \left(\mathbf{A}_{G \setminus \{j, \mathbf{k}\}}^m \right)_{\{j\}, (P \setminus \{j^*\})} \\ &= \left(d \prod_{\mathbf{u} \in C} b_{\mathbf{u}}^2 \right)^{-1} \text{tr} \left[h_C^\dagger (h_{\mathbf{k}} \chi) \text{ad}_{H'}^m (\chi h_j) \right] \end{aligned} \quad (3.187)$$

$$= (-1)^m \left(d \prod_{\mathbf{u} \in C} b_{\mathbf{u}}^2 \right)^{-1} \text{tr} \left\{ (h_j \chi) \text{ad}_{H'}^m \left[h_C^\dagger (\chi h_{\mathbf{k}}) \right] \right\} \quad (3.188)$$

where we have applied the identity

$$\text{tr} (X \text{ad}_{iH} Y) = -\text{tr} (Y \text{ad}_{iH} X) \quad (3.189)$$

m times in succession. We next sum over all deformations of P to obtain

$$\begin{aligned} \sum_{P \in \langle P \rangle} \left(\prod_{\mathbf{u} \in C} b_{\mathbf{u}}^2 \right) (\mathbf{A}^m)_{\{j^*\}, P} \\ = (-1)^m \text{tr} \{ (h_j \chi) \text{ad}_{H'}^m [J_G[\langle C \rangle] (\chi h_{\mathbf{k}})] \} \end{aligned} \quad (3.190)$$

$$= (-1)^m \text{tr} \{ (h_j \chi) J_G[\langle C \rangle] \text{ad}_{H'}^m [(\chi h_{\mathbf{k}})] \} \quad (3.191)$$

$$= (-1)^m \sum_{P \in \langle P \rangle} \text{tr} \{ (h_j \chi) h_C^\dagger \text{ad}_{H'}^m (\chi h_{\mathbf{k}}) \} \quad (3.192)$$

$$= (-1)^{m+|C|} \sum_{P \in \langle P \rangle} \left(\prod_{\mathbf{u} \in C} b_{\mathbf{u}}^2 \right) (\mathbf{A}^m)_{\{j^*\}, P^*} \quad (3.193)$$

Applying Lemma 3.15, we have that the matrix amplitude in the sum is a constant, so we have the result Eq. (3.182). By pairing corresponding walks to P and P^* with the same first $g-1$ steps in Eq. (3.181), we have the full result Eq. (3.179). Therefore, in case (b.iv), contributions from odd holes cancel, and contributions from even holes add. This therefore proves the theorem. \square

3.8 Numerical Example

We now apply our formalism to a two dimensional model that has previously not been discussed in the literature. The system is supported on a two-dimensional square lattice, with five qubits located on the links of the lattice, such that there is a spin at each of the positions $(j + \frac{\alpha}{6}, k)$ and $(j, k + \frac{\alpha}{6})$ for $\alpha = \{1, 2, 3, 4, 5\}$. The frustration graph of the model is shown in Fig. 3.5. The frustration graph is not a line graph, thus admitting no obvious map to free fermions [22]; also, since the graph is two-dimensional the model necessarily contains even holes, and thus falls beyond the scope of Ref. [126]. Nevertheless, the frustration graph is claw-free and contains a simplicial clique, thus admitting a free-fermion solution of the form Eq. (3.2). The model was constructed by first designing a two-dimensional, claw-free, simplicial graph which is not a line graph and finding a qubitization of the model, which we provide in Sect. 3.F. As we have shown, the free-fermion solution does not depend on this particular realization, so we do not write it explicitly here. We stress that, while the solution can be found by mapping the model to a line graph through a local unitary transformation, the model was not constructed to have this property.

For small system sizes it is possible to construct the full independence polynomial and generalized characteristic polynomial of the graph, from which the single particle energies and fermionic modes can be extracted. However, in the thermodynamic limit this is not practical. It is perhaps more informative

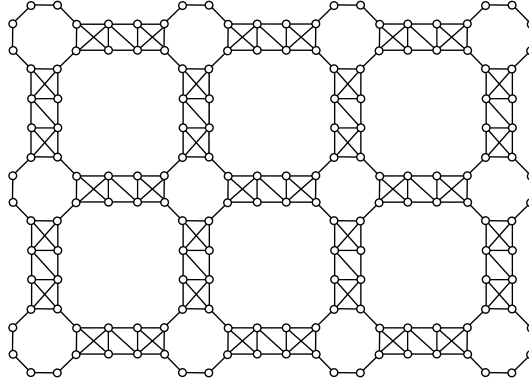


Figure 3.5: The frustration graph for the two-dimensional model analyzed below. The frustration graph is simplicial and claw-free. The model is neither a line graph nor (even-hole, claw)-free and so exists beyond the scope of Refs. [22, 126]

to use our knowledge of the existence of such a solution to construct a unitary (and therefore spectrum-preserving) transformation which maps the model from its present form to one whose frustration graph is a line graph.

The unit cell of the model contains sixteen Hamiltonian terms acting on ten qubits; however, there is an obvious symmetry between the horizontal and vertical links of the lattice. It is sufficient therefore to consider the transformation on a single arm of the graph containing eight vertices (Hamiltonian terms) applied to five qubits; we thus denote the Hamiltonian on each of the arms of the graph as

$$H_{\text{arm}} = h_a + h_b + h_c + h_d + h_e + h_f + h_g + h_h$$

with each term associated to the Pauli realization given in Eq. (3.263) in the natural way.

The transformation is depicted graphically in Fig. 3.6a. In each step the Hamiltonian is conjugated by a unitary generated by the product of a pair of terms, choosing the generating angle to remove one of the terms. This will generally introduce new terms in the Hamiltonian with interaction strengths depending on the rotation angle of our previous steps. By choosing our rotations appropriately, we can iterate this procedure until the frustration graph is a line graph. While our result guarantees that such a unitary circuit exists, in general cases it may be difficult to find in practice.

We begin by applying a unitary rotation to contract the edge between the vertices c and d . This rotation is generated by the product of the Hamiltonian terms h_c and h_d in each of the halved unit cells so that $U_{cd} = \prod_{j,k} e^{\theta h_c h_d}$ with $\theta = \frac{1}{2} \arctan\left(\frac{c}{d}\right)$ and chosen such that $U_{cd}(h_c + h_d)U_{cd}^\dagger = h_\delta$

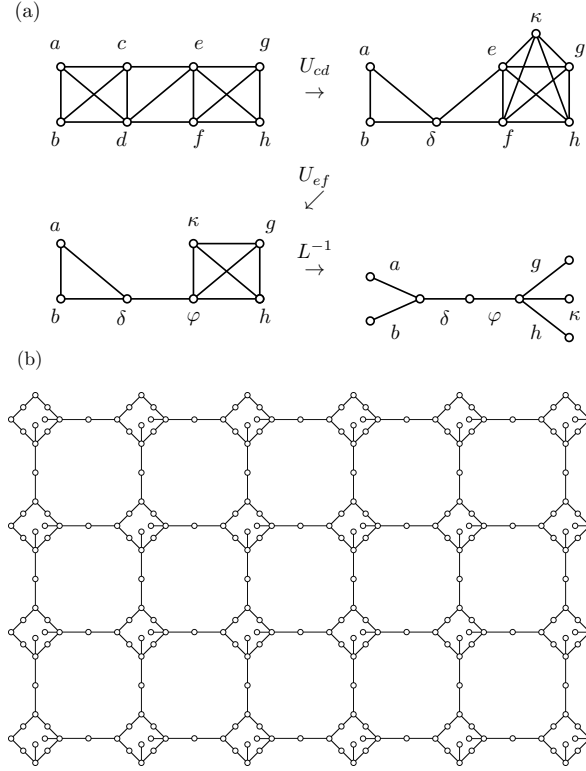


Figure 3.6: A 2-dimensional simplicial claw-free frustration graph. (a) A graphical depiction of the unitary circuit to map the model as given to a model whose frustration graph is a line graph and so admits a Jordan-Wigner solution. In the last step, we show the generalized Jordan-Wigner solution applied to a single unit cell, though it is not always the case that such a solution extends globally. (b) The generalized Jordan-Wigner transformation on the entire model.

where

$$h_\delta := \frac{1}{c} \sqrt{c^2 + d^2} h_d. \quad (3.194)$$

That is, the Hamiltonian term associated with the vertex c is removed from the model. Note that vertices a, b and e each neighbor both c and d , thus commuting with the unitary U_{cd} . However, vertex f neighbors only d , so this rotation introduces an additional term to the Hamiltonian h_κ with a coupling strength defined by $\kappa = f \sin(2\theta)$ for each arm in the lattice via $U_{cd} h_f U_{cd}^\dagger = \cos(2\theta) h_f + h_\kappa$. The frustration graph of the rotated model is shown in the top right of Fig. 3.6a. This graph is one of the forbidden subgraphs of a line graph and so another rotation needs to be applied in order to find the hopping graph. We now apply a rotation to contract the edge between vertices e and f .

This rotation is given by the unitary $U_{ef} = \prod_{j,k} e^{\phi h_e h_f}$ with $\phi = -\frac{1}{2} \arctan\left(\frac{f \cos(2\theta)}{e}\right)$ and chosen such that $U_{ef}(h_e + \cos(2\theta) h_f) U_{ef}^\dagger = h_\varphi$. We now see that the frustration graph shown in the bottom left of Fig. 3.6a is a line graph. Finding the root graph, as shown in the bottom right of Fig. 3.6a,

gives the hopping graph of an arm of the lattice. Though it is not always the case that a local transformation will extend globally, in this case we have transformed the entire Hamiltonian into a line-graph free-fermion model with a local unitary circuit.

With the majorana hopping graph identified it is then possible to numerically construct and plot the dispersion relation for the model. The dispersion relation for the model is shown in Fig. 3.7. Note that when h_κ term is turned off (that is when $f \sin \theta = 0$), the dispersion relation model has a conical shape and is critical at $p = (0, 0)$ with critical exponent $z_c = 1$. Thus, when $\kappa = 0$, the model is in the same phase as the Kitaev honeycomb model [12]. On the contrary, as κ is increased, the gap opens and the other bands hybridize. Thus, we have constructed a gapped, two-dimensional phase which can be realized by a two-local Hamiltonian. Such a model could well prove useful for applications in error correction or general condensed matter physics.

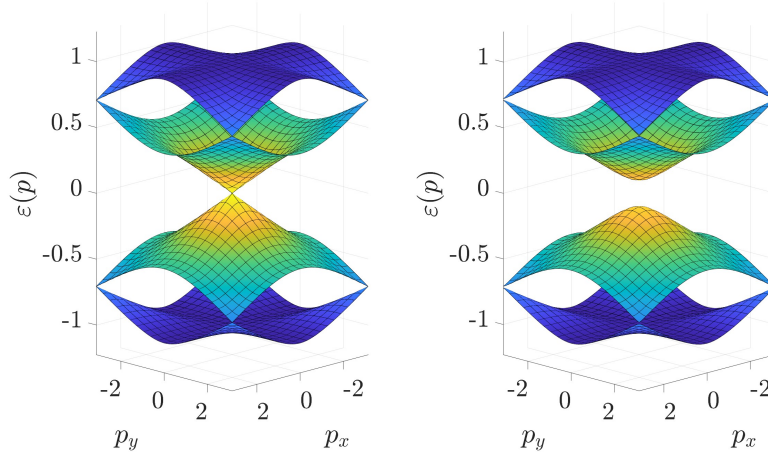


Figure 3.7: Dispersion relation $\varepsilon(p)$ for the two-dimensional model studied here with κ turned off (left) and on (right). When h_κ is turned off, the model reverts to the same phase as the Kitaev honeycomb model as can be seen from the Dirac cone shape [12]. When h_κ is turned on, a gap opens up and the other bands hybridize as in the periodic model.

3.9 Discussion

Quantum circuits describing the evolution of time-dependent free-fermion systems under the Jordan-Wigner transform are the focus of fermionic linear optics, where these are also known as matchgate circuits. These circuits were initially proposed by Valiant as an instance of a *holographic algorithm* [86], inspired by the Fisher-Kastelyn-Temperley algorithm [133–135] for counting weighted perfect matchings in a graph, and they illustrate the deep connection between fermions and combinatorial structures. While matchgate circuits can be efficiently simulated classically in a fixed basis, simple changes to this

setting will make them classically intractable or even universal for quantum computation [77–79, 81, 82]. It is interesting to see that efficient classical algorithms are reflected in the exact solvability of quantum models, much as with Valiant’s original proposal for matchgates. This work can be viewed as an extension to this line of reasoning.

In recent work [22, 41, 126] a relationship has been established between the frustration graph of a Hamiltonian and the free-fermion solvability of the model. Fig. 3.1 depicts how the results of Chapman and Flammia [22] and Elman *et al.* [126] overlap, but neither result contains completely the other. Here, we have developed a graph-theoretic framework for free-fermion solvability, which unifies the results of the previous work. Our results show that the absence of a claw and the presence of a simplicial clique in the frustration graph of a Hamiltonian are sufficient to prove that the model has a generic free-fermion solution. Our key insight in this proof is the identification of a family of mutually commuting Hamiltonian symmetries - the generalized cycle symmetries (see Sect. 3.5). The identification of these symmetries has also developed further the connection, previously established in Ref. [126], between the absence of a claw in the frustration graph of a quantum many-body model and the integrability of the model.

While the sufficient condition of an SCF frustration graph encompasses the previous work in this area, SCF Hamiltonians do not span the entirety of the free-fermionic Hamiltonian space. For one thing we know that there exist models which are free for specific coefficients; for another there are models whose spectrum is the union of an super linearly increasing number free-fermionic spectra. In Sect. 3.8, we have considered two models that are equivalent to a Jordan-Wigner solvable free-fermion model under a constant-depth circuit. On the contrary the four-fermion model introduced by Fendley [23] is equivalent to a line-graph model under a quantum circuit which grows linearly with the size of the system. One could even imagine a class of models that can be mapped to a Jordan-Wigner solvable model via a circuit whose depth grows exponentially. Thus, it is clear that a characterization of free-fermion models could be developed based on the depth of the circuit needed to transform the models frustration graph into a line-graph. Such a characterization could theoretically help to categorize those models which do not have a gapless phase, and thus fall beyond the scope of the characterization by critical exponents and quantum field theories [136, 137].

Because the claw is a forbidden induced subgraph of both previous graph-theoretic characterizations, it seems to be a natural criterion for any free-fermion solution to apply. However, it is perhaps mysterious that we require the presence of a simplicial clique as well. Indeed, the graph families of both previous characterizations are guaranteed to also contain a simplicial clique. This was recently

shown in Ref. [56] for a family generalizing (even-hole, claw)-free graphs, as inspired by this precise question. Intuitively, we can view a simplicial clique as a kind of fermionic boundary mode, and its existence in a claw-free graph implies a recursive structure that forces the model to be fermionic in some sense. We capture this intuition by connecting these models to a polynomial divisibility result for the independence polynomial of a graph given by Godsil [129] and later generalized to the multivariate setting in Ref. [100]. While our characterization does not capture all free-fermion solutions to spin models (there are well-known examples of non-generic solutions), we expect that it will be difficult to remove the simplicial clique assumption in the generic case.

Regarding quantum circuits, there is also the question of whether the extended class of free-fermion models also extends the class of free-fermionic quantum gates. It is known that the matchgates [77–79, 81, 82] represent a non-universal set of quantum gates. It is also known that a quantum circuit constructed entirely from matchgates results in Gaussian states which are ground states of a Jordan-Wigner-type Hamiltonians [82]. This then raises the question of whether there is an overlapping, but not universal, gate set which produces the SCF Hamiltonians developed here. Also related to quantum circuits is the notion of simulability. It has been suggested [138] that free-fermion states can be more efficiently prepared using quantum optimization algorithms than their interacting counterparts. It would be interesting to know whether the ground states (or thermal states) of SCF models are more efficiently preparable using quantum optimization algorithms. It is clear then, that while the current work extends the class of known free-fermion-solvable models, there are avenues for further work regarding both free-fermion solutions to many-body physics, and using the mathematical framework of graph theory to probe our understanding of physics.

Certainly, it appears as though free-fermion-solvable models are more abundant than was previously known, so an obvious question to ask would be: just how abundant are free-fermionic Hamiltonians? Even if the class of Hamiltonians was restricted to those currently known to have a generic solution it remains unknown what the likelihood is of a random Hamiltonian admitting an SCF free-fermion solution. There are also unanswered questions pertaining to whether free-fermionic systems can be leveraged for purposes within the field of quantum information. A strong link between the Jordan-Wigner-type free-fermion models of Chapman and Flammia [22] and error correcting codes for quantum computing has been established and studied by Chapman and Flammia [124]. However it remains to be seen whether such a link can be extended to include the (even-hole, claw)-free models developed in Ref. [126] or the SCF models developed in the current work. The ability to leverage free-fermionic solutions might also appear useful in the development of more compact fermion-to-qubit

mappings [118], which could have a plethora of uses in the fields of quantum chemistry, condensed matter physics, and high-energy physics.

Another example of future work that could be probed within the mathematical framework of graph theory pertains to the question of qudit many-body models and *free parafermions*. In particular, it would be interesting to understand whether there exists a graph-theoretic characterization of free parafermions in the same way that we have developed for fermions. Some examples of free parafermionic models have been studied in isolation [59, 139, 140], while families of spin chains have also been constructed [57, 58, 141, 142]. However, as of yet, there is no systematic identification mechanism akin to the simplicial, claw-free characterization of free fermions. We conjecture that such a characterization is possible.

Appendix

3.A Proof of Lemmas 3.6, 3.7, 3.8

3.A.1 Proof of Lemma 3.6

Suppose we have a vertex $\mathbf{d}^{(s)} \in \Gamma_{C'}(\mathbf{a}_s) \setminus \Gamma_{C'}(\mathbf{c}^{(s)})$.

We first show (a) $s < \ell - 1$, and so $\ell > 1$. Suppose to the contrary that $s = \ell - 1$, we first show that $\mathbf{a}_s = \mathbf{a}_{\ell-1} \notin C'$. Suppose to the contrary that $\mathbf{a}_{\ell-1} \in C'$, then because $\mathbf{c}^{(\ell-1)} \in \Gamma_{C'}(\mathbf{a}_{\ell-1})$, $\mathbf{a}_{\ell-1}$ must have two neighbors in C'_c , but this contradicts the assumption that $\mathbf{a}_{\ell-1}$ is the endpoint of $P^{(0)}$ (alternatively, if $\mathbf{a}_{\ell-1} \in C'$, then it cannot have neighbors in both C'_c and C'_d). Thus, $\mathbf{a}_{\ell-1} \notin C'$. Because $\mathbf{a}_{\ell-1}$ has neighbors $\mathbf{c}^{(\ell-1)} \in C'_c$ and $\mathbf{d}^{(\ell-1)} \in C'_d$, which are themselves non-neighboring, $\mathbf{a}_{\ell-1}$ must neighbor C' as case (a.iii) such that $\Gamma_{C'}(\mathbf{a}_{\ell-1})$ induces two disconnected paths, each of length 1. However, this would again imply that $\mathbf{a}_{\ell-1}$ has two neighbors in C'_c , contradicting the assumption that $\mathbf{a}_{\ell-1}$ is the endpoint of $P^{(0)}$. Thus, $s < \ell - 1$ and $\ell > 1$.

We now show (b), there exists an $s' > s$ such that $\mathbf{d}^{(s)} \in \Gamma_{C'}(\mathbf{c}^{(s')}) \setminus \Gamma_{C'}(\mathbf{a}'_s)$. We must have $\mathbf{c}^{(s+1)} \in \Gamma(\mathbf{d}^{(s)})$ to avoid the claw $\{\mathbf{a}_s, \mathbf{c}^{(s)}, \mathbf{c}^{(s+1)}, \mathbf{d}^{(s)}\}$. If $\mathbf{a}_{s+1} \notin \Gamma(\mathbf{d}^{(s)})$, then the statement holds for $s' = s + 1$, so assume $\mathbf{a}_{s+1} \in \Gamma(\mathbf{d}^{(s)})$. Suppose $k > 2$, then we must have $\mathbf{b}_{s+1} \in \Gamma(\mathbf{d}^{(s)})$ by Lemma 3.4. If $\mathbf{d}^{(s)}$ has another neighbor in C , it must be \mathbf{b}_{s+2} . $\mathbf{d}^{(s)}$ must have an additional neighbor $\mathbf{u} \in C'_c$, since it does not neighbor $\mathbf{c}^{(s)}$. We cannot have $\mathbf{u} \in C$, since all possible neighbors \mathbf{a}_s - \mathbf{b}_{s+1} - \mathbf{a}_{s+1} - \mathbf{b}_{s+2} to $\mathbf{d}^{(s)}$ in C have at least one neighbor in C'_c . We must have that \mathbf{u} neighbors at least one of $\{\mathbf{a}_s, \mathbf{a}_{s+1}\}$ to avoid $\{\mathbf{d}^{(s)}, \mathbf{a}_s, \mathbf{a}_{s+1}, \mathbf{u}\}$, but \mathbf{a}_s has two neighbors $\mathbf{c}^{(s)}, \mathbf{c}^{(s+1)} \in C'_c$ already. Thus, $\mathbf{u} = \mathbf{c}^{(s+2)} \in \Gamma_{C'_c}(\mathbf{a}_{s+1})$ and we have $\ell > 2$. If $\mathbf{a}_{s+2} \notin \Gamma(\mathbf{d}^{(s)})$, then the statement holds for $s' = s + 2$, so assume $\mathbf{a}_{s+2} \in \Gamma(\mathbf{d}^{(s)})$, but then $\{\mathbf{d}^{(s)}, \mathbf{a}_s, \mathbf{a}_{s+1}, \mathbf{a}_{s+2}\}$ induces a claw. Thus, the statement holds for $k > 2$. Assume $k = 2$, which gives $\ell = 2$, and assume $\Gamma_C(\mathbf{d}^{(s)}) = \mathbf{a}_{s+1}$ - \mathbf{b}_s - \mathbf{a}_s (the case not covered for $k > 2$). $\mathbf{d}^{(s)}$ must have an additional neighbor $\mathbf{u} \in C'_c$, since it does not neighbor $\mathbf{c}^{(s)}$. We cannot have $\mathbf{u} \in C$, since all vertices in C have a neighbor in C'_c . We must have that \mathbf{u} neighbors at least one of $\{\mathbf{a}_s, \mathbf{a}_{s+1}\}$ to avoid $\{\mathbf{d}^{(s)}, \mathbf{a}_s, \mathbf{a}_{s+1}, \mathbf{u}\}$, but \mathbf{a}_s has two neighbors $\mathbf{c}^{(s)}, \mathbf{c}^{(s+1)} \in C'_c$ already. Thus, $\mathbf{u} = \mathbf{c}^{(s+2)} \in \Gamma_{C'_c}(\mathbf{a}_{s+1})$ and we have $\ell > 2$, but this is a contradiction to the conclusion that $\ell = 2$. This therefore proves Lemma 3.6. \square

3.A.2 Proof of Lemma 3.7

Suppose there is a vertex in $\mathbf{d}^{(s)} \in C'_d$ such that $\mathbf{d}^{(s)} \in \Gamma_{C'}(\mathbf{c}^{(s)}) \setminus \Gamma_{C'}(\mathbf{a}_s)$. Suppose $s = 0$, then by lemma 4 applied to $\mathbf{c}_0 \prec_C \mathbf{a}_0$, we have

$$\Gamma_{(\{\mathbf{c}_0\} \cup C)}(\mathbf{d}^{(0)}) = \begin{cases} \mathbf{a}_{k-1} - \mathbf{b}_0 - \mathbf{c}_0 & \text{(i)} \\ \mathbf{b}_{k-1} - \mathbf{a}_{k-1} - \mathbf{b}_0 - \mathbf{c}_0 & \text{(ii)} \\ \mathbf{c}_0 - \mathbf{b}_1 - \mathbf{a}_1 & \text{(iii)} \\ \mathbf{c}_0 - \mathbf{b}_1 - \mathbf{a}_1 - \mathbf{b}_2 & \text{(iv)} \end{cases} \quad (3.195)$$

Thus, it is not possible to have $\Delta_C(\mathbf{d}^{(0)}) = 4$ in this case. In cases (i) and (ii), if $\mathbf{a}_{k-1} \in P^{(0)}$, then by our labeling, $\ell = k$. By Lemma 3.6(a), we must have $\mathbf{c}^{(k-1)} \in \Gamma(\mathbf{d}^{(0)})$ as well. This gives

$$\begin{cases} \Gamma_C(\mathbf{d}^{(0)}) = \mathbf{a}_{k-1} - \mathbf{b}_0 \\ \Gamma_C(\mathbf{d}^{(0)}) = \mathbf{b}_{k-1} - \mathbf{a}_{k-1} - \mathbf{b}_0 \end{cases} \begin{cases} \Gamma_{C^{(0)}}(\mathbf{d}^{(0)}) = \mathbf{a}_{k-1} - \mathbf{b}_0 - \mathbf{c}_0 & \mathbf{a}_{k-1} \notin P^{(0)} \\ \Gamma_{C^{(0)}}(\mathbf{d}^{(0)}) = \mathbf{c}^{(k-1)} - \mathbf{b}_0 - \mathbf{c}_0 & \mathbf{a}_{k-1} \in P^{(0)} \\ \Gamma_{C^{(0)}}(\mathbf{d}^{(0)}) = \mathbf{b}_{k-1} - \mathbf{a}_{k-1} - \mathbf{b}_0 - \mathbf{c}_0 & \mathbf{a}_{k-1} \notin P^{(0)} \\ \Gamma_{C^{(0)}}(\mathbf{d}^{(0)}) = \mathbf{b}_{k-1} - \mathbf{c}^{(k-1)} - \mathbf{b}_0 - \mathbf{c}_0 & \mathbf{a}_{k-1} \in P^{(0)} \end{cases} \quad (3.196)$$

So $\Delta_{C^{(0)}}(\mathbf{d}^{(0)}) = \Delta_C(\mathbf{d}^{(0)}) + 1$, and

$$\begin{cases} \mathbf{d}^{(s)} \prec_C \mathbf{a}_{k-1} \in C_a & \Delta_C(\mathbf{d}^{(s)}) = 3 \\ \mathbf{d}^{(s)} \prec_{C^{(0)}} \mathbf{b}_0 \in C_b & \Delta_{C^{(0)}}(\mathbf{d}^{(s)}) = 3 \end{cases} \quad (3.197)$$

so the statement holds in cases (i) and (ii). In cases (iii) and (iv), if $\mathbf{a}_1 \in P^{(0)}$, then if $\mathbf{c}^{(1)} \notin \Gamma(\mathbf{d}^{(0)})$, we have $\ell > 2$ by Lemma 3.6(a). We must have $\mathbf{c}^{(2)} \in \Gamma(\mathbf{d}^{(0)})$ to avoid the claw $\{\mathbf{a}_1, \mathbf{c}^{(1)}, \mathbf{c}^{(2)}, \mathbf{d}^{(0)}\}$, but since $\mathbf{a}_2 \notin \Gamma(\mathbf{d}^{(0)})$, we must have $\mathbf{c}^{(1)} - \mathbf{b}_2 \subset \Gamma(\mathbf{d}^{(0)})$ by Lemma 3.4, together with the above. However, this clearly contradicts our assumption, so we have $\mathbf{c}^{(1)} \in \Gamma(\mathbf{d}^{(0)})$. This gives

$$\begin{cases} \Gamma_C(\mathbf{d}^{(0)}) = \mathbf{b}_1 - \mathbf{a}_1 \\ \Gamma_C(\mathbf{d}^{(0)}) = \mathbf{b}_1 - \mathbf{a}_1 - \mathbf{b}_2 \end{cases} \begin{cases} \Gamma_{C^{(0)}}(\mathbf{d}^{(0)}) = \mathbf{c}_0 - \mathbf{b}_1 - \mathbf{c}_1 & \mathbf{a}_{k-1} \notin P^{(0)} \\ \Gamma_{C^{(0)}}(\mathbf{d}^{(0)}) = \mathbf{c}_0 - \mathbf{b}_1 - \mathbf{c}^{(1)} & \mathbf{a}_{k-1} \in P^{(0)} \\ \Gamma_{C^{(0)}}(\mathbf{d}^{(0)}) = \mathbf{c}_0 - \mathbf{b}_1 - \mathbf{a}_1 - \mathbf{b}_2 & \mathbf{a}_{k-1} \notin P^{(0)} \\ \Gamma_{C^{(0)}}(\mathbf{d}^{(0)}) = \mathbf{c}_0 - \mathbf{b}_1 - \mathbf{c}^{(1)} - \mathbf{b}_2 & \mathbf{a}_{k-1} \in P^{(0)} \end{cases} \quad (3.198)$$

So $\Delta_{C^{(0)}}(\mathbf{d}^{(0)}) = \Delta_C(\mathbf{d}^{(0)}) + 1$, and

$$\begin{cases} \mathbf{d}^{(s)} \prec_C \mathbf{a}_1 \in C_a & \Delta_C(\mathbf{d}^{(s)}) = 3 \\ \mathbf{d}^{(s)} \prec_{C^{(0)}} \mathbf{b}_1 \in C_b & \Delta_{C^{(0)}}(\mathbf{d}^{(s)}) = 3 \end{cases} \quad (3.199)$$

In cases (i) and (ii) as well.

Suppose $s > 0$ and $k > 3$. If $\mathbf{a}_{s-1} \notin \Gamma(\mathbf{d}^{(s)})$, then $\{\mathbf{c}^{(s)}, \mathbf{d}^{(s)}, \mathbf{a}_{s-1}, \mathbf{a}_s\}$ induces a claw, so $\mathbf{a}_{s-1} \in \Gamma(\mathbf{d}^{(s)})$. If $\mathbf{b}_s \notin \Gamma(\mathbf{d}^{(s)})$, then considering Lemma 3.4 with respect to $\mathbf{c}^{(s)} \prec_{C^{(0,s-1)}} \mathbf{a}_s$ gives that we must have $\mathbf{c}^{(s)}\text{-}\mathbf{b}_{s+1}\text{-}\mathbf{a}_{s+1} \subset \Gamma(\mathbf{d}^{(s)})$, but this also implies $\mathbf{b}_{s-1} \in \Gamma_C(\mathbf{d}^{(s)})$ by Corollary 1 applied to $\mathbf{a}_{s-1} \in C$.

We then have that $\mathbf{b}_{s-1}\text{-}\mathbf{a}_{s-1}\text{-}\mathbf{c}^{(s)}\text{-}\mathbf{b}_{s+1}\text{-}\mathbf{a}_{s+1} \subset \Gamma(\mathbf{d}^{(s)})$, so $\{\mathbf{d}^{(s)}, \mathbf{b}_{s-1}, \mathbf{c}^{(s)}, \mathbf{a}_{s+1}\}$ induces a claw if $k > 3$ (if $k = 3$, then \mathbf{b}_{s-1} is neighboring to \mathbf{a}_{s+1} in C). Thus, $\mathbf{b}_s \in \Gamma(\mathbf{d}^{(s)})$. By Lemma 3.4 with $\mathbf{c}^{(s)} \prec_{C^{(0,s-1)}} \mathbf{a}_s$, we must have $\mathbf{c}^{(s-1)} \in \Gamma(\mathbf{d}^{(s)})$. If $\mathbf{d}^{(s)}$ has another neighbor in $C^{(0,s-1)}$, it must be \mathbf{b}_{s-1} again by Lemma 3.4 with $\mathbf{c}^{(s)} \prec_{C^{(0,s-1)}} \mathbf{a}_s$. Because $\mathbf{b}_{s-1}\text{-}\mathbf{a}_{s-1}\text{-}\mathbf{b}_s \subset \Gamma_C(\mathbf{d}^{(s)})$, then if $\mathbf{d}^{(s)}$ has another neighbor in C , it must be \mathbf{a}_{s-2} . If $\mathbf{a}_{s-2} \in \Gamma(\mathbf{c}^{(s-1)})$, then $\{\mathbf{d}^{(s)}, \mathbf{c}^{(s-1)}, \mathbf{c}^{(s)}, \mathbf{a}_{s-2}\}$ induces a claw. Thus, we must have $\mathbf{a}_{s-2} \in P^{(0)}$, so $s \geq 2$ and $\ell \geq 3$. We cannot have that $\mathbf{d}^{(s)}$ has more than four neighbors in C or more than two neighbors in C' , so this gives

$$\Gamma_{(C \cup C')}(\mathbf{d}^{(s)}) = \begin{cases} \{\mathbf{c}^{(s-1)}, \mathbf{c}^{(s)}, \mathbf{a}_{s-1}, \mathbf{b}_s\} \\ \{\mathbf{c}^{(s-1)}, \mathbf{c}^{(s)}, \mathbf{b}_{s-1}, \mathbf{a}_{s-1}, \mathbf{b}_s\} \\ \{\mathbf{c}^{(s-1)}, \mathbf{c}^{(s)}, \mathbf{a}_{s-2}, \mathbf{b}_{s-1}, \mathbf{a}_{s-1}, \mathbf{b}_s\} \quad (s \geq 2, \ell \geq 3) \end{cases} \quad (3.200)$$

theses cases are depicted in Fig. 3.8 and this gives

$$\begin{cases} \Gamma_C(\mathbf{d}^{(s)}) = \mathbf{a}_{s-1}\text{-}\mathbf{b}_s & \Gamma_{C^{(0)}}(\mathbf{d}^{(s)}) = \mathbf{c}^{(s-1)}\text{-}\mathbf{b}_s\text{-}\mathbf{c}^{(s)} \\ \Gamma_C(\mathbf{d}^{(s)}) = \mathbf{b}_{s-1}\text{-}\mathbf{a}_{s-1}\text{-}\mathbf{b}_s & \Gamma_{C^{(0)}}(\mathbf{d}^{(s)}) = \mathbf{b}_{s-1}\text{-}\mathbf{c}^{(s-1)}\text{-}\mathbf{b}_s\text{-}\mathbf{c}^{(s)} \\ \Gamma_C(\mathbf{d}^{(s)}) = \mathbf{a}_{s-2}\text{-}\mathbf{b}_{s-1}\text{-}\mathbf{a}_{s-1}\text{-}\mathbf{b}_s & \Gamma_{C^{(0)}}(\mathbf{d}^{(s)}) = \mathbf{b}_{s-1}\text{-}\mathbf{c}^{(s-1)}\text{-}\mathbf{b}_s\text{-}\mathbf{c}^{(s)} \end{cases} \quad (3.201)$$

So the statement holds in this case.

Suppose $\Delta_C(\mathbf{d}^{(s)}) = 4$. Let $\mathbf{d}^{(s-1)}$ be the additional neighbor to $\mathbf{c}^{(s-1)}$ in C'_d . We cannot have $\mathbf{d}^{(s-1)} \in C$, since all neighbors to $\mathbf{c}^{(s-1)}$ also neighbor $\mathbf{d}^{(s)}$ (we only need to show this for \mathbf{b}_{s-1} and \mathbf{b}_s , because any vertices in $P^{(0)} \cap C_a$ must have a neighbor in C'_d , so these vertices cannot be in C'_d). If $\mathbf{d}^{(s-1)}$ does not neighbor \mathbf{a}_{s-1} , then we can apply Lemma 3.7 to $\mathbf{d}^{(s-1)} \in \Gamma_{C'}(\mathbf{c}^{(s-1)}) \setminus$

$\Gamma_{C'}(\mathbf{a}_{s-1})$, so assume $\mathbf{d}^{(s-1)}$ does neighbor \mathbf{a}_{s-1} . We must have $\mathbf{b}_{s-1} \in \Gamma_C(\mathbf{d}^{(s-1)})$ to avoid the claw $\{\mathbf{a}_{s-1}, \mathbf{d}^{(s-1)}, \mathbf{b}_{s-1}, \mathbf{c}^{(s)}\}$, since we cannot have $\mathbf{d}^{(s-1)}$ neighboring $\mathbf{c}^{(s)}$ or $k' = 2 < \ell$.

By Lemma 3.4 applied to $\mathbf{d}^{(s)} \prec_{C(0, s-2)} \mathbf{a}_{s-1}$, we must have $\mathbf{c}^{(s-2)} \in \Gamma(\mathbf{d}^{(s-1)})$. If $\mathbf{d}^{(s-1)}$ does not neighbor \mathbf{a}_{s-2} , then we can apply Lemma 3.7 to $\mathbf{d}^{(s-1)} \in \Gamma_{C'}(\mathbf{c}^{(s-2)}) \setminus \Gamma_{C'}(\mathbf{a}_{s-2})$, so assume $\mathbf{d}^{(s-1)}$ does neighbor \mathbf{a}_{s-2} . We must have $\mathbf{b}_{s-2} \in \Gamma(\mathbf{d}^{(s-1)})$ to avoid the claw $\{\mathbf{a}_{s-2}, \mathbf{b}_{s-2}, \mathbf{d}^{(s-1)}, \mathbf{d}^{(s)}\}$. Let $\mathbf{d}^{(s-2)}$ be the additional neighbor to $\mathbf{c}^{(s-2)}$ in C'_d . We cannot have $\mathbf{d}^{(s-2)}$ in C because both $\mathbf{b}_{s-2}, \mathbf{b}_{s-1}$ have a neighbor in C'_d . $\mathbf{d}^{(s-2)}$ cannot neighbor \mathbf{a}_{s-2} because $\Gamma_{C'}(\mathbf{a}_{s-2}) = \mathbf{c}^{(s-2)}\text{-}\mathbf{d}^{(s-1)}\text{-}\mathbf{c}^{(s-1)}\text{-}\mathbf{d}^{(s)}$, so we can apply the Lemma 3.7 to $\mathbf{d}^{(s-2)} \in \Gamma_{C'}(\mathbf{c}^{(s-2)}) \setminus \Gamma_{C'}(\mathbf{a}_{s-2})$. Thus, there must be a vertex $\mathbf{d}^{(s')} \in \Gamma_{C'}(\mathbf{c}^{(s')}) \setminus \Gamma_{C'}(\mathbf{a}_{s'})$ such that $\Delta_C(\mathbf{d}^{(s')}) < 4$, or we will always have an additional vertex neighboring a vertex in $P^{(0)} \cap C'_c$ without neighboring its clone. In all cases, this vertex $\mathbf{d}^{(s')}$ lies in the same path component of $G[C_b \oplus C'_d]$ as $\mathbf{d}^{(s)}$.

Suppose $s > 0$ and $k = 3$, and $\mathbf{b}_s \notin \Gamma(\mathbf{d}^{(s)})$, so

$$\Gamma(\mathbf{d}^{(s)}) = \mathbf{b}_{s+1}\text{-}\mathbf{a}_{s+1}\text{-}\mathbf{b}_{s-1}\text{-}\mathbf{a}_{s-1}. \quad (3.202)$$

We must have $\mathbf{c}^{(s-1)} \in \Gamma(\mathbf{d}^{(s)})$ to avoid the claw $\{\mathbf{a}_{s-1}, \mathbf{c}^{(s-1)}, \mathbf{d}^{(s)}, \mathbf{b}_s\}$. We must have $\mathbf{a}_{s+1} \in \Gamma(\mathbf{c}^{(s-1)})$ to avoid the claw $\{\mathbf{d}^{(s)}, \mathbf{c}^{(s-1)}, \mathbf{c}^{(s)}, \mathbf{a}_s\}$. Thus, $\ell = k = 3$, but then $\{\mathbf{b}_{s+1}, \mathbf{d}^{(s)}, \mathbf{a}_s, \mathbf{c}^{(s+1)}\}$ induces a claw. Therefore, we must have $\mathbf{b}_s \in \Gamma(\mathbf{d}^{(s)})$, and we recover the cases for $k > 3$.

$$\Gamma_{(C \cup C')}(\mathbf{d}^{(s)}) = \begin{cases} \{\mathbf{c}^{(s-1)}, \mathbf{c}^{(s)}, \mathbf{a}_{s-1}, \mathbf{b}_s\} \\ \{\mathbf{c}^{(s-1)}, \mathbf{c}^{(s)}, \mathbf{b}_{s-1}, \mathbf{a}_{s-1}, \mathbf{b}_s\} \\ \{\mathbf{c}^{(s-1)}, \mathbf{c}^{(s)}, \mathbf{a}_{s-2}, \mathbf{b}_{s-1}, \mathbf{a}_{s-1}, \mathbf{b}_s\} \end{cases} \quad (s = 2, \ell = 3) \quad (3.203)$$

and this gives

$$\begin{cases} \Gamma_C(\mathbf{d}^{(s)}) = \mathbf{a}_{s-1}\text{-}\mathbf{b}_s & \Gamma_{C(0)}(\mathbf{d}^{(s)}) = \mathbf{c}^{(s-1)}\text{-}\mathbf{b}_s\text{-}\mathbf{c}^{(s)} \\ \Gamma_C(\mathbf{d}^{(s)}) = \mathbf{b}_{s-1}\text{-}\mathbf{a}_{s-1}\text{-}\mathbf{b}_s & \Gamma_{C(0)}(\mathbf{d}^{(s)}) = \mathbf{b}_{s-1}\text{-}\mathbf{c}^{(s-1)}\text{-}\mathbf{b}_s\text{-}\mathbf{c}^{(s)} \\ \Gamma_C(\mathbf{d}^{(s)}) = \mathbf{a}_{s-2}\text{-}\mathbf{b}_{s-1}\text{-}\mathbf{a}_{s-1}\text{-}\mathbf{b}_s & \Gamma_{C(0)}(\mathbf{d}^{(s)}) = \mathbf{b}_{s-1}\text{-}\mathbf{c}^{(s-1)}\text{-}\mathbf{b}_s\text{-}\mathbf{c}^{(s)} \end{cases} \quad (3.204)$$

and the remaining part of the statement holds as well.

Finally, suppose $s > 0$ and $k = 2$, so $\ell = 2$ and $s = 1$. We cannot have $\Delta_C(\mathbf{d}^{(1)}) = 4$ since

$a_1 \notin \Gamma(\mathbf{d}^{(1)})$. If $\mathbf{b}_1 \in \Gamma(\mathbf{d}^{(1)})$, we have by Lemma 3.4

$$\begin{cases} \mathbf{a}_0\mathbf{b}_1 = \Gamma_C(\mathbf{d}^{(1)}) & \mathbf{c}_0\mathbf{b}_1\mathbf{c}^{(1)} = \Gamma_{C^{(0)}}(\mathbf{d}^{(1)}) \\ \mathbf{b}_0\mathbf{a}_0\mathbf{b}_1 = \Gamma_C(\mathbf{d}^{(1)}) & \mathbf{b}_0\mathbf{c}_0\mathbf{b}_1\mathbf{c}^{(1)} = \Gamma_{C^{(0)}}(\mathbf{d}^{(1)}) \end{cases} \quad (3.205)$$

so the statement holds in this case.

If $\mathbf{b}_1 \notin \Gamma(\mathbf{d}^{(1)})$, then $\mathbf{b}_0 \in \Gamma_C(\mathbf{d}^{(1)})$ by Lemma 3.4, and

$$\mathbf{b}_0\mathbf{a}_0 = \Gamma_C(\mathbf{d}^{(1)}) \quad \text{and} \quad \mathbf{c}_0\mathbf{b}_0\mathbf{c}^{(1)} = \Gamma_{C^{(0)}}(\mathbf{d}^{(1)}) \quad (3.206)$$

which proves the lemma for this case, and therefore Lemma 3.7 is proved. \square

3.A.3 Proof of Lemma 3.8

Clearly, this is the case for $s > 0$, or $\mathbf{d}^{(s)}$ will have three neighbors in C'_c , giving a claw. Thus, the only possibility is for $s = s' = 0$, and there is an additional vertex neighboring to $\mathbf{d}^{(s)}$ in C_a that is neighboring to neither $\mathbf{c}^{(0)}$ nor $\mathbf{j}^{(0)}$. This therefore gives a claw unless the statement holds. \square

3.A.4 Proof of Lemma 3.9

If $\llbracket h_{P^{(j)}}, h_{P^{(k)}} \rrbracket = -1$ and $P^{(k)}$ precedes $P^{(j)}$ in \mathcal{O} then there exists a vertex $\mathbf{v} \in P^{(j)}$ such that $h_{\mathbf{v}}$ anticommutes with $h_{P^{(k)}}$. If $\mathbf{v} \in C'_d$, then \mathbf{v} depends on $P^{(k)}$. If $\mathbf{v} \in C_b$, then \mathbf{v} has a neighbor in $P^{(k)} \cap C_a$, otherwise, by Table 3.2, \mathbf{v} neighbors $\mathbf{c}^{(0)} \notin C$, so $\{\mathbf{v}, \mathbf{a}_{k-1}, \mathbf{a}_0, \mathbf{c}^{(0)}\}$ induces a claw.

Let $\mathbf{b}^{(s)} := \mathbf{v}$ with neighbor $\mathbf{a}_s \in P^{(k)}$. We have $\mathbf{c}^{(s)} \prec_{C^{(k,s-1)}} \mathbf{a}_s$, but $\mathbf{b}^{(s)} \in C^{(k,s-1)}$, so $\mathbf{b}^{(s)}$ neighbors $\mathbf{c}^{(s)}$. If $\mathbf{d}^{(s)}$ doesn't neighbor $\mathbf{c}^{(s)}$, then this contradicts $\mathbf{d}^{(s)} \prec_{C^{(j,s-1)}} \mathbf{b}^{(s)}$. If $\mathbf{b}^{(s)}$ has another neighbor, $\mathbf{a}_{s-1} \in P^{(k)}$, then it must neighbor $\mathbf{c}^{(s-1)} \prec_{C^{(k,s-2)}} \mathbf{a}_{s-1}$, but this contradicts $h_{\mathbf{b}^{(s)}}$ anticommuting with $h_{P^{(k)}}$. This rules out cases (b.iii) and (b.iv) from Table 3.2, therefore we have (b.i) $\ell > 1$. Therefore $\{\mathbf{b}^{(s)}, \mathbf{a}_{s-1}, \mathbf{c}^{(s)}, \mathbf{c}^{(s+1)}\}$ gives a claw.

This shows that if $h_{P^{(j)}}$ and $h_{P^{(k)}}$ anticommute and $P^{(k)}$ precedes $P^{(j)}$ in \mathcal{O} , $P^{(j)}$ depends on $P^{(k)}$. Next, we show the other direction: if $P^{(j)}$ depends on $P^{(k)}$, then $h_{P^{(j)}}$ and $h_{P^{(k)}}$ anticommute. We show that there is precisely one vertex in $\mathbf{j} \in P^{(j)}$ that depends on $P^{(k)}$ with $\Delta_C(\mathbf{j}) < 4$, and so $h_{\mathbf{j}}$ is the only factor of $h_{P^{(j)}}$ that anticommutes with $h_{P^{(k)}}$. By our construction of \mathcal{O} , there is at least one such vertex, so suppose \mathbf{j} is this vertex, and that, without loss of generality, $\mathbf{d}^{(s)} := \mathbf{j} \in C'_d$ with $P^{(k)} \in G[C_a \oplus C'_c]$ and $\mathbf{d}^{(s)} \in \Gamma_{C'}(\mathbf{c}^{(s)}) \setminus \Gamma_{C'}(\mathbf{a}_s)$. If $\Delta_C(\mathbf{d}^{(s)}) > 2$, then if there is another vertex $\mathbf{d}^{(s+1)} \in \Gamma_{C'_d}(\mathbf{b}_s)$ in $P^{(j)}$, then it must also neighbor $\mathbf{c}^{(s)}$ by our assumption on \mathcal{O} that $P^{(j)}$ is

untethered with respect to $C^{(k)}$. By our assumption on \mathcal{O} in Eq. (3.103), there is no additional vertex in $P^{(j)}$ that depends on $P^{(k)}$ with degree in C less than four in this case.

Thus, we show that if $\Delta_C(\mathbf{d}^{(s)}) = 2$, then if there is another vertex $\mathbf{u} \in \Gamma_{C'_d}(\mathbf{b}_s)$ in $P^{(j)}$, then it must also neighbor $\mathbf{c}^{(s)}$. Suppose to the contrary that $\mathbf{d}^{(s-1)} := \mathbf{u}$ does not neighbor $\mathbf{c}^{(s)}$, then $|C'| > 4$, and by Lemma 3.4 applied to $\mathbf{d}^{(s)} \prec_{C^{(k)}} \mathbf{b}_s$, we must have

$$\mathbf{b}_{s-1}-\mathbf{a}_{s-1}-\mathbf{b}_s \subseteq \Gamma_C(\mathbf{d}^{(s-1)}) \quad (3.207)$$

If $\mathbf{a}_s \notin \Gamma(\mathbf{d}^{(s-1)})$, then $\{\mathbf{b}_s, \mathbf{a}_s, \mathbf{d}^{(s)}, \mathbf{d}^{(s-1)}\}$ is a claw. Thus, $\mathbf{a}_s \in \Gamma(\mathbf{d}^{(s-1)})$ and $|C| = 4$ by Lemma 3.4 together with the assumption that $\mathbf{d}^{(s-1)} \notin \Gamma(\mathbf{c}^{(s)})$. This gives

$$\mathbf{a}_{s-1}-\mathbf{b}_s-\mathbf{a}_s-\mathbf{b}_{s-1} = \Gamma_C(\mathbf{d}^{(s-1)}) \quad (3.208)$$

Now, $\mathbf{c}^{(s)}$ has another neighbor $\mathbf{u} \in C'_d$, which cannot be in C because every neighbor to $\mathbf{c}^{(s)}$ in C has a neighbor in C'_d . Thus, let $\mathbf{d}^{(s+1)} := \mathbf{u}$. If $\mathbf{a}_s \notin \Gamma_C(\mathbf{d}^{(s+1)})$, then $\{\mathbf{c}^{(s)}, \mathbf{d}^{(s)}, \mathbf{a}_s, \mathbf{d}^{(s+1)}\}$ is a claw. If $\mathbf{b}_{s-1} \notin \Gamma_C(\mathbf{d}^{(s+1)})$ $\{\mathbf{a}_s, \mathbf{d}^{(s-1)}, \mathbf{b}_{s-1}, \mathbf{d}^{(s+1)}\}$ is a claw. We thus have $\{\mathbf{d}^{(s-1)}, \mathbf{c}^{(s)}, \mathbf{d}^{(s+1)}\} \subset \Gamma_{C'}(\mathbf{a}_s)$, $\{\mathbf{d}^{(s-1)}, \mathbf{c}^{(s)}, \mathbf{d}^{(s+1)}\} \subset \Gamma_{C'}(\mathbf{b}_{s-1})$, and $\{\mathbf{d}^{(s-1)}, \mathbf{d}^{(s)}, \mathbf{c}^{(s)}\} \subset \Gamma_{C'}(\mathbf{b}_s)$, which allows us to infer $\Delta_{C'}(\mathbf{a}_s) = \Delta_{C'}(\mathbf{b}_{s-1}) = \Delta_{C'}(\mathbf{b}_s) = 4$ from Lemma 3.3. Thus, the only possibility for h_C and $h_{C'}$ to anticommute is for

$$\Gamma_{C'}(\mathbf{a}_{s-1}) = \mathbf{d}^{(s-1)}-\mathbf{c}^{(s-1)}-\mathbf{d}^{(s)} \quad (3.209)$$

(i.e. $\mathbf{a}_{s-1} \prec_{C'} \mathbf{c}^{(s-1)}$). By Lemma 3.4, \mathbf{b}_s neighbors $\mathbf{c}^{(s-1)}$. Now, $\mathbf{d}^{(s-1)}$ has another neighbor $\mathbf{u} \in C'_c$, which again cannot be in C since all of the neighbors to $\mathbf{d}^{(s-1)}$ in C have a neighbor in C'_c . If \mathbf{u} does not neighbor \mathbf{a}_s , then $\{\mathbf{d}^{(s-1)}, \mathbf{u}, \mathbf{a}_{s-1}, \mathbf{a}_s\}$ gives a claw. Since $\mathbf{u} \notin \Gamma_{C'}(\mathbf{c}^{(s)}) = \{\mathbf{d}^{(s)}, \mathbf{d}^{(s+1)}\}$, we have $\mathbf{b}_{s-1} \in \Gamma_C(\mathbf{u})$ by Lemma 3.4 applied to $\mathbf{c}^{(s)} \prec_{C^{(k,s-1)}} \mathbf{a}_s$ and the fact that the neighborhoods in C' to \mathbf{b}_s and \mathbf{a}_{s-1} are fixed. However, then $\{\mathbf{b}_{s-1}, \mathbf{a}_{s-1}, \mathbf{c}^{(s)}, \mathbf{u}\}$ gives a claw. Thus, if \mathbf{b}_s has an additional neighbor $\mathbf{u} \in C'_d$, it must also neighbor $\mathbf{c}^{(s)}$, so by the argument above, there can be no additional vertex in $P^{(j)}$ whose corresponding operator anticommutes with $h_{P^{(k)}}$. Therefore, if $P^{(j)}$ depends on $P^{(k)}$, there is precisely one vertex $\mathbf{j} \in P^{(j)}$ for which $h_{\mathbf{j}}$ anticommutes with $h_{P^{(k)}}$, so $h_{P^{(j)}}$ and $h_{P^{(k)}}$ anticommute, and this proves the lemma. \square

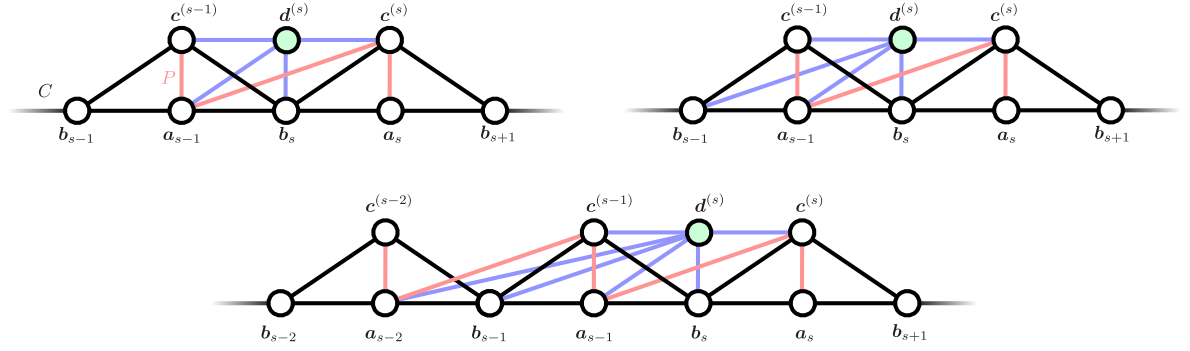


Figure 3.8: Diagram of the possible cases given in Eq. (3.200).

3.B Proof of Lemma 3.10

Proof of Lemma 3.10. By definition,

$$Z_G(-u^2) = T_G(u)T_G(-u) \quad (3.210)$$

$$= \left(\sum_{s=0}^{\alpha(G)} (-u)^s Q_G^{(s)} \right) \left(\sum_{t=0}^{\alpha(G)} u^t Q_G^{(t)} \right) \quad (3.211)$$

$$= \sum_{s,t=0}^{\alpha(G)} (-1)^s u^{s+t} Q_G^{(s)} Q_G^{(t)} \quad (3.212)$$

If $s + t = 1 \pmod{2}$, then, by Theorem 3.1,

$$(-1)^s Q_G^{(s)} Q_G^{(t)} + (-1)^t Q_G^{(t)} Q_G^{(s)} = (-1)^s [Q_G^{(s)}, Q_G^{(t)}] = 0 \quad (3.213)$$

Hence,

$$Z_G(-u^2) = \sum_{\substack{s,t=0 \\ s+t=0 \pmod{2}}}^{\alpha(G)} (-1)^s u^{s+t} Q_G^{(s)} Q_G^{(t)} \quad (3.214)$$

$$= \sum_{\substack{S,T \in \mathcal{S}_G \\ |S|+|T|=0 \pmod{2}}} (-1)^{|S|} u^{|S|+|T|} h_S h_T \quad (3.215)$$

$$= \sum_{\substack{S,T \in \mathcal{S}_G \\ |S|+|T|=0 \pmod{2}}} (-1)^{|S|} u^{|S|+|T|} (h_{S \cap T})^2 h_{S \setminus T} h_{T \setminus S}. \quad (3.216)$$

As in the proof of Eq. (3.80a), we use the fact that every factor h_j with $j \in S \cap T$ commutes with every factor in $h_S h_T$. Commuting a given factor of h_j for $j \in S \setminus T$ through $h_{T \setminus S}$ gives a factor of

(-1) for every neighbor to j in $T \setminus S$. Using

$$S \oplus T = (S \setminus T) \cup (T \setminus S) \quad (3.217)$$

gives

$$h_{S \setminus T} h_{T \setminus S} = (-1)^{|E[S \oplus T]|} h_{T \setminus S} h_{S \setminus T} \quad (3.218)$$

since $G[S \oplus T]$ is bipartite by Lemma 3.2. Thus, if $|E[S \oplus T]| \equiv 1 \pmod{2}$, then $h_{S \setminus T} h_{T \setminus S} + h_{T \setminus S} h_{S \setminus T} = 0$. Hence,

$$Z_G(-u^2) = \sum_{\substack{S, T \in \mathcal{S}_G \\ |S|+|T| \equiv 0 \pmod{2} \\ |E[S \oplus T]| \equiv 0 \pmod{2}}} (-1)^{|S|} u^{|S|+|T|} (h_{S \cap T})^2 h_{S \setminus T} h_{T \setminus S} \quad (3.219)$$

$$= \sum_{\substack{S, T \in \mathcal{S}_G \\ |S|+|T| \equiv 0 \pmod{2} \\ |E[S \oplus T]| \equiv 0 \pmod{2}}} (-1)^{|S|} u^{|S|+|T|} h_S h_T. \quad (3.220)$$

Again by Lemma 3.2, $G[S \oplus T]$ is a disjoint union of paths and even holes. Suppose $G[S \oplus T]$ contains a path component P . Since P either has odd-many vertices or odd-many edges, it cannot be the only component of $G[S \oplus T]$. Define

$$\tilde{S} = S \oplus P$$

$$\tilde{T} = T \oplus P$$

this gives distinct independent sets \tilde{S} and \tilde{T} for which $S \oplus T = \tilde{S} \oplus \tilde{T}$ and $|S| + |T| = |\tilde{S}| + |\tilde{T}|$. This gives

$$(-1)^{|\tilde{S}|} u^{|\tilde{S}|+|\tilde{T}|} h_{\tilde{S}} h_{\tilde{T}} = (-1)^{|\tilde{S}|} u^{|\tilde{S}|+|\tilde{T}|} h_{S \setminus P} h_{T \cap P} h_{S \cap P} h_{T \setminus P} \quad (3.221)$$

$$= (-1)^{|\tilde{S}|+|E[P]|} u^{|\tilde{S}|+|\tilde{T}|} h_{S \setminus P} h_{S \cap P} h_{T \cap P} h_{T \setminus P} \quad (3.222)$$

$$(-1)^{|\tilde{S}|} u^{|\tilde{S}|+|\tilde{T}|} h_{\tilde{S}} h_{\tilde{T}} = -(-1)^{|S|} u^{|S|+|T|} h_S h_T \quad (3.223)$$

Hence,

$$(-1)^{|S|} u^{|S|+|T|} h_S h_T + (-1)^{|\tilde{S}|} u^{|\tilde{S}|+|\tilde{T}|} h_{\tilde{S}} h_{\tilde{T}} = 0 \quad (3.224)$$

where we have used the fact that, if P has odd length, then $|\tilde{S}| = |S|$, and if P has even length, then $|\tilde{S}| = |S| \pm 1$. Thus, $(-1)^{|\tilde{S}|+|E[P]|} = -(-1)^{|S|}$. For a given collection of pairs (S, T) such that $G[S \oplus T]$ is fixed, we can choose a fiducial path component by which to pair terms to cancel. Therefore, $G[S \oplus T]$ can contain no path components, so it must be a collection of disjoint and non-neighboring even holes. In this case $|S| = |T|$, and we have

$$Z_G(-u^2) = \sum_{\substack{S, T \in \mathcal{S}_G \\ S \oplus T = \partial \mathcal{X} \\ \mathcal{X} \in \mathcal{C}_G^{(\text{even})}}} (-u^2)^{|S|} h_S h_T \quad (3.225)$$

$$Z_G(-u^2) = \sum_{\mathcal{X} \in \mathcal{C}_G^{(\text{even})}} (-u^2)^{|\partial \mathcal{X}|/2} 2^{|\mathcal{X}|} I_{G \setminus \Gamma[\mathcal{X}]}(-u^2) \prod_{C \in \mathcal{X}} h_C \quad (3.226)$$

By Lemma 3.5, this gives

$$Z_G(-u^2) = \sum_{\langle \mathcal{X} \rangle \in \langle \mathcal{C}_G^{(\text{even})} \rangle} (-u^2)^{|\partial \langle \mathcal{X} \rangle|/2} 2^{|\mathcal{X}|} I_{G \setminus \Gamma[\langle \mathcal{X} \rangle]}(-u^2) \prod_{\langle C_0 \rangle \in \langle \mathcal{X} \rangle} J_G[\langle C_0 \rangle] \quad (3.227)$$

completing the proof. \square

3.C Proofs of Lemmas 3.1 and 3.11

Proof of Lemma 3.1. From Eq. (3.57), we have

$$Q_G^{(k)} = Q_{G \setminus K_s}^{(k)} + \sum_{j \in K_s} Q_{G \setminus (K_s \cup K_j)}^{(k-1)} h_j, \quad (3.228)$$

and

$$Q_{G \setminus K_j}^{(k-1)} = Q_{G \setminus (K_s \cup K_j)}^{(k-1)} + \sum_{\mathbf{k} \in K_s \setminus \{j\}} Q_{G \setminus (K_s \cup K_j \cup K_{\mathbf{k}})}^{(k-2)} h_{\mathbf{k}}, \quad (3.229)$$

where, again, $Q_G^{(k)} = 0$ for $k < 0$. This gives

$$Q_G^{(k)} = Q_{G \setminus K_s}^{(k)} + \sum_{j \in K_s} \left(Q_{G \setminus K_j}^{(k-1)} - \sum_{\mathbf{k} \in K_s \setminus \{j\}} Q_{G \setminus (K_s \cup K_j \cup K_{\mathbf{k}})}^{(k-2)} h_{\mathbf{k}} \right) h_j \quad (3.230)$$

$$= Q_{G \setminus K_s}^{(k)} + \sum_{j \in K_s} Q_{G \setminus K_j}^{(k-1)} h_j - \sum_{j, \mathbf{k} \in K_s, j \neq \mathbf{k}} Q_{G \setminus (K_s \cup K_j \cup K_{\mathbf{k}})}^{(k-2)} h_{\mathbf{k}} h_j. \quad (3.231)$$

The third term vanishes because $Q_{G \setminus (K_s \cup K_j \cup K_k)}^{(k-2)}$ is symmetric in \mathbf{j} and \mathbf{k} , but $h_{\mathbf{j}}$ and $h_{\mathbf{k}}$ anticommute for $\mathbf{j}, \mathbf{k} \in K_s$ and $\mathbf{j} \neq \mathbf{k}$. Therefore

$$Q_G^{(k)} = Q_{G \setminus K_s}^{(k)} + \sum_{\mathbf{j} \in K_s} Q_{G \setminus K_j}^{(k-1)} h_{\mathbf{j}} \quad (3.232)$$

and proves the lemma. \square

Proof of Lemma 3.11. By Def. 3.7, it is sufficient to show that

$$\left(1 + u \sum_{\mathbf{j} \in K_s} h_{\mathbf{j}}\right) \chi T_G(-u) = T_G(-u) \left(1 - u \sum_{\mathbf{j} \in K_s} h_{\mathbf{j}}\right) \chi. \quad (3.233)$$

By equating coefficients of u^k , this is equivalent to showing that

$$\chi Q_G^{(k)} + \sum_{\mathbf{j} \in K_s} h_{\mathbf{j}} \chi Q_G^{(k-1)} = \left(Q_G^{(k)} - Q_G^{(k-1)} \sum_{\mathbf{j} \in K_s} h_{\mathbf{j}}\right) \chi. \quad (3.234)$$

We expand the left-hand side by applying Eq. (3.57) to the clique K_s in the first term and the clique $K_{\mathbf{j}} \equiv \Gamma[G] \setminus (K_s \setminus \{\mathbf{j}\})$ in the second term. This gives

$$\chi Q_G^{(k)} + \sum_{\mathbf{j} \in K_s} h_{\mathbf{j}} \chi Q_G^{(k-1)} = \chi \left(Q_{G \setminus K_s}^{(k)} + \sum_{\mathbf{j}' \in K_s} h_{\mathbf{j}'} Q_{G \setminus (K_s \cup K_{\mathbf{j}'})}^{(k-1)}\right) + \sum_{\mathbf{j} \in K_s} h_{\mathbf{j}} \chi \left(Q_{G \setminus K_j}^{(k-1)} + \sum_{\mathbf{j}' \in K_j} h_{\mathbf{j}'} Q_{G \setminus \Gamma[\mathbf{j}']}^{(k-2)}\right) \quad (3.235)$$

For $\mathbf{j} \in K_s$, we see that $h_{\mathbf{j}} \chi$ only anticommutes with $h_{\mathbf{k}}$ if $\mathbf{k} \in K_j$. Thus

$$\chi Q_G^{(k)} + \sum_{\mathbf{j} \in K_s} h_{\mathbf{j}} \chi Q_G^{(k-1)} = \left(Q_{G \setminus K_s}^{(k)} - \sum_{\mathbf{j}' \in K_s} h_{\mathbf{j}'} Q_{G \setminus (K_s \cup K_{\mathbf{j}'})}^{(k-1)}\right) \chi + \sum_{\mathbf{j} \in K_s} \left(Q_{G \setminus K_j}^{(k-1)} - \sum_{\mathbf{j}' \in K_j} h_{\mathbf{j}'} Q_{G \setminus \Gamma[\mathbf{j}']}^{(k-2)}\right) h_{\mathbf{j}} \chi \quad (3.236)$$

$$= \left(Q_{G \setminus K_s}^{(k)} + \sum_{\mathbf{j} \in K_s} Q_{G \setminus K_j}^{(k-1)} h_{\mathbf{j}}\right) \chi - \sum_{\mathbf{j} \in K_s} \left(Q_{G \setminus (K_s \cup K_j)}^{(k-1)} + \sum_{\mathbf{j}' \in K_j} h_{\mathbf{j}'} Q_{G \setminus \Gamma[\mathbf{j}']}^{(k-2)}\right) h_{\mathbf{j}} \chi \quad (3.237)$$

$$= Q_G^{(k)} \chi - \sum_{\mathbf{j} \in K_s} \left(Q_{G \setminus (K_s \cup K_j)}^{(k-1)} + Q_G^{(k-1)} - Q_{G \setminus K_j}^{(k-1)}\right) h_{\mathbf{j}} \chi \quad (3.238)$$

and

$$Q_{G \setminus (K_s \cup K_j)}^{(k-1)} - Q_{G \setminus K_j}^{(k-1)} = - \sum_{j' \in K_s \setminus \{j\}} Q_{G \setminus (K_s \cup K_j \cup K_{j'})}^{(k-2)} h_{j'}. \quad (3.239)$$

This gives

$$\chi Q_G^{(k)} + \sum_{j \in K_s} h_j \chi Q_G^{(k-1)} = Q_G^{(k)} \chi - Q_G^{(k-1)} \sum_{j \in K_s} h_j \chi + \sum_{j, j' \in K_s, j \neq j'} Q_{G \setminus (K_s \cup K_j \cup K_{j'})}^{(k-2)} h_{j'} h_j \chi \quad (3.240)$$

In the last term, $Q_{G \setminus (K_s \cup K_j \cup K_{j'})}^{(k-2)}$ is symmetric in j and j' , but h_j anticommutes with $h_{j'}$ for $j, j' \in K_s$ with $j \neq j'$. Thus, this term vanishes, and we have

$$\chi Q_G^{(k)} + \sum_{j \in K_s} h_j \chi Q_G^{(k-1)} = \left(Q_G^{(k)} - Q_G^{(k-1)} \sum_{j \in K_s} h_j \right) \chi \quad (3.241)$$

completing the proof. \square

3.D Proof of Lemma 3.13

Proof of Lemma 3.13. We have

$$T_G(u) \psi_{\mathcal{J},+j} T_G(-u) = \frac{1}{N_{\mathcal{J},j}} T_G(u) [\Pi_{\mathcal{J}} T_G(-u_{\mathcal{J},j}) \chi T_G(u_{\mathcal{J},j})] T_G(-u) \quad (3.242)$$

$$= \frac{1}{N_{\mathcal{J},j}} \Pi_{\mathcal{J}} T_G(-u_{\mathcal{J},j}) [T_G(u) \chi T_G(-u)] T_G(u_{\mathcal{J},j}) \quad (3.243)$$

$$= \frac{1}{N_{\mathcal{J},j}} \Pi_{\mathcal{J}} T_G(-u_{\mathcal{J},j}) \left[Z_G(-u^2) \left(1 - u \sum_{j \in K_s} h_j \right) \chi - T_G(u) \left(u \sum_{j \in K_s} h_j \right) \chi T_G(-u) \right] T_G(u_{\mathcal{J},j}) \quad (3.244)$$

where we have applied Lemma 3.11 in the last line. From our proof of Lemma 3.12, we have

$$T_G(u) \psi_{\mathcal{J},+j} T_G(-u) = \frac{1}{N_{\mathcal{J},j}} \Pi_{\mathcal{J}} T_G(-u_{\mathcal{J},j}) \left\{ Z_G(-u^2) \chi - \frac{u}{2} Z_G(-u^2) [H, \chi] - \frac{u}{2} T_G(u) [H, \chi] T_G(-u) \right\} T_G(u_{\mathcal{J},j}) \quad (3.245)$$

$$= Z_G(-u^2) \psi_{\mathcal{J},+j} - \frac{u}{2} Z_G(-u^2) [H, \psi_{\mathcal{J},+j}] - \frac{u}{2} T(u) [H, \psi_{\mathcal{J},+j}] T_G(-u) \quad (3.246)$$

$$= Z_G(-u^2) \psi_{\mathcal{J},+j} - \frac{u}{u_{\mathcal{J},j}} Z_G(-u^2) \psi_{\mathcal{J},+j} - \frac{u}{u_{\mathcal{J},j}} T(u) \psi_{\mathcal{J},+j} T_G(-u) \quad (3.247)$$

$$T_G(u) \psi_{\mathcal{J},+j} T_G(-u) = \frac{1}{u_{\mathcal{J},j}} [Z_G(-u^2) (u_{\mathcal{J},j} - u) \psi_{\mathcal{J},+j} - u T_G(u) \psi_{\mathcal{J},+j} T_G(-u)]. \quad (3.248)$$

where we applied Lemma 3.12 directly in Eq. (3.247). Now, by rearranging, we have

$$(u_j + u)T_G(u)\psi_{+j} = (u_j - u)\psi_{+j}T_G(u). \quad (3.249)$$

where we have applied $Z_G^{-1}(-u^2)T_G(u)$ to the right on both sides. This requires choosing $u \neq \pm u_{\mathcal{J},j}$ for any pair (\mathcal{J}, j) , as $Z_G(-u_{\mathcal{J},j})$ is not invertible. Applying this allows us to write

$$\{\psi_{\mathcal{J},+j}, T_G(u)\chi T_G(-u)\} = \frac{u_{\mathcal{J},j} + u}{u_{\mathcal{J},j} - u} T_G(u) \{\psi_{\mathcal{J},+j}, \chi\} T_G(-u). \quad (3.250)$$

We compute the anticommutation relation $\{\psi_{\mathcal{J},+j}, \chi\}$ as

$$\{\psi_{\mathcal{J},+j}, \chi\} = \frac{4}{N_{\mathcal{J},j}} \Pi_{\mathcal{J}} Z_{G \setminus K_s}(-u_{\mathcal{J},j}^2) \quad (3.251)$$

By setting

$$N_{\mathcal{J},j} = 4u_{\mathcal{J},j} \left(Z_{G \setminus K_s}(-u_{\mathcal{J},j}^2) \frac{\partial Z_G(x)}{\partial x} \Big|_{x=-u_{\mathcal{J},j}^2} \right)^{\frac{1}{2}}, \quad (3.252)$$

we have

$$\{\psi_{\mathcal{J},+j}, \psi_{\mathcal{J}',-k}\} = \delta_{\mathcal{J},\mathcal{J}'} \delta_{jk} \Pi_{\mathcal{J}}, \quad (3.253)$$

completing the proof. \square

3.E Proof of Lemma 3.14

Proof of Lemma 3.14. By following a similar analysis to the proof of Lemma 3.13, the commutator $[\psi_{+j}, \psi_{-j}]$ may be expressed as

$$[\psi_{+j}, \psi_{-j}] = \frac{1}{N_j} \lim_{u \rightarrow u_j} \left(\frac{u_j + u}{u_j - u} T(u) [\psi_{+j}, \chi] T(-u) \right). \quad (3.254)$$

$$= -\frac{2u_j}{N_j} \left(\frac{\partial T_G(u_j)}{\partial u_j} [\psi_{+j}, \chi] T(-u_j) + T(u_j) [\psi_{+j}, \chi] \frac{\partial T_G(-u_j)}{\partial u_j} \right) \quad (3.255)$$

$$= -\frac{2u_j}{N_j} \left(\frac{\partial T_G(u_j)}{\partial u_j} \psi_{+j} \chi T(-u_j) - T(u_j) \chi \psi_{+j} \frac{\partial T_G(-u_j)}{\partial u_j} \right). \quad (3.256)$$

Now, by using the anticommutation relation from the proof of Lemma 3.13, we obtain

$$[\psi_{+j}, \psi_{-j}] = -\frac{8u_j}{N_j^2} \left(T(-u_j) \frac{\partial T_G(u_j)}{\partial u_j} - T(u_j) \frac{\partial T_G(-u_j)}{\partial u_j} \right) \quad (3.257)$$

$$= -\frac{1}{2u_j} \left(\frac{\partial Z_G(x)}{\partial x} \Big|_{x=-u_j^2} \right)^{-1} \left(T(-u_j) \frac{\partial T_G(u_j)}{\partial u_j} - T(u_j) \frac{\partial T_G(-u_j)}{\partial u_j} \right). \quad (3.258)$$

Then,

$$\sum_{j=1}^{\alpha(G)} \varepsilon_j [\psi_{+j}, \psi_{-j}] = - \sum_{j=1}^{\alpha(G)} \frac{1}{2u_j^2} \left(\frac{\partial Z_G(x)}{\partial x} \Big|_{x=-u_j^2} \right)^{-1} \left(T_G(-u_j) \frac{\partial T_G(u_j)}{\partial u_j} - T_G(u_j) \frac{\partial T_G(-u_j)}{\partial u_j} \right). \quad (3.259)$$

By using

$$\frac{\partial Z_G(x)}{\partial x} \Big|_{x=-u_j^2} = \frac{1}{u_j^2} \prod_{\substack{k=1 \\ k \neq j}}^{\alpha(G)} \left(\frac{u_k^2 - u_j^2}{u_k^2} \right), \quad (3.260)$$

we have

$$\sum_{j=1}^{\alpha(G)} \varepsilon_j [\psi_{+j}, \psi_{-j}] = -\frac{1}{2} \sum_{j=1}^{\alpha(G)} \left(T_G(-u_j) \frac{\partial T_G(u_j)}{\partial u_j} - T_G(u_j) \frac{\partial T_G(-u_j)}{\partial u_j} \right) \prod_{\substack{k=1 \\ k \neq j}}^{\alpha(G)} \left(\frac{-u_k^2}{u_j^2 - u_k^2} \right). \quad (3.261)$$

Finally, by the Lagrange interpolation formula,

$$\sum_{j=1}^{\alpha(G)} \varepsilon_j [\psi_{+j}, \psi_{-j}] = \left(T_G(u) \frac{\partial T_G(u)}{\partial u} \right) \Big|_{u=0} = H, \quad (3.262)$$

completing the proof. \square

3.F Numerical model definition

In this appendix we give the full qubitization of the many-body model defined in Sect. 3.8. The model is defined on a two-dimensional square lattice, with five qubits residing on the links of the lattice such that there is a spin at each of the positions $(j + \frac{\alpha}{6}, k)$ and $(j, k + \frac{\alpha}{6})$. The model is two-local, with each term bilinear in Pauli operators. Due to the obvious symmetry of the lattice we collect the terms along each link of the lattice in the Hamiltonian by their couplig strength and label each term as h_μ

for $\mu \in \{a, b, c, d, e, f, g, h\}$. We then give the full Hamiltonian as

$$\begin{aligned}
H = \sum_{j,k} & \left(a \left(\sigma_{j+\frac{2}{6},k}^y \sigma_{j+\frac{1}{6},k}^x + \sigma_{j,k+\frac{2}{6}}^y \sigma_{j,k+\frac{1}{6}}^x \right) + b \left(\sigma_{j+\frac{2}{6},k}^x \sigma_{j-\frac{1}{6},k}^y + \sigma_{j,k+\frac{2}{6}}^x \sigma_{j+\frac{1}{6},k}^y \right) \right. \\
& + c \left(\sigma_{j+\frac{2}{6},k}^z \sigma_{j+\frac{3}{6},k}^y + \sigma_{j,k+\frac{2}{6}}^z \sigma_{j,k+\frac{3}{6}}^y \right) + d \left(\sigma_{j+\frac{2}{6},k}^z \sigma_{j+\frac{3}{6},k}^z + \sigma_{j,k+\frac{2}{6}}^z \sigma_{j,k+\frac{3}{6}}^z \right) \\
& + e \left(\sigma_{j+\frac{3}{6},k}^x \sigma_{j+\frac{4}{6},k}^z + \sigma_{j,k+\frac{3}{6}}^x \sigma_{j,k+\frac{4}{6}}^z \right) + f \left(\sigma_{j+\frac{3}{6},k}^y \sigma_{j+\frac{4}{6},k}^z + \sigma_{j,k+\frac{3}{6}}^y \sigma_{j,k+\frac{4}{6}}^z \right) \\
& \left. + g \left(\sigma_{j+\frac{4}{6},k}^x \sigma_{j+1,k+\frac{1}{6}}^y + \sigma_{j,k+\frac{4}{6}}^x \sigma_{j-\frac{1}{6},k}^y \right) + h \left(\sigma_{j+\frac{4}{6},k}^y \sigma_{j+\frac{5}{6},k}^x + \sigma_{j,k+\frac{4}{6}}^y \sigma_{j,k+\frac{5}{6}}^x \right) \right). \tag{3.263}
\end{aligned}$$

With this in mind we can now explicitly define the unitary rotations discussed in Sect. 3.8 in terms of their Paulis. Note that the unitaries are defined as products of local unitaries across all links, that is for all values of j and k within the lattice. Thus we can write

$$U_{cd} = \prod_{j,k} \exp \left\{ -i\theta \sigma_{j+\frac{3}{6},k}^x \right\} \exp \left\{ -i\theta \sigma_{j,k+\frac{3}{6}}^x \right\} \tag{3.264}$$

$$U_{ef} = \prod_{j,k} \exp \left\{ -i\phi \sigma_{j+\frac{3}{6},k}^z \right\} \exp \left\{ -i\phi \sigma_{j,k+\frac{3}{6}}^z \right\}. \tag{3.265}$$

We can also give an explicit expression for the extraneous term, h_κ , which is introduced by the rotation of h_f by U_{cd} :

$$h_\kappa := \begin{cases} f \sin(2\theta) \sigma_{j+\frac{3}{6},k}^z \sigma_{j+\frac{4}{6},k}^z & \text{on horizontal links} \\ f \sin(2\theta) \sigma_{j,k+\frac{3}{6}}^z \sigma_{j,k+\frac{4}{6}}^z & \text{on vertical links.} \end{cases} \tag{3.266}$$

Chapter 4

Boundary topological entanglement entropy in two and three dimensions

The topological entanglement entropy is used to measure long-range quantum correlations in the ground space of topological phases. Here we obtain closed form expressions for the topological entropy of (2+1)- and (3+1)-dimensional loop gas models, both in the bulk and at their boundaries, in terms of the data of their input fusion categories and algebra objects. Central to the formulation of our results are generalized \mathcal{S} -matrices. We conjecture a general property of these \mathcal{S} -matrices, with proofs provided in many special cases. This includes constructive proofs for categories up to rank 5.

4.1 Introduction

The classification of topological phases is fundamental to the study of modern condensed matter physics [16, 143–145]. Moreover, they have properties that may be valuable for the robust storage and manipulation of quantum information [146, 147]. Their characteristics include a stable gap at zero temperature and quasiparticle excitations with non-trivial braid statistics [148, 149].

An important class of topological phases are represented by topological loop-gas models [13, 25]. These models can be defined in terms of an input unitary fusion category, and their ground states by superpositions of string diagrams labeled by objects from the category. The categorical framework

provides a collection of local relations that ensure topological invariance of the ground states. In $(2+1)$ -dimensions, these models are called Levin-Wen models [13]. Levin-Wen models have point-like excitations, commonly called anyons, with non-trivial fusion rules and braid statistics. In $(3+1)$ -dimensions, the input category must be equipped with a premodular braiding, leading to a Walker-Wang model [25]. Generically, Walker-Wang models support point-like and loop-like excitations. In contrast to Levin-Wen models, the excitations in the bulk of a Walker-Wang model may be trivial, specifically if the input category is modular.

Loop-gas models can be defined on manifolds with boundaries by modifying the local relations governing the strings in the vicinity of the boundary. One way to define a boundary to a topological loop-gas is to allow some strings to terminate on the boundary. This is captured in the current work using particular objects called algebras [150, 151]. Despite their trivial bulk excitations, Walker-Wang models may have highly non-trivial boundary excitations.

Intimately connected to the topological properties of these phases is the long-range entanglement present in the ground state of the Hamiltonians describing these phases [152, 153]. The long-range quantum correlations found in the ground states of topological phases can be measured using the topological entanglement entropy [154–156]. We typically expect that the entanglement entropy shared between two subsystems of the ground state of a gapped many body system to respect an area law [157]. However, supposing a sensible choice of bipartition, the entanglement entropy of the ground state of topological phases has a constant universal correction [154]. In $(2+1)$ -dimensions, it is known that this correction relates to the total quantum dimension of the quasiparticle excitations supported by the phase [155, 156]. We can also evaluate the quantum dimensions of individual excitations [158] and defects [159, 160] of a phase using topological entanglement entropy. Other work has shown we can use the topological entanglement entropy to calculate the fusion rules [161] and braid statistics [162] of $(2+1)$ -dimensional phases.

Generalizations of topological entanglement entropy diagnostics have been found [163, 164] for $(3+1)$ -dimensional phases with bulk topological order. These diagnostics were first demonstrated using the $(3+1)$ -dimensional toric code model [165] as an example. This phase gives rise to one species of bosonic excitation that braids non-trivially with a loop-like excitation in the bulk of the system. In contrast, particular classes of Walker-Wang models [25] have been shown to behave differently using the same diagnostics. Modular examples of these models demonstrate zero bulk topological entanglement entropy [55, 166], even though, at their boundary, they realize quasiparticle excitations with non-trivial braid statistics [55].

In Ref. [167], two new diagnostics were found to interrogate the long-range entanglement at the boundary of a (3+1)-dimensional topological phase. The behavior of the diagnostics was determined by making quite generic considerations of the support of creation operators for topological excitations, without assuming any knowledge of the underlying particle theory of the phase. It was shown that the diagnostics will show a null outcome only if all the particles that can be created at the boundary have trivial braid statistics. Conversely, boundary topological order must necessarily show positive topological entanglement entropy if quasi-particles that demonstrate non-trivial braid statistics can be created. In that work, the diagnostics were tested at the different boundaries of the (3+1)-dimensional toric code where null outcomes were obtained at boundaries where the appropriate types of particles condense. However, a limitation of the diagnostics presented in that paper is that the meaning of a positive outcome is not well understood.

From the input fusion category perspective, the topological entanglement entropies can be understood as arising from constraints on the ‘string flux’ passing through a surface. In (3+1)-dimensions, there are also additional corrections due to braiding. Allowing strings to terminate in the vicinity of a physical boundary alters the flux (and braiding) constraints in the vicinity, thereby altering the topological entropy.

In this work, we obtain closed form expressions for bulk and boundary topological entanglement entropy diagnostics for topological loop-gas models. We obtain our results by evaluating the entanglement entropy of various regions of ground states of Levin-Wen and Walker-Wang models. This requires careful analysis of various string diagrams, such as generalized \mathcal{S} -matrices which encode the braiding properties of the input category. Additionally, we examine how the inclusion of boundaries, via algebra objects, alter these diagrams, and so the topological entropy. In all cases, we find that the entropy can be expressed in terms of the quantum dimension of the input category and the quantum dimension of the algebra object. In the bulk of (3+1)-dimensional models, we conjecture, and prove in many cases, that the entropy is the logarithm of the total quantum dimension of the particle content of the theory, extending the results of Ref. [166].

Overview

Following a brief summary of our results, the remainder of this chapter is structured as follows. In Sect. 4.2, we introduce some notation and minor results that are required for the remainder of the chapter. In Sect. 4.3, we briefly review the models of interest, and discuss the class of boundaries we consider. In Sect. 4.4, we explain the origin and meaning of topological entanglement entropy, and

define the diagnostics used to detect boundary topological entanglement entropy. In Sect. 4.5, we compute the entropy of bulk regions for Levin-Wen models. These computations are required for the Walker-Wang models, and provide a good warm-up. We then discuss the additional considerations for Walker-Wang models, and extend the computations to these. In Sect. 4.6, we compute the boundary entropy diagnostics for Levin-Wen models with boundary, followed by some classes of Walker-Wang models with boundary. We summarize in Sect. 4.7.

We include two appendices. In Sect. 4.A, we provide proofs of some results concerning generalized S -matrices. In Sect. 4.B, we provide proofs of some results concerning loop-gas models, and their entropies.

Summary of results

In Table 4.1, we summarize our main results. The models we discuss will be introduced in the following sections, followed by the proofs of these results. We note that many of these results were previously known, for example the bulk Levin-Wen appears in Refs. [155, 156]. When the Levin-Wen model is defined by the fusion category $\mathbf{Vec}(G)$, the boundary Levin-Wen results appear in Ref. [168]. The bulk results for symmetric and modular Walker-Wang models appear in Ref. [166]. We extend this to include all pointed inputs (all quantum dimensions equal to 1), as well as all input categories up to rank 5. This allows us to conjecture a general result. To the best of our knowledge, there are no results concerning boundary entropies of Walker-Wang models beyond the (3+1)-dimensional toric code [167].

4.2 Preliminaries

In this work, each of the (3+1)-dimensional models we are interested in are described by a *unitary premodular category*. Boundaries of these models can be specified using *algebra objects* in the input category. For definitions of the various algebraic objects, we refer to Ref. [169], or for the physically minded reader Refs. [12, 170, 171]. Here, we briefly review the notation we use to describe these objects.

Let \mathcal{C} be a fusion category (Ref. [169], Def. 4.1.1). Without loss of generality, we assume \mathcal{C} is skeletal (isomorphic objects are equal), and the unit is strict. The number of simple objects is called the *rank* of \mathcal{C} , denoted $\mathrm{rk}(\mathcal{C})$. In all cases, we denote the unit object of \mathcal{C} by 1 , and the dual of an object x by \bar{x} .

The category \mathcal{C} is equipped with a bilinear functor $\otimes : \mathcal{C} \times \mathcal{C} \rightarrow \mathcal{C}$. Once we fix a basis for the

Model	Bulk strings	Boundary Q-system	Topological entropy
Levin-Wen	\mathcal{C} fusion		$\gamma = \log \mathcal{D}_{\mathcal{Z}(\mathcal{C})}^2$
		A	$\Gamma = \log \mathcal{D}^2$
Walker-Wang	\mathcal{C} premodular		$\delta = \log \mathcal{D}_{\mathcal{Z}_2(\mathcal{C})}^2$ ^a
		A	$\Delta_{\bullet} = ?$ ^b
		$A = 1$	$\Delta_{\circ} = \log d_A^2 - \log \mathcal{D}^2 + \Delta_{\bullet}$ $\Delta_{\bullet} = \log \mathcal{D}^2$ $\Delta_{\circ} = 0$
Walker-Wang	\mathcal{C} symmetric		$\delta = \log \mathcal{D}_{\mathcal{Z}_2(\mathcal{C})}^2$
		A	$\Delta_{\bullet} = \log \mathcal{D}^2 - \log d_A$ $\Delta_{\circ} = \log d_A$
Walker-Wang	\mathcal{C} pointed		$\delta = \log \mathcal{D}_{\mathcal{Z}_2(\mathcal{C})}^2$
		A such that $A \cap \mathcal{Z}_2(\mathcal{C}) = \{1\}$ ^c	$\Delta_{\bullet} = \log \mathcal{D}^2 - 2 \log d_A$ $\Delta_{\circ} = 0$
		A such that $A \cap \mathcal{Z}_2(\mathcal{C}) = A$	$\Delta_{\bullet} = \log \mathcal{D}^2 - \log d_A$ $\Delta_{\circ} = \log d_A$

^a Conjectured, proven in many cases as indicated in Theorem 3.

^b We do not have a general form at present.

^c Includes the case \mathcal{C} modular.

Table 4.1: Summary of results, technical terms defined in Sect. 4.2. The bulk strings are labeled by a unitary fusion category \mathcal{C} , possibly with extra structure. The number \mathcal{D} denotes the total quantum dimension of \mathcal{C} , A is a Q-system (with extra structure, see Sect. 4.2) of dimension d_A , $\mathcal{Z}(\mathcal{C})$ and $\mathcal{Z}_2(\mathcal{C})$ are the Drinfeld and Müger centers of \mathcal{C} respectively. Topological entanglement entropies for Levin-Wen models are denoted γ and Γ for the bulk and near the boundary respectively. These quantities are defined in Eq. (4.10), Eq. (4.11) and Fig. 4.2. The corresponding quantities in (3+1)-dimensions are denoted δ for the bulk entropy (Eq. (4.12) and Fig. 4.3), and Δ_{\bullet} (Δ_{\circ}) for the boundary entropy detecting point-like (loop-like) excitations as defined in Eq. (4.13) and Fig. 4.4 (Eq. (4.14) and Fig. 4.5).

fusion space $\mathcal{C}(a \otimes b, c)$, we denote a basis vector μ using a trivalent vertex ¹

$$\begin{array}{c} c \\ | \\ \mu \\ / \backslash \\ a \quad b \end{array} . \quad (4.1)$$

The (vector space) dimension of $\mathcal{C}(a \otimes b, c)$ is denoted $N_{a,b}^c$. We call these tensors the fusion rules of \mathcal{C} . If all $N_{a,b}^c \in \{0, 1\}$, we call the category *multiplicity free*. We normalize these bases following Ref. [170].

The natural isomorphism $(- \otimes -) \otimes - \cong - \otimes (- \otimes -)$ is realized as the F -matrices [12] of \mathcal{C} , and we refer to such a re-association as an F -move. If these are unitary, we say that \mathcal{C} is a *unitary fusion category*. Henceforth, we restrict to the unitary setting. We assume that \mathcal{C} is equipped with the unique unitary spherical structure [172], meaning that all diagrams can be treated as though they are drawn on the surface of a sphere.

The dimension of a simple object a is denoted d_a , while the total dimension of \mathcal{C} is denoted $\mathcal{D}_{\mathcal{C}}^2 := \sum_a d_a^2$, where the sum is over all simple objects. When it is clear from context, we omit the subscript. In string diagrams, a loop labeled by a is assigned d_a . We refer to insertion or removal of a loop, and the associated division or multiplication by the dimension, as a *loop move*. If $\mathcal{D}^2 = \text{rk}(\mathcal{C})$, we say that \mathcal{C} is *pointed*. This property is also commonly called Abelian in the physics literature.

Braided unitary fusion categories (Ref. [169], Def. 8.1.2) can be uniquely equipped with a unitary premodular structure [173]. For the results in this manuscript, it is important to understand which strings can be ‘uncrossed’. This is captured by the Müger center (Ref. [174], Def. 2.9), denoted $\mathcal{Z}_2(\mathcal{C})$. A premodular category is *symmetric* if $\mathcal{Z}_2(\mathcal{C}) = \mathcal{C}$, and *modular* if $\mathcal{Z}_2(\mathcal{C}) = \mathbf{Vec}$. We will refer to premodular categories which are neither symmetric nor modular as *properly premodular*.

We will make extensive use of an operator we call the *connected \mathcal{S} -matrix* \mathcal{S}_c , with matrix elements

$$[\mathcal{S}_c]_{(a,\alpha),(b,\beta)} = \frac{1}{\mathcal{D}} \begin{array}{c} \text{diagram} \end{array} . \quad (4.2)$$

The usual \mathcal{S} -matrix (Ref. [174], Def. 2.2) occurs as a special case, namely $\mathcal{S}_{a,b} = [\mathcal{S}_1]_{a,b}$. The connected \mathcal{S} -matrix appears in Theorem 3.1.17 of Ref. [175], and is closely related to the punctured \mathcal{S} -matrix of

¹We refrain from drawing arrows on the diagrams, instead using the convention that all lines are oriented upwards.

Ref. [176]. We will need the following result concerning the connected \mathcal{S} -matrix.

Lemma 4.1. Let \mathcal{C} be a unitary premodular category, then

$$\sum_{c \in \mathcal{C}} \text{Tr } \mathcal{S}_c^\dagger \mathcal{S}_c = \mathcal{D}^2, \quad (4.3)$$

where \mathcal{S}_c is the connected \mathcal{S} -matrix and \mathcal{D} is the total dimension of \mathcal{C} .

Proof. Provided in Appendix 4.A. □

We now briefly review the notation we use to describe algebra objects in \mathcal{C} . Let (A, m, η) be a Q-system, also called a unitary Frobenius algebra, in \mathcal{C} (Ref. [177], Def. 5.4). Since \mathcal{C} is semi-simple, we can decompose the object $A = 1 \oplus a_1 \oplus a_2 \oplus \dots$. In this work, we restrict to the multiplicity free case, so each a_i appears at most once. We represent the multiplication morphism m as

$$m = \begin{array}{c} A \\ \diagup \quad \diagdown \\ A \quad A \end{array} = \sum_{a,b,c \in A} m_{a,b}^c \begin{array}{c} c \\ \diagup \quad \diagdown \\ a \quad b \end{array}. \quad (4.4)$$

To simplify the notation, we define $m_{x,y}^z = 0$ whenever any of the labels do not occur in the decomposition of A . This allows us to always sum over simple objects in \mathcal{C} . Additionally, we suppress the A label. Any unlabeled lines carry an implicit A . We can always normalize the unit morphism $\eta = 1$, and the multiplication morphism

$$\sum_{a,b \in A} |m_{a,b}^c|^2 \sqrt{d_a d_b} = \delta_{c \in A} \sqrt{d_c} d_A, \quad (4.5)$$

where $d_A = \sum_{a \in A} d_a$. When it does not cause confusion, we will indicate a Q-system by its object, for example $A = 1$, the ‘unit algebra’.

If the underlying category \mathcal{C} is braided, we say the algebra is *commutative* if it commutes in the category (Ref. [169], Def. 8.8.1).

4.2.1 Examples

We use the following examples throughout our work to illustrate our results. The unitary fusion category $\mathbf{Vec}^\omega(\mathbb{Z}_2)$ is the category of finite dimensional \mathbb{Z}_2 -graded vector spaces. The simple objects of this pointed category are group elements $\mathbb{Z}_2 := \{1, x \mid x^2 = 1\}$. We neglect to draw the unit object,

1. As such, the only nonzero trivalent vertex is

$$\begin{array}{c} \diagup \\ \diagdown \end{array} . \quad (4.6)$$

There are exactly two inequivalent associators compatible with the fusion rule, namely

$$\begin{array}{c} \diagup \\ \diagdown \end{array} = \omega \begin{array}{c} \diagdown \\ \diagup \end{array} , \quad (4.7)$$

with $\omega = \pm 1$. With the associator fixed, there are two compatible braidings

$$\begin{array}{c} \diagup \\ \diagdown \end{array} = \varphi \begin{array}{c} \diagdown \\ \diagup \end{array} , \quad (4.8)$$

with $\varphi^2 = \omega$. We denote by $\mathbf{Vec}^{\omega, \varphi}(\mathbb{Z}_2)$ the braided category, with associator ω and braiding φ . The categories $\mathbf{Vec}^{-1, \pm i}(\mathbb{Z}_2)$ are modular, while $\mathbf{Vec}^{1, \pm 1}(\mathbb{Z}_2)$ are symmetric.

For these examples, there are two possible Q-systems, namely $A_0 := 1$, with trivial m morphism, and $A_1 := 1 \oplus x$. The unit algebra, A_0 , is compatible as a commutative Q-system. For A_1 , compatibility as a Q-system reduces to $m_{x,x}^1 \omega = m_{x,x}^1$, so is only a valid algebra object when $\omega = 1$. In that case, A_1 is commutative when $m_{x,x}^1 \varphi = m_{x,x}^1$, which required $\varphi = 1$.

4.3 Loop-gas models in (3+1) dimensions

Walker-Wang [25, 52–54] models are three-dimensional Hamiltonian models that give rise to topological loop-gas states as their ground states. Hamiltonians for these models are given in Ref. [25]. Our results do not depend on the particular form of the Hamiltonian, rather on universal properties of the ground states in the associated topological phase.

Quasiparticle excitations in these models are defects in the ground state, corresponding to a local change in the rules. Far from the excitations, the excited state remains invariant under the original moves but, for example, a string may be allowed to terminate at the location of the excitation.

4.3.1 Bulk

We now briefly introduce the categorical description of the models of interest far from any physical boundary.

Given a unitary fusion category \mathcal{C} , and a given lattice embedded on a three-dimensional manifold,

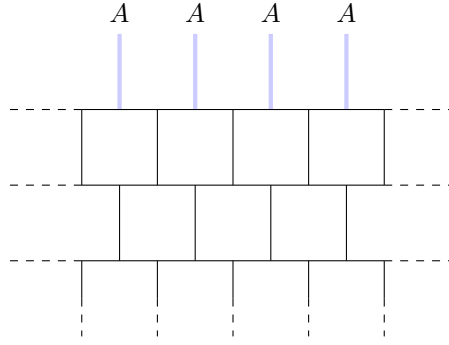


Figure 4.1: An algebra specifies a boundary for a Levin-Wen model on a ‘comb lattice’. Dashed lines indicate the lattice continues. The top, thick blue lines are labeled by an algebra A that defines a physical boundary to the lattice.

the ground states of Walker-Wang models are super-positions of closed diagrams from the category. Strings lie along the edges of the lattice, and closed means they cannot terminate. To produce a lattice model, \mathcal{D} -dimensional vector spaces are assigned to each edge. These vector spaces are equipped with an orthogonal basis consisting of the objects of \mathcal{C} . If the category is multiplicity free, vector spaces corresponding to the fusion spaces are assigned to the vertices. An abstract string configuration is realized by the vector consisting of the appropriate basis vector on each edge. At the vertices, the fusion rules of the category dictate which strings can fuse. If a given configuration occurs in a particular ground state, then any other configuration that is obtainable by local moves (i.e. F - or loop-moves) also occurs in that ground state. The relative coefficients are dictated by the F -symbols, and consistency is ensured by the pentagon equation. Since the allowed moves are all local, there may be multiple ground states on manifolds with nontrivial genus. For example, a loop enclosing a cycle of the torus cannot be removed with the local loop move.

In (3+1)-dimensions, for Walker-Wang models, the diagrams can also include crossings. This required additional data to be added to the category, in particular a braiding. If we picture these diagrams embedded in 3 dimensional space, there is an ambiguity involved in these crossing. For example, if we look at a crossing from ‘the side’, there is no crossing. This ambiguity can be resolved by widening the strings into ribbons. This is implemented by insisting that the braided category is premodular.

In addition to the F - and loop- moves, R - moves and insertion of links (or knots), such as the S -matrix are allowed. Again, given any closed string configuration, any other configuration that can be reached via these rules is included in the ground state superposition.

4.3.2 Boundaries

To include a physical boundary in a loop-gas model, the rules must be modified. For the topological loop-gas models, these rules are again defined by local moves in the vicinity of the boundary. These must be compatible with the bulk moves, and ensure topological/retriangulation invariance at the boundary. We restrict our attention to gapped boundaries.

Levin-Wen models

There are various equivalent classifications for the gapped boundaries of Levin-Wen models [150, 151, 178–181]. In this work, we use an internal classification. In this framework, gapped boundary conditions for Levin-Wen models are labeled by *indecomposable Q -systems* in \mathcal{C} up to Morita equivalence [150, 151]. We restrict to multiplicity free algebras for simplicity. These algebra objects are (not necessarily simple) objects in \mathcal{C} , and their simple subjects are roughly the string types that are allowed to terminate on the boundary.

On the comb lattice (Fig. 4.1), for example, the dangling edges only take values in the chosen algebra. Far from the boundary, the ground states look just like those with no boundary. Near the boundary, loops are no longer required to be closed, rather they can terminate on the boundary if their label occurs within the algebra. We refer to Refs. [150, 151] for more details, including an explicit Hamiltonian.

Walker-Wang models

Just as in the bulk, when we move to (3+1)-dimensions, the braiding must be taken into account. A general classification of gapped boundaries for Walker-Wang models has not been established, so we proceed for a class of boundaries generalizing those for Levin-Wen introduced above. As before, a boundary is labeled by an algebra object. Since the bulk is braided, an additional compatibility condition is required, namely that the algebra is commutative (Ref. [169], Def. 8.8.1). Finally, in this work, an *indecomposable, commutative, Q -systems* labels a gapped boundary condition of a Walker-Wang model ².

4.3.3 Examples

Recall the examples from Sect. 4.2.1. In (2+1)-dimensions, $\mathbf{Vec}^{1,\pm 1}(\mathbb{Z}_2)$ lead to the same loop-gas model, since the Levin-Wen construction doesn't make use of the braiding. This model is the equally

²Private communications with David Aasen

weighted superposition of all loop diagrams (with no branching due to the fusion rules). This is the ground state of the toric code model [146].

Likewise, $\mathbf{Vec}^{\pm i}(-1)$ correspond to the same loop-gas model. Due to the nontrivial Frobenius-Schur indicator [12], it is convenient to associate -1 to a loop rather than $+1$ (otherwise we can take extra care when bending lines). The ground state is therefore a superposition of loops, but weighted by $(-1)^{\text{number of loops}}$. This is commonly called the double-semion model.

There are two possible (gapped) boundaries for the toric code, the ‘smooth’ boundary, corresponding to the algebra A_0 , and the ‘rough’ boundary, corresponding to A_1 . We refer to Ref. [182] for more details. The double-semion model only allows for one kind of (gapped) boundary, labeled by A_0 .

In (3+1)-dimensions, each of these models labels a distinct Walker-Wang model. The models $\mathbf{Vec}^{1,1}(\mathbb{Z}_2)$, $\mathbf{Vec}^{1,-1}(\mathbb{Z}_2)$ are commonly called the *bosonic*- and *fermionic*- toric code models respectively [165, 183]. Since these categories both have $\mathcal{Z}_2(\mathcal{C}) = \{1, x\}$, they both have a single particle excitation, in addition to the trivial excitation, whose self-statistics lead to the names of the models. The two models $\mathbf{Vec}^{\pm i}(-1)$ are both referred to as semion models.

In (3+1)-dimensions, the bosonic toric code still has two kinds of boundaries, but the remaining models are only compatible with the trivial boundary labeled by A_0 .

4.4 Entropy diagnostics

In what follows we describe the universal correction to the area law that we expect for topological phases. We then define two diagnostics that can be used to probe the properties of the excitations at the boundary of (3+1)-dimensional topological phases.

4.4.1 The universal correction to the area law

The ground states of topological phases of matter demonstrate robust long-range entanglement that is not present in trivial phases [154–156]. Typically, we expect the entanglement entropy shared between a subsystem of a ground state of a gapped phase with the rest of the system to respect an area law, i.e., the entanglement will scale with the size of the surface area of the subsystem. The long-range entanglement manifests as a universal correction to the area law. More precisely, we expect that if we partition the ground state of a system into two subsystems, R and its complement R^c , the entanglement entropy, S_R , will satisfy

$$S_R = \alpha|\partial R| - b_R\gamma. \quad (4.9)$$

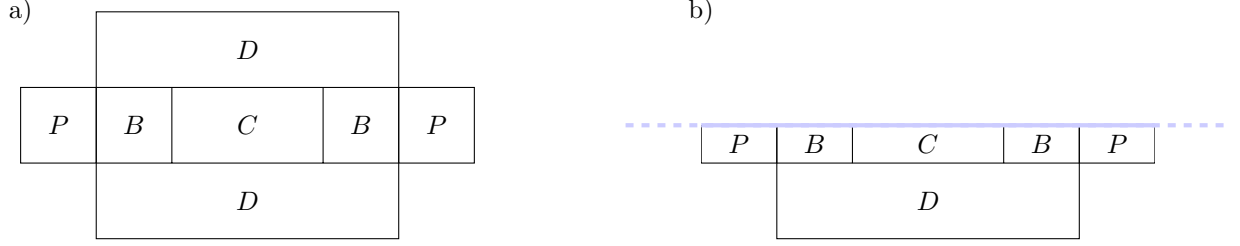


Figure 4.2: Example of subsystems that can be used to find topological entropies in (2+1)-dimensions. The region A is the complement of BCD . The regions a) are used to find the bulk entropy γ , and the regions b) are used for the boundary entropy Γ .

Here α is a non-universal coefficient that depends on the microscopic details of the system, $|\partial R|$ is the surface area of the interface between the partitioned regions, b_R is the number of disjoint components of the interface between R and R^c , and γ is a universal constant commonly known as the topological entanglement entropy. We have assumed that R is large compared to the correlation length of the system, and its shape has no irregular features.

4.4.2 (2+1)-dimensional models

Intimately connected to the long-range entanglement of a topological phase are the properties of its low-energy excitations. A large class of topological models in (2+1)-dimensions are the Levin-Wen string-net models [13]. These models support topological point-like excitations that can be braided to change the state of the system.

Throughout this work we will be interested in the boundaries of topological phases. Importantly, topological particles can behave differently in the vicinity of the boundary of a phase. For instance, topological particles found in the bulk may become trivial particles close to certain boundaries. This is because topological particles can condense at the boundary such that non-trivial charges can be created locally.

As the physics of the quasi-particles of a topological phase can change close to its boundary, so to do we expect that the nature of its long-range entanglement to change. In Ref. [167], several topological entanglement entropy diagnostics were found to probe long-range entanglement of a model, both in the bulk and near to a boundary. The first is the bulk topological entanglement entropy

$$\gamma := S_{BC} + S_{CD} - S_B - S_D, \quad (4.10)$$

where the regions are depicted in Fig. 4.2a, and $XY := X \cup Y$. If $\gamma = 0$, all point-like excitations can be created on the distinct parts of P with a creation operator that has no support on ACD , where A is the region that is complement to those shown in the figure. In this case, we declare them trivial. Conversely, if there are non-trivial topological excitations, for example created with string-like operators, γ is necessarily non-zero.

In the presence of a gapped boundary, the excitations may differ. If a bulk topological excitation can be discarded or ‘condensed’ on the boundary, it is possible to locally create such an excitation near the boundary. This is detected using the diagnostic

$$\Gamma := S_{BC} + S_{CD} - S_B - S_D, \quad (4.11)$$

where the regions are depicted in Fig. 4.2b. If $\Gamma = 0$, all point-like excitations on P can be created with an operator that has no support on ACD , while non-trivial excitations require non-zero Γ .

4.4.3 (3+1)-dimensional models

Walker-Wang models give rise to both point- and line-like topological particles in the bulk, in addition to boundary excitations. Unlike Levin-Wen models, in some instances topological particles are only found at the boundary.

Since there are two kinds of topological excitations in (3+1)-dimensions, we might expect that there are two bulk diagnostics generalizing γ . However, as it has been shown [164, 166], these coincide. We define the bulk topological entanglement entropy

$$\delta := S_{BC} + S_{CD} - S_B - S_D, \quad (4.12)$$

where the regions are depicted in Fig. 4.3. We obtained this choice of region following intuition given in Ref. [167] where we consider the creating point excitations at the distinct parts of region P using a string operator supported on ACD . We find δ is zero only if all the excitations can be created using an operator with local support. The boundary diagnostics that we describe next are obtained by bisecting the regions shown in Fig. 4.3 along different planes where the boundary lies.

In Ref. [167] two topological entanglement entropy diagnostics were found to probe long-range entanglement of a model near to a boundary. The first boundary diagnostic is an indicator that point-like topological particles can be created at the boundary of the system, and the second indicates that the boundary supports extended one-dimensional ‘loop-like’ topological particles. Unlike in the

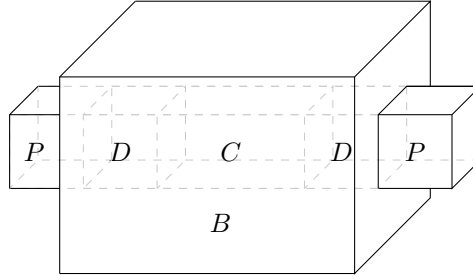


Figure 4.3: Partitioning of the lattice for detecting excitations in the bulk. B encircles CD , and A is the complement of BCD . If δ is small, excitations on P can be created by only acting on PD and so have trivial statistics.

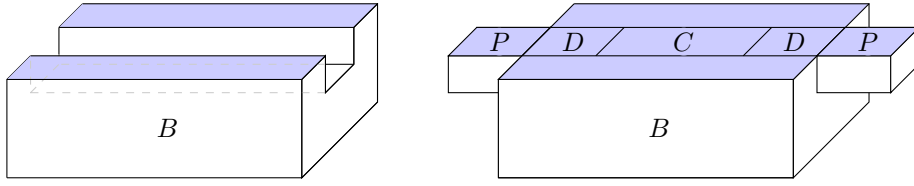


Figure 4.4: Partitioning of the lattice for detecting point-like excitations on the boundary. The top (blue) surface is on the physical boundary of the lattice. If Δ_\bullet is small, excitations on P can be created by only acting on PD and so have trivial statistics.

bulk, these diagnostics do not necessarily coincide. The first

$$\Delta_\bullet := S_{BC} + S_{CD} - S_B - S_D, \quad (4.13)$$

defined using the regions in Fig. 4.4, is non-zero if non-trivial point-like excitations can be created near the boundary. If $\Delta_\bullet = 0$, all point-like excitations on P can be created with a local operator, so they are necessarily trivial. Conversely, if there are non-trivial point-like particles near the boundary, $\Delta_\bullet > 0$.

The final diagnostic is designed to detect nontrivial loop-like excitations. Using the regions depicted in Fig. 4.5, this diagnostic is

$$\Delta_\circ := S_{BC} + S_{CD} - S_B - S_D. \quad (4.14)$$

Similarly to the other diagnostics, if Δ_\circ is zero, then line-like excitations must be trivial. Conversely, Δ_\circ must be nonzero if non-trivial loop excitations can be created at the boundary.

The diagnostics presented in Ref. [167] were found using generic arguments about the support of deformable operators that are used to create excitations. As such, it was shown rigorously that the null outcome is obtained only if a boundary does not give rise to topological particles. Conversely, a boundary that gives rise to topological excitations must give a positive reading for these diagnostics.

However, due to spurious contributions [184–187], the generic arguments cannot guarantee that the diagnostics do not give false positives and, moreover, the work gives no interpretation for the magnitude of a positive reading. In our work, we restrict to loop-gas models. In that setting, for a large class of models, we obtain expressions for the topological entanglement entropy near the boundary.

4.5 Bulk entropy of topological loop-gasses

We now show how the entanglement entropy of ground states of Levin-Wen models is computed far from any boundary, before moving on to Walker-Wang models. To make the calculation we take the Schmidt decomposition of the ground state

$$|\psi\rangle = \sum_{\lambda=1}^r \Phi_{\lambda} |\psi_R^{\lambda}\rangle |\psi_{R^c}^{\lambda}\rangle, \quad (4.15)$$

for regions R , where the sets $\{|\psi_R^{\lambda}\rangle\}$ and $\{|\psi_{R^c}^{\lambda}\rangle\}$ are orthonormal, and r is the Schmidt rank of the state $|\psi\rangle$. This allows us to compute the reduced state ρ_R on R . Diagonalizing this matrix yields the entanglement entropy.

In what follows, we will need to parameterize the states $|\psi_R^{\lambda}\rangle$ and $|\psi_{R^c}^{\lambda}\rangle$. Recall from Sect. 4.3 that ground states of the loop-gas models can be understood as classes of diagrams which are related by local moves. It is convenient to parameterize $|\psi_R^{\lambda}\rangle$ in a similar way. Far from the interface (since the correlation length is 0, far means one site), the state behaves exactly like the ground state. Unlike in the bulk, the interface defines a fixed boundary condition for the diagram in R . States $|\psi_R^{\lambda}\rangle$ will therefore be represented by some fiducial diagram T , and are understood to consist of a superposition of all diagrams that can be obtained from T by local moves *restricted to R* as indicated in Fig. 4.6. Particular lattices may provide geometric complications, but the topological invariance of the ground state will mean these are of no consequence. In all cases, we will choose a particular class of fusion trees as fiducial diagrams. For the following, we will therefore need several results concerning fusion

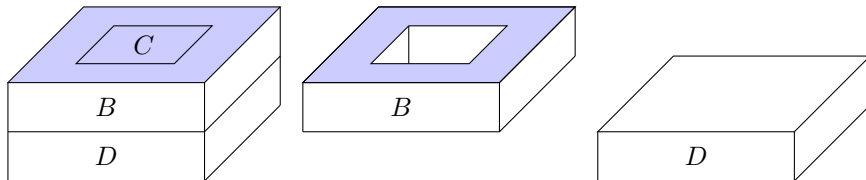


Figure 4.5: Partitioning of the lattice for detecting line-like excitations on the boundary. The top (blue) surface is on the boundary of the lattice. If Δ_{\circ} is small, excitations on B can be created without acting on C and so have trivial statistics.

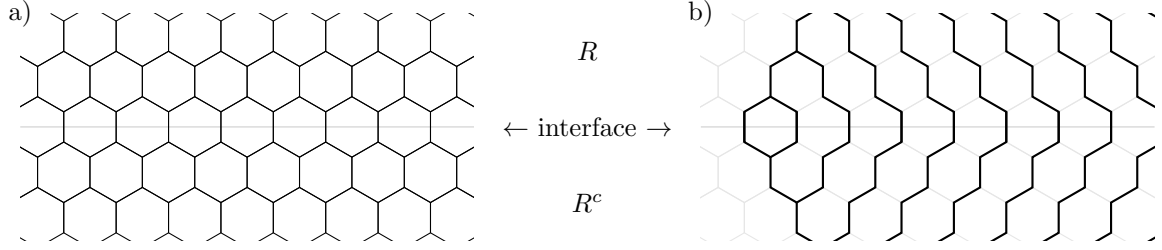


Figure 4.6: To compute the Schmidt decomposition, we need to parameterize states contained on one sub-region. Given a generic configuration on the lattice (a), we can utilize the ‘moves’ outlined in Sect. 4.2, restricted to either side of the interface, to deform into a tree (b). The lattice sites on the boundary provide boundary conditions for the states in R and R^c . We utilize constraints on the total fusion outcome in each region to parameterize the allowed trees.

trees. Consider fusing n strings labeled $\vec{x} := (x_1, x_2, \dots, x_n)$ to a fixed object a . Using F -moves, we can bring the fusion tree for this process into the canonical form

where $1 \leq \mu \leq N_{a,b}^c$ parameterizes the distinct fusion channels $a \otimes b \rightarrow c$. In the following, sums over x_i, y_i are over all simple objects in \mathcal{C} . First, we need two results concerning summing over trees.

Lemma 4.2. Let \mathcal{C} a unitary fusion category, then for a fixed simple fusion outcome a ,

$$\sum_{\vec{x}, \vec{y}} N_{x_1 x_2}^{y_1} N_{y_1 x_3}^{y_2} \cdots N_{y_{n-2} x_n}^a \prod_{j \leq n} d_{x_j} = d_a \mathcal{D}^{2(n-1)}, \quad (4.17)$$

where $\mathcal{D} = \sqrt{\sum_i d_i^2}$ is the total quantum dimension of \mathcal{C} .

Proof. Provided in Appendix 4.B. □

Lemma 4.3. Let \mathcal{C} a unitary fusion category, then for a fixed simple fusion outcome a ,

$$\sum_{\vec{x}, \vec{y}} N_{x_1 x_2}^{y_1} N_{y_1 x_3}^{y_2} \cdots N_{y_{n-2} x_n}^a \frac{\prod_{j \leq n} d_{x_j}}{\mathcal{D}^{2(n-1)}} \log \prod_{k \leq n} d_{x_k} = n d_a \sum_x \frac{d_x^2 \log d_x}{\mathcal{D}^2}. \quad (4.18)$$

Proof. Provided in Appendix 4.B. □

Finally, we need the probability of a given fusion tree in a topological loop-gas model.

Lemma 4.4 (Probability of trees). Let \mathcal{C} a unitary fusion category. Given a fusion outcome a on n edges, the probability of the tree in Eq. (4.16) is

$$\Pr[\vec{x}, \vec{y}, \vec{\mu}|a] = \frac{\prod_{j \leq n} d_{x_j}}{d_a \mathcal{D}^{2(n-1)}}. \quad (4.19)$$

Proof. Provided in Appendix 4.B. □

Throughout the remainder of this section, we use the following condensed notation

$$\sum_{\vec{x}, \vec{y}, \vec{\mu}} := \sum_{x_1, \dots, x_n} \sum_{y_1, \dots, y_{n-2}} \sum_{\mu_1, \dots, \mu_{n-2}} \quad (4.20)$$

$$= \sum_{x_1, \dots, x_n} \sum_{y_1, \dots, y_{n-2}} N_{x_1 x_2}^{y_1} N_{y_1 x_3}^{y_2} \dots N_{y_{n-2} x_n}^a, \quad (4.21)$$

where we frequently leave the fusion outcome a implicit.

4.5.1 Levin-Wen models

Theorem 4.1 (Topological entropy of (2+1)-dimensional Levin-Wen models in the bulk [155, 156, 188]).

Consider the regions shown in Fig. 4.2a, then the Levin-Wen model defined by a unitary spherical fusion category \mathcal{C} , with total dimension \mathcal{D} , has topological entropy

$$\gamma = 2 \log \mathcal{D}^2 = \log \mathcal{D}_{\mathcal{Z}(\mathcal{C})}^2, \quad (4.22)$$

where $\mathcal{Z}(\mathcal{C})$ is the modular category called the *Drinfeld center* [169] of \mathcal{C} which describes the anyons of the theory.

Examples. Recall the examples from Sect. 2.5. As discussed in Sect. 4.3.3, these label two distinct loop-gas models in (2+1)-dimensions, the toric code and double semion models. Since all the input categories for these examples have $\mathcal{D}^2 = 2$, the topological entanglement entropy is $\gamma = 2 \log 2$ for both.

Lemma 4.5 (Entropy of (union of) simply connected bulk regions [156, 166, 188]). On a region R in

the bulk consisting of the disjoint union of simply connected sub-regions, the entropy is

$$S_R = nS[\mathcal{C}] - b_0 \log \mathcal{D}^2, \quad (4.23)$$

where b_0 is the number of disjoint interface components of R , n is the number of links crossing the entanglement interface, and

$$S[\mathcal{C}] := \log \mathcal{D}^2 - \sum_x \frac{d_x^2 \log d_x}{\mathcal{D}^2}. \quad (4.24)$$

Proof of Lemma 4.5. Consider a ball R with n sites along the interface, in the configuration $\vec{x} = x_1, x_2, \dots, x_n$. Since any configuration must be created by inserting closed loops into the empty state, the total ‘charge’ crossing the interface must be 1. For a fixed \vec{x} , there are now many ways for this to happen, parameterized by trees depicted in Eq. (4.16) with fusion outcome $a = 1$.

Trees with distinct labelings (in \vec{x} , \vec{y} or $\vec{\mu}$) are orthogonal. This means that if the tree Eq. (4.16) occurs adjacent to the interface within R , it must also occur on the other side of the interface

$$\propto \delta_{\vec{z}=\vec{y}} \delta_{\vec{v}=\vec{\mu}} \delta_{d=c}. \quad (4.25)$$

If the trees on either side of the cut had different branching structures, we could use local moves on either side of the cut to bring them to this standard form.

We take the Schmidt decomposition of the ground state as follows

$$|\psi\rangle = \sum_{\vec{x}, \vec{y}, \vec{\mu}} \Phi_{\vec{x}, \vec{y}, \vec{\mu}} \left| \psi_R^{\vec{x}, \vec{y}, \vec{\mu}} \right\rangle \left| \psi_{R^c}^{\vec{x}, \vec{y}, \vec{\mu}} \right\rangle, \quad (4.26)$$

where the notation $\vec{x}, \vec{y}, \vec{\mu}$ indicates the labeling of a valid tree as in Eq. (4.16). The state $\left| \psi_R^{\vec{x}, \vec{y}, \vec{\mu}} \right\rangle$

includes any state that can be reached from Eq. (4.16) (with $a = 1$) by acting only on R . The reduced state on R is

$$\rho_R = \sum_{\vec{x}, \vec{y}, \vec{\mu}} |\Phi_{\vec{x}, \vec{y}, \vec{\mu}}|^2 \left| \psi_R^{\vec{x}, \vec{y}, \vec{\mu}} \right\rangle \left\langle \psi_R^{\vec{x}, \vec{y}, \vec{\mu}} \right| \quad (4.27)$$

$$= \sum_{\vec{x}, \vec{y}, \vec{\mu}} \text{Pr}[\vec{x}, \vec{y}, \vec{\mu}|1] \left| \psi_R^{\vec{x}, \vec{y}, \vec{\mu}} \right\rangle \left\langle \psi_R^{\vec{x}, \vec{y}, \vec{\mu}} \right|, \quad (4.28)$$

where $\text{Pr}[\vec{x}, \vec{y}, \vec{\mu}|1]$ is the probability of the labeled tree, given that \vec{x} fuses to 1. From Lemma 4.4, the reduced state is

$$\rho_R = \sum_{\vec{x}, \vec{y}, \vec{\mu}} \frac{\prod_{j \leq n} d_{x_j}}{\mathcal{D}^{2(n-1)}} \left| \psi_R^{\vec{x}, \vec{y}, \vec{\mu}} \right\rangle \left\langle \psi_R^{\vec{x}, \vec{y}, \vec{\mu}} \right|. \quad (4.29)$$

The von Neumann entropy of ρ_R is therefore

$$S_R := -\text{tr } \rho_R \log \rho_R \quad (4.30)$$

$$= - \sum_{\vec{x}, \vec{y}, \vec{\mu}} \frac{\prod_{j \leq n} d_{x_j}}{\mathcal{D}^{2(n-1)}} \log \frac{\prod_{k \leq n} d_{x_k}}{\mathcal{D}^{2(n-1)}} \quad (4.31)$$

$$= \frac{\log \mathcal{D}^{2(n-1)}}{\mathcal{D}^{2(n-1)}} \sum_{\vec{x}, \vec{y}, \vec{\mu}} \prod_{j \leq n} d_{x_j} - \sum_{\vec{x}, \vec{y}, \vec{\mu}} \frac{\prod_{j \leq n} d_{x_j}}{\mathcal{D}^{2(n-1)}} \log \prod_{k \leq n} d_{x_k} \quad (4.32)$$

$$= n(\log \mathcal{D}^2 - \sum_x \frac{d_x^2 \log d_x}{\mathcal{D}^2}) - \log \mathcal{D}^2 \quad (4.33)$$

$$= nS[C] - \log \mathcal{D}^2 \quad (4.34)$$

where Lemmas 4.2 and 4.3 are applied to the left and right terms of line (4.32), respectively, and

$$S[C] := \log \mathcal{D}^2 - \sum_x \frac{d_x^2 \log d_x}{\mathcal{D}^2}. \quad (4.35)$$

It is straightforward to check that this holds on each sub-region of R . □

Applying Lemma 4.5 to the regions in Fig. 4.2a completes the proof of Thm. 4.1.

4.5.2 Walker-Wang models

In this section, we prove the following result for the bulk diagnostic for Walker-Wang models. The essential arguments in this section were made in Ref. [166], however we use slightly different language that allows the result to be applied more generally.

Theorem 4.2. For a Walker-Wang model defined by a unitary premodular category \mathcal{C} , the topological entanglement entropy (defined using the regions in Fig. 4.3) in the bulk is given by

$$\delta = \sum_{c, \lambda_c} \frac{\lambda_c}{\mathcal{D}^2} \log \frac{\lambda_c}{d_c}, \quad (4.36)$$

where $\{\lambda_c\}$ are the eigenvalues of $\mathcal{S}_c^\dagger \mathcal{S}_c$, and \mathcal{S}_c is the connected \mathcal{S} -matrix (Eq. (4.2)).

Proof. In simply connected regions, the arguments from Lemma 4.5 still hold. The other type of region in Fig. 4.2a is a torus. In this case, we cannot simply decompose the ground state as in Eq. (4.26), with the sum over configurations on the interface. Recall that the reason we could do this for a simple region was ground states are created by inserting closed loops, and all closed loops except those crossing the interface can be added entirely within either R or R^c . This is not the case for a toroidal region. Consider, for example, the configuration depicted in Fig. 4.7. The closed string inside R (red, dashed) cannot be altered by acting entirely within R , so contributes additional entanglement to the ground state, which is not witnessed by the interface configuration. Additionally, the two loops may be connected by a string, such that the global charge is trivial. Therefore, unlike for simply connected regions, the net charge crossing the boundary is not necessarily trivial. With these considerations, we can decompose the ground state as

$$|\psi\rangle = \sum_{\substack{\vec{x}, \vec{y}, \vec{\mu} \\ c, a, \alpha, b, \beta}} \Phi_{\vec{x}, \vec{y}, \vec{\mu}, c} \frac{[\mathcal{S}_c]_{(b, \beta)(a, \alpha)}}{\mathcal{D}} \left| \psi_R^{\vec{x}, \vec{y}, \vec{\mu}, c, a, \alpha} \right\rangle \left| \psi_{R^c}^{\vec{x}, \vec{y}, \vec{\mu}, c, b, \beta} \right\rangle, \quad (4.37)$$

where \mathcal{S}_c is the connected \mathcal{S} -matrix defined in Eq. (4.2). The indices $\vec{x}, \vec{y}, \vec{\mu}$ are as in Eq. (4.26), b labels the loop encircling R , while a is the loop within R , and c is the total charge crossing the boundary (the top label in Eq. (4.16)). The reduced state on R is

$$\rho_R = \sum_{\substack{\vec{x}, \vec{y}, \vec{\mu} \\ a_1, \alpha_1, a_2, \alpha_2, c}} \frac{\text{Pr}[\vec{x}, \vec{y}, \vec{\mu} | c]}{\mathcal{D}^2} [\mathcal{S}_c^\dagger \mathcal{S}_c]_{(a_2, \alpha_2)(a_1, \alpha_1)} \left| \psi_R^{\vec{x}, \vec{y}, \vec{\mu}, a_1, \alpha_1, c} \right\rangle \left\langle \psi_R^{\vec{x}, \vec{y}, \vec{\mu}, a_2, \alpha_2, c} \right| \quad (4.38)$$

$$= \sum_{\substack{\vec{x}, \vec{y}, \vec{\mu} \\ a_1, \alpha_1, a_2, \alpha_2, c}} \frac{\prod_{j \leq n} d_{x_j}}{d_c \mathcal{D}^{2n}} [\mathcal{S}_c^\dagger \mathcal{S}_c]_{(a_2, \alpha_2)(a_1, \alpha_1)} \left| \psi_R^{\vec{x}, \vec{y}, \vec{\mu}, a_1, \alpha_1, c} \right\rangle \left\langle \psi_R^{\vec{x}, \vec{y}, \vec{\mu}, a_2, \alpha_2, c} \right|. \quad (4.39)$$

To compute the entropy of this state, it is convenient to diagonalize it. Denote the eigenvalues of $\mathcal{S}_c^\dagger \mathcal{S}_c$

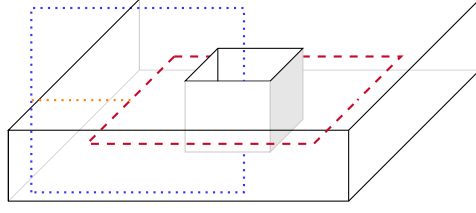


Figure 4.7: When the region R is not simply connected, the computation of entropy is more subtle. There is additional entanglement in the system due to intersecting loops that cannot be created in R or R^c separately. This is not witnessed by the configuration of strings on the interface.

by $\{\lambda_c\}$. By a unitary change of basis, we have

$$U \rho_R U^\dagger = \sum_{\substack{\vec{x}, \vec{y}, \vec{\mu}, \\ c, \lambda_c}} \frac{\prod_{j \leq n} d_{x_j}}{d_c \mathcal{D}^{2n}} \lambda_c \left| \varphi_{\lambda_c}^{\vec{x}, \vec{y}, \vec{\mu}, c} \right\rangle \left\langle \varphi_{\lambda_c}^{\vec{x}, \vec{y}, \vec{\mu}, c} \right|, \quad (4.40)$$

with von Neumann entropy

$$S_R = nS[\mathcal{C}] - \sum_{c, \lambda_c} \frac{\lambda_c}{\mathcal{D}^2} \log \frac{\lambda_c}{d_c}, \quad (4.41)$$

where Lemmas 4.1 to 4.3 are used. Combining with Lemma 4.5 completes the proof. \square

Conjecture 4.1. Let \mathcal{C} be a unitary premodular category \mathcal{C} , and define the connected \mathcal{S} -matrix via its matrix elements

$$[\mathcal{S}_c]_{(a, \alpha), (b, \beta)} = \frac{1}{\mathcal{D}} \bar{a} \begin{array}{c} \text{diagram of two overlapping circles} \end{array} \bar{c}. \quad (4.42)$$

The diagram shows two overlapping circles. The left circle is labeled with α at the top and \bar{b} at the bottom. The right circle is labeled with β at the bottom and b at the right. A line labeled c connects the top of the left circle to the top of the right circle. A line labeled \bar{c} connects the bottom of the right circle to the bottom of the left circle.

The connected \mathcal{S} -matrix obeys

$$\sum_{c, \lambda_c} \frac{\lambda_c}{\mathcal{D}^2} \log \frac{\lambda_c}{d_c} = \log \mathcal{D}_{\mathcal{Z}_2(\mathcal{C})}^2, \quad (4.43)$$

where $\{\lambda_c\}$ are the eigenvalues of $\mathcal{S}_c^\dagger \mathcal{S}_c$, and $\mathcal{Z}_2(\mathcal{C})$ is the Müger center of \mathcal{C} .

We conjecture that Eq. (4.43) holds in general, however we are currently unable to compute the spectrum of \mathcal{S}_c beyond the families outlined in Thm. 4.3.

Theorem 4.3. For a Walker-Wang model defined by a unitary premodular category of one of the following types:

- $\mathcal{C} = \mathcal{A} \boxtimes \mathcal{B}$, where \mathcal{A} is symmetric and \mathcal{B} is modular [166],
- \mathcal{C} pointed,
- $\text{rk}(\mathcal{C}) < 6$ and multiplicity free,
- $\text{rk}(\mathcal{C}) = \text{rk}(\mathcal{Z}_2(\mathcal{C})) + 1$ and $d_x = \mathcal{D}_{\mathcal{Z}_2(\mathcal{C})}$, where x is the additional object (as a special case, \mathcal{C} is a Tambara-Yamagami category [189, 190]),

then Eq. (4.43) holds. As a consequence, the topological entanglement entropy (defined using the regions in Fig. 4.3) in the bulk is given by

$$\delta = \log \mathcal{D}_{\mathcal{Z}_2(\mathcal{C})}^2, \quad (4.44)$$

where $\mathcal{Z}_2(\mathcal{C})$ is the Müger center of \mathcal{C} . As special cases, this includes

$$\delta_{\text{modular}} = 0 \quad (4.45)$$

$$\delta_{\text{symmetric}} = \log \mathcal{D}^2 \quad (4.46)$$

We conjecture that Eq. (4.44) holds in generality. Physically, this is seen by noting that the particle content of the bulk Walker-Wang model is given by the Müger center $\mathcal{Z}_2(\cdot)$ [191].

Proof. Provided in Appendix 4.B. □

Examples. Recall the examples from Sect. 2.5. As discussed in Sect. 4.3.3, these label four distinct loop-gas models in (3+1)-dimensions, the bosonic and fermionic toric code models, and two semion models. All four input categories are pointed, so we can apply Thm. 4.3 to obtain the topological entanglement entropy. The first two models are symmetric, so $\delta = \log 2$ for both. The inputs to the semion models are modular, so the bulk is trivial [55]. In this case $\delta = 0$.

4.6 Boundary entropy of topological loop-gasses

We now turn to the computation of the boundary diagnostics from Sect. 4.4. As before, we begin with Levin-Wen models.

4.6.1 Levin-Wen models

Theorem 4.4 (Topological entropy of (2+1)-dimensional Levin-Wen models at a boundary).

Consider the regions shown in Fig. 4.2b. The Levin-Wen model defined by unitary spherical fusion category \mathcal{C} , with boundary specified by an indecomposable Q-system $A \in \mathcal{C}$ has boundary entropy

$$\Gamma = \log \mathcal{D}^2, \quad (4.47)$$

where \mathcal{D} is the total quantum dimension of \mathcal{C} .

Examples. Recall the examples from Sect. 2.5. As discussed in Sect. 4.3.3, these label two distinct loop-gas models in (2+1)-dimensions, the toric code, and the double semion. The toric code has two possible boundary conditions, while the double semion only allows for the trivial boundary. All boundaries have $\Gamma = \log 2$.

Recall that a boundary for a Levin-Wen model defined by \mathcal{C} is specified by an algebra object $A \in \mathcal{C}$. The algebra encodes the strings that can terminate on the boundary. This interpretation leads us to the following lemma.

Lemma 4.6 (Entropy of (union of) simply connected regions, with boundary). On a region R consisting of the disjoint union of simply connected sub-regions, the entropy is

$$S_R = nS[\mathcal{C}] + \frac{b_1}{2} \log d_A - b_0 \log \mathcal{D}^2, \quad (4.48)$$

where b_0 is the number of disjoint interface components of R , b_1 is the number of points where the entanglement surface intersects the physical boundary, and n is the number of links crossing the entanglement interface.

Proof. Consider a ball R with n sites along the interface, which is in contact with the boundary. Recall that in the bulk, the fusion of the strings crossing the boundary was required to be 1. In the presence of the boundary, this conservation rule is modified, since loops can terminate. All that is

now required is that the fusion is in A

The ground state can be decomposed as

$$|\psi\rangle = \sum_{\substack{\vec{x}, \vec{y}, \vec{\mu} \\ a \in A}} \Phi_{\vec{x}, \vec{y}, \vec{\mu}, a} \left| \psi_R^{\vec{x}, \vec{y}, \vec{\mu}, a} \right\rangle \left| \psi_{R^c}^{\vec{x}, \vec{y}, \vec{\mu}, a} \right\rangle. \quad (4.50)$$

As before, the state $\left| \psi_R^{\vec{x}, \vec{y}, \vec{\mu}, a} \right\rangle$ includes any state that can be reached from Eq. (4.49) by acting only on R . The reduced state on R is

$$\rho_R = \sum_{\substack{\vec{x}, \vec{y}, \vec{\mu} \\ a \in A}} |\Phi_{\vec{x}, \vec{y}, \vec{\mu}, a}|^2 \left| \psi_R^{\vec{x}, \vec{y}, \vec{\mu}, a} \right\rangle \left\langle \psi_R^{\vec{x}, \vec{y}, \vec{\mu}, a} \right| \quad (4.51)$$

$$= \sum_{\substack{\vec{x}, \vec{y}, \vec{\mu} \\ a \in A}} \text{Pr}[\vec{x}, \vec{y}, \vec{\mu} | a] \text{Pr}[a] \left| \psi_R^{\vec{x}, \vec{y}, \vec{\mu}, a} \right\rangle \left\langle \psi_R^{\vec{x}, \vec{y}, \vec{\mu}, a} \right|, \quad (4.52)$$

where $\text{Pr}[\vec{x}, \vec{y}, \vec{\mu} | a]$ is the probability of the labeled tree, given that \vec{x} fuses to a , and $\text{Pr}[a \in A] = d_a/d_A$.

Therefore,

$$\rho_R = \sum_{\substack{\vec{x}, \vec{y}, \vec{\mu} \\ a \in A}} \frac{\prod_{j \leq n} d_{x_j}}{\mathcal{D}^{2(n-1)} d_A} \left| \psi_R^{\vec{x}, \vec{y}, \vec{\mu}, a} \right\rangle \left\langle \psi_R^{\vec{x}, \vec{y}, \vec{\mu}, a} \right|. \quad (4.53)$$

Applying Lemmas 4.2 and 4.3 completes the proof for this region. It is straightforward to check that this holds on each sub-region of R , where Lemma 4.5 is used for any bulk sub-region. \square

Applying Lemma 4.6 to the regions in Fig. 4.2b completes the proof of Thm. 4.4.

We can make sense of this halving of the entropy by considering folding the plane. Suppose we fold the model in Fig. 4.2a so that it resembles Fig. 4.2b. This turns the bulk of a model defined by \mathcal{C} to a boundary of a model labeled by $\mathcal{C} \boxtimes \mathcal{C}^{\text{op}}$. The quantum dimension of the folded theory is $\mathcal{D}_{\mathcal{C} \boxtimes \mathcal{C}^{\text{op}}} = \mathcal{D}_{\mathcal{C}}^2$, so the bulk diagnostic for \mathcal{C} matches the boundary diagnostic computed for this folded

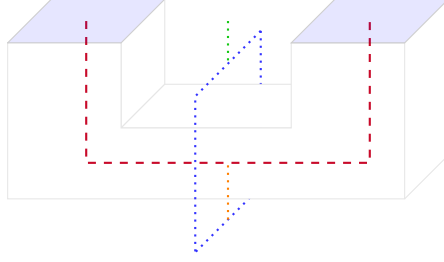


Figure 4.8: When the region R is in non-simple contact with a boundary on which strings can terminate, the computation of entropy is more subtle. There is additional entanglement in the system due to intersecting loops that cannot be created in R (red, dashed) or R^c (blue, dotted) separately. The red (internal) strings can terminate on the boundary. Also, the blue loop can emit a string which can terminate on the boundary.

theory.

4.6.2 Walker-Wang models

In (3+1)-dimensions, just like in (2+1)-dimensions, strings can terminate at the boundary. In addition, loops can interlock as discussed in Sect. 4.5.2. In the vicinity of the boundary, these two effects can occur simultaneously as depicted in Fig. 4.8.

For simply connected regions in contact with a boundary, we can apply Lemma 4.6, replacing $b_1/2$ with the number of lines where the region contacts the physical boundary. By applying the results so far, it is straightforward to check that the two diagnostics Eq. (4.13) and Eq. (4.14) are related by

$$\Delta_{\circ} = \Delta_{\bullet} + \log d_A^2 - \log \mathcal{D}^2, \quad (4.54)$$

so we only need to consider Δ_{\bullet} . We are currently unable to compute this in general, however in this section we prove the following results:

Theorem 4.5. For a Walker-Wang model defined by a unitary premodular category \mathcal{C} , the entropy diagnostic Δ_{\bullet} for a boundary labeled by an indecomposable, commutative Q-system A is given by

$$\Delta_{\bullet} = \begin{cases} \log \mathcal{D}^2 & A = 1, \\ \log \mathcal{D}^2 - \log d_A & \mathcal{C} \text{ symmetric}, \\ \log \mathcal{D}^2 - 2 \log d_A & \mathcal{C} \text{ pointed and } \mathcal{Z}_2(\mathcal{C}) \cap A = \{1\}. \text{ In particular } \mathcal{C} \text{ modular.} \\ \log \mathcal{D}^2 - \log d_A & \mathcal{C} \text{ pointed and } \mathcal{Z}_2(\mathcal{C}) \cap A = A. \end{cases} \quad (4.55)$$

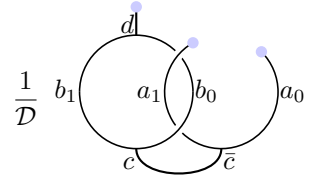
Examples. Recall the examples from Sect. 2.5. As discussed in Sect. 4.3.3, these label four distinct

loop-gas models in (3+1)-dimensions, the bosonic and fermionic toric code models, and two semion models. All four input categories are pointed, so we can apply Thm. 4.5 to obtain the boundary topological entanglement entropy.

The bosonic toric code is compatible with two distinct gapped boundary conditions, labeled by A_0 and A_1 (see Sect. 2.5), with $d_{A_0} = d_1 = 1$, and $d_{A_1} = d_1 + d_x = 2$. Since the input category is symmetric, $\mathcal{Z}_2(\mathcal{C}) \cap A_i = A_i$, so the entropy diagnostics are $\Delta_\bullet(A_0) = \log 2 - \log 1 = \log 2$ and $\Delta_\bullet(A_1) = \log 2 - \log 2 = 0$.

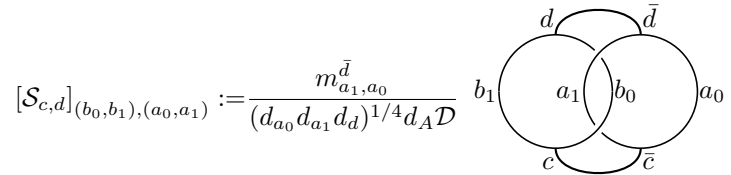
For the remaining examples, only the boundary labeled by A_0 is compatible, and $\Delta_\bullet = \log 2$ in all cases.

Proof. To capture configurations like the one in Fig. 4.8, we need new boundary \mathcal{S} -matrices resembling



$$\frac{1}{\mathcal{D}} \quad b_1 \quad a_1 \quad b_0 \quad a_0 \quad , \quad (4.56)$$

where the dots indicate where a string meets the boundary. We use boundary retriangulation invariance, as defined in Refs. [150, 151] to evaluate this diagram on the ground space. Using this, we define the new \mathcal{S} -matrix elements as



$$[\mathcal{S}_{c,d}]_{(b_0,b_1),(a_0,a_1)} := \frac{m_{a_1,a_0}^{\bar{d}}}{(d_{a_0} d_{a_1} d_d)^{1/4} d_A \mathcal{D}} \quad b_1 \quad a_1 \quad b_0 \quad a_0 \quad , \quad (4.57)$$

where $a_0, a_1, d \in A$ and $b_0, b_1, c \in \mathcal{C}$. With this, the ground state can be written

$$|\psi\rangle = \sum_{\substack{\vec{x}, \vec{y}, \vec{\mu} \\ c, b_0, b_1 \in \mathcal{C} \\ d, a_0, a_1 \in A}} \Phi_{\vec{x}, \vec{y}, \vec{\mu}, c} \frac{[\mathcal{S}_{c,d}]_{(b_0,b_1),(a_0,a_1)}}{N_A} \left| \psi_R^{\vec{x}, \vec{y}, \vec{\mu}, c, a_0, a_1} \right\rangle \left| \psi_{R^c}^{\vec{x}, \vec{y}, \vec{\mu}, c, b_0, b_1, d} \right\rangle, \quad (4.58)$$

where N_A is a normalizing factor. The reduced state on R is

$$\rho_R = \sum_{\substack{\vec{x}, \vec{y}, \vec{\mu} \\ c \in \mathcal{C} \\ d, a_0, a_1, a_2, a_3 \in A}} \frac{\prod_{j \leq n} d_{x_j} [\mathcal{S}_{c,d}^\dagger \mathcal{S}_{c,d}]_{(a_2, a_3), (a_0, a_1)}}{d_c \mathcal{D}^{2(n-1)} N_A} \left| \psi_R^{\vec{x}, \vec{y}, \vec{\mu}, c, a_0, a_1} \right\rangle \left\langle \psi_R^{\vec{x}, \vec{y}, \vec{\mu}, c, a_2, a_3} \right|. \quad (4.59)$$

$A = 1$

When the algebra is trivial, no strings can terminate. In that case, $\mathcal{S}_{1,1}^\dagger \mathcal{S}_{1,1} = 1$, so the reduced state is

$$\rho_R = \sum_{\vec{x}, \vec{y}, \vec{\mu}} \frac{\prod_{j \leq n} d_{x_j}}{\mathcal{D}^{2(n-1)}} \left| \psi_R^{\vec{x}, \vec{y}, \vec{\mu}} \right\rangle \left\langle \psi_R^{\vec{x}, \vec{y}, \vec{\mu}} \right|, \quad (4.60)$$

which is diagonal and has entropy

$$S_R = nS[C] - \log \mathcal{D}^2. \quad (4.61)$$

\mathcal{C} symmetric

When \mathcal{C} is symmetric, the rings in Eq. (4.57) separate, so

$$[\mathcal{S}_{c,d}]_{(b_0, b_1), (a_0, a_1)} = \delta_{c=d} \sqrt{d_{b_0} d_{b_1}} \frac{(d_{a_0} d_{a_1})^{1/4} m_{a_1, a_0}^{\bar{d}}}{d_d^{1/4} d_A^2 \mathcal{D}}, \quad (4.62)$$

$$\left[\mathcal{S}_{c,d}^\dagger \mathcal{S}_{c,d} \right]_{(a_2, a_3), (a_0, a_1)} = \delta_{c=d} \sum_{b_0, b_1} N_{b_0 b_1}^d \frac{d_{b_0} d_{b_1}}{\sqrt{d_d}} (d_{a_0} d_{a_1} d_{a_2} d_{a_3})^{1/4} \frac{m_{a_1, a_0}^{\bar{d}} \left(m_{a_3, a_2}^{\bar{d}} \right)^*}{d_A^4 \mathcal{D}^2} \quad (4.63)$$

$$= \delta_{c=d} (d_{a_0} d_{a_1} d_{a_2} d_{a_3})^{1/4} \sqrt{d_d} \frac{m_{a_1, a_0}^{\bar{d}} \left(m_{a_3, a_2}^{\bar{d}} \right)^*}{d_A^2}. \quad (4.64)$$

It can readily be verified that this matrix is rank 1. The eigenvalue can be found using Eq. (4.5), giving $\lambda = d_d/d_A$. We can therefore write the state on R as

$$\rho_R = \sum_{\substack{\vec{x}, \vec{y}, \vec{\mu} \\ c \in \mathcal{C} \\ d \in A}} \delta_{c=d} \frac{\prod_{j \leq n} d_{x_j}}{\mathcal{D}^{2(n-1)} d_A} \left| \psi_R^{\vec{x}, \vec{y}, \vec{\mu}, c} \right\rangle \left\langle \psi_R^{\vec{x}, \vec{y}, \vec{\mu}, c} \right| \quad (4.65)$$

$$= \sum_{\substack{\vec{x}, \vec{y}, \vec{\mu} \\ c \in A}} \frac{\prod_{j \leq n} d_{x_j}}{\mathcal{D}^{2(n-1)} d_A} \left| \psi_R^{\vec{x}, \vec{y}, \vec{\mu}, c} \right\rangle \left\langle \psi_R^{\vec{x}, \vec{y}, \vec{\mu}, c} \right|. \quad (4.66)$$

Using Lemmas 4.2 and 4.3, we find that the entropy of this state is

$$\mathcal{S}_R = nS[\mathcal{C}] - \log \mathcal{D}^2 + \log d_A. \quad (4.67)$$

\mathcal{C} pointed

When all quantum dimensions are equal to 1, the boundary \mathcal{S} -matrix is

$$[\mathcal{S}_{c,d}]_{(b_0,b_1),(a_0,a_1)} = \delta_{c=d} \frac{m_{a_1,a_0}^{\bar{d}}}{d_A} [\mathcal{S}_1]_{b_0,\bar{a}_1}, \quad (4.68)$$

where $[\mathcal{S}_1]_{b_0,a_1}$ is the \mathcal{S} -matrix from Eq. (4.2). This gives

$$\left[\mathcal{S}_{c,d}^\dagger \mathcal{S}_{c,d} \right]_{(a_2,a_3),(a_0,a_1)} = \delta_{c=d} \frac{m_{a_1,a_0}^{\bar{d}} (m_{a_3,a_2}^{\bar{d}})^*}{d_A^2} \sum_{b_0} [\mathcal{S}_1]_{b_0,\bar{a}_3}^* [\mathcal{S}_1]_{b_0,\bar{a}_1}. \quad (4.69)$$

Using Lemmas 2.4 and 2.13 of Ref. [174], this can be simplified to

$$\left[\mathcal{S}_{c,d}^\dagger \mathcal{S}_{c,d} \right]_{(a_2,a_3),(a_0,a_1)} = \delta_{c=d} \frac{m_{a_1,a_0}^{\bar{d}} (m_{a_3,a_2}^{\bar{d}})^*}{d_A^2} \delta_{a_3 \otimes \bar{a}_1 \in \mathcal{Z}_2(\mathcal{C})}. \quad (4.70)$$

Pointed braided categories have fusion rules given by an Abelian group G [169, 192], and algebras are twisted group algebras [193, 194] of subgroups of G . Moreover, $\mathcal{Z}_2(\mathcal{C})$ also has fusion rules given by a subgroup.

Since $a_3 \otimes \bar{a}_1 \in A$ and $a_3 \otimes \bar{a}_1 \in \mathcal{Z}_2(\mathcal{C})$, there must be some $h \in \mathcal{Z}_2(\mathcal{C}) \cap A$ so that $a_3 = a_1 h$. We can then write

$$\rho_R = \sum_{\substack{\vec{x} \\ d,a \in A \\ h \in \mathcal{Z}_2(\mathcal{C}) \cap A}} \frac{m_{a,(ad)^{-1}}^{d^{-1}} (m_{ah,(ahd)^{-1}}^{d^{-1}})^*}{d_A^2 \mathcal{D}^{2(n-1)} N_A} \left| \psi_R^{\vec{x},d,a} \right\rangle \left\langle \psi_R^{\vec{x},d,ah} \right|. \quad (4.71)$$

In the case that $\mathcal{Z}_2(\mathcal{C}) \cap A = A$, this reduces to the symmetric case, since summing over $h \in A$ is the same as summing over $A \ni h' = ah$.

When $\mathcal{Z}_2(\mathcal{C}) \cap A = \{1\}$, the unit, the reduced state on R simplifies to

$$\rho_R = \sum_{\substack{\vec{x} \\ d,a \in A}} \frac{m_{a,(ad)^{-1}}^{d^{-1}} (m_{a,(ad)^{-1}}^{d^{-1}})^*}{d_A^2 \mathcal{D}^{2(n-1)} N_A} \left| \psi_R^{\vec{x},d,a} \right\rangle \left\langle \psi_R^{\vec{x},d,a} \right|. \quad (4.72)$$

This reduced state is diagonal, and has entropy

$$S_R = - \sum_{\substack{\vec{x} \\ d, a \in A}} \frac{|m_{a, (ad)^{-1}}^{d^{-1}}|^2}{\mathcal{D}^{2(n-1)} d_A^2} \log \left(\frac{|m_{a, (ad)^{-1}}^{d^{-1}}|^2}{\mathcal{D}^{2(n-1)} d_A^2} \right) \quad (4.73)$$

$$= - \sum_{\substack{\vec{x} \\ d, a \in A}} \frac{|m_{a, (ad)^{-1}}^{d^{-1}}|^2}{\mathcal{D}^{2(n-1)} d_A^2} \log \left(|m_{a, (ad)^{-1}}^{d^{-1}}|^2 \right) + \log \left(\mathcal{D}^{2(n-1)} d_A^2 \right), \quad (4.74)$$

where we have made use of Eq. (4.5). Since A is a twisted group algebra, we may assume $|m_{ab}^c| \in \{0, 1\}$.

Finally, this gives

$$S_R = \log \left(\mathcal{D}^{2(n-1)} d_A^2 \right) \quad (4.75)$$

$$= S[\mathcal{C}] - \log \mathcal{D}^2 + 2 \log d_A, \quad (4.76)$$

completing the proof. \square

4.7 Remarks

To summarize, we have evaluated the long-range entanglement in the bulk, and at the boundary, of (2+1)- and (3+1)-dimensional topological phases. In (2+1)-dimensions, we found the entropy diagnostic $\Gamma = \log \mathcal{D}^2$ regardless of the choice of boundary algebra A . This is in contrast to the results for (3+1)-dimensions, where a signature of the boundary, namely its dimension as an algebra, can be seen in the diagnostics Δ_\bullet and Δ_\circ .

The most natural boundary for these models is defined by the algebra $A = 1$, which (uniquely) always exists. At this boundary, we found that the point-like diagnostic Δ_\bullet recovers the total dimension of the input category. In particular, when \mathcal{C} is a (2+1)-dimensional anyon model, this is consistent with a boundary that supports the anyons. Conversely, the loop-like diagnostic Δ_\circ is zero at these boundaries, ruling out loop-like excitations in the vicinity.

We have conjectured a general property of the connected \mathcal{S} -matrix which, if proven in general, allows computation of bulk Walker-Wang topological entropy. Such a proof may also be interesting for the classification of premodular categories in general. To the best of our knowledge, there is no complete classification of boundaries for Walker-Wang models. Such a classification is complicated by requiring, as a sub-classification, a complete understanding of (2+1)-dimensional theories. This goes beyond the scope of the current work, and we have therefore specialized to boundaries described by

Q-systems and to particular families of input fusion category. Extending these results may provide a more complete understanding of the possible boundary excitations and their properties.

Appendix

4.A Properties of the connected \mathcal{S} -matrix

Proposition 4.A.1 (Premodular trap). Let \mathcal{C} be a unitary premodular category, then

$$\frac{1}{\mathcal{D}^2} \sum_a d_a \bigcup_{x \ y} a = \sum_{z \in \mathcal{Z}_2(\mathcal{C}), \mu} \sqrt{\frac{d_z}{d_x d_y}} \bigcup_{x \ y}^{\mu z \mu} x \ y. \quad (4.77)$$

Proof. This is a slight generalization of Prop. 3.1 of Ref. [195], following from Lemmas 2.4 and 2.13 of Ref. [174]. \square

Lemma (4.1). Let \mathcal{C} be a unitary premodular category, then

$$\sum_{c \in \mathcal{C}} \text{Tr } \mathcal{S}_c^\dagger \mathcal{S}_c = \mathcal{D}^2, \quad (4.78)$$

where \mathcal{S}_c is the connected \mathcal{S} -matrix and \mathcal{D} is the total dimension of \mathcal{C} .

Proof. The operator \mathcal{S}_c acts on the fusion spaces as [12]

$$\mathcal{S}_c \begin{array}{c} b \quad \bar{b} \\ \diagdown \quad \diagup \\ \beta \\ | \\ c \end{array} = \frac{\sqrt{d_c}}{\mathcal{D}} \sum_x d_x \begin{array}{c} \bar{x} \quad x \\ | \quad \diagup \\ \bigcirc \\ \diagdown \quad | \\ \beta \\ | \\ c \end{array}. \quad (4.79)$$

Using Eq. (4.79), we have

$$\sum_c \text{Tr } \mathcal{S}_c^\dagger \mathcal{S}_c = \sum_{a, \alpha, c} [\mathcal{S}_c^\dagger \mathcal{S}_c]_{(a, \alpha), (a, \alpha)} \quad (4.80)$$

$$= \sum_{a, \alpha, c} \frac{\sqrt{d_c}}{\mathcal{D}^2} \sum_x d_x \quad \text{Diagram (4.81)} \quad (4.81)$$

$$= \sum_{a, \alpha, c} \frac{\sqrt{d_c}}{\mathcal{D}^2} \sum_x d_x \quad \text{Diagram (4.82)} \quad (4.82)$$

using the properties of the trace. Applying the premodular trap (Proposition 4.A.1), this gives

$$\sum_c \text{Tr } \mathcal{S}_c^\dagger \mathcal{S}_c = \sum_{\substack{a, \alpha, c, \\ z \in \mathcal{Z}_2(\mathcal{C}), \mu}} \sqrt{\frac{d_c d_z}{d_a^2}} \quad \text{Diagram (4.83)} \quad (4.83)$$

$$= \sum_{a, z \in \mathcal{Z}_2(\mathcal{C}), \mu} \sqrt{d_z} \quad \text{Diagram (4.84)} \quad (4.84)$$

$$= \sum_{a, z \in \mathcal{Z}_2(\mathcal{C}), \mu} |\varkappa_a|^2 \delta_{z=1} d_a^2 \quad (4.85)$$

$$= \mathcal{D}^2, \quad (4.86)$$

where \varkappa_a is the Frobenius-Schur indicator [12]. □

4.B Loop-gas results

In this section, given a fusion category \mathcal{C} , an n -tuple of simple objects $\vec{x}_n := (x_1, x_2, \dots, x_n)$, and a fixed simple object a , we use the notation

$$N_a(\vec{x}_n) := \sum_{\vec{y}_{n-2}} N_{x_1, x_2}^{y_1} N_{y_1, x_3}^{y_2} \dots N_{y_{n-2}, x_n}^a, \quad (4.87)$$

where $\vec{y}_{n-2} := (y_1, y_2, \dots, y_{n-2})$, and the sum is over all tuples of simple objects in \mathcal{C} . $N_a(\vec{x}_n)$ counts the number of ways \vec{x}_n can fuse to a . When it can easily be inferred, we omit the subscript on the tuple \vec{x} .

Lemma (4.2). Let \mathcal{C} be a unitary fusion category, then

$$\sum_{\vec{x}_n} N_a(\vec{x}_n) \prod_{j \leq n} d_{x_j} = d_a \mathcal{D}^{2(n-1)}, \quad (4.88)$$

where $\mathcal{D} = \sqrt{\sum_a d_a^2}$ is the total quantum dimension of \mathcal{C} .

Proof. We proceed inductively.

When $n = 1$, $N_a(x) = \delta_{x=a} = N_{1,x}^a$, and Eq. (4.88) reduces to $d_a = d_a$.

Assume Eq. (4.88) holds for the fusion of n objects. Recall that in any fusion category, we have

$$d_a d_b = \sum_c N_{bc}^a d_c, \quad (4.89)$$

and this holds for any cyclic permutation of the indices on N_{bc}^a . We now obtain

$$\sum_{\vec{x}_{n+1}} N_a(\vec{x}_{n+1}) \prod_{j \leq n+1} d_{x_j} = \sum_{\vec{x}_n, y_{n-1}} N_{y_{n-1}}(\vec{x}_n) \prod_{j \leq n} d_{x_j} \sum_{x_{n+1}} N_{y_{n-1}, x_{n+1}}^a d_{x_{n+1}} \quad (4.90)$$

$$= \mathcal{D}^{2(n-1)} \sum_{x_{n+1}, y_{n-1}} N_{y_{n-1}, x_{n+1}}^a d_{y_{n-1}} d_{x_{n+1}} \quad (4.91)$$

$$= \mathcal{D}^{2(n-1)} d_a \sum_{y_{n-1}} d_{y_{n-1}}^2 \quad (4.92)$$

$$= d_a \mathcal{D}^{2n}, \quad (4.93)$$

where in the second line we used the induction assumption (Eq. (4.88)), and in the third line we used Eq. (4.89). \square

Lemma (4.3). Let \mathcal{C} a unitary fusion category. For the fusion of n objects $\vec{x} = (x_1, x_2, \dots, x_n)$, with $n > 1$, we have

$$\sum_{\vec{x}_n} N_a(\vec{x}_n) \frac{\prod_{j \leq n} d_{x_j}}{\mathcal{D}^{2(n-1)}} \log \prod_{k \leq n} d_{x_k} = n d_a \sum_x \frac{d_x^2 \log d_x}{\mathcal{D}^2}. \quad (4.94)$$

Proof. We prove the claim inductively. The base case is when $n = 2$.

$$\sum_{x_1, x_2} N_{x_1, x_2}^a \frac{d_{x_1} d_{x_2}}{\mathcal{D}^2} (\log d_{x_1} + \log d_{x_2}) = \sum_{x_1, x_2} N_{x_1, x_2}^a \frac{d_{x_1} d_{x_2}}{\mathcal{D}^2} \log d_{x_1} + \sum_{x_1, x_2} N_{x_1, x_2}^a \frac{d_{x_1} d_{x_2}}{\mathcal{D}^2} \log d_{x_2} \quad (4.95)$$

$$= d_a \sum_{x_1} \frac{d_{x_1}^2}{\mathcal{D}^2} \log d_{x_1} + d_a \sum_{x_2} \frac{d_{x_2}^2}{\mathcal{D}^2} \log d_{x_2} \quad (4.96)$$

$$= 2 d_a \sum_x \frac{d_x^2 \log d_x}{\mathcal{D}^2}. \quad (4.97)$$

Assume Eq. (4.94) holds for n -tuples, then

$$\sum_{\vec{x}_n, x_{n+1}} N_a(\vec{x}_{n+1}) \frac{\prod_{j \leq n+1} d_{x_j}}{\mathcal{D}^{2n}} \log \prod_{k \leq n+1} d_{x_k} = \sum_{\substack{\vec{x}_n \\ y_{n-1}, x_{n+1}}} N_{y_{n-1}}(\vec{x}_n) N_{y_{n-1}, x_{n+1}}^a \frac{\prod_{j \leq n} d_{x_j}}{\mathcal{D}^{2n}} d_{x_{n+1}} \log \left(\prod_{k \leq n} d_{x_k} d_{x_{n+1}} \right) \quad (4.98)$$

$$= \sum_{\substack{\vec{x}_n \\ y_{n-1}, x_{n+1}}} N_{y_{n-1}}(\vec{x}_n) \frac{\prod_{j \leq n} d_{x_j}}{\mathcal{D}^{2n}} N_{y_{n-1}, x_{n+1}}^a d_{x_{n+1}} \left(\log \prod_{k \leq n} d_{x_k} + \log d_{x_{n+1}} \right) \quad (4.99)$$

$$= n \sum_x \frac{d_x^2 \log d_x}{\mathcal{D}^2} \sum_{y_{n-1}, x_{n+1}} \frac{N_{y_{n-1}, x_{n+1}}^a d_{y_{n-1}} d_{x_{n+1}}}{\mathcal{D}^2} + \sum_{y_{n-1}, x_{n+1}} N_{y_{n-1}, x_{n+1}}^a \frac{d_{y_{n-1}} d_{x_{n+1}} \log d_{x_{n+1}}}{\mathcal{D}^2} \quad (4.100)$$

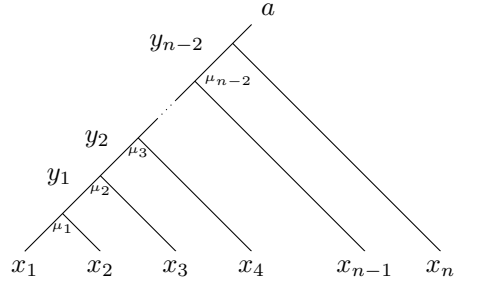
$$= n d_a \sum_x \frac{d_x^2 \log d_x}{\mathcal{D}^2} \sum_{x_{n+1}} \frac{d_{x_{n+1}}^2}{\mathcal{D}^2} + d_a \sum_{x_{n+1}} \frac{d_{x_{n+1}}^2 \log d_{x_{n+1}}}{\mathcal{D}^2} \quad (4.101)$$

$$= (n+1) d_a \sum_x \frac{d_x^2 \log d_x}{\mathcal{D}^2}. \quad (4.102)$$

□

Lemma (4.B). Let \mathcal{C} a unitary fusion category. Given a fixed fusion outcome a on n simple objects,

the probability of the tree


(4.103)

in the ground state of a topological loop-gas (Levin-Wen or Walker-Wang) model is

$$\Pr[\vec{x}, \vec{y}, \vec{\mu}|a] = \frac{\prod_{j \leq n} \Pr[x_j]}{\Pr[a] \prod_{k \leq n} d_{x_k}} d_a \quad (4.104)$$

$$= \frac{\prod_{j \leq n} d_{x_j}}{d_a \mathcal{D}^{2(n-1)}}. \quad (4.105)$$

Proof. Given a pair of objects a, b , the probability that they fuse to c is given by [166, 196]

$$\Pr[a \otimes b \rightarrow c] = \frac{N_{ab}^c d_c}{d_a d_b}, \quad (4.106)$$

so the probability that $x_1 \otimes x_2 \otimes \dots \otimes x_n \rightarrow a$ is

$$\Pr[x_1 \otimes x_2 \otimes x_3 \otimes \dots \otimes x_n \rightarrow a] = \sum_{\vec{y}} \Pr[x_1 \otimes x_2 \rightarrow y_1] \Pr[y_1 \otimes x_3 \rightarrow y_2] \dots \Pr[y_{n-2} \otimes x_n \rightarrow a] \quad (4.107)$$

$$= \frac{N_a(\vec{x})}{\prod_{j \leq n} d_{x_j}} d_a, \quad (4.108)$$

where

$$N_a(\vec{x}) := \sum_{\vec{y}} N_{x_1 x_2}^{y_1} N_{y_1 x_3}^{y_2} \dots N_{y_{n-2} x_n}^a \quad (4.109)$$

$$= \sum_{\vec{y}} N_a(\vec{x}, \vec{y}). \quad (4.110)$$

The probability of a configuration is

$$\Pr[\vec{x}, \vec{y}|a] = \Pr[x_1 \otimes x_2 \otimes x_3 \otimes \dots \otimes x_n \rightarrow a] \frac{\prod_{j \leq n} \Pr[x_j]}{\Pr[a]} \quad (4.111)$$

$$= \frac{N_a(\vec{x}, \vec{y}) d_a}{\prod_{k \leq n} d_{x_k}} \frac{\prod_{j \leq n} \Pr[x_j]}{\Pr[a]}, \quad (4.112)$$

where $\Pr[x_i] = d_{x_i}^2 / \mathcal{D}^2$. For a fixed \vec{x} and \vec{y} , all (allowed) $\vec{\mu}$ are equally likely, and there are $N_a(\vec{x}, \vec{y})$ such configurations, so

$$\Pr[\vec{x}, \vec{y}, \vec{\mu}|a] = \frac{\prod_{j \leq n} \Pr[x_j]}{\Pr[a] \prod_{k \leq n} d_{x_k}} d_a \quad (4.113)$$

$$= \frac{\prod_{j \leq n} d_{x_j}}{d_a \mathcal{D}^{2(n-1)}}. \quad (4.114)$$

Lemma 4.2 can be used to show these are properly normalized. \square

Theorem (4.3). For a Walker-Wang model defined by a unitary premodular category of one of the following types:

1. $\mathcal{C} = \mathcal{A} \boxtimes \mathcal{B}$, where \mathcal{A} is symmetric and \mathcal{B} is modular [166],
2. \mathcal{C} pointed,
3. $\text{rk}(\mathcal{C}) < 6$ and multiplicity free,
4. $\text{rk}(\mathcal{C}) = \text{rk}(\mathcal{Z}_2(\mathcal{C})) + 1$ and $d_x = \mathcal{D}_{\mathcal{Z}_2(\mathcal{C})}$, where x is the additional object,

then Eq. (4.43) holds. As a consequence, the topological entanglement entropy (defined using the regions in Fig. 4.3) in the bulk is given by

$$\delta = \log \mathcal{D}_{\mathcal{Z}_2(\mathcal{C})}^2. \quad (4.115)$$

As special cases, this includes

$$\delta_{\text{modular}} = 0 \quad (4.116)$$

$$\delta_{\text{symmetric}} = \log \mathcal{D}^2 \quad (4.117)$$

Proof.

4.B.1 Case 1

Using the premodular trap (Proposition 4.A.1), we have the matrix elements of $\mathcal{S}_c^\dagger \mathcal{S}_c$

$$[\mathcal{S}_c^\dagger \mathcal{S}_c]_{(a,\alpha),(b,\beta)} = \sqrt{\frac{d_c}{d_a d_b}} \sum_{x \in \mathcal{Z}_2(\mathcal{C}), \mu} \sqrt{d_x} \cdot \text{diagram} \quad (4.118)$$

If \mathcal{C} is symmetric, $\mathcal{Z}_2(\mathcal{C}) = \mathcal{C}$, and

$$[\mathcal{S}_c^\dagger \mathcal{S}_c]_{(a,\alpha),(b,\beta)} = \delta_{c=1} d_a d_b. \quad (4.119)$$

This matrix is rank 1, with eigenvalue \mathcal{D}^2 . If \mathcal{C} is modular, $\mathcal{Z}_2(\mathcal{C}) = \mathbf{Vec}$, and

$$[\mathcal{S}_c^\dagger \mathcal{S}_c]_{(a,\alpha),(b,\beta)} = \delta_{a=b} \delta_{\alpha=\beta} \delta_{\bar{a} \otimes a = c} d_c. \quad (4.120)$$

For fixed c , this matrix is rank $\sum_c N_{\bar{a},a}^c$, with all eigenvalues equal to d_c .

4.B.2 Case 2

If \mathcal{C} is pointed (every simple object has dimension 1), then $\mathcal{S}_c = 0$ unless $c = 1$. In this case, the fusion rules are given by a finite Abelian group A [169, 192], and $\mathcal{Z}_2(\mathcal{C}) = A'$ has fusion rules given by a subgroup. From Lemmas 2.4 and 2.13 of Ref. [174], along with symmetries of the \mathcal{S}_1 matrix proven in Ref. [12] we know that

$$[\mathcal{S}_1^\dagger \mathcal{S}_1]_{ab} = \sum_{c \in \mathcal{Z}_2(\mathcal{C})} N_{ab}^c d_c, \quad (4.121)$$

so

$$[\mathcal{S}_1^\dagger \mathcal{S}_1]_{ab} = 1 \iff a \in bA'. \quad (4.122)$$

Therefore, $[\mathcal{S}_1^\dagger \mathcal{S}_1]$ is a block matrix, with $[A : A'] = |A|/|A'|$ blocks, labeled by the cosets of A' , each full of ones. Therefore, there are $[A : A']$ eigenvalues, identically $\mathcal{D}_{\mathcal{Z}_2(\mathcal{C})}^2$. The entropy is given by

$$\delta = \log \mathcal{D}_{\mathcal{Z}_2(\mathcal{C})}^2. \quad (4.123)$$

4.B.3 Case 3

Case 3 is proven explicitly in the Mathematica file provided with the chapter Ref. [197]. Classification of the fusion rings for ranks 2-5 can be found in Ref. [195, 198–201], along with Ref. [202]. Additionally, all multiplicity free fusion rings for ranks 1-6 can be found at Ref. [203]. From this, explicit F and R data can be found. The list of categories, along with their properties, is included beginning on Page 165.

4.B.4 Case 4

It is straightforward to check that if a or b are in $\mathcal{Z}_2(\mathcal{C})$, then

$$[\mathcal{S}_c^\dagger \mathcal{S}_c]_{(a,\alpha),(b,\beta)} = \delta_{c=1} d_a d_b \delta_{a \in \mathcal{Z}_2(\mathcal{C})} \delta_{b \in \mathcal{Z}_2(\mathcal{C})}, \quad (4.124)$$

so $\mathcal{S}_c^\dagger \mathcal{S}_c$ has the form

$$[\mathcal{S}_c^\dagger \mathcal{S}_c] = \begin{matrix} & \mathcal{Z}_2(\mathcal{C}) \\ \mathcal{Z}_2(\mathcal{C}) & \begin{bmatrix} d_a d_b \delta_{c=1} & 0 \\ 0 & X_c \end{bmatrix} \end{matrix} = U \begin{matrix} & \mathcal{Z}_2(\mathcal{C}) \\ \mathcal{Z}_2(\mathcal{C}) & \begin{bmatrix} \mathcal{D}_{\mathcal{Z}_2(\mathcal{C})}^2 \delta_{c=1} & 0 & \cdots \\ 0 & 0 & \cdots & 0 \\ \vdots & \vdots & \ddots & \\ 0 & & & \tilde{X}_c \end{bmatrix} \end{matrix} U^\dagger. \quad (4.125)$$

From the top left block, we have an eigenvector of $\mathcal{S}_1^\dagger \mathcal{S}_1$ with entries $v_a = \delta_{a \in \mathcal{Z}_2(\mathcal{C})} d_a$ with eigenvalue $\mathcal{D}_{\mathcal{Z}_2(\mathcal{C})}^2$. From Lemmas 2.4 and 2.13 of Ref. [174], along with symmetries of the \mathcal{S}_1 matrix proven in Ref. [12] we know that

$$[\mathcal{S}_1^\dagger \mathcal{S}_1]_{ab} = \sum_{c \in \mathcal{Z}_2(\mathcal{C})} N_{ab}^c d_c. \quad (4.126)$$

The vector with entries $w_a = d_a$ is also an eigenvector with the same eigenvalue:

$$\sum_{b \in \mathcal{C}} \sum_{c \in \mathcal{Z}_2(\mathcal{C})} N_{ab}^c d_c d_b = \sum_{c \in \mathcal{Z}_2(\mathcal{C})} d_a d_c^2 \quad (4.127)$$

$$= \mathcal{D}_{\mathcal{Z}_2(\mathcal{C})}^2 d_a, \quad (4.128)$$

so we have an orthogonal vector $w - v$ with eigenvalue $\mathcal{D}_{\mathcal{Z}_2(\mathcal{C})}^2$.

If $\text{rk}(\mathcal{C}) = \text{rk}(\mathcal{Z}_2(\mathcal{C})) + 1$ and the additional object has $d_x = \mathcal{D}_{\mathcal{Z}_2(\mathcal{C})}$, then all other eigenvalues must be 0 since $\text{Tr } S_1^\dagger S_1 = 2\mathcal{D}_{\mathcal{Z}_2(\mathcal{C})}^2$ and $\mathcal{D}^2 = \mathcal{D}_{\mathcal{Z}_2(\mathcal{C})}^2 + d_x^2$. The entropy of the Walker-Wang model in the bulk is

$$\delta = \log \mathcal{D}_{\mathcal{Z}_2(\mathcal{C})}^2. \quad (4.129)$$

□

4.B.5 Small category data

Data for small categories. “Valid” indicates that the pentagon, hexagon, and ribbon equations, along with unitarity, are true. “TY” indicates that the category has the property defined in Case 4 of Thm. 4.3.

Full data, including explicit F and R symbols is provided in the attached Mathematica files, also available at Ref. [197]. Note that these may take *a very long time* to check. This is due to the complicated algebraic integers occurring, and Mathematica needing to simplify using the functions “Simplify” and “RootReduce”.

Categories are named $\text{FR}_{c;x}^{a,b}$ according to their fusion ring $\text{FR}_c^{a,b}$ from Ref. [203], along with their categorification ID x . Highlighted categories do not fall within any of the other cases in Thm. 4.3.

Cat. ID	Rank	\mathcal{D}^2	Valid	$\text{rk}(\mathcal{Z}_2(\mathcal{C}))$	Premodular?	Pointed?	TY?	TEE	$\log \mathcal{D}_{\mathcal{Z}_2(\mathcal{C})}^2$	Conjecture true?
FR _{1;0} ^{2,0}	2	2	✓	2	Symm.	✓		log 2	log 2	✓
FR _{1;1} ^{2,0}	2	2	✓	1	Mod.	✓	✓	0	0	✓
FR _{1;2} ^{2,0}	2	2	✓	2	Symm.	✓		log 2	log 2	✓
FR _{1;3} ^{2,0}	2	2	✓	1	Mod.	✓	✓	0	0	✓
FR _{2;0} ^{2,0}	2	$\frac{1}{2}(\sqrt{5}+5)$	✓	1	Mod.			0	0	✓
FR _{2;1} ^{2,0}	2	$\frac{1}{2}(\sqrt{5}+5)$	✓	1	Mod.			0	0	✓
FR _{1;0} ^{3,0}	3	4	✓	1	Mod.			0	0	✓
FR _{1;1} ^{3,0}	3	4	✓	1	Mod.			0	0	✓
FR _{1;2} ^{3,0}	3	4	✓	1	Mod.			0	0	✓
FR _{1;3} ^{3,0}	3	4	✓	1	Mod.			0	0	✓
FR _{1;4} ^{3,0}	3	4	✓	1	Mod.			0	0	✓
FR _{1;5} ^{3,0}	3	4	✓	1	Mod.			0	0	✓
FR _{1;6} ^{3,0}	3	4	✓	1	Mod.			0	0	✓
FR _{1;7} ^{3,0}	3	4	✓	1	Mod.			0	0	✓
FR _{2;0} ^{3,0}	3	6	✓	3	Symm.			log 6	log 6	✓
FR _{2;1} ^{3,0}	3	6	✓	2	✓			log 2	log 2	✓
FR _{2;2} ^{3,0}	3	6	✓	2	✓			log 2	log 2	✓
FR _{3;0} ^{3,0}	3	~ 9.30	✓	1	Mod.			0	0	✓
FR _{3;1} ^{3,0}	3	~ 9.30	✓	1	Mod.			0	0	✓
FR _{1;0} ^{3,2}	3	3	✓	3	Symm.	✓		log 3	log 3	✓
FR _{1;1} ^{3,2}	3	3	✓	1	Mod.	✓		0	0	✓
FR _{1;2} ^{3,2}	3	3	✓	1	Mod.	✓		0	0	✓

Cat. ID	Rank	\mathcal{D}^2	Valid	$\text{rk}(\mathcal{Z}_2(\mathcal{C}))$	Premodular?	Pointed?	TY?	TEE	$\log \mathcal{D}_{\mathcal{Z}_2(\mathcal{C})}^2$	Conjecture true?
FR _{1:0} ^{4,0}	4	4	✓	4	Symm.	✓		log 4	log 4	✓
FR _{1:1} ^{4,0}	4	4	✓	1	Mod.	✓		0	0	✓
FR _{1:2} ^{4,0}	4	4	✓	4	Symm.	✓		log 4	log 4	✓
FR _{1:3} ^{4,0}	4	4	✓	1	Mod.	✓		0	0	✓
FR _{1:4} ^{4,0}	4	4	✓	2	✓	✓		log 2	log 2	✓
FR _{1:5} ^{4,0}	4	4	✓	2	✓	✓		log 2	log 2	✓
FR _{1:6} ^{4,0}	4	4	✓	2	✓	✓		log 2	log 2	✓
FR _{1:7} ^{4,0}	4	4	✓	2	✓	✓		log 2	log 2	✓
FR _{1:8} ^{4,0}	4	4	✓	4	Symm.	✓		log 4	log 4	✓
FR _{1:9} ^{4,0}	4	4	✓	1	Mod.	✓		0	0	✓
FR _{1:10} ^{4,0}	4	4	✓	4	Symm.	✓		log 4	log 4	✓
FR _{1:11} ^{4,0}	4	4	✓	1	Mod.	✓		0	0	✓
FR _{1:12} ^{4,0}	4	4	✓	2	✓	✓		log 2	log 2	✓
FR _{1:13} ^{4,0}	4	4	✓	2	✓	✓		log 2	log 2	✓
FR _{1:14} ^{4,0}	4	4	✓	2	✓	✓		log 2	log 2	✓
FR _{1:15} ^{4,0}	4	4	✓	2	✓	✓		log 2	log 2	✓
FR _{1:16} ^{4,0}	4	4	✓	1	Mod.	✓		0	0	✓
FR _{1:17} ^{4,0}	4	4	✓	2	✓	✓		log 2	log 2	✓
FR _{1:18} ^{4,0}	4	4	✓	1	Mod.	✓		0	0	✓
FR _{1:19} ^{4,0}	4	4	✓	2	✓	✓		log 2	log 2	✓
FR _{1:20} ^{4,0}	4	4	✓	1	Mod.	✓		0	0	✓
FR _{1:21} ^{4,0}	4	4	✓	1	Mod.	✓		0	0	✓
FR _{1:22} ^{4,0}	4	4	✓	1	Mod.	✓		0	0	✓
FR _{1:23} ^{4,0}	4	4	✓	1	Mod.	✓		0	0	✓
FR _{1:24} ^{4,0}	4	4	✓	1	Mod.	✓		0	0	✓
FR _{1:25} ^{4,0}	4	4	✓	2	✓	✓		log 2	log 2	✓
FR _{1:26} ^{4,0}	4	4	✓	1	Mod.	✓		0	0	✓
FR _{1:27} ^{4,0}	4	4	✓	2	✓	✓		log 2	log 2	✓
FR _{1:28} ^{4,0}	4	4	✓	1	Mod.	✓		0	0	✓
FR _{1:29} ^{4,0}	4	4	✓	1	Mod.	✓		0	0	✓
FR _{1:30} ^{4,0}	4	4	✓	1	Mod.	✓		0	0	✓
FR _{1:31} ^{4,0}	4	4	✓	1	Mod.	✓		0	0	✓
FR _{2:0} ^{4,0}	4	$\sqrt{5} + 5$	✓	2	✓			log 2	log 2	✓
FR _{2:1} ^{4,0}	4	$\sqrt{5} + 5$	✓	1	Mod.			0	0	✓
FR _{2:2} ^{4,0}	4	$\sqrt{5} + 5$	✓	2	✓			log 2	log 2	✓
FR _{2:3} ^{4,0}	4	$\sqrt{5} + 5$	✓	1	Mod.			0	0	✓
FR _{2:4} ^{4,0}	4	$\sqrt{5} + 5$	✓	2	✓			log 2	log 2	✓
FR _{2:5} ^{4,0}	4	$\sqrt{5} + 5$	✓	1	Mod.			0	0	✓
FR _{2:6} ^{4,0}	4	$\sqrt{5} + 5$	✓	2	✓			log 2	log 2	✓
FR _{2:7} ^{4,0}	4	$\sqrt{5} + 5$	✓	1	Mod.			0	0	✓
FR _{3:0} ^{4,0}	4	10	✓	4	Symm.			log 10	log 10	✓
FR _{3:1} ^{4,0}	4	10	✓	2	✓			log 2	log 2	✓
FR _{3:2} ^{4,0}	4	10	✓	2	✓			log 2	log 2	✓
FR _{3:3} ^{4,0}	4	10	✓	2	✓			log 2	log 2	✓
FR _{3:4} ^{4,0}	4	10	✓	2	✓			log 2	log 2	✓
FR _{4:0} ^{4,0}	4	$4\sqrt{2} + 8$	✓	2	✓			log 2	log 2	✓
FR _{4:1} ^{4,0}	4	$4\sqrt{2} + 8$	✓	2	✓			log 2	log 2	✓
FR _{5:0} ^{4,0}	4	$\frac{1}{2}(5\sqrt{5} + 15)$	✓	1	Mod.			0	0	✓
FR _{5:1} ^{4,0}	4	$\frac{1}{2}(5\sqrt{5} + 15)$	✓	1	Mod.			0	0	✓
FR _{5:2} ^{4,0}	4	$\frac{1}{2}(5\sqrt{5} + 15)$	✓	1	Mod.			0	0	✓
FR _{5:3} ^{4,0}	4	$\frac{1}{2}(5\sqrt{5} + 15)$	✓	1	Mod.			0	0	✓
FR _{6:0} ^{4,0}	4	~ 19.24	✓	1	Mod.			0	0	✓
FR _{6:1} ^{4,0}	4	~ 19.24	✓	1	Mod.			0	0	✓
FR _{1:0} ^{4,2}	4	4	✓	4	Symm.	✓		log 4	log 4	✓
FR _{1:1} ^{4,2}	4	4	✓	1	Mod.	✓		0	0	✓
FR _{1:2} ^{4,2}	4	4	✓	2	✓	✓		log 2	log 2	✓
FR _{1:3} ^{4,2}	4	4	✓	1	Mod.	✓		0	0	✓
FR _{1:4} ^{4,2}	4	4	✓	4	Symm.	✓		log 4	log 4	✓
FR _{1:5} ^{4,2}	4	4	✓	1	Mod.	✓		0	0	✓
FR _{1:6} ^{4,2}	4	4	✓	2	✓	✓		log 2	log 2	✓
FR _{1:7} ^{4,2}	4	4	✓	1	Mod.	✓		0	0	✓

Cat. ID	Rank	\mathcal{D}^2	Valid	$\text{rk}(\mathcal{Z}_2(\mathcal{C}))$	Premodular?	Pointed?	TY?	TEE	$\log \mathcal{D}_{\mathcal{Z}_2(\mathcal{C})}^2$	Conjecture true?
FR _{3,0} ^{1,0}	5	8	✓	2	✓			log 2	log 2	✓
FR _{5,0} ^{1,1}	5	8	✓	5	Symm.			log 8	log 8	✓
FR _{5,0} ^{1,2}	5	8	✓	2	✓			log 2	log 2	✓
FR _{5,0} ^{1,3}	5	8	✓	5	Symm.			log 8	log 8	✓
FR _{5,0} ^{1,4}	5	8	✓	2	✓			log 2	log 2	✓
FR _{5,0} ^{1,5}	5	8	✓	4	✓		✓	log 4	log 4	✓
FR _{5,0} ^{1,6}	5	8	✓	2	✓			log 2	log 2	✓
FR _{5,0} ^{1,7}	5	8	✓	4	✓		✓	log 4	log 4	✓
FR _{5,0} ^{1,8}	5	8	✓	2	✓			log 2	log 2	✓
FR _{5,0} ^{1,9}	5	8	✓	4	✓		✓	log 4	log 4	✓
FR _{5,0} ^{1,10}	5	8	✓	2	✓			log 2	log 2	✓
FR _{5,0} ^{1,11}	5	8	✓	4	✓		✓	log 4	log 4	✓
FR _{5,0} ^{1,12}	5	8	✓	2	✓			log 2	log 2	✓
FR _{5,0} ^{1,13}	5	8	✓	5	Symm.			log 8	log 8	✓
FR _{5,0} ^{1,14}	5	8	✓	2	✓			log 2	log 2	✓
FR _{5,0} ^{1,15}	5	8	✓	5	Symm.			log 8	log 8	✓
FR _{5,0} ^{1,16}	5	8	✓	2	✓			log 2	log 2	✓
FR _{5,0} ^{1,17}	5	8	✓	5	Symm.			log 8	log 8	✓
FR _{5,0} ^{1,18}	5	8	✓	2	✓			log 2	log 2	✓
FR _{5,0} ^{1,19}	5	8	✓	2	✓			log 2	log 2	✓
FR _{5,0} ^{1,20}	5	8	✓	4	✓		✓	log 4	log 4	✓
FR _{5,0} ^{1,21}	5	8	✓	2	✓			log 2	log 2	✓
FR _{5,0} ^{1,22}	5	8	✓	2	✓			log 2	log 2	✓
FR _{5,0} ^{1,23}	5	8	✓	4	✓		✓	log 4	log 4	✓
FR _{5,0} ^{1,24}	5	8	✓	2	✓			log 2	log 2	✓
FR _{5,0} ^{1,25}	5	8	✓	2	✓			log 2	log 2	✓
FR _{5,0} ^{1,26}	5	8	✓	5	Symm.			log 8	log 8	✓
FR _{5,0} ^{1,27}	5	8	✓	2	✓			log 2	log 2	✓
FR _{5,0} ^{1,28}	5	8	✓	2	✓			log 2	log 2	✓
FR _{5,0} ^{1,29}	5	8	✓	2	✓			log 2	log 2	✓
FR _{5,0} ^{1,30}	5	8	✓	2	✓			log 2	log 2	✓
FR _{5,0} ^{1,31}	5	8	✓	2	✓			log 2	log 2	✓
FR _{5,0} ^{1,32}	5	8	✓	2	✓			log 2	log 2	✓
FR _{5,0} ^{1,33}	5	8	✓	2	✓			log 2	log 2	✓
FR _{5,0} ^{1,34}	5	8	✓	2	✓			log 2	log 2	✓
FR _{5,0} ^{1,35}	5	8	✓	2	✓			log 2	log 2	✓
FR _{5,0} ^{1,36}	5	8	✓	2	✓			log 2	log 2	✓
FR _{5,0} ^{1,37}	5	8	✓	2	✓			log 2	log 2	✓
FR _{5,0} ^{1,38}	5	8	✓	2	✓			log 2	log 2	✓
FR _{5,0} ^{1,39}	5	8	✓	2	✓			log 2	log 2	✓
FR _{5,0} ^{1,40}	5	8	✓	2	✓			log 2	log 2	✓
FR _{5,0} ^{1,41}	5	8	✓	2	✓			log 2	log 2	✓
FR _{5,0} ^{1,42}	5	8	✓	2	✓			log 2	log 2	✓
FR _{5,0} ^{1,43}	5	8	✓	2	✓			log 2	log 2	✓
FR _{5,0} ^{1,44}	5	8	✓	2	✓			log 2	log 2	✓
FR _{5,0} ^{1,45}	5	8	✓	2	✓			log 2	log 2	✓
FR _{5,0} ^{1,46}	5	8	✓	2	✓			log 2	log 2	✓
FR _{5,0} ^{1,47}	5	8	✓	2	✓			log 2	log 2	✓
FR _{5,0} ^{1,48}	5	8	✓	2	✓			log 2	log 2	✓
FR _{5,0} ^{1,49}	5	8	✓	2	✓			log 2	log 2	✓
FR _{5,0} ^{1,50}	5	8	✓	2	✓			log 2	log 2	✓
FR _{5,0} ^{1,51}	5	8	✓	2	✓			log 2	log 2	✓
FR _{5,0} ^{1,52}	5	8	✓	2	✓			log 2	log 2	✓
FR _{5,0} ^{1,53}	5	8	✓	5	Symm.			log 8	log 8	✓
FR _{5,0} ^{1,54}	5	8	✓	4	✓		✓	log 4	log 4	✓
FR _{5,0} ^{1,55}	5	8	✓	4	✓		✓	log 4	log 4	✓
FR _{5,0} ^{1,56}	5	8	✓	5	Symm.			log 8	log 8	✓
FR _{5,0} ^{1,57}	5	8	✓	2	✓			log 2	log 2	✓
FR _{5,0} ^{1,58}	5	8	✓	2	✓			log 2	log 2	✓
FR _{5,0} ^{1,59}	5	8	✓	2	✓			log 2	log 2	✓
FR _{5,0} ^{1,60}	5	8	✓	2	✓			log 2	log 2	✓
FR _{5,0} ^{1,61}	5	8	✓	2	✓			log 2	log 2	✓
FR _{5,0} ^{1,62}	5	8	✓	2	✓			log 2	log 2	✓
FR _{5,0} ^{1,63}	5	8	✓	2	✓			log 2	log 2	✓
FR _{3,0} ^{3,0}	5	12	✓	1	Mod.			0	0	✓
FR _{3,1} ^{3,1}	5	12	✓	1	Mod.			0	0	✓
FR _{3,2} ^{3,2}	5	12	✓	1	Mod.			0	0	✓
FR _{3,3} ^{3,3}	5	12	✓	1	Mod.			0	0	✓
FR _{3,4} ^{3,4}	5	12	✓	1	Mod.			0	0	✓
FR _{3,5} ^{3,5}	5	12	✓	1	Mod.			0	0	✓
FR _{3,6} ^{3,6}	5	12	✓	1	Mod.			0	0	✓
FR _{3,7} ^{3,7}	5	12	✓	1	Mod.			0	0	✓
FR _{3,0} ^{4,0}	5	14	✓	5	Symm.			log 14	log 14	✓
FR _{4,1} ^{4,1}	5	14	✓	2	✓			log 2	log 2	✓
FR _{4,2} ^{4,2}	5	14	✓	2	✓			log 2	log 2	✓
FR _{4,3} ^{4,3}	5	14	✓	2	✓			log 2	log 2	✓
FR _{4,4} ^{4,4}	5	14	✓	2	✓			log 2	log 2	✓
FR _{4,5} ^{4,5}	5	14	✓	2	✓			log 2	log 2	✓
FR _{4,6} ^{4,6}	5	14	✓	2	✓			log 2	log 2	✓
FR _{5,0} ^{5,0}	5	24	✓	5	Symm.			log 24	log 24	✓
FR _{6,0} ^{6,0}	5	24	✓	3	✓			log 6	log 6	✓
FR _{5,0} ^{6,2}	5	24	✓	5	Symm.			log 24	log 24	✓
FR _{6,3} ^{6,3}	5	24	✓	3	✓			log 6	log 6	✓
FR _{5,0} ^{7,0}	5	$5\sqrt{5}+15$	✓	2	✓			log 2	log 2	✓
FR _{5,0} ^{7,1}	5	$5\sqrt{5}+15$	✓	2	✓			log 2	log 2	✓
FR _{10,0} ^{10,0}	5	~ 34.65	✓	1	Mod.			0	0	✓
FR _{10,1} ^{10,1}	5	~ 34.65	✓	1	Mod.			0	0	✓
FR _{1,0} ^{5,4}	5	5	✓	5	Symm.	✓		log 5	log 5	✓
FR _{1,1} ^{5,4}	5	5	✓	1	Mod.	✓		0	0	✓
FR _{1,2} ^{5,4}	5	5	✓	1	Mod.	✓		0	0	✓
FR _{1,3} ^{5,4}	5	5	✓	1	Mod.	✓		0	0	✓
FR _{1,4} ^{5,4}	5	5	✓	1	Mod.	✓		0	0	✓

Chapter 5

Outlook

Over the next century, two of the greatest challenges that humanity will face are climate change and the antibiotics crisis [204]. Studying many-body quantum systems has the potential to alleviate and even solve both of these problems. For example, understanding mechanisms which allow for superconductivity at low temperatures could help with engineering new materials that operate at higher temperatures. The ability to design and fabricate high temperature superconductors could drastically change the energy consumption and production around the world [5]. Similarly, understanding the subatomic physical interactions that take place when drugs interact with living cells could also allow for more precise drug design [205, 206]. Beyond these two major challenges, many-body physics is important for a myriad of fundamental research areas [16].

A vast majority of quantum many-body models are currently insoluble. The Hilbert space dimension of these models grows exponentially with system size, leaving the calculations necessary to solve them intractable. There are, however, classes of models for which a tractable method of extracting a solution is known. These models are called exactly soluble models. Exactly soluble many-body models are important precisely because they are soluble. Furthermore, such models remain of interest even when their exact solubility comes at the expense of the accuracy of the model's description of a known physical system [16]. The underlying message of this thesis is exactly this: the insight gained from exactly soluble models reaches far beyond the scope of the specific physical system that those models purport to describe. Through these simplistic and tractable models we are able to gain a physical intuition that informs our understanding of universal phenomena and provide a scope with which we can probe new physics.

This thesis considers two distinct classes of exactly soluble, quantum many-body systems to differ-

ent ends. In the first part of this thesis, we uncover a class of models which were previously unknown to be exactly soluble and provide a solution method as well as a criteria for the recognition of this class. In the second part of the thesis, we study the entanglement structure of another class of models, such a calculation is made possible due to the fact that this class of model is exactly soluble.

New solution methods are of great interest within the field of quantum many-body physics. Arguably, the novelty of a solution method can be just as important as the existence of the solution itself. Often, new methods are discovered through their application to a specific model. In many cases, the newly developed solution method can then be modified and applied more broadly, to a larger class of system. As such, a new solution method can expand the class of models which are known to be exactly solvable. To this day, the discovery of the free-fermion solution for the one-dimensional Ising model [24, 28] is lauded as a wonderful piece of ingenuity and informs our understanding of free-fermion models at large.

The standard approach to finding a free-fermion solution to a many-body spin model is the blind application of Jordan-Wigner, followed by the identification of symmetries such that the Hamiltonian terms are reduced to quadratic order. The success of such an approach has largely been down to luck and intuition. The introduction of a recognition scheme [22] for many-body spin models that admit a generalized Jordan-Wigner type free-fermion solution was therefore significant because such a characterization reduces the guesswork for solving free-fermion models. However, not all models that admit a free-fermion solution do so via a generator-to-generator mapping. Examples of such models are few and far between in the literature, however, in Ref. [23], Paul Fendley solved a one-dimensional many-body spin model that was previously considered to be interacting, by identifying the free-fermion modes and single particle energies. The solution method is elegant and simple; the modes are defined by sets of Hamiltonian terms which mutually commute and single-particle energies are given by reciprocals of roots of a polynomial. The obvious questions that followed were, ‘why does this solution work?’ and ‘when can this solution method be applied more broadly to many-body models?’ In Chapters 2 and 3 we answer these by identifying the graph theoretic invariants that allow for such an elegant and simple solution to work.

Graph theory has been utilized throughout the literature of quantum many-body physics, and indeed mathematical physics at large. Notwithstanding, the application of graph theory in Chapters 2 and 3 is unique: the graphs are defined in an unusual way, being dependent on a particular Pauli basis. In many cases, (hyper)graphs are used with vertices defined by Hilbert spaces and hyperedges

defined by the support of the Hamiltonian terms (in a basis independent way)¹ [207]; such hypergraphs have an equivalent graph representation² where the vertices are identified with the basis-independent Hamiltonian terms and adjacency determined by overlap in support of those terms [208]. As in Chapters 2 and 3, many-body models have been classified via a forbidden subgraph characterization before [209]. However, beyond the definition of the graphs used here, there also is an inherent novelty in the work presented as the solutions themselves are constructed using the graphical features; indeed, it would be difficult to imagine identifying the symmetries that are identified in either chapter, but perhaps more explicitly so those in Chapter 3, without doing so directly by their graphical structures. Furthermore, there is scope for this to continue. It would be completely unsurprising to discover an entirely new class of exactly soluble models that can be identified and then solved by graphical means.

In Chapter 2, we develop a general construction for finding and solving quantum lattice models with a free-fermion structure in one spatial dimension, using exactly the method introduced by Paul Fendley in Ref. [23]. Surprisingly, the results in Chapter 2 are neither contained within, nor do they completely contain, the traditional qubit-to-fermion maps given by Ref. [22]. This means that not all models which admit a free-fermion solution via a generalized Jordan-Wigner map can be solved using the methods developed in this chapter.

This disunity between the two classes of free-fermion model is rectified in Chapter 3. Here, the construction is expanded from one-dimensional systems to arbitrary spatial dimension. This expansion of Fendley’s method requires the identification of a new set of ‘local’ symmetries and the modification of the solution method. The expansion also unifies the new framework with those of more traditional methods (Jordan-Wigner). The new classification for models which admit a free-fermion solution is a much larger class of graphs, meaning that the class of exactly soluble models has been greatly expanded.

As discussed in Chapter 3, the recognition condition is not conclusive, as it is not a necessary and sufficient condition. Indeed, it is known that there are free-fermion models beyond this set of results. Thus, one obvious avenue for further work would be to understand how these models might fit within the framework, and attempt to find a more complete set of conditions for free-fermion solubility, which includes those models which are non-generic. Another avenue that presents itself as interesting for further research is the inverse problem of finding fermion-to-qubit maps; in particular, finding compact qubit encodings for (interacting) fermion Hamiltonians. With the arrival of programmable quantum computers seemingly becoming closer with every passing day, it seems reasonable that we might want

¹A hypergraph is a graph where the edges can connect more than two vertices

²This is actually the line graph of the corresponding hypergraph

to understand systems of interacting fermions. Simulating such systems would be made simpler if there was an effective description of the interacting fermionic system in terms of fewer spins.

In Chapter 4, we investigated the entanglement properties of a class of models which describe topologically ordered phases in two and three spatial dimensions. This family of models were never intended to describe any known physical system; rather, they are interesting because they can be solved exactly. Furthermore, this family of models capture the long-wavelength physics of topological states of matter that are known to exist in certain laboratory settings. Thus, the models provide a framework in which to study the physical properties of their ‘more realistic’ cousins, including properties of their anyonic excitations and their long-range entanglement.

It is precisely this last property that we have investigated in Chapter 4, where the topological entanglement entropy was calculated for two- and three-dimensional loop-gas models in the bulk and in the boundary. We show that the correction to the area law of entanglement is only present in the locality of the model where anyons are supported. Furthermore, we show how the magnitude of the correction is dependent on the properties of the anyon model that is present. This work is an extension of previous results which calculate the entanglement properties of Walker-Wang models in the bulk [156, 165, 166]. This extension to the understanding of topological entanglement entropy is made possible by the introduction of new diagnostics specifically for identifying topological order at the boundary of three-dimensional systems [167].

The consequences of the results derived in this chapter extend far beyond limited reach of the Walker-Wang and Levin-Wen exactly soluble models discussed. Such a understanding of the entanglement structure of topological systems can be applied more generally, which may be of particular interest to physical systems that can be fabricated in a lab for the purpose of developing the building blocks of topological quantum computing.

Bibliography

- [1] L. Du, S. Wang, D. Scarabelli, L. N. Pfeiffer, K. W. West, S. Fallahi, G. C. Gardner, M. J. Manfra, V. Pellegrini, S. J. Wind, and A. Pinczuk. Emerging many-body effects in semiconductor artificial graphene with low disorder. *Nat. Comms.*, 9(1), August 2018.
- [2] C. S. Chiu, G. Ji, A. Bohrdt, M. Xu, M. Knap, E. Demler, F. Grusdt, M. Greiner, and D. Greif. String patterns in the doped hubbard model. *Science*, 365(6450):251–256, July 2019.
- [3] J. Bardeen, L. N. Cooper, and J. R. Schrieffer. Theory of superconductivity. *Phys. Rev.*, 108(5):1175–1204, December 1957.
- [4] R. A. Hart, P. M. Duarte, T.-L. Yang, X. Liu, T. Paiva, E. Khatami, R. T. Scalettar, N. Trivedi, D. A. Huse, and R. G. Hulet. Observation of antiferromagnetic correlations in the hubbard model with ultracold atoms. *Nature*, 519(7542):211–214, February 2015.
- [5] E. Fradkin. *Field Theories of Condensed Matter Physics*. Cambridge University Press, 2013.
- [6] S. Xu, L. Susskind, Y. Su, and B. Swingle. A sparse model of quantum holography. arXiv:2008.02303, 2020.
- [7] A Kitaev. A simple model of quantum holography.
- [8] S.-K. Jian and H. Yao. Solvable sachdev-ye-kitaev models in higher dimensions: From diffusion to many-body localization. *Phys. Rev. Lett.*, 119(20), November 2017.
- [9] D. J Griffiths and D. F Schroeter. *Introduction to quantum mechanics*. Cambridge university press, 2018.
- [10] J. K Pachos. *Introduction to topological quantum computation*. Cambridge University Press, 2012.
- [11] A. Kitaev. Unpaired Majorana fermions in quantum wires. *Phys. Usp.*, 44:131, 2000.

- [12] A. Kitaev. Anyons in an exactly solved model and beyond. *Ann. Phys. (N. Y.)*, 321(1):2 – 111, 2006.
- [13] M. A. Levin and X.-G. Wen. String-net condensation: A physical mechanism for topological phases. *Phys. Rev. B*, 71:045110, Jan 2005.
- [14] F. J. Burnell, X. Chen, L. Fidkowski, and A. Vishwanath. Exactly soluble model of a three-dimensional symmetry-protected topological phase of bosons with surface topological order. *Phys. Rev. B*, 90(24):245122, 2014.
- [15] M. A Nielsen and I. Chuang. *Quantum computation and quantum information*. American Association of Physics Teachers, 2002.
- [16] X.-G. Wen. *Quantum field theory of many-body systems: from the origin of sound to an origin of light and electrons*. Oxford University Pres, 2004.
- [17] P. W. Shor. Polynomial-time algorithms for prime factorization and discrete logarithms on a quantum computer. *SIAM J. Comput.*, 26(5):1484–1509, October 1997.
- [18] D. Deutsch and R. Jozsa. Rapid solution of problems by quantum computation. *Proc. Math. Phys. Eng. Sci. P ROY SOC A-MATH PHY*, 439(1907):553–558, December 1992.
- [19] S. Lloyd. Universal quantum simulators. *Science*, 273(5278):1073–1078, August 1996.
- [20] R. Orús. Tensor networks for complex quantum systems. *Nat. Rev. Phys.*, 1(9):538–550, August 2019.
- [21] D. A. R. Sakthivadivel. Magnetisation and mean field theory in the ising model. *SciPost Phys.*, January 2022.
- [22] A. Chapman and S. T. Flammia. Characterization of solvable spin models via graph invariants. *Quantum*, 4:278, June 2020.
- [23] P. Fendley. Free fermions in disguise. *J. Phys. A*, 52(33):335002, July 2019.
- [24] E. Lieb, T. Schultz, and D. Mattis. Two soluble models of an antiferromagnetic chain. *Ann. Phys.*, 16(3):407 – 466, 1961.
- [25] K. Walker and Z. Wang. (3+1)-TQFTs and topological insulators. *Front. Phys.*, 7:150, 2012.
- [26] C. J. Turner, K. Meichanetzidis, Z. Papić, and J. Pachos. Optimal free descriptions of many-body theories. *Nat. Comms.*, 8:14926, 2017.

- [27] K. Meichanetzidis, C. J. Turner, A. Farjami, Z. Papić, and J. K. Pachos. Free-fermion descriptions of parafermion chains and string-net models. *Phys. Rev. B*, 97:125104, 2018.
- [28] P. Jordan and E. Wigner. Über das paulische Äquivalenzverbot. *Z. Physik*, 47(9-10):631–651, September 1928.
- [29] X.-G. Wen. Quantum order from string-net condensations and the origin of light and massless fermions. *Phys. Rev. D*, 68(6), September 2003.
- [30] E. Fradkin. Jordan-Wigner transformation for quantum-spin systems in two dimensions and fractional statistics. *Phys. Rev. Lett.*, 63(3):322–325, July 1989.
- [31] Y. R. Wang. Ground state of the two-dimensional antiferromagnetic Heisenberg model studied using an extended Wigner-Jordon transformation. *Phys. Rev. B*, 43(4):3786–3789, February 1991.
- [32] L. Huerta and J. Zanelli. Bose-Fermi transformation in three-dimensional space. *Phys. Rev. Lett.*, 71(22):3622–3624, November 1993.
- [33] C. D. Batista and G. Ortiz. Generalized Jordan-Wigner transformations. *Phys. Rev. Lett.*, 86(6):1082–1085, February 2001.
- [34] S. Bravyi and A. Kitaev. Fermionic quantum computation. *Ann Phys (N.Y.)*, 298(1):210–226, May 2002.
- [35] F. Verstraete and J. I. Cirac. Mapping local Hamiltonians of fermions to local Hamiltonians of spins. *J. Stat. Mech. Theory Exp.*, 2005(09):P09012–P09012, September 2005.
- [36] Z. Nussinov, G. Ortiz, and E. Cobanera. Arbitrary dimensional Majorana dualities and architectures for topological matter. *Phys. Rev. B*, 86(8):085415, August 2012.
- [37] Y.-A. Chen, A. Kapustin, and D. Radičević. Exact bosonization in two spatial dimensions and a new class of lattice gauge theories. *Ann Phys (N.Y.)*, 393:234–253, June 2018.
- [38] Y.-A. Chen and A. Kapustin. Bosonization in three spatial dimensions and a 2-form gauge theory. *Phys. Rev. B*, 100(24), December 2019.
- [39] S. Backens, A. Shnirman, and Y. Makhlin. Jordan–Wigner transformations for tree structures. *Sci. Rep.*, 9(1):2598, February 2019.

- [40] N. Tantivasadakarn. Jordan-Wigner dualities for translation-invariant Hamiltonians in any dimension: Emergent fermions in fracton topological order. *Phys. Rev. Res.*, 2(2), June 2020.
- [41] M. Ogura, Y. Imamura, N. Kameyama, K. Minami, and M. Sato. Geometric criterion for solvability of lattice spin systems. *Phys. Rev. B*, 102:245118, Dec 2020.
- [42] R. J. Trudeau. *Introduction to Graph Theory*. Dover, 2013.
- [43] G. Alan. *Algorithmic Graph Theory*. Cambridge University Press, 1985.
- [44] N. Deo. *Graph theory with applications to engineering and computer science*. Courier Dover Publications, 2017.
- [45] C. J. Garroway, J. Bowman, D. Carr, and P. J Wilson. Applications of graph theory to landscape genetics. *Evol. Appl.*, 1(4):620–630, 2008.
- [46] A. B. Lee, D. Luca, L. Klei, B. Devlin, and K. Roeder. Discovering genetic ancestry using spectral graph theory. *Genet. Epidemiol.*, 34(1):51–59, 2010.
- [47] A. T. Balaban. Applications of graph theory in chemistry. *J. Chem. Inf. Comput.*, 25(3):334–343, 1985.
- [48] D. H. Rouvray. Graph theory in chemistry. *Chem. Soc. Rev.*, 4(2):173–195, 1971.
- [49] N. Trinajstić. *Chemical graph theory*. CRC press, 2018.
- [50] Wai-Kai Chen. *Graph theory and its engineering applications*, volume 5. World Scientific, 1997.
- [51] X.-G. Wen. Quantum orders in an exact soluble model. *Phys. Rev. Lett.*, 90:016803, Jan 2003.
- [52] D. J. Williamson and Z. Wang. Hamiltonian models for topological phases of matter in three spatial dimensions. *Ann. Phys.*, 377:311–344, 2017.
- [53] L. Crane and D. Yetter. A categorical construction of 4D topological quantum field theories. *Quant. Topol.*, 3:120, 1993.
- [54] L. Crane, L. H Kauffman, and D. N. Yetter. State-sum invariants of 4-manifolds. *J. Knot Theory Ramif.*, 6(02):177–234, 1997.
- [55] C. W. von Keyserlingk, F. J. Burnell, and S. H. Simon. Three-dimensional topological lattice models with surface anyons. *Phys. Rev. B*, 87(4):045107, 2013.

- [56] M. Chudnovsky, A. Scott, P. Seymour, and S. Spirkl. A note on simplicial cliques. *Discrete Math.*, 344:112470, 2021.
- [57] F. C. Alcaraz and R. A. Pimenta. Free fermionic and parafermionic quantum spin chains with multispin interactions. *Phys. Rev. B*, 102:121101(R), Dec 2020.
- [58] F. C. Alcaraz and R. A. Pimenta. Integrable quantum spin chains with free fermionic and parafermionic spectrum. *Phys. Rev. B*, 102:235170, Dec 2020.
- [59] P. Fendley. Free parafermions. *J. Phys. A Math*, 47:075001, 2014.
- [60] M. Planat and M. Saniga. On the pauli graphs of N -qudits. arXiv:quant-ph/0701211, 2007.
- [61] W. Shaofeng. Jordan-Wigner transformation in a higher-dimensional lattice. *Phys. Rev. E*, 51(2):1004–1005, February 1995.
- [62] Z. Nussinov and G. Ortiz. Bond algebras and exact solvability of Hamiltonians: Spin $S = 1/2$ multilayer systems. *Phys. Rev. B*, 79(21):214440, June 2009.
- [63] V. Galitski. Fermionization transform for certain higher-dimensional quantum spin models. *Phys. Rev. B*, 82(6):060411(R), August 2010.
- [64] E. Cobanera, G. Ortiz, and Z. Nussinov. The bond-algebraic approach to dualities. *Adv. Phys.*, 60(5):679–798, October 2011.
- [65] L. Onsager. Crystal statistics. I. a two-dimensional model with an order-disorder transition. *Phys. Rev.*, 65(3-4):117–149, February 1944.
- [66] T. D. Schultz, D. C. Mattis, and E. H. Lieb. Two-dimensional Ising model as a soluble problem of many fermions. *Rev. Mod. Phys.*, 36:856–871, Jul 1964.
- [67] M. S. Kochmański. Generalized Jordan-Wigner transformations and the Ising-Onsager problem. *J. Exp. Theor.*, 84(5):940–947, May 1997.
- [68] G. Ortiz, J. E. Gubernatis, E. Knill, and R. Laflamme. Quantum algorithms for fermionic simulations. *Phys. Rev. A*, 64(2):022319, July 2001.
- [69] S. Bravyi, J. M. Gambetta, A. Mezzacapo, and K. Temme. Tapering off qubits to simulate fermionic Hamiltonians. arXiv:1701.08213, 2017.
- [70] V. Havlíček, M. Troyer, and J. D. Whitfield. Operator locality in the quantum simulation of fermionic models. *Phys. Rev. A*, 95(3):032332, March 2017.

- [71] M. Steudtner and S. Wehner. Fermion-to-qubit mappings with varying resource requirements for quantum simulation. *New J. Phys.*, 20(6):063010, June 2018.
- [72] K. Setia, S. Bravyi, A. Mezzacapo, and J. D. Whitfield. Superfast encodings for fermionic quantum simulation. *Phys. Rev. Res.*, 1(3):033033, October 2019.
- [73] Z. Jiang, J. McClean, R. Babbush, and Hartmut Neven. Majorana loop stabilizer codes for error mitigation in fermionic quantum simulations. *Phys. Rev. Appl.*, 12(6):064041, December 2019.
- [74] Z. Jiang, A. Kalev, W. Mroczkiewicz, and H. Neven. Optimal fermion-to-qubit mapping via ternary trees with applications to reduced quantum states learning. *Quantum*, 4:276, June 2020.
- [75] M. Levin and X.-G. Wen. Fermions, strings, and gauge fields in lattice spin models. *Phys. Rev. B*, 67(24), June 2003.
- [76] R. C. Ball. Fermions without fermion fields. *Phys. Rev. Lett.*, 95(17), October 2005.
- [77] E. Knill. Fermionic Linear Optics and Matchgates. arXiv:quant-ph/0108033, 2001.
- [78] B. M. Terhal and D. P. DiVincenzo. Classical simulation of noninteracting-fermion quantum circuits. *Phys. Rev. A*, 65(3), March 2002.
- [79] S. Bravyi. Universal quantum computation with the $\nu = 5/2$ fractional quantum Hall state. *Phys. Rev. A*, 73(4), April 2006.
- [80] R. Jozsa and A. Miyake. Matchgates and classical simulation of quantum circuits. *Proc. Math. Phys. Eng. Sci. P ROY SOC A-MATH PHY*, 464(2100):3089–3106, 2008.
- [81] D. J. Brod and E. F. Galvão. Extending matchgates into universal quantum computation. *Phys. Rev. A*, 84(2), August 2011.
- [82] M. Hebenstreit, R. Jozsa, B. Kraus, S. Strelchuk, and M. Yoganathan. All pure fermionic non-Gaussian states are magic states for matchgate computations. *Phys. Rev. Lett.*, 123(8), August 2019.
- [83] L. G. Valiant. Quantum circuits that can be simulated classically in polynomial time. *SIAM J. Comput.*, 31(4):1229–1254, January 2002.
- [84] J.-Y. C. and V. Choudhary. Valiant’s holant theorem and matchgate tensors. In *Lecture Notes in Computer Science*, pages 248–261. Springer Berlin Heidelberg, 2006.

- [85] J.-Y. Cai, V. Choudhary, and P. Lu. On the theory of matchgate computations. In *CCC'07*. IEEE, June 2007.
- [86] L. G. Valiant. Holographic algorithms. *SIAM J. Comput.*, 37(5):1565–1594, 2008.
- [87] O. Crawford, B. van Straaten, D. Wang, T. Parks, E. Campbell, and S. Brierley. Efficient quantum measurement of Pauli operators in the presence of finite sampling error. arXiv:1908.06942, 2019.
- [88] A. F. Izmaylov, T.-C. Yen, R. A. Lang, and V. Verteletskyi. Unitary partitioning approach to the measurement problem in the variational quantum eigensolver method. *J. Chem. Theory Comput.*, 16(1):190–195, November 2019.
- [89] X. Bonet-Monroig, R. Babbush, and T. E. O’Brien. Nearly Optimal Measurement Scheduling for Partial Tomography of Quantum States. arXiv:1908.05628, 2019.
- [90] P. Gokhale, O. Angiuli, Y. Ding, K. Gui, T. Tomesh, M. Suchara, M. Martonosi, and F. T. CH. Minimizing State Preparations in Variational Quantum Eigensolver by Partitioning into Commuting Families. arXiv:1907.13623, July 2019.
- [91] T.-C. Yen, V. Verteletskyi, and A. F. Izmaylov. Measuring all compatible operators in one series of single-qubit measurements using unitary transformations. *J. Chem. Theory Comput.*, 16(4):2400–2409, March 2020.
- [92] V. Verteletskyi, T.-C. Yen, and A. F. Izmaylov. Measurement optimization in the variational quantum eigensolver using a minimum clique cover. *J. Chem. Phys.*, 152(12):124114, March 2020.
- [93] A. Zhao, A. Tranter, W. M. Kirby, S. F. Ung, A. Miyake, and P. J. Love. Measurement reduction in variational quantum algorithms. *Phys. Rev. A*, 101(6), June 2020.
- [94] A. J. Kollár, M. Fitzpatrick, P. Sarnak, and A. A. Houck. Line-graph lattices: Euclidean and non-euclidean flat bands, and implementations in circuit quantum electrodynamics. *Commun. Math. Phys.*, 376(3):1909–1956, December 2019.
- [95] A. J. Kollár, M. Fitzpatrick, and A. A. Houck. Hyperbolic lattices in circuit quantum electrodynamics. *Nature*, 571(7763):45–50, July 2019.
- [96] M. Chudnovsky and P. Seymour. The structure of claw-free graphs. In *Surveys in Combinatorics 2005*, pages 153–172. Cambridge University Press, July 2005.

- [97] R. Faudree, E. Flandrin, and Z. Ryjáček. Claw-free graphs — a survey. *Discrete Math.*, 164(1-3):87–147, February 1997.
- [98] J. Krausz. Démonstration nouvelle d’une théorème de Whitney sur les réseaux. *Középisk. Mat. és Fiz. Lapok*, 50, 1943.
- [99] M. Cavers, S. M. Cioabă, S. Fallat, D. A. Gregory, W. H. Haemers, S. J. Kirkland, J. J. McDonald, and M. Tsatsomeros. Skew-adjacency matrices of graphs. *Lin. Algebra Its Appl.*, 436(12):4512–4529, June 2012.
- [100] J. Leake and N. Ryder. Generalizations of the Matching Polynomial to the Multivariate Independence Polynomial. *arXiv e-prints*, page arXiv:1610.00805, October 2016.
- [101] A. Engström. Inequalities on well-distributed point sets on circles. *J. Inequalities Pure App.*, 2007.
- [102] M. Chudnovsky and P. Seymour. The roots of the independence polynomial of a clawfree graph. *J. Comb. Theory. Ser. B*, 97(3):350–357, May 2007.
- [103] R. Descartes. *La géométrie de René Descartes*, volume 1. A. Hermann, 1886.
- [104] L. W. Beineke. Characterizations of derived graphs. *J. Comb. Theory*, 9(2):129–135, September 1970.
- [105] K. Cameron, S. Chaplick, and Chính T. Hoàng. On the structure of (pan, even hole)-free graphs. *J. Graph Theory*, 87(1):108–129, June 2017.
- [106] T. Kloks, D. Kratsch, and H. Müller. Finding and counting small induced subgraphs efficiently. *Inf. Process. Lett.*, 74(3-4):115–121, May 2000.
- [107] M. Chudnovsky and P. Seymour. Growing without cloning. *SIAM J. Discrete Math.*, 26(2):860–880, January 2012.
- [108] G. Wegner. *Eigenschaften der Nerven homologisch-einfacher Familien im \mathbb{R}^n* . PhD thesis, Göttingen University, Göttingen, Germany, 1967.
- [109] R. M. Beam and R. F. Warming. The asymptotic spectra of banded Toeplitz and quasi-Toeplitz matrices. *SIAM J. Sci. Comput.*, 14(4):971–1006, July 1993.
- [110] F. L. Pedrocchi A. Jaffe. Reflection positivity for parafermions. *Commun. Math. Phys.*, 377(1):455, 2015.

- [111] P. Fendley and K. Schoutens. Cooper pairs and exclusion statistics from coupled free-fermion chains. *J. Stat. Mech. Theory Exp.*, 2007(02):P02017–P02017, February 2007.
- [112] B. A. van Voorden and K. Schoutens. Topological quantum pump of strongly interacting fermions in coupled chains. *New J. Phys.*, 21(1):013026, January 2019.
- [113] S. Bravyi and D. Gosset. Complexity of quantum impurity problems. *Commun. Math. Phys.*, 356(2):451–500, August 2017.
- [114] R. Babbush, D. W. Berry, I. D. Kivlichan, A. Y. Wei, P. J. Love, and A. Aspuru-Guzik. Exponentially more precise quantum simulation of fermions in second quantization. *New J. Phys.*, 18(3):033032, March 2016.
- [115] S. McArdle, S. Endo, A. Aspuru-Guzik, S. Benjamin, and X. Yuan. Quantum computational chemistry. *Rev. Mod. Phys.*, 92:15003, August 2020.
- [116] Q. Wang, M. Li, C. Monroe, and Y. Nam. Resource-optimized fermionic local-hamiltonian simulation on a quantum computer for quantum chemistry. *Quantum*, 5:509, July 2021.
- [117] D. Leykam. Making fermionic quantum simulators more affordable. *Quantum Views*, 5:57, August 2021.
- [118] C. Derby, J. Klassen, J. Bausch, and T. Cubitt. Compact fermion to qubit mappings. *Phys. Rev. B*, 104(3):035118, July 2021.
- [119] C. Derby and J. Klassen. A Compact Fermion to Qubit Mapping Part 2: Alternative Lattice Geometries. *arXiv e-prints*, page arXiv:2101.10735, January 2021.
- [120] Y.-A. Chen and Y. Xu. Equivalence between fermion-to-qubit mappings in two spatial dimensions. *arXiv e-prints*, page arXiv:2201.05153, January 2022.
- [121] S. Bravyi, B. M. Terhal, and B. Leemhuis. Majorana fermion codes. *New J. Phys.*, 12(8):083039, aug 2010.
- [122] D. Aasen, M. Hell, R. V. Mishmash, A. Higginbotham, J. Danon, M. Leijnse, T. S. Jespersen, J. A. Folk, C. M. Marcus, K. Flensberg, and J. Alicea. Milestones toward majorana-based quantum computing. *Phys. Rev. X*, 6(3):031016, August 2016.
- [123] J. Alicea. New directions in the pursuit of majorana fermions in solid state systems. *Rep. Prog. Phys.*, 75(7):076501, June 2012.

- [124] A. Chapman, Steven T. Flammia, and Alicia J. Kollár. Free-fermion subsystem codes. *PRX Quantum*, 3:030321, Aug 2022.
- [125] D. I. Pikulin, B. van Heck, T. Karzig, E. A. Martinez, B. Nijholt, T. Laeven, G. W. Winkler, J. D. Watson, S. Heedt, M. Temurhan, V. Svidenko, R. M. Lutchyn, M. Thomas, G. de Lange, L. Casparis, and C. Nayak. Protocol to identify a topological superconducting phase in a three-terminal device. *arXiv e-prints*, page arXiv:2103.12217, March 2021.
- [126] S. J. Elman, A Chapman, and S. T. Flammia. Free fermions behind the disguise. *Commun. Math. Phys*, 388:969, 2021.
- [127] M. Chudnovsky, A. Scott, P. Seymour, and Sophie Spirkl. A note on simplicial cliques. *arXiv e-prints*, page arXiv:2012.05287, December 2020.
- [128] P. Bonsma, Marcin Kamiński, and Marcin Wrochna. Reconfiguring Independent Sets in Claw-Free Graphs. *arXiv e-prints*, page arXiv:1403.0359, March 2014.
- [129] C. Godsil. *Algebraic Combinatorics*. 1993.
- [130] P. Caputa, J. M. Magan, and D. Patramanis. Geometry of krylov complexity. *Phys. Rev. Res.*, 4(1), January 2022.
- [131] E. Rabinovici, A. Sánchez-Garrido, R. Shir, and J. Sonner. Operator complexity: a journey to the edge of krylov space. *J. High Energy Phys.*, 2021(6), June 2021.
- [132] D. E. Parker, Xiangyu Cao, A.ander Avdoshkin, Thomas Scaffidi, and Ehud Altman. A universal operator growth hypothesis. *Phys. Rev. X*, 9(4), October 2019.
- [133] H. N. V. Temperley and M. E Fisher. Dimer problem in statistical mechanics-an exact result. *Philos. Mag. Lett.*, 6(68):1061–1063, 1961.
- [134] P. W. Kasteleyn. Dimer statistics and phase transitions. *J. Math. Phys.*, 4(2):287–293, 1963.
- [135] P. W. Kasteleyn. Graph theory and crystal physics. In *Graph Theory and Theoretical Physics*, pages 43–110. Academic Press, 1967.
- [136] T. J. Osborne and A. Stottmeister. Conformal field theory from lattice fermions. arXiv:2107.13834, 2021.
- [137] T. J. Osborne and A. Stottmeister. Quantum simulation of conformal field theory. arXiv:2109.14214, 2021.

- [138] G. Matos, S. Johri, and Z. Papić. Quantifying the efficiency of state preparation via quantum variational eigensolvers. *PRX Quantum*, 2:010309, 2021.
- [139] F. C. Alcaraz and M. T. Batchelor. Anomalous bulk behavior in the free parafermion $Z(N)$ spin chain. *Phys. Rev. E*, 97:062118, Jun 2018.
- [140] F. C. Alcaraz, M. T. Batchelor, and Z. H. Liu. Energy spectrum and critical exponents of the free parafermion $Z(N)$ spin chain. *J. Phys. A Math*, 50(16):16LT03, March 2017.
- [141] F. C. Alcaraz and R. A. Pimenta. Free-parafermionic $Z(N)$ and free-fermionic XY quantum chains. *Phys. Rev. E*, 104:054121, Nov 2021.
- [142] F. C. Alcaraz, J. A. Hoyos, and R. A. Pimenta. Powerful method to evaluate the mass gaps of free-particle quantum critical systems. *Phys. Rev. B*, 104:174206, Nov 2021.
- [143] F. D. M. Haldane and E. H. Rezayi. Periodic Laughlin-Jastrow wave functions for the fractional quantized Hall effect. *Phys. Rev. B*, 31:2529–2531, Feb 1985.
- [144] X. G. Wen. Vacuum degeneracy of chiral spin states in compactified space. *Phys. Rev. B*, 40:7387–7390, 1989.
- [145] X. G. Wen and Q. Niu. Ground-state degeneracy of the fractional quantum hall states in the presence of a random potential and on high-genus riemann surfaces. *Phys. Rev. B*, 41:9377–9396, May 1990.
- [146] A. Yu. Kitaev. Fault-tolerant quantum computation by anyons. *Ann. Phys.*, 303:2, 2003.
- [147] B. J. Brown, D. Loss, J. K. Pachos, C. N. Self, and J. R. Wootton. Quantum memories at finite temperature. *Rev. Mod. Phys.*, 88:045005, 2016.
- [148] F. Wilczek. Magnetic flux, angular momentum, and statistics. *Phys. Rev. Lett.*, 48:1144–1146, Apr 1982.
- [149] F. Wilczek. Quantum mechanics of fractional-spin particles. *Phys. Rev. Lett.*, 49:957–959, 1982.
- [150] Y. Hu, Z.-X. Luo, R. Pankovich, Y. Wan, and Y.-S. Wu. Boundary hamiltonian theory for gapped topological phases on an open surface. *J. High Energy Phys.*, 2018:134, 2018.
- [151] Y. Hu, Y. Wan, and Y.-S. Wu. Boundary hamiltonian theory for gapped topological orders. *Chin. Phys. Lett.*, 34:077103, 2017.

- [152] X. Chen, Z.-C. Gu, and X.-G. Wen. Local unitary transformation, long-range quantum entanglement, wave function renormalization, and topological order. *Phys. Rev. B*, 82:155138, 2010.
- [153] Z. Wang and X. Chen. Twisted gauge theories in three-dimensional Walker-Wang models. *Phys. Rev. B*, 95:115142, 2017.
- [154] A. Hamma, R. Ionicioiu, and P. Zanardi. Bipartite entanglement and entropic boundary law in lattice spin systems. *Phys. Rev. A*, 71:022315, 2005.
- [155] A. Kitaev and J. Preskill. Topological entanglement entropy. *Phys. Rev. Lett.*, 96:110404, 2006.
- [156] M. Levin and X.-G. Wen. Detecting topological order in a ground state wave function. *Phys. Rev. Lett.*, 96:110405, Mar 2006.
- [157] J. Eisert, M. Cramer, and M. B. Plenio. Colloquium: Area laws for the entanglement entropy. *Rev. Mod. Phys.*, 82:277–306, 2010.
- [158] S. Dong, E. Fradkin, R. G. Leigh, and S. Nowling. Topological entanglement entropy in Chern-Simons theories and quantum Hall fluids. *J. High Energy Phys.*, 2008(05):016, 2008.
- [159] B. J. Brown, S. D. Bartlett, A. C. Doherty, and S. D. Barrett. Topological entanglement entropy with a twist. *Phys. Rev. Lett.*, 111:220402, 2013.
- [160] P. Bonderson, C. Knapp, and K. Patel. Anyonic entanglement and topological entanglement entropy. *Ann. Phys.*, 385:399, 2017.
- [161] B. Shi, K. Kato, and I. H. Kim. Fusion rules from entanglement. *Ann. Phys.*, 418:168164, July 2020.
- [162] Y. Zhang, T. Grover, A. Turner, M. Oshikawa, and A. Vishwanath. Quasiparticle statistics and braiding from ground-state entanglement. *Phys. Rev. B*, 85:235151, 2012.
- [163] C. Castelnovo and C. Chamon. Topological order in a three-dimensional toric code at finite temperature. *Phys. Rev. B*, 78:155120, 2008.
- [164] T. Grover, A. M. Turner, and A. Vishwanath. Entanglement entropy of gapped phases and topological order in three dimensions. *Phys. Rev. B*, 84:195120, 2011.
- [165] A. Hamma, P. Zanardi, and X.-G. Wen. String and membrane condensation on three-dimensional lattices. *Phys. Rev. B*, 72:035307, Jul 2005.

- [166] A. Bullivant and J. K. Pachos. Entropic manifestations of topological order in three dimensions. *Phys. Rev. B*, 93(12):125111, 2016.
- [167] I. H. Kim and B. J. Brown. Ground-state entanglement constrains low-energy excitations. *Phys. Rev. B*, 92(11):115139, 2015.
- [168] B. Shi and Y.-M. Lu. Characterizing topological order by the information convex. *Phys. Rev. B*, 99:035112, 2019.
- [169] P. Etingof, S. Gelaki, D. Nikshych, and V. Ostrik. *Tensor categories*, volume 205 of *Mathematical Surveys and Monographs*. American Mathematical Society, Providence, RI, 2015.
- [170] P. H. Bonderson. *Non-Abelian anyons and interferometry*. California Institute of Technology, 2012.
- [171] K. Beer, D. Bondarenko, A. Hahn, M. Kalabakov, N. Knust, L. Niermann, T. J. Osborne, C. Schridde, S. Seckmeyer, D. E. Stiegemann, et al. From categories to anyons: a travelogue. arXiv:1811.06670, 2018.
- [172] P. Etingof, D. Nikshych, and V. Ostrik. On fusion categories. *Ann. Math.*, 162(2):581–642, September 2005.
- [173] C. Galindo. On braided and ribbon unitary fusion categories. arXiv:1209.2022, 2013.
- [174] M. Müger. On the structure of modular categories. *Proc. London Math. Soc.*, 87(2):291–308, 2003.
- [175] Bojko Bakalov and Alexander A Kirillov. *Lectures on tensor categories and modular functors*, volume 21. American Mathematical Soc., 2001.
- [176] P. Bonderson, C. Delaney, C. Galindo, E. C. Rowell, A. Tran, and Z. Wang. On invariants of modular categories beyond modular data. *J Pure Appl Algebra*, 223(9):4065–4088, 2019.
- [177] M. Müger. From Subfactors to Categories and Topology I. Frobenius algebras in and Morita equivalence of tensor categories. *J. Pure Appl. Algebra*, 180:81–157, 2003.
- [178] J. Fuchs, I. Runkel, and C. Schweigert. TFT construction of RCFT correlators i: partition functions. *Nucl. Phys. B.*, 646(3):353–497, December 2002.
- [179] A Y Kitaev and Liang Kong. Models for gapped boundaries and domain walls. *Commun. Math. Phys.*, 313:351–373, 2012.

- [180] J. Fuchs, C. Schweigert, and A. Valentino. Bicategories for boundary conditions and for surface defects in 3-d TFT. *Commun. Math. Phys.*, 321(2):543–575, May 2013.
- [181] J. Fuchs, J. Priel, C. Schweigert, and A. Valentino. On the brauer groups of symmetries of abelian dijkgraaf–witten theories. *Commun. Math. Phys.*, 339(2):385–405, July 2015.
- [182] S. B. Bravyi and A. Yu. Kitaev. Quantum codes on a lattice with boundary. arXiv:quant-ph/9811052, 1998.
- [183] C. W. von Keyserlingk and F. J. Burnell. Walker-Wang models and axion electrodynamics. *Phys. Rev. B*, 91(4):045134, 2015.
- [184] J. Cano, T. L. Hughes, and M. Mulligan. Interactions along an entanglement cut in $2 + 1d$ abelian topological phases. *Phys. Rev. B*, 92(7), August 2015.
- [185] L. Zou and J. Haah. Spurious long-range entanglement and replica correlation length. *Phys. Rev. B*, 94(7), August 2016.
- [186] D. J. Williamson, A. Dua, and M. Cheng. Spurious topological entanglement entropy from subsystem symmetries. *Phys. Rev. Lett.*, 122(14), April 2019.
- [187] K. Kato and F. G. S. L. Brandão. Toy model of boundary states with spurious topological entanglement entropy. *Phys. Rev. Res.*, 2(3), July 2020.
- [188] M. Levin. *String-net condensation and topological phases in quantum spin systems*. PhD thesis, Massachusetts Institute of Technology, 2006.
- [189] D. Tambara and S. Yamagami. Tensor categories with fusion rules of self-duality for finite abelian groups. *J. Algebra*, 209(2):692–707, November 1998.
- [190] J. A. Siehler. Braided near-group categories. arXiv:math/0011037, 200.
- [191] Z. Wang. *Topological Phases of Matter: Exactly Solvable Models and Classification*. PhD thesis, California Institute of Technology, 2019.
- [192] A. Joyal and R. Street. Braided tensor categories. *Adv. Math.*, 102(1):20–78, November 1993.
- [193] V. Ostrik. Module categories over the Drinfeld double of a finite group. *Int. Math. Res. Not.*, 2003:1507–1520, 2003.
- [194] A. Bullivant and C. Delcamp. Gapped boundaries and string-like excitations in (3+1)d gauge models of topological phases. *J. High Energy Phys.*, 2021(7), July 2021.

- [195] P. Bruillard. Rank 4 premodular categories. *N. Y. J. Math.*, 22:775, 2016.
- [196] J. Preskill. Lecture notes for physics 219: Quantum computation. *Caltech Lecture Notes*, page 7, 1999.
- [197] J. C. Bridgeman, B. J. Brown, and S. J. Elman. Boundary topological entanglement entropy in two and three dimensions. *Commun. Math. Phys.*, 389(2):1241–1276, August 2021.
- [198] V. Ostrik. Fusion categories of rank 2. *Math. Res. Lett.*, 10(2):177–183, 2003.
- [199] V. Ostrik. Pre-modular categories of rank 3. *Mosc. Math. J.*, 8(1):111–118, 2008.
- [200] E. Rowell, R. Stong, and Z. Wang. On classification of modular tensor categories. *Commun. Math. Phys.*, 292:343, 2009.
- [201] P. Bruillard and C. M. Ortiz-Marrero. Classification of rank 5 premodular categories. *J. Math. Phys.*, 59(1):011702, January 2018.
- [202] Z. Yu. On slightly degenerate fusion categories. *J. Algebra*, 559:408–431, October 2020.
- [203] [List of small multiplicity-free fusion rings](#).
- [204] Ventola C. L. The antibiotic resistance crisis: part 1: causes and threats. *P. & T*, 40(4):277–283, 2015.
- [205] Y. Cao, J. Romero, and A. Aspuru-Guzik. Potential of quantum computing for drug discovery. *IBM J. Res. Dev.*, 62(6):6:1–6:20, November 2018.
- [206] N. S. Blunt, J. Camps, O. Crawford, R. Izsák, S. Leontica, et al. Perspective on the current state-of-the-art of quantum computing for drug discovery applications. *J. Chem. Theory Comput*, 18(12):7001–7023, November 2022.
- [207] Á. M. Alhambra. Quantum many-body systems in thermal equilibrium. *arXiv e-prints*, 2022.
- [208] J. Haah, R. Kothari, and E. Tang. Optimal learning of quantum hamiltonians from high-temperature gibbs states. *arXiv e-prints*, 2021.
- [209] W. Brown and D. Poulin. Quantum markov networks and commuting hamiltonians. *arXiv e-prints*, 2012.